LUMINESCENCE STUDY OF ION-IMPLANTED AND MBE-Grown Er-DOPED GaAs AND $Al_xGa_{1-x}As$

José E. Colón, B.S., M.S.

Captain, USAF

AFIT/DS/ENP/93-01

DEPARTMENT OF THE AIR FORCE
AIR UNIVERSITY
AIR FORCE INSTITUTE OF TECHNOLOGY

Wright-Patterson Air Force Base, Ohio

AFIT/DS/ENP/93-01

LUMINESCENCE STUDY OF ION-IMPLANTED AND MBE-Grown Er-DOPED GaAs AND $Al_xGa_{1-x}As$

José E. Colón, B.S., M.S.

Captain, USAF

AFIT/DS/ENP/93-01

Approved for public release: distribution unlimited

AFIT/DS/ENP/93-01

LUMINESCENCE STUDY OF ION-IMPLANTED AND MBE-Grown Er-DOPED GaAs AND $Al_xGa_{1-x}As$

DISSERTATION

Presented to the Faculty of the School of Engineering
of the Air Force Institute of Technology
Air University
In Partial Fulfillment of the
Requirements for the Degree of
Doctor of Philosophy

José E. Colón, B.S., M.S.
Captain, USAF

March 1993

Approved for public release: distribution unlimited

Preface

It is true that no man is an island. It is also true that the completion of a project like this can not be the work of just one person. It requires the work and talent of many people other than the author. Here, I would like to recognize the contributions of many wonderful people who offered me their assistance and support. Their friendship and continuous support made this experience a remarkable one. First, I would like to thank my advisors Dr. Y. K. Yeo and Dr. R. L. Hengehold for their continuous support and encouragement during the course of this program. Their guidance was truly instrumental in accomplishing this work. Thanks to Dr. Yeo for bearing with me during all those years. Their role was more than just professional assistance. They always care deeply about my success in this program, and will always have my gratitude for all their efforts.

I must also recognize the technical assistance by Greg Smith, who always kept my equipment in working conditions. Thanks Greg for those long hours repairing different pieces of equipment. Thanks also to Mr. Bill Evans for his help in the acquisition of new equipment, ion implantation, and for maintaining the supply of liquid helium. Also, thanks to Dr. Keith Evans from the Solid State Electronics Directorate of Wright Laboratory for providing the MBE samples and for many hours of stimulating discussions on the physics of Er-doped

semiconductors. I must also thanks Wright Laboratory for allowing the use of their RTA furnace, and Jim Solomon who did the SIMS measurements.

Special thanks to the secretaries of the Physics department: Diana Jordan, Nancy Loy, and Karen Dobbyn for their outstanding support during all these years and their wonderful friendship. They were always there whenever I needed them. This acknowledgement would not be complete without recognizing the contribution of Lt Col Pomrenke from AFOSR to this work. Gernot introduced to me this field of study back in 1989 during my master's thesis work. He not only provided funding for this study, but also the numerous conversations with him on this research topic were always an inspiration.

In this long list of friends who contributed to this work, I must highlight the many contributions of my fellow PhD student and rare earth scholar David W. Elsaesser. Dave wrote the program used to plot all the figures in this document. He also wrote the program used in the selective excitation luminescence experiments, and did numerous trips to the Solid State Electronics Directorate building to anneal my samples. Thanks to Dave for those long hours we spent together working on this project.

I must also thank several people from the Phillips Laboratory who greatly helped me finishing this project. First, I must thank my boss, Lt Col Wilhelm who gave me the

time necessary to complete this work. Also, Capt David Bell, Capt Robert Pugh, and Capt Karen Wink who let me use their Sun workstations to do my plots.

To conclude, I want to thank from the bottom of my heart my wife Carmen and my daughters Tania, Carla, Amanda, and Erica for all their sacrifices during the duration of this program. Their love and support through these years were always an inspiration. It would be impossible to replace the many precious moments that were lost because I had to work on weekends or late at night. During all these years, Carmen did the hard job of taking care of our children as well as encouraging me. We shared many difficult moments, although at times she had to bear most of the burden. For all the sacrifice and hard work by Carmen and the girls, this document represents as much their work as it does mine. Thanks for all your love and faith in me.

José E. Colón

Table of Contents

List of Figures

List of Tables

Abstract

The excitation and de-excitation mechanisms of the 1.54 μm emissions, from ion implanted and MBE grown GaAs:Er and $Al_xGa_{1-x}As$:Er, were studied through luminescence experiments. Experimental techniques included photoluminescence, time resolved photoluminescence, and selective excitation photoluminescence. The Er^{3+} emissions were studied as a function of Er concentration, aluminum mole fraction, n- and p-type doping level, and annealing temperature. In addition oxygen co-doping studies were done in order to determine the role played by oxygen in the Er^{3+} luminescence.

Photoluminescence and selective excitation photoluminescence revealed the presence of multiple Er-related luminescence centers in ion implanted GaAs:Er and $Al_xGa_{1-x}As$:Er. It was found that various emissions, originating from a particular luminescence center, can be excited very efficiently with below-bandgap laser excitation. The 1.54 μm emissions exhibit a broad selective excitation band that extends from the bandedge to pass 1.0 μm. A model of the excitation mechanism involving an energy transfer from electron-hole recombination at an Er-related hole trap is proposed. Time resolved measurements showed that the decay of the 1.54 μm emission is, mainly, a single exponential with a characteristic lifetime of approximately 1 msec. The lifetime decreases with sample temperature. In GaAs:Er, it decreases with an activation energy of 169 meV.

The Er^{3+} emissions from MBE grown GaAs:Er and $Al_xGa_{1-x}As$:Er were studied as a function of various growth parameters. Photoluminescence and time resolved measurements showed that the Er^{3+} emissions from $Al_xGa_{1-x}As$:Er originate from three distinct centers. Emissions from two of these centers have characteristic lifetimes on the order of 1.1 and 1.2 msec, while emissions from the other centers have lifetimes of approximately 200 μsec. $Al_xGa_{1-x}As$:Er samples showed various sharp emissions near 988 nm, which were assigned to the intra-4f-shell transition between the $^4I_{11/2}$ excited state and the $^4I_{15/2}$ ground state of Er^{3+}.

Oxygen co-doping consistently resulted in stronger Er^{3+} emissions from $Al_xGa_{1-x}As$:Er, but not from GaAs:Er. The 1.54 μm emissions from the co-doped samples were studied as a function of Er concentration, oxygen concentration, aluminum mole fraction, and annealing temperature. Lifetime measurements on $Al_xGa_{1-x}As$:Er showed that emissions from the co-doped samples have longer lifetimes, thus suggesting smaller losses due to nonradiative processes. The enhancement of the Er^{3+} emissions from $Al_xGa_{1-x}As$:(Er+O) was attributed to the formation of an Er-Al-O complex.

I. Introduction

Rare Earth (RE) compounds, which are very important in many applications because of their magnetic, chemical, and optical, properties have been studied intensively in the last five decades. In this current study we are concerned with their optical properties. The emission spectra of solids containing RE elements show very sharp emission lines due to internal 4f-shell transitions of the particular RE ion. This phenomenon is a result of their electronic configuration, which can be written for the Er^{3+} ions as (Boyn [1988])

$$[Pd]4f^n5s^25p^6,$$

where [Pd] refers to the electronic configuration of Pd, and n varies from 1 to 13 (not including La that some experts also classify as a RE element). The rare earths are unique in that their partially filled 4f shell is shielded from the environment by the 5s and 5p filled shells.

The Hamiltonian of a RE ion in a solid can be written as

$$H = H_o + H_{EE} + H_{so} + H_{CF},$$

where H_o is the Hartree-Fock part of the Hamiltonian, H_{EE} is the Coulomb interaction between the electrons (part not contained in H_o), H_{SO} is the spin orbit interaction, and H_{CF} is the crystal field potential. Of these terms, H_{EE} and H_{SO} have comparable effect, while H_{CF} has a much smaller effect and is

normally treated as a perturbation. Because H_{EE} and H_{SO} are comparable, the spin orbit coupling can be treated using the so called "intermediate" coupling scheme in which J is the only good quantum number.

Because the 4f-shell is shielded from the local crystalline environment, the 4f emissions are observed at nearly the same wavelength independent of the host material. In addition, the 4f emissions have very narrow linewidths and their positions vary very little (if at all) with temperature variations. These properties make RE doped materials ideal for laser sources. Indeed, ionic crystals doped with RE elements are some of the most important laser sources used today. Rare earth doped semiconductors can be used in the fabrication of novel optoelectronic devices with very sharp emissions whose wavelengths are temperature stable. From the application point of view, the study of RE doped III-V semiconductors and alloys is particularly important, because these are among the most used materials in optoelectronic devices. For example, Erbium (Er) doped III-V semiconductors and alloys show very sharp, temperature independent emissions at 1.54 μm, which is the wavelength of minimum attenuation in silica based fiber optics. Therefore, development of an Er based injection laser could greatly improve optical communications.

Although the optical properties of rare earth doped materials have been studied extensively since the 1940s, most of the work was done on rare earths in ionic hosts and to a

lesser extent in II-VI semiconducting compounds. The study of RE doped III-V semiconductors is relatively recent, dating back to the late 1970s (Pyhskin [1975], Ennen [1987], Pomrenke [1989]). Although there have been some advances in understanding the physics of these materials, knowledge in this area is still very limited. Specifically, many questions remain regarding the incorporation of the RE elements in the lattice and the excitation and de-excitation mechanisms of the 4f shell. In order to address these questions, optical studies of ion implanted and MBE-grown GaAs:Er and $Al_xGa_{1-x}As$:Er have been carried out. The experimental techniques used included photoluminescence, lifetime measurements, and selective excitation photoluminescence. In addition, the enhancement of the Er^{3+} emissions with oxygen co-doping has been studied. It is these measurements and their implications about the behavior of the rare-earth Er in these III-V hosts that forms the essence of this dissertation.

The different topics presented in this dissertation have been organized into five chapters. Following this introductory chapter, a review of the research done on rare earth doped semiconductors is presented in chapter II. A brief overview of the physics of rare earth doped II-VI compounds with a special emphasis in the excitation and de-excitation mechanisms of the 4f-shell is given, followed by a comprehensive review of the work done on rare earth doped III-V semiconductors. A description of the experimental set-up

used to perform the various experiments is given in chapter III. As mentioned above, this dissertation involved the study of ion implanted as well as MBE-grown GaAs:Er and AlGaAs:Er. The results for the ion implanted samples are presented in sections 4.1, 4.2, and 4.3. In sections 4.1 and 4.2, the results from photoluminescence and selective excitation luminescence are given, in addition a model of the excitation mechanism is proposed in section 4.2. The results from lifetime measurements of the main Er^{3+} emission near 1.54 μm are discussed in section 4.3. In section 4.4 the results obtained from photoluminescence, selective excitation luminescence, and lifetime measurements on the MBE samples are presented and they are compared with the results obtained for the ion implanted samples and with those obtained by other researchers in this field. The effect of oxygen co-implantation into GaAs:Er and AlGaAs:Er on the Er^{3+} emissions was also studied, and the results are presented in section 4.5. Finally, a summary of the results obtained in this dissertation work will be given in chapter V along with recommendations for further work on this area of research.

II. Background

This chapter introduces some concepts that will be used later in chapter IV, and reviews the work done so far in this area. A discussion of the configuration coordinate diagram is given in section 2.1. The ideas presented here are very important in understanding the excitation mechanism. A brief overview of the physics of rare earth doped II-VI semiconductors, particularly the excitation mechanisms of the 4f shell is presented in section 2.2. As mentioned, most of the work on RE doped semiconductors have been done on II-VI compounds. Therefore, a review of these systems will be very useful in our understanding of the excitation mechanisms of the 4f shell. Finally, a comprehensive review of previous studies of RE doped III-V semiconductors is presented in section 2.3.

2.1 Configuration Coordinate Diagram

The configuration coordinate (CC) diagram provides a framework for qualitative discussions of excitation and relaxation processes in semiconductors, and it will be very useful in the description of the 4f-shell excitation mechanisms. The qualitative basis of the CC diagram is the recognition that a change in the charge state of a defect causes a change in the bonding to the neighboring atoms, and

consequently a change in the relative position of these atoms (Böer [1990], pp. 494-501). Therefore, after trapping a charged particle, the surrounding atoms will relax to a new equilibrium position. In addition, the electronic eigenstate of the defect will also be affected by the change in the charge state. Consequently, after the trapping of a charge carrier, the defect relaxes and the electronic defect level changes. A similar process occurs when an electron within the defect is excited from the ground state into an excited state with a different wavefunction. The excited state will require a somewhat longer space. This will cause a change in the bonding to the neighboring atoms, thus resulting in a change of the atomic configuration. The CC diagram presents a pictorial representation of these processes. It depicts the coupling between the elastic energy and the electron-lattice interaction energy. In the simple harmonic approximation, the Hamiltonian of the lattice energy is given by:

$$H_o = \frac{1}{2}M(\frac{du}{dt})^2 + \frac{1}{2}\beta u^2,$$

where u is the lattice distortion and ß is the restoring force constant. Using normal coordinates:

$$H_o = \frac{1}{2}M(p^2 + M^2\omega^2 q^2),$$

where p = Mdu/dt and q = u = R - R_o. The basic assumption of the CC diagram is that the effect of the electronic transition can be treated as a linear perturbation of H_o which results in

a shift in the equilibrium position, i.e. the total Hamiltonian is:

$$H = H_o - \tau q,$$

where τ is the electronic interaction force. This Hamiltonian gives a displaced parabola. This is easily seen with a change of coordinates:

$$Q = q - \frac{\tau}{\beta},$$

then

$$\begin{aligned} H &= \frac{1}{2}M\dot{q}^2 + \frac{1}{2}\beta q^2 - \tau q \\ &= \frac{1}{2}M\dot{Q}^2 + \frac{1}{2}\beta\left(Q + \frac{\tau}{\beta}\right)^2 - \tau Q - \frac{\tau^2}{\beta} \\ &= \frac{1}{2}\dot{Q}^2 + \frac{1}{2}Q\beta - \frac{1}{2}\frac{\tau^2}{\beta}. \end{aligned}$$

Therefore, after capturing of an electron the energy as a function of the distortion coordinate will be given by a displaced parabola with its minimum at $(E - \tau^2/2\beta, q + \tau\beta)$, and the relaxation energy is given by $E_{relax} = -\tau^2/2\beta$. The electronic interaction force, τ, is proportional to a coupling constant called the Huang-Rhys factor, and β is proportional to the square of the breathing mode frequency (close to the LO phonon frequency). Actual systems deviate somewhat from this simple model, and higher order terms must be taken into account in the Hamiltonian describing the lattice distortion and electron lattice interaction. As a result, the displaced

parabola is deformed in addition to being shifted. Deep level defects show strong lattice coupling, therefore optical transitions from these defects are characterized by linewidths of several hundred meV. Various experimental techniques have been developed to obtain the CC diagram for a particular system. However, in this work our use of the CC diagram will be mainly descriptive since more work needs to be done in order to obtain the necessary parameters.

2.2 Rare Earth Doped II-VI Semiconductors

In II-VI compounds, the RE ions are substitutional and usually occupy metal sites. However, RE elements have a tendency to form complexes with other impurities such as P atoms and with group I elements (Boyn [1988]). Knowledge of the relative position of the energy levels of the RE ions with respect to those of the crystal is very limited. The RE^{3+} ground state lies most probably within the valence band, while the RE^{2+} ground state level should be located near the conduction band. Exceptions to this are Yb^{2+} and Eu^{2+} in ZnS which lie in the middle of the bandgap (Przybylinska et al. [1989]). Theoretical estimates by Świątek et al. [1990] indicate that in ZnS the RE^{2+} level of Yb, Eu, Sm, and Tm lies in the bandgap.

In order to maintain charge neutrality, group I elements are normally used as charge compensators in RE doped II-VI

compounds. The addition of group I elements facilitates the introduction of RE ions into the lattice, and have been found to strongly enhance the RE^{3+} emissions (Boyn, [1988]).

2.2.1 Excitation Mechanisms

Boyn [1988] classifies the excitation mechanisms of the 4f shell according to three types of processes:

a. Direct excitation of the 4f shell;

b. Excitation of impurity states outside the 4f shell, followed by non-radiative energy transfer to the 4f shell;

c. Excitation by (free) excitons and electron-hole pairs.

Direct excitation of the 4f shell is characterized by the presence of sharp lines in the excitation spectrum, while type b and c processes appear as broad bands in the excitation spectrum.

In type b processes, the primary excitation process is followed by nonradiative energy transfer to the 4f shell. These processes can be further subdivided into three categories:

b1. Excitation of RE ions by sensitizing impurities or centers. An example of such a process is the excitation of the 4f shell in ZnS:(RE+Cu) where Cu acts as the sensitizing center (Kröger and Dikhoff [1950]). Another example is the transfer of the

ecombination energy from donor-acceptor pairs, a theoretical discussion of which can be found in Shaffer and Williams [1970].

b2. Transitions between external states of RE centers. Examples of this type of process are charge transfer and 5d to 4f transitions, which are common in ionic hosts.

b3. Excitation of donor-acceptor pairs involving the RE ions as the donors and some other impurity as the acceptor. According to Boyn [1988], in this transition an electron is promoted from an acceptor state to a spatially overlapping (shallow) donor state. Due to the strong coupling to phonons, these transitions will give rise to broad bands well below E_g in the excitation spectrum. A variation of this type of process occurs when complex RE centers act as acceptors.

Since all three subtypes of type b processes, as well as type c processes, give rise to broad excitation bands, it is very difficult to distinguish between them. Type b2 processes are characteristic of a specific center, therefore, they will be observed in different samples containing that center. On the other hand, type b2 processes are characteristic of the samples, i.e., will be observed for all the centers in the sample. In the case of b3 processes, there are no simple rules to differentiate them from b1 and b2 processes.

Furthermore, the excitation spectra of some samples exhibit all these types of excitation mechanisms.

2.3 Rare Earth Doped III-V Semiconductors

Research efforts on the physical properties of rare earth doped III-V semiconductors have intensified during the past few years due to potential applications in new optoelectronic devices. However, these materials are still poorly understood. In particular the excitation and de-excitation mechanisms of the 4f shell are not well understood. This section presents a comprehensive review of the work done on this research area.

2.3.1 Ytterbium

Among the RE elements, Yb has been the subject of most investigations on RE doped III-V semiconductors, in particular InP:Yb. Ytterbium intra-4f-shell emissions have been observed in InP, GaP, GaAs (Ennen and Sneider [1984], Ennen et al. [1985]), AlGaAs (Colón [1988]), and GaInP (Kozanecki et al. [1989]). The emissions are observed near 1.0 μm and are due to the transition between the crystal field split states $^4F_{5/2}$ and $^4F_{7/2}$ of Yb^{3+}. Photoluminescence excitation (Wagner et al. [1984]) and Zeeman experiments (Azodi et al. [1985]) on InP:Yb have shown all emissions around 1 μm originate from a single center with cubic symmetry, assumed to be a substitutional Yb ion in a cation site. This is also indicated by the fact that

all InP:Yb samples show the same emissions near 1.0 μm, independent of doping method and sample treatment (such as annealing). The Yb emission spectrum changes significantly in $Ga_xIn_{1-x}P$:Yb (Kozanecki et al. [1989]) due to the presence of a second luminescent center emitting near 1.0 μm. This center has noncubic symmetry and it appears even with very small concentrations of Ga (x = .5%). It has been assigned to an Yb ion on a substitutional cation site perturbed by the presence of a Ga ion in the next nearest neighbor position. Kozanecki et al. noticed that the ratio of the intensities of the emissions from the cubic center to those of the noncubic center exceeds the ratio of the respective probabilities for each center by a factor of 4 to 5. According to the authors, this is due either to a more efficient excitation mechanism of the noncubic center or to an energy transfer from the cubic to the lower symmetry center. Also, for x > 0.1, all Yb emissions broaden, forming a broad structureless band. The same results were obtained for the ion implanted samples and for the samples where Yb was doped during the growth process (Kozanecki et al. [1989]). Another interesting variation of the InP:Yb system is $InAs_xP_{1-x}$, where the hope is to narrow the bandgap energy to obtain a resonant effect.

Photoluminescence studies of these systems were done by Neuhalfen and Wessels [1991] for x = 0 to 0.98. For x = 0, 0.11, 0.12 , and 0.17, it was found that the main Yb peak shifts toward smaller energies as x increases,i.e., as the

bandgap energy decreases. Of all the alloys, x = 0.17 showed the stronger Yb^{3+} emissions (although somewhat weaker than Yb emissions from InP) presumably because of a resonant effect. No intra-4f emissions can be seen from the samples with x > 0.2, which is interpreted by the authors as evidence that the Yb level for $x \geq 0.2$ is either resonant with the valence band or below the valence band.

It should be pointed out that the behavior of Yb in InP does not seem to be characteristic of Yb in other III-V hosts or other RE elements in III-V semiconductors. Indeed, Rutherford backscattering experiments (Kozanecki and Groetzschel [1988, 1990]) have shown that Yb in GaAs, GaP, and AlGaAs occupies non-substitutional sites in the lattice. Also, Rutherford backscattering (RBS) experiments have shown that in these hosts Yb diffuses to the surface and forms precipitates. Contrary to the case in InP:Yb, in these materials the PL emission spectra around 1.0 μm depend upon the particular doping method used. Furthermore, strong luminescence near 1.0 μm is only observed in In based semiconductors, whereas Ga based semiconductors show very weak or no Yb emissions.

2.3.2 Erbium

Erbium has been introduced into III-V semiconductors using different techniques such as ion implantation (Pomrenke et al. [1986]), molecular beam epitaxy (Ennen et al. [1987]), liquid

phase epitaxy (Bantien et al. [1987]), MOCVD (Uwai et al. [1987]), and diffusion (Zhao et al. [198]). The host semiconductors have included InP, GaP, GaAs, AlGaAs, GaInAsP, and the quantum well GaAs/AlGaAs (Galtier et al. [1988]). The Er^{3+} emissions are observed near 1.54 μm and are due to the intra-4f transition between the crystal field split states $^4I_{13/2}$ and $^4I_{15/2}$ of Er^{3+}. Figure 1 shows an energy level diagram of Er^{3+}. The figure also indicates the bandgaps of GaAs and $Al_xGa_{1-x}As$ for comparison purposes. Note that the energy difference between other excited states (i.e., at higher energy than the $^4I_{13/2}$ level) and the ground state is smaller than the bandgap of the host semiconductor. In particular, the $^4I_{11/2}$ state is approximately 1.3 eV from the ground state, which is smaller than the GaAs bandgap, and therefore it should be possible to observe the transitions originating from this level. Also, the $^4I_{9/2}$ level is approximately 1.5 eV from the ground state, i.e. nearly resonant with the GaAs bandgap. However, in the low temperature PL of GaAs, only the $^4I_{13/2} \rightarrow {}^4I_{15/2}$ transition is observed. We will return to this point later when discussing the results. As mentioned, the 4f levels are shielded from the crystalline environment by the filled outer shells. As a result, the crystal field splitting is only 10% (or less) of the spin-orbit splitting. This is illustrated in figure 2, which shows the splitting of the $^4I_{13/2}$ and $^4I_{15/2}$ levels in a cubic field, and the order of magnitude of the crystal field and spin-orbit splitting. As shown in the figure, in a

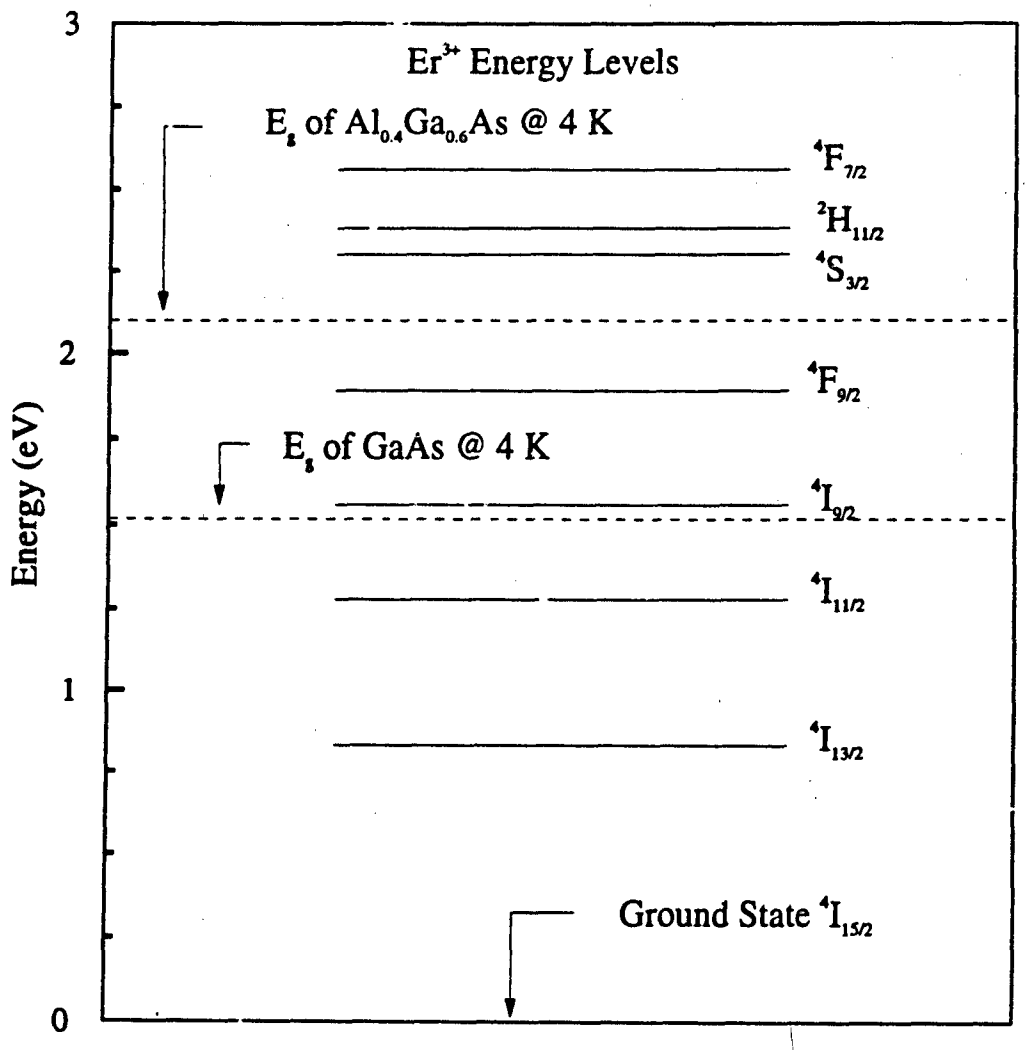

Figure 1 Energy levels of Er^{3+} compared to the bandgap energies of GaAs and $Al_{0.4}Ga_{0.6}As$

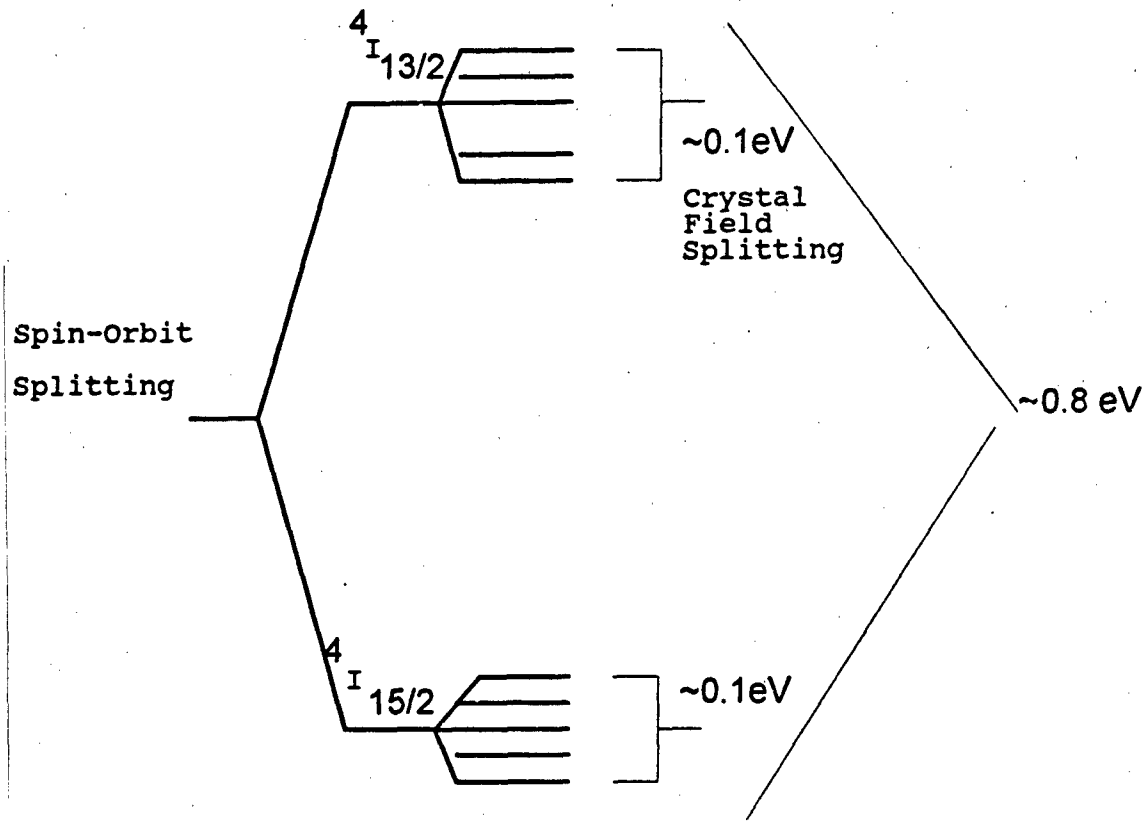

Figure 2 Stark splitting of the $^4I_{13/2}$ and $^4I_{15/2}$ energy levels of Er^{3+} in a cubic crystal field

cubic field both levels are split into five sublevels. The spacing among sublevels in a multiplet was selected arbitrarily because the exact value will change for each individual case. Transitions among sublevels in a given multiplet will occur in the order of one nanosecond or less, while the radiative transition between the $^4I_{13/2}$ and $^4I_{15/2}$ levels has a lifetime of approximately one millisecond. Thus, we can expect that all emissions observed in the low temperature PL spectrum are due to transitions between the lowest level in the upper multiplet and the ground state multiplet, as shown in the figure. Therefore, for a single Er center in a cubic field, only five emissions are expected. When the Er ion occupies a site with the lowest symmetry, the ground state will split into eight sublevels, and thus only eight emissions would be expected from a given Er-related center. However, in most cases the low temperature PL of GaAs:Er shows many more emissions than expected for a single center. The spectra of Er in III-V semiconductors are dependent upon both the particular conditions of the sample preparation and the host semiconductor. For example, ion implanted samples have very complex emission spectra with up to 40 Er related emission lines, while erbium doped LPE samples show rather simple emission spectra with only five Er lines. This would indicate that the Er emissions originate from multiple luminescent centers. In fact, isochronal annealing studies of ion implanted GaAs:Er (Klein et al. [1991]) have shown that the

1.54 μm emissions originate from at least five different luminescent centers. The presence of multiple luminescent centers is due to Er ions at different lattice locations and/or the formation of complexes between Er and other impurities. The exact nature of these centers is not known. Electron spin resonance (ESR) studies of InP:Er (Masterov et al. [1987]), and EPR studies of GaAs:Er by Baeumber et al. [1987], as well as an RBS study of MBE-grown GaAs:Er (Galtier et al. [1988]) have given results that are consistent with Er occupying substitutional sites. However, because of the tendency of Er to form different luminescent centers, the nature of which depends upon the particular growth or doping method used, such studies are far from conclusive.

A very important question that must be addressed is the charge state of the Er ion in III-V semiconductors. Although the emissions near 1.54 μm are due to transitions between 4f states of Er^{3+}, electron paramagnetic experiments (EPR) on ion implanted GaAs:Er done by Klein et al. [1991a, 1991b] showed that the great majority of Er ions (99.9%) are in the 2+ state. Therefore, excitation of Er^{3+} must involve an ionization process. However, this seems to contradict the previous reports of resonant excitation of the Er emissions from MBE-grown GaAs:Er by Ennen et al. [1987], since resonant excitation would not be possible if Er were in the 2+ state. More experimental and theoretical work is necessary to resolve these contradictory results. Another important question that

might be related to the charge state of Er is why the transition from the $^4I_{11/2}$ excited state to the $^4I_{15/2}$ ground state is normally not observed in photoluminescence experiments. Such transitions have been observed around 988 nm in the electroluminescence spectrum of GaAs:Er but not in the PL spectrum (Isshiki et al. [1990]). Recently, it was reported that the 988 nm emissions were observed in the photoluminescence of MBE-grown $Al_{0.55}Ga_{0.45}As$:Er (Benyattou et al. [1992]).

2.3.3 Other Rare Earth Systems

There are very few studies of III-V semiconductors doped with RE elements other than Yb or Er. Intra-4f luminescence has been observed in the cases of Nd, Pr, and Tm doped into either GaAs, GaP, AlGaAs, or InP as the host semiconductor. The RE elements Ce, Gd, and Dy have also been introduced as dopants into III-V semiconductors (Zakharenkov et al. [1985], Berman et al. [1985], Bagraev et al. [1983], Physkin et al. [1968]), however, no intra-4f luminescence from these systems has been reported. Electron spin resonance experiments have shown that Eu in InP is in the Eu^{2+} state (Zakharenkov et al. [1985]). Also, the effect of adding Eu to the melt (in InP) was studied using Raman spectroscopy by Bairamov et al. [1990] however, the objective of that work was to study the so-called "purification" effect of the RE elements (i.e., addition of RE elements to the melt reduces accidental

impurities by forming precipitates) and no mention was made of the luminescence from InP:Eu. There are some luminescence studies of GaP:Dy and GaP:Ce films (Kasatkin et al. [1978], [1979]), but only broadband luminescence was observed.

Neodymium has been introduced as a dopant into GaP, GaAs, and AlGaAs by ion implantation (Müller et al. [1986], Wagner et al. [1986], Kozanecki and Groetzschel [1991]) and MOCVD (Nakagome and Takahei [1989]). In all cases, the luminescence spectrum shows three sets of sharp lines near 0.92, 1.1, and 1.4 μm, corresponding to the transitions from the state $^4F_{3/2}$ to the states $^4I_{9/2}$, $^4I_{13/2}$, $^4I_{15/2}$ of Nd^{3+}, respectively. Selective excitation luminescence experiments (SEL) have shown that in GaP:Nd the 4f emissions originate from more than one luminescent center with noncubic symmetry. An interesting result from the SEL experiments is that excitation of Nd^{3+} with energy greater than the bandgap is about five times more efficient than resonant excitation (in GaP). Also, RBS experiments (Kozanecki and Groetzschel [1991]) have shown that Nd occupies non-substitutional sites in GaP, GaAs, and AlGaAs.

The luminescence spectrum of GaP:Pr has been studied by Kasatkin et al. [1981], Kasatkin [1985], Gippius et al. [1986], and Pomrenke [1989]. Kasatkin [1985] found four sets of sharp emissions in the ranges 1.24-1.35, 1.68-1.75, 1.9-2.04, and 2.2-2.3 eV that were interpreted as due to intra-4f transitions of Pr^{3+}. Pomrenke [1989] studied the luminescence from GaAs:Pr and InP:Pr. Three sets of sharp lines were

observed around 1.6, 1.35, and 1.05 μm. These emissions were assigned to the transitions of $^3F_3 \rightarrow {}^1H_4$, $^1G_4 \rightarrow {}^3H_5$, $^1G_4 \rightarrow {}^3H_4$ of Pr^{3+}, respectively. Pomrenke [1989] also studied the luminescence of Tm implanted GaAs and InP, and Ho implanted GaAs. The emission spectrum of GaAs:Tm consisted of several sharp lines near 1.22 μm assigned to the transition of $^3H_5 \rightarrow {}^3H_6$ of Tm^{3+}, whereas InP:Tm only showed a very weak emission near 1.23 μm. The results for GaAs:Ho were not clear, although a very weak emission that might be due to Ho^{3+} was observed.

2.3.4 Electrical properties

Very little is known about the electrical behavior of RE ions in III-V semiconductors. Theoretical studies by Hemstreet [1986] predicted that Yb in InP would behave as an acceptor, however, EPR measurements (Lambert et al. [1989]) have shown that the Yb^{2+} acceptor level is not in the bandgap. Later results indicate that RE ions tend to introduce isoelectronic traps into the bandgap. These traps do not contribute carriers by themselves but can capture free carriers and bind excitons (Thonke et al. [1991]). In the case of Yb, an electron trap of 30 meV below the conduction band was found from DLTS measurements (Withney et al. [1988]). Within experimental error, the trap concentration was found to be the same as the concentration of Yb. Similar results were reported by Lambert et al. [1989] from temperature dependent Hall measurements on InP:Yb and InP:Er. It was found that

both Yb and Er introduce electron traps at 30 and 60 meV below the conduction band, respectively. Admittance spectroscopy experiments (Smith et al. [1987]) have shown that in MBE-grown GaAs:Er, Er introduces a trapping level in the bandgap of GaAs, unfortunately neither the nature of the trapping level (hole or electron trap) nor the energy of the level could be determined from the experiments. Another case where RE ions have been found to introduce isoelectronic traps is GaAs:Yb. A band of trapping levels near 0.7 eV were reported by Takahei et al. [1990] in MOCVD grown GaAs:Er. More recent results have shown that Yb also introduces a hole trap in p-type InP at 40 ± 10 meV above the valence band (Seghier et al. [1991]). Lambert et al. [1991] and Seghier et al. [1991] believe that Yb introduces an isoelectronic trap in InP that can bind either holes or electrons. As it will be discussed in the next section, the tendency of RE ions to introduce isoelectronic traps into the bandgap is closely related to the excitation mechanism of the intra-4f emissions.

2.3.5 Excitation Mechanism

One of the most important obstacles to the development of optoelectronic devices based on RE doped III-V semiconductors is the lack of understanding of the intra-4f-shell excitation mechanism. Most of the work in this area has been done on InP:Yb, although there has been some work on GaP:Yb, GaAs:Er,

and GaP:Nd (Kasatkin and Savel'ev [1984], Tagushi et al. [1990], Ennen et al. [1987], and Donegan [1990]). Experimental techniques used to understand the excitation mechanism include photoluminescence excitation (Wagner et al. [1984], Kasatkin and Savel'ev [1984], Körber and Hangleiter [1988]), ESR measurements (Masterov et al. [1983]), time resolved electroluminescence (Kasatkin et al. [1985]), time resolved PL (Klein [1988], Körber and Hangleiter [1988], and Benyattou et al. [1991]), electrical measurements (Kasatkin and Romanov [1985]), EPR measurements (Klein et al. [1991]), and optically detected cyclotron resonance (Godlewski et al. [1990], and Heijmink et al. [1991]). An overview of the work done up to the present will be presented in this section.

2.3.5.1 Ytterbium in InP, GaP, and GaAs

The most important disagreement among researchers has been whether below-bandgap states are involved in the excitation of Yb^{3+} or not. Kasatkin and Savel'ev [1984] believe D-A pairs are involved in the excitation of Yb emissions from GaP and InP. In their SEL experiments, the excitation spectrum of the main Yb emission from GaP:Yb was virtually the same as the D-A excitation spectrum, independent of the Yb concentration. In contrast, both the emission and excitation spectrum of InP:Yb showed a dependence on the Yb concentration. For Yb concentrations smaller than the concentration of D-A pairs, the luminescence spectrum showed D-A emissions. However, for

Yb concentrations equal or greater than the D-A concentrations, the luminescence due to D-A recombination was quenched. At high Yb concentrations, the excitation spectrum showed a decrease of the Yb luminescence as the excitation energy was decreased below bandgap, but it showed a peak at the same energy position where the excitation of D-A pairs was maximum (i.e., in the InP samples without Yb). Based on these results, Kasatkin and Savel'ev concluded that excitation of Yb^{3+} in InP and GaP proceeds through an Auger recombination process, in which the recombination energy of an exciton or a D-A pair is transferred nonradiatively (by the Coulomb interaction) to the 4f shell. Kasatkin et al. [1985] used this model to interpret their results from the time resolved eletroluminescence experiments. In this model the rate equation for the Yb^{3+} excitation can be written as

$$\frac{dn(t)_a}{dt} = \frac{kn(t)}{\tau} - \frac{n(t)_a}{\tau_a}.$$

The solution to this equation is

$$n(t)_a = \frac{kn_o\tau_a}{\tau_a-\tau}\left[\exp\left(-\frac{t}{\tau_a}\right) - \exp\left(-\frac{t}{\tau}\right)\right],$$

where τ_a is the lifetime of Yb ions in an excited state, k is the fraction of donor-acceptor pairs participating in the excitation, n(t) is the concentration of donor-acceptor pairs, τ is the lifetime of an excited pair, and n_o is the number of donor-acceptor pairs. Kasatkin et al. found that this last

equation fit their data with values of τ_a = 9 μsec and τ = 2 μsec.

Contrary to these results, SEL experiments on InP:Yb by Körber and Hangleiter [1988] showed no evidence of Yb^{3+} excitation by below bandgap states (such as D-A). Also lifetime measurements (Körber and Hangleiter [1988], Klein [1988], Pomrenke [1989]) did not show the time delay in the rise of the Yb^{3+} signal seen by Kasatkin et al. [1985].

More recently, Takahei et al. [1989] proposed a model in which excitation of Yb^{3+} in InP proceeds through the Yb electron trap (see section on electrical properties). Figure 3a shows the configuration coordinate diagram representing different energy states (host + 4f shell) during the excitation process. In the diagram, the horizontal axis is the lattice distortion around Yb. The vertical axis is the total energy of the 4f electrons, host electrons, and lattice distortion. Four energy states are shown. Figure 3b shows the configuration of the host and the 4f shell for each state illustrated in Fig. 3a. In state (1), the 4f shell is in the ground state and the Yb trap is empty. In state (2), the 4f shell is in the ground state, and one electron is excited from the valence band to the conduction band, leaving a hole in the valence band. In state (3), an electron is trapped by Yb. Because the electron attractive potential is a short range potential (non-Coulombic), the electron is localized around the Yb site, probably causing large distortions in the lattice

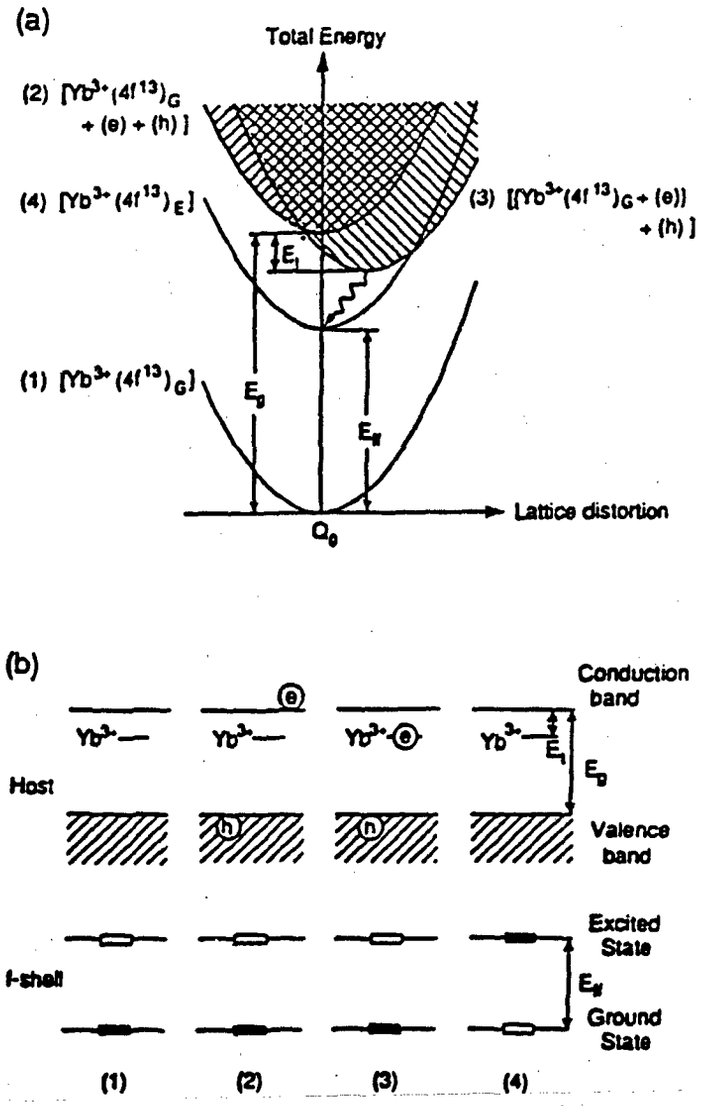

Figure 3 Configuration coordinate diagram illustrating the excitation mechanism of the 4f-shell in InP:Yb according to Takahei et al. [1991]

as indicated by the shift in the horizontal direction. In state (4), the electron at the Yb trap has recombined with a hole in the valence band, while the 4f shell is in the excited state. Above-bandgap excitation of Yb^{3+} would proceed as follows:

i. Activation from state (1) to state (2), either by photo-excitation or by carrier injection into a pn junction;

ii. Relaxation from state (2) to state (3) by capture of an electron by the Yb trap;

iii. Relaxation from state (3) to state (4) due to recombination of the electron-hole pair and nonradiative transfer to the 4f-shell.

iv. Relaxation from state (4) to state (1) by radiative transition of the intra-4f-shell electrons.

The excitation spectrum of InP:Yb shows a small peak for some samples around the D-A energy position. Takahei et al. [1989] proposed two possible mechanisms of below-bandgap excitation of Yb^{3+} (other than resonant excitation that occurs near 910 nm, Wagner et al. [1984]). These mechanisms proceed as follows:

I.

1. Excitation of electrons at acceptors into the conduction band;

2. Capture of electrons by the electron trap associated with Yb^{3+};

3. Recombination of electrons at the trap and holes at acceptors with simultaneous excitation of Yb^{3+}.

II.

1. Excitation of electrons from the valence band to the electron trap associated with Yb^{3};

2. Recombination of electrons at the trap with holes in the valence band, or at neutral acceptors, with the simultaneous excitation of Yb^{3+}.

Mechanism I can only take place in the samples with a high concentration of either Yb or acceptors. This is because the average distance between the Yb ion and the acceptors will be larger in samples with low Yb concentration, thus making the interaction between the Yb ions and the acceptors less probable. For mechanism II, to be effective there must be empty states in the electron trap, which will require the donor concentration to be smaller than the sum of acceptors and trap concentration. This condition is necessary because electrons ionized from donors will occupy some of the states in the electron trap. Therefore, below- bandgap excitation of Yb is possible only in a p-type sample or in a heavily Yb doped sample.

Although further experimental evidence implying excitation of Yb^{3+} in InP by excitons bound at the Yb related trap has been reported, there is some discussion about whether the 30 meV electron trap found by DLTS is the level involved in the 4f shell excitation. Absorption experiments by Thonke et al.

[1990] indicated only a small fraction of Yb ions was optically active, while DLTS experiments (Withney et al. [1989]) showed the concentration of the electron trap was approximately the same as the Yb concentration. Furthermore, photoconductivity (PC) experiments by Thonke et al. [1990] seem to favor a model in which Yb^{3+} excitation proceeds through a hole trap. Ytterbium doped samples showed a strong decrease in PC upon excitation with energies greater than the InP bandgap (E_g) when compared to the samples without Yb. The PC spectrum of InP (without Yb) showed a strong peak at E_g, as well as sharp and strong peaks in the free exciton (FE) region. However, the PC spectrum of the Yb doped sample did not show the bandedge peak, and it had a minimum in the FE region. These results suggest very efficient trapping of free carriers and excitons by an Yb trap right upon generation. Additionally, in the Yb doped sample, a strong PC peak appears at 1.39 eV (approximately 30 meV less than the bandgap). This peak can be interpreted as due to excitation of electrons from an Yb hole trap (30 meV above the valence band) to the conduction band. If an electron trap is assumed (such as the one found in DLTS experiments), a negative PC signal would be expected at this position, because electrons from the valence band would be excited to the electron trap. As was mentioned in the previous section, a hole trap in p-type InP:Yb was found later by Seghier et al. [1991]. Also, temperature dependent Hall measurements by L'homer et al. [1991] found the

presence of both an electron and a hole trap, both with activation energies of 40 meV. Measurements of the bandedge luminescence decay time from n-type InP:Yb (L'homer et al. [1991]) seem to confirm the hypothesis by Thonke et al. [1990]. In the experiment, the bandedge luminescence decay from InP:Yb was studied as a function of temperature and excitation density. Their data gives a lifetime of 350 nsec for the Yb BE. A very high hole capture cross section of $2 \times 10^{13}/cm^{-2}$ was determined, which is two orders of magnitude higher than the capture cross section for the electron trap. The binding energy of the Yb BE was found to be approximately 90 meV. The model by L'homer et al. implies that, in n-type InP, the bandedge luminescence decay time and subsequently the PL efficiency of Yb^{3+} are essentially governed by the trapping of photocreated holes.

2.3.5.2 Erbium

In comparison with InP:Yb, fewer studies dealt with the excitation mechanism of the 4f emissions from Er doped III-V semiconductors. Bantien et al. [1987] and Smith et al. [1987] found a linear increase in PL intensity as the laser excitation power increases, with no sign of saturation. Such behavior is similar to the near edge excitonic luminescence. However, PL studies of the 1.54 μm emissions from $Al_{0.55}Ga_{0.45}As$:Er have shown a sublinear relationship. Benyattou et al. [1990, 1991] found that the PL intensity varied as the

square root of the laser excitation power. A two beam experiment was carry out by Benyattou et al. in order to understand this behavior. In that experiment, a HeNe laser was used to pump the 1.54 μm emissions, while a chopped argon laser was used as a probe beam. The probe beam was used to generate free carriers. In order to avoid any pumping of the PL signal by the probe beam, the lock-in amplifier was set such that the signal was completely out of phase with the probe beam. When the probe beam and the pump beam spots overlap, the PL intensity decreased. These results were explained by assuming an excitation model similar to that of Yb in InP. In analogy with Yb, it was assumed that Er introduces an isoelectronic trap in the bandgap that can bind excitons. An exciton at the Er trap would transfer its recombination energy to the 4f shell, thus exciting the Er^{3+}. However, the bound exciton might instead transfer its energy to a free carrier by an Auger process. The probability of this competing Auger process will be proportional to the free carrier concentration, i.e., the probability of such process will be Bn, where B is a transfer constant and n is the carrier concentration. The total probability for the bound exciton to transfer its energy to an Er ion is (Benyattou et al. [1990, 1991]) given by

$$P = \frac{P_e}{P_e + Bn},$$

where P_e is the Er excitation rate. The rate of Er excitation is given by

$$\frac{dn_e^*}{dt} = A\phi\frac{P_e}{P_e + Bn} - \frac{n_e}{\tau_f},$$

where n_e^* is the excited Er concentration, $A\phi$ is the number of created bound excitons, ϕ is the light flux, and τ_f is the excited state decay constant. Assuming high flux and a bimolecular recombination of free carriers, the steady state solution of the rate equation is

$$n_e^* = \frac{\tau_f A P_e}{C}\sqrt{\phi}.$$

Therefore, this model can explain the square root dependence of the PL intensity as a function of the excitation power. Furthermore, Benyattou et al. found a good fit with the results from their two beam experiments. An oversight of the work done by Benyattou et al. is that the energy of the probe beam is actually smaller than the bandgap of $Al_{0.55}Ga_{0.45}As$. This issue will be addressed in the discussion of the results of this current study.

2.3.6 Quenching Mechanism

The PL intensity of the intra-4f emissions from RE doped

III-V semiconductors depends strongly on the sample temperature, i.e., the PL intensity decreases as the temperature increases. The quenching mechanism responsible for this behavior is probably related to the specifics of the excitation mechanism but it is not yet understood. Most of the knowledge in this area has been obtained from lifetime experiments and from studies of the temperature dependence of the PL intensity. Again, the system that has been studied the most is InP:Yb, although some work has been done on GaAs:Er, AlGaAs:Er, and GaAs:Nd.

2.3.6.1 Ytterbium

Lifetime studies by Körber and Hangleiter [1988] on InP:Yb showed a single exponential decay with a time constant of 12.5 μsec, independent of the Yb concentration. However, Klein [1988] found an initial non-exponential component with a much shorter time constant. The time constant of the long decay found by Klein was essentially the same as that reported by Körber and Hangleiter. In order to explain the fast non-exponential component, Klein made use of Hemstreet's theoretical results (Hemstreet [1986]), which predicts a ground state of Yb in InP consisting of a linear combination of Yb^{3+} and Yb^{2+}. In Klein's model, the photoneutralization of Yb^{2+} produces an electron that may be captured by an Yb^{3+} ion in the excited state, thus interrupting the intra-4f emission. Since not all the Yb^{3+} ions are affected in this way, this

would result in a non-exponential decay. A similar model was proposed by Körber and Hangleiter to explain the temperature quenching of the Yb emissions.

Takahei et al. [1989] presented two objections to Klein's model. First, photoexcited carriers should recombine or relax to trap related states on the order of nanoseconds, while the non-exponential component observed in some InP:Yb samples was of the order of μsec. Second, EPR experiments (Lambert et al. [1988]) showed that the Yb^{2+} state is not in the InP bandgap. The initial non-exponential fast decay was explained by Takahei et al. [1989] and by Tagushi et al. [1991] as follows. After excitation of the 4f shell by electron-hole recombination at the Yb electron trap, the trap with excited 4f-shell becomes empty. Such traps may capture electrons from distant shallow donors. These electrons can be excited into the conduction band by an energy transfer from the excited 4f-shell. This process would be efficient only when the concentration of shallow donors (N_D) is greater than the concentration of Yb traps (N_T). This model was also used by Tagushi et al. [1991] to explain the temperature dependence of the PL intensity from the samples with $N_D > N_T$.

However, the model discussed above cannot explain the decay of Yb^{3+} emissions from p-type InP:Yb. According to the above model, the decay of Yb for the p-type samples should be the same as for the n-type samples with $N_D << N_T$. Also, the decay for the p-type samples should be purely exponential, because

quenching by donors will be very inefficient. However, Takahei et al. [1989] found for the p-type samples, a slightly non-exponential decay with a time constant of 17.4 μsec. In Takahei's excitation model, this can be explained by the presence of two different excitation mechanisms for the p-type samples. As discussed in the previous section, for the p-type samples, electrons at the Yb trap can recombine with either holes in the valence band or holes captured at the acceptor levels. The former process is much faster than the latter. The presence of a fast excitation process with a slow excitation process deforms the exponential decay, and thus results in larger apparent decay times. Incidentally, this will also explain the initial rise in the decay curve of the Yb electroluminescence observed by Kasatkin and Savel'ev [1985]. The sample used by Kasatkin and Savel'ev was melt grown Yb doped InP, which is likely to contain high impurity concentrations. Takahei's model can also explain the dependence of the Yb^{3+} PL intensity on the carrier concentration that was observed by Zakharenkov et al. [1989]. As would be expected from Takahei's model, the Yb^{3+} PL intensity initially increases with increasing free electron concentration until it reaches a maximum, and then decreases very quickly as the free electron concentration increases further. Unfortunately, the authors couldn't determine the Yb concentration in the samples studied. According to Takahei's model the maximum intensity should occur when the electron

concentration is approximately the same as the Yb concentration.

As mentioned above, Tagushi et al. [1991] used Takahei's model to explain the temperature dependence of the PL intensity. These authors found two different processes involved in the temperature quenching of Yb^{3+}. Below 70 K, the PL intensity of the samples with $N_D > N_T$ decreases as the temperature increases. This was explained by the capture of electrons from the shallow donors by Yb traps with excited 4f-shells, and subsequent transfer of energy from the 4f shell to these electrons, exciting the electrons into the conduction band and quenching the 4f emissions. On the other hand, the samples with $N_D < N_T$ showed constant intensity as the temperature was raised, to approximately 50 K. After 50 K, the intensity of the Yb emissions from these samples showed a slight increase. This was correlated with an increase in the free carrier concentration above 50 K. Tagushi et al. attributed this phenomenon to the capture of electrons from shallow donors by Yb traps with the 4f- shell in the ground state. Successive capture of holes by these traps would result in the increase in the number of excited Yb 4f-shells. Above 70 K, the PL intensity of all the samples decreased with increasing temperature, independent of the carrier concentration, while the intensity of the near edge emissions increased. Tagushi et al. [1991] believe this is due to an energy backtransfer from the 4f-shell to the host.

Other researchers have also found two different processes involved in the temperature quenching of Yb^{3+}. Klein [1988] fitted the PL intensity to an expression of the form

$$I(T) = \frac{I(0)}{1 + A_1 \exp\left(\frac{-E_1}{kT}\right) + A_2 \exp\left(\frac{-E_2}{kT}\right)}$$

with E_1 = 115 meV, E_2 = 10.8 meV, $A_1 = 4.7 \times 10^7$, and A_2 = 3.2. Similar results were obtained by Stapor et al. [1989], Thonke et al. [1990], and L'homer et al. [1991]. The magnitude of A_2, when compared to A_1, indicates the process with activation energy E_2 is very inefficient in quenching the Yb^{3+} emissions. The nature of that process is not known. The activation energy E_1 has been related to the excitation mechanism. The same activation energy has been found from the temperature dependence of the lifetime (Stapor et al. [1989] and Thonke et al. [1990]). The value of E_1 fits neatly in Lambert's excitation model (Lambert et al. [1991]). Indeed, in Lambert's model, E_1 corresponds to the dissociation energy of the Yb bound exciton, i.e.,

$$E_1 = E_{binding} + E_{trap},$$

where $E_{binding}$ is the binding energy of the exciton (90 meV as determined by Lambert et al. [1990]), and E_{trap} is the energy of the Yb trap (35 meV). However, Agushi et al. [1991] estimated an activation energy of 150 meV for the temperature quenching, and attributed it to an energy backtransfer process from the 4f shell to the host. as discussed in the previous paragraph.

2.3.6.2 Erbium

Decay times of Er^{3+} from Er doped III-V semiconductors have been measured by several researchers. Not surprisingly, the decay time and the temperature quenching of the Er^{3+} emissions depend on both the host semiconductor and the method of doping used as indicated by the results obtained by Klein and Pomrenke [1988]. These differences are most probably due to the presence of different Er related luminescent centers, as was already mentioned. Another example is provided by comparing the temperature dependence of Er emissions from MOCVD and doped samples by diffusion. The energy and linewidth of Er emissions from diffusion doped samples are independent of sample temperature (Zhao et al. [1988, 1989]), whereas MOCVD samples show a shift of the emission wavelength of approximately 1×10^{-3} nm/deg, and a broadening of the emissions with increasing temperature (Takahei et al. [1989]). In addition, the temperature quenching seems to be correlated with the bandgap of the host semiconductor (Favennec et al. [1989]). As the bandgap increases, the temperature quenching of the 4f emissions is much less effective. Similar results were obtained from the study of the Er^{3+} emissions from $In_xGa_{1-x}P$ as a function of x (Neuhalfen and Wessels (1991b)). This behavior is the opposite of that found for $InAs_xP_{1-x}$:Yb (Neuhalfen and Wessels [1991]).

III. Experiment

Experimental techniques used in present studies of ion implanted and MBE-grown GaAs:Er and AlGaAs:Er involved photoluminescence (PL), selective excitation photoluminescence (SEL), and lifetime measurements. For our purposes, the term PL will be used to denote the observation of the emission spectrum upon laser excitation, while SEL experiments involve scanning the excitation energy while monitoring a particular emission. Specifics of each experiment will be given in the respective section in this chapter. Our optical observations were correlated with electrical measurements (Hall measurements and deep level transient spectroscopy (DLTS)) done by David Elsaesser as part of his dissertation research. In addition, Er incorporation was monitored for a limited number of samples by secondary ion mass spectroscopy (SIMS) and Rutherford backscattering (RBS). This chapter will present a description of the experimental setup and of samples studied. A brief description of the substrates used for Er ion implantation will be presented in section 3.5 and information on particular MBE samples studied will be given in chapter 4.

Figure 4 illustrates the major components of the experimental setup that was used to do PL and SEL. Several configurations are possible. For PL experiments, the argon ion laser was used as the excitation source. The path of the

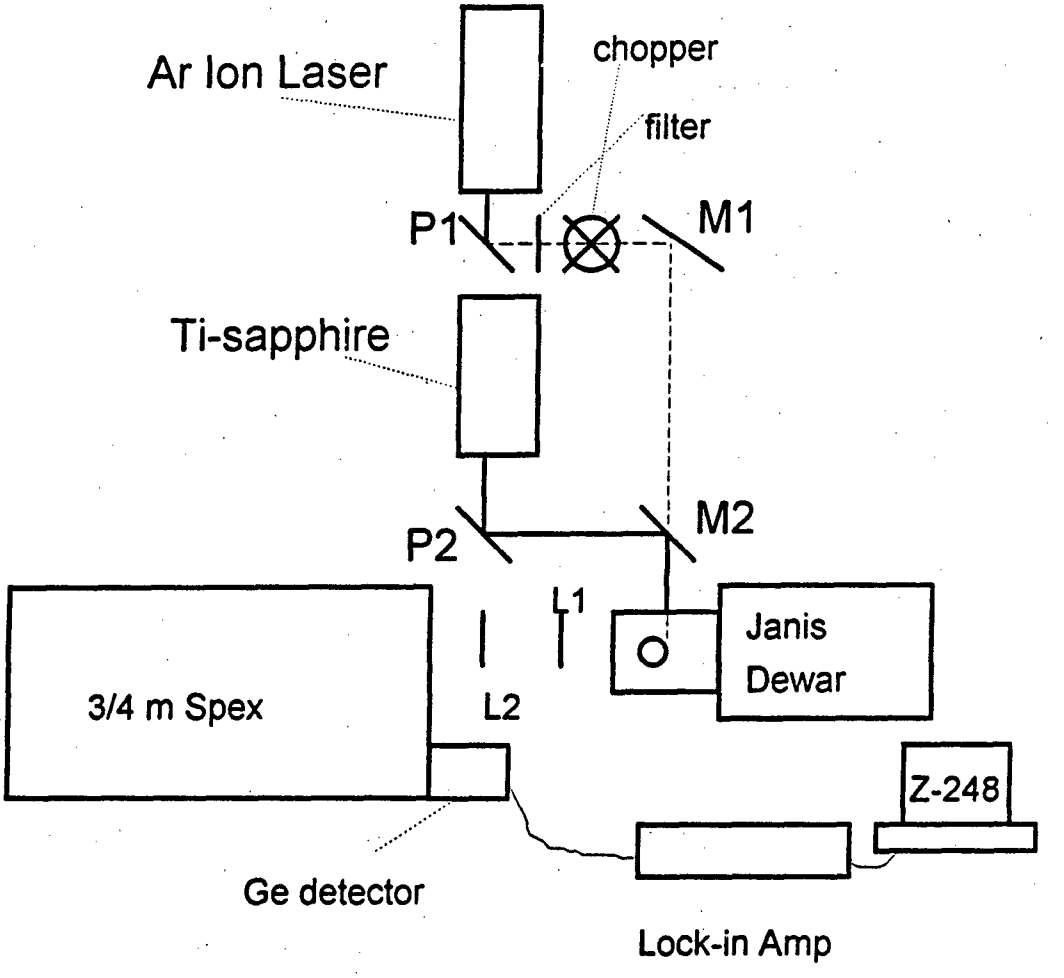

Figure 4 Experimental set-up used for photo-luminescence and selective excitation luminescence experiments

beam is indicated by the dashed line. A periscope, p1, was used to bring the beam to the appropriate height. After p1, a narrow band filter at 488 nm was used to eliminate unwanted plasma lines. A chopper, c1, provided the reference signal for the lock-in amplifier. After being chopped, the beam was deflected by mirror M1 to the sample chamber. The excitation beam power was measured after M1, just before the sample chamber. This will take into account all the losses after passing each optical component, except for transmission losses at the sample chamber's quartz windows. For SEL experiments and for below-bandgap laser excitation, a Ti-sapphire laser pumped by the argon ion laser was used as the excitation source. The path of the excitation beam, when using the Ti-sapphire laser, is illustrated by the solid line in figure 4. The chopper, C2, located in front of the Ti-sapphire laser provided the reference signal for the lock-in amplifier. After being chopped, the beam was deflected to mirror M2 by the use of a periscope (P2), which directed the beam to the sample chamber. The excitation power was measured after M2 before each experiment. Two lenses, L1 and L2, were used to collect the luminescence beam into the spectrometer. Further details about each specific experiment will be given in later sections.

3.1 Photoluminescence

As mentioned, a filtered argon ion laser was used as the excitation source. This laser has a beam diameter (at the $1/e^2$ point) of 1.25 mm and divergence of 0.69 mrad. The excitation power varied for each particular experiment. For most experiments, it was between 10 and 100 mW, which translates into an irradiance value ranging from .81 to 8.1 W/cm^2. These calculations do not take into account approximately 10 % losses after passing through the quartz windows of the sample chamber.

A Janis Research model 10DT Super Varitemp cryostat was used as the sample chamber. This dewar has a liquid nitrogen reservoir which surrounds an inner liquid helium reservoir. Liquid helium flowed into the sample chamber via a capillary tube, while the sample chamber was pumped with a mechanical pump. This arrangement allowed control of the sample temperature from 2 to 300 K. Prior to cooling it down, the dewar was evacuated using an Alcatel turbomolecular pump. The sample was mounted on a copper sample holder with the use of standard rubber cement. Since the cryostat works on the principle of cooling by flowing helium vapor, the quality of thermal conductivity between the sample and the sample holder was not critical. The sample holder was attached to a copper cylinder in which the temperature sensor and heating cable were located. A second temperature sensor was located in the vaporizer assembly. The sensors were silicon diodes from Lake

Shore Cryogenics, one calibrated and one matched. Temperature display and control were performed by a Lake Shore model 805 temperature controller. The temperature controller was set so that it used the sensor in contact with the sample holder as the controlling sensor.

The luminescence from the sample was collected by two lenses, L1 and L2 shown in figure 4. A long pass filter in front of the spectrometer's entrance slit was used to eliminate second order effects from the excitation beam and from near edge emissions. A 1.0 μm filter was used when looking in the range of 1.0 to 1.7 μm, while a 0.78 μm filter was used when looking at signals below 1 μm. The luminescence signal was dispersed with a Spex 3/4-m Czerny-Turner spectrometer using a 1.25 μm blazed grating. Slitwidths were varied for each sample, mainly due to the weak nature of the Er emissions from most of the samples investigated. For maximum throughput, it is recommended to use an exit slit width at least twice as wide as the entrance slit. However, there is a trade off between resolution and throughput. Different slit widths were used depending on whether maximum throughput was required for observing a very weak signal, or whether within the limits of the signal's strength, the best resolution possible was required.

A North Coast model 805P germanium slow detector was used in all the experiments except lifetime measurements. The detector's signal was sent to a Scientech lock-in amplifier.

The reference signal was provided by chopping the excitation beam as shown in figure 4. There are two main reasons for chopping the excitation beam instead of the sample's luminescence. First, this configuration was found to give stronger signals, and since most of the Er emissions were weak, this was an important consideration. Second, this configuration also reduced the noise level. Since a small vibration is introduced due to pumping of the sample chamber, chopping the beam provided a more stable reference signal. The output signal from the lock-in amplifier was sent to a PC via an A/D converter for storage and later analysis.

3.2 Selective Excitation Luminescence (SEL)

As mentioned, a Ti-sapphire laser was used as the excitation source for SEL experiments. The beam path in SEL experiments was explained in section 3.1. A Spectra Physics model 3900 Ti-sapphire laser pumped by a 20 watt argon ion laser was used. This laser has a linewidth of less than 40 GHz, and a beam diameter of .95 mm at $1/e^2$ points (at 790 nm) with a beam divergence of 1 mrad. The laser has a tunable range from 660 to 1100 nm, which requires the use of four different optics sets that have tunable ranges of 660-750 nm, 700-850 nm, 850-1000 nm, and 950 to 1100 nm, respectively. A birefringent filter provided wavelength selection. Very precise positioning of the birefringent filter was obtained with the use of a Burleigh inchworm and a Burleigh 6000

inchworm controller. The inchworm could be positioned from 0 to 21000 μm in step of .5 μm. Each time when the Ti-sapphire optics set was changed, a new calibration chart was obtained to determine the laser wavelength at selected inchworm positions. Typical calibration charts are shown in figure 5. Between these selected inchworm positions, a linear interpolation was used to determine the wavelength.

Selective excitation luminescence experiments were done by setting the spectrometer at the wavelength of the emission to be monitored and scanning the excitation laser wavelength. In order to do this, a computer interface card (Burleigh model 6200) was used to connect the inchworm controller to the IEEE port of a Z-248 computer. Also, the output from the lock-in amplifier was sent to a Keithley 238 current source measure unit connected to the same computer. This set-up allowed simultaneous control of the excitation laser wavelength and data taking. A computer program was written in Quick Basic 4.5 that performed both functions: control of the inchworm position and data taking and display. The program let the user select the inchworm travel distance and step size. After moving the inchworm by the step size specified it read a specified number of data points from the lock-in amplifier and averaged them. It continues to do this until the inchworm has moved the desired travel distance. The program then creates a file containing both the inchworm position and the signal intensity. The inchworm position can then be converted into

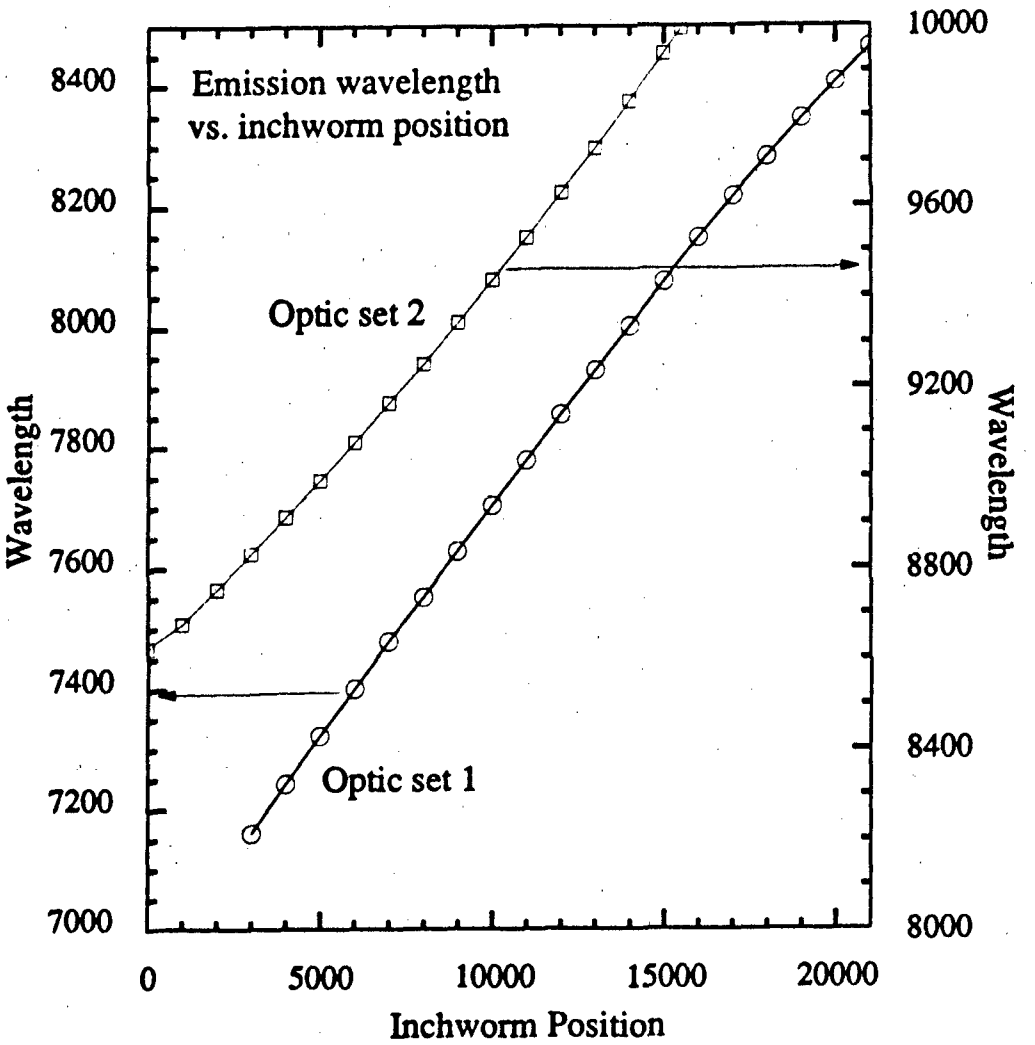

Figure 5 Ti-sapphire laser emission wavelength as a function of inchworm position

the corresponding laser excitation energy with the use of a calibration file, thus giving the excitation spectrum of the monitored emission in the spectral range covered. As mentioned, the maximum step distance is 21000 μm and minimum step size is .5 μm, therefore the excitation energy will be known with very good precision. In our case, most measurements were done with a step size of either 10 or 20 μm.

3.3 Lifetime Measurements

Figure 6 shows a simplified diagram of the experimental set-up used for lifetime measurements. Similar to the PL set-up, it includes cryogenics, an excitation source and detection subsystems consisting of the spectrometer, detector, and data acquisition.

The cryogenic subsystem consisted of an Air Products LT-3-110A Helitran system pumped with a fore-pump-backed and water-cooled Leybold-Harreus NT 220 turbo molecular pump. Sample temperature control was achieved using an Air Products Digital Temperature Indicator/Controller that employed an iron doped chrome versus gold thermocouple. The controller was calibrated using liquid nitrogen and freezing water as reference points. The sample was mounted on the cold finger using crycon grease. This was done to obtain the best thermal contact possible.

The excitation laser source was the 337.1 nm line of a

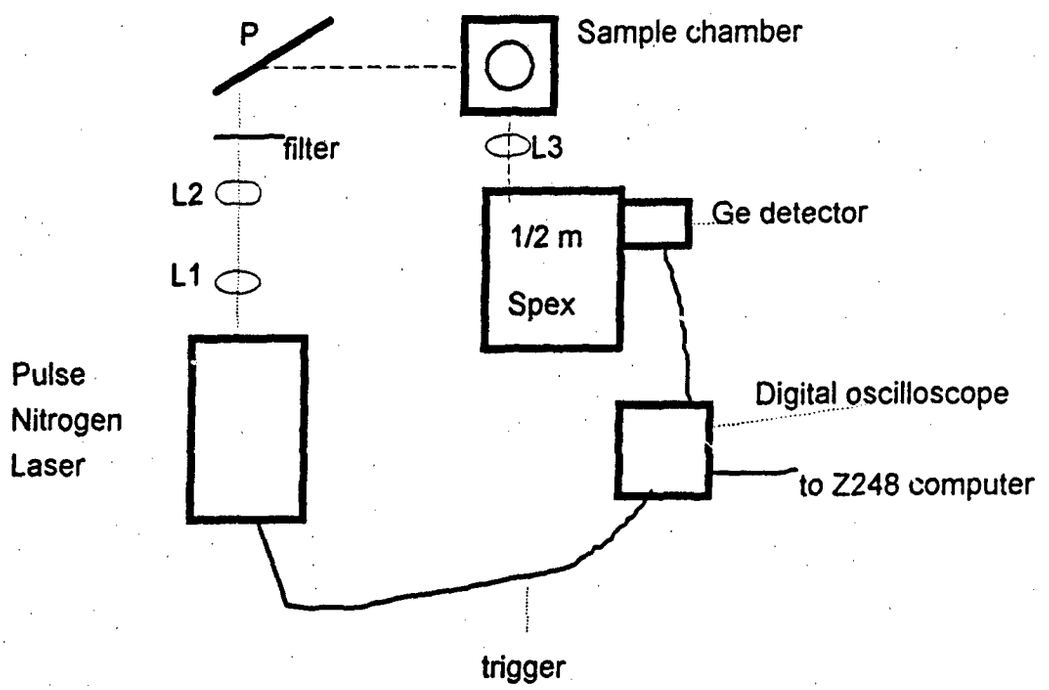

Figure 6 Experimental set-up used for lifetime measurements

Laser Photonics UV-24 pulse nitrogen laser. The pulse width was 5 to 7 nsec. The maximum repetition rate of the laser is 50 Hz. As can be seen from figure 6, a series of lenses and other optical components were used to focus the beam onto the sample. Lens L1 was used to control the spot size together with a second cylindrical lens, L2. After the second lens, the beam passes through a UV narrow band pass filter to eliminate unwanted plasma lines. A periscope is then used to bring the beam to the appropriate height, while a third lens, L3, helps focus the beam onto the sample. The luminescence was collected with the help of two lenses into the spectrometer. A long pass 850 nm filter was used in front of the entrance slit.

A 1/2-m Spex 500 spectrometer was used with a 1.6 μm blazed grating. Slitwidths varied with the particular sample under study. Although high resolution was not critical in this experiment, if the signal was strong enough the slits were closed as much as possible to be able to distinguish between different Er^{3+} emissions.

A North Coast model 805L germanium fast detector was used. The time constant of this detector is switch selectable between 10 and 100 μsec. The fast response setting was used in these investigations. The signal from the detector was sent to a LeCroy 9400A digital oscilloscope with the trigger signal from the oscilloscope provided by the nitrogen laser. This oscilloscope can average any number of waveforms as

selected by the user, up to a maximum of 50,000, a feature which reduces the noise considerably. However, since a 20 Hz repetition rate was used, such averaging could be time consuming. In practice, the number of decays averaged depended on the signal strength. Decays of the stronger Er emissions were averaged 100 to 200 times, while decays from the weaker emissions were averaged up to 5000 times. The averaged decay was then sent to a PC for storage and later analysis.

The system response time was determined by measuring the decay of one of the laser plasma lines. The measured decay is shown in figure 7 along with the calculated fit. Further discussion on the effect of the system response on the measured decays and details on the data analysis will be given in chapter 4.

3.4 Sample Information

Most of the samples studied were doped with Er using ion implantation. Erbium was implanted at room temperature using an implantation energy of 1 MeV. Erbium doses of 5×10^{12}, 1×10^{13}, and $5 \times 10^{13}/cm^2$ were used. The substrates included undoped GaAs and $Al_xGa_{1-x}As$ (x = 0.1, 0.2, 0.3, and 0.4) samples, and MOCVD-grown GaAs and $Al_{0.29}Ga_{0.71}As$ layers doped with either Si or Zn. Table I lists the various substrates used for ion implantation. In addition to the MOCVD-grown layers, some p-type substrates were prepared by implanting Mg into SI-

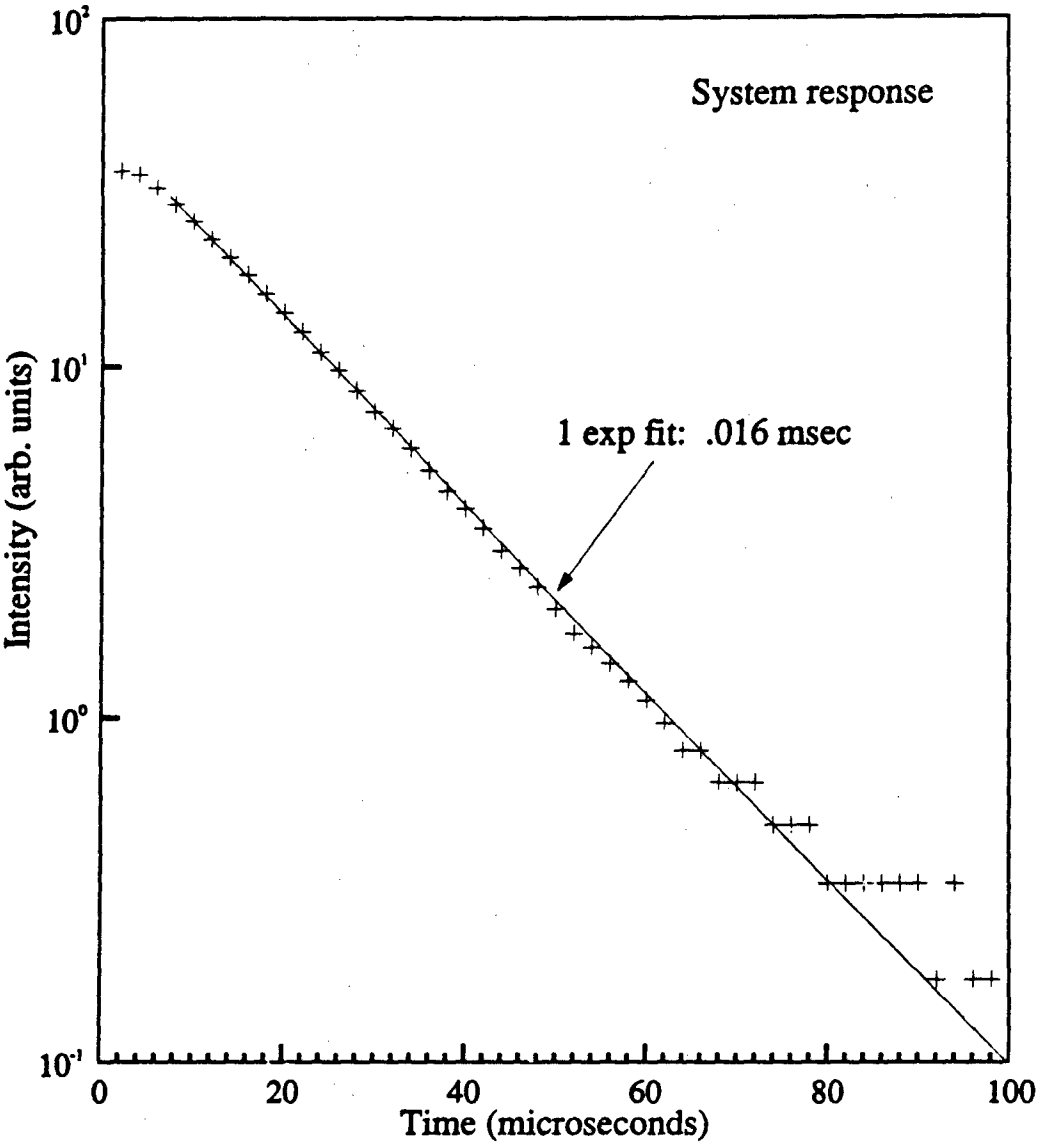

Figure 7 Time decay of a nitrogen laser plasma line illustrating the system response of the experimental set-up used for lifetime measurements

Table I

Samples used for Er ion Implantation

Sample	Growth	Doping Method	Carrier Concentration (cm^{-3})	Type
GaAs	LEC	undoped	-----	SI
GaAs	MOCVD	Zn	6.8×10^{16}	p
GaAs	MOCVD	Si	4.9×10^{15}	n
GaAs	MOCVD	Si	2.8×10^{17}	n
GaAs	MOCVD	Si	1×10^{18}	n
$Al_{0.10}Ga_{0.90}As$	MOCVD	undoped	1.6×10^{16}	n
$Al_{0.20}Ga_{0.80}As$	MOCVD	undoped	2.9×10^{16}	n
$Al_{0.30}Ga_{0.70}As$	MOCVD	undoped	7.3×10^{16}	n
$Al_{0.40}Ga_{0.60}As$	MOCVD	undoped	------	SI
$Al_{0.29}Ga_{0.71}As$	MOCVD	undoped	------	SI
$Al_{0.29}Ga_{0.71}As$	MOCVD	Zn	------	p
$Al_{0.29}Ga_{0.71}As$	MOCVD	Si	------	SI

GaAs. An oxygen co-doping study was also made. Information on the samples used for this study will be given in section 4.5.2. In addition to ion implanted samples, various MBE-grown GaAs:Er and $Al_xGa_{1-x}As$:Er layers were studied. The information on the MBE samples will be given in section 4.4, when discussing the results obtained for each particular case.

IV. Results and Discussion

4.1 Photoluminescence of Er Implanted GaAs and $Al_xGa_{1-x}As$

The luminescence spectrum of Er doped III-V semiconductors is characterized by a series of sharp peaks near 1.54 μm. These sharp emissions are due to the intra-4f transitions between the crystal field split states of $^4I_{13/2}$ and $^4I_{15/2}$ of Er^{3+}. Although the crystal field splitting of these levels is relatively small, the emission spectrum is very sensitive to variations in the crystalline environment. As a result, Er^{3+} emissions originating from different Er complexes will occur at slightly different energies. Also, the number of emission lines observed in the spectra will vary, depending on the symmetry of the Er related luminescent center. The emission spectrum of Er doped III-V semiconductors is clearly dependent upon the doping method and sample treatment such as annealing. This indicates a tendency of the Er ions to form multiple types of complexes in these hosts. Indeed, we have observed the presence of multiple Er related luminescent centers in most of our samples as indicated by the sample dependence of the PL emission spectrum. That is, the PL spectrum shows different emissions near 1.54 μm, and the relative intensities among these emissions vary differently, depending upon the doping method (MBE vs ion implantation), annealing conditions, and Er concentration.

4.1.1 GaAs:Er

Conventional furnace annealing (CFA) of Er implanted samples resulted in very weak emissions near 1.54 μm. The strongest Er^{3+} emissions obtained with CFA were observed for samples annealed at temperatures between 650 and 700 °C. The low temperature PL spectrum from samples annealed using CFA showed different emissions around 1.54 μm, depending on the annealing temperature. Also, the relative intensity among the sharp 1.54 μm emissions varied, depending on sample preparation. This behavior is indicative of the formation of different Er complexes. Emissions from different centers may occur at slightly different wavelengths, thus resulting in the observed variations in the PL spectrum. These results agree with observations made by Klein et al [1991]. These authors observed the presence of at least five different luminescence centers in ion implanted GaAs:Er samples annealed using CFA. Unfortunately, due to the weakness of these emissions, the PL spectra had to be recorded using very wide slit openings (up to 3 mm), thus resulting in low resolution. Because of this, it was almost impossible to distinguish among specific emission peaks from different centers. The weak emission problem was partially resolved in this work by using rapid thermal annealing (RTA). Samples annealed using RTA showed stronger Er^{3+} emissions than those annealed using CFA. Figure 8 shows the low temperature PL spectra from n-type and SI-GaAS samples implanted with an Er dose of $5 \times 10^{13}/cm^2$ at 1 MeV. The

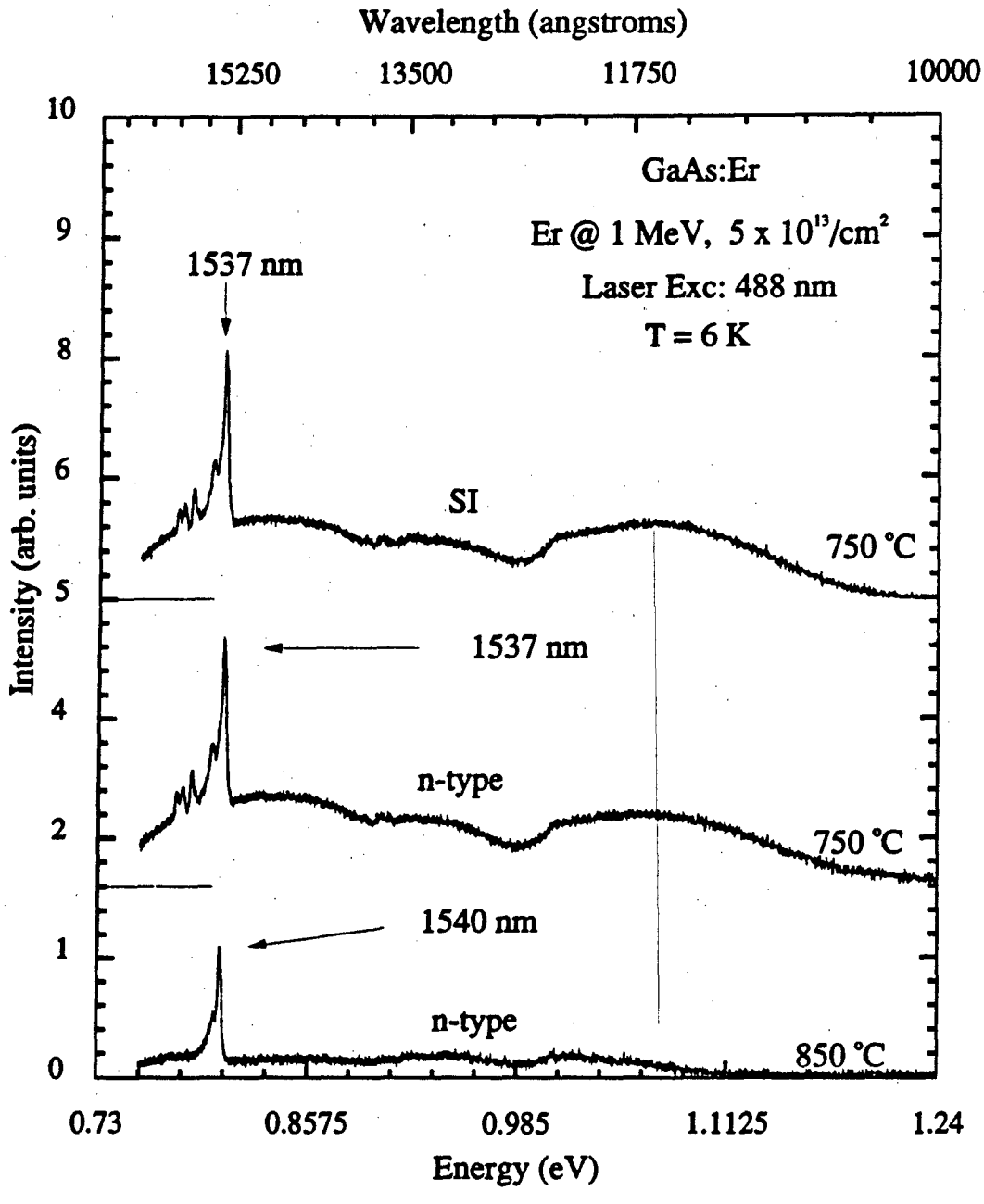

Figure 8 Photoluminescence of n-type and SI-GaAs:Er implanted at 1 MeV with a dose of 5 x $10^{13}/cm^2$ and annealed at different temperatures

SI- and one of the n-type samples were annealed at 750 °C for 15 seconds using RTA, and another n-type sample was annealed at 850 °C for 15 seconds. The horizontal lines beneath the two uppermost spectra show the zero level for each respective spectrum. All three samples show several sharp emissions near 1.54 μm, which are assigned to the intra-4f transitions between the $^4I_{13/2}$ and $^4I_{15/2}$ multiplets of Er^{3+}. The 1.54 emissions seen in this figure are really composed of several sharp peaks, which are not apparent due to the low resolution. This will be evident when we discuss higher resolution spectra. In addition, at least two broadband (bb) emissions can be distinguished from the figure. The spectra shown were not corrected for the system response, and thus this is partially responsible for the strange asymmetrical shape of the bb emissions. The addition of two or more bb emissions of comparable intensity also contributes to the asymmetrical shape observed. These bb emissions have been observed in all our ion implanted samples. The exact nature of these emissions is not completely known yet. One possible explanation is that they are due to implantation damage. This is supported by the decrease in PL intensity of these bb emissions with increasing annealing temperature, as seen from the figure. The bb emission underlying the sharp 1.54 μm emissions is most probably due to the EL2 defect. The EL2 defect in GaAs introduces a structureless bb centered around 0.8 eV with a full width at half maximum of approximately

0.3 eV (Tajima [1987]), similar to the bb emission observed in our spectra. In fact, DLTS studies have also revealed the presence of the EL2 defect in our ion implanted samples (Colón et al [1991]).

Figure 8 also shows very clearly the annealing behavior that is typical of ion implanted GaAs:Er samples. Note that the Er^{3+} emissions from the sample annealed at 850 °C are weaker than those from the two other samples. This observation is not only true for the n-type sample but it is also typical of results obtained for all the samples studied. Although a complete annealing study was not done, we have consistently observed that samples annealed at 750 °C using RTA showed the strongest Er^{3+} emissions. Annealing at higher temperatures (or lower temperatures) resulted in weaker Er^{3+} emissions. Also, note that the strongest emissions from the samples annealed at 750 °C are centered around 1.5[illegible] / μm, while those from the sample annealed at 850 °C are shifted toward 1.54 μm. In addition, some of the minor peaks near 1.54 μm disappeared at higher annealing temperatures. The shifting of the main peak from 1.537 to 1.54 μm is due to the presence of various sharp emissions, some of which are enhanced or quenched at different annealing temperatures. This suggests the presence of multiple luminescence centers in our samples due to the formation of several Er related complexes. Clearly, these complexes are not completely stable and can be easily broken by annealing at temperatures of 850 °C or

higher. Annealing at further higher temperatures may result in quenching of the Er^{3+} emissions. These results can be correlated with Rutherford backscattering (RBS) studies of Er implanted into GaAs (Kozanecki et al [1992]). Their study showed that at low annealing temperatures, most of the Er ions occupy non-substitutional sites in the GaAs lattice. However, raising the annealing temperature, T_A, increases the percentage of substitutional Er ions, and at $T_A \geq 1000$ °C, almost all Er ions were on substitutional sites, but no Er^{3+} luminescence was observed at these high annealing temperatures. Thus, since substitutional Er in GaAs seems to be optically inactive, the intra-4f luminescence may originate either from Er at interstitial sites or Er complexes involving other impurities or defects.

The emission spectra of Er implanted GaAs samples also showed a dependence on the Er dose. Figure 9 shows the low temperature photoluminescence spectra from GaAs:Er samples implanted at 1 MeV with different Er doses. In all cases shown, an undoped SI-GaAs substrate was used for Er implantation. All three spectra were recorded under identical experimental conditions. The Er doses used were 5×10^{12}, 1×10^{13}, and $5 \times 10^{13}/cm^2$. The excitation source was the 488 nm line of the Ar ion laser. As the figure shows, the emission spectra from samples implanted at the two lowest Er doses are essentially the same except for the PL intensity. In both cases, the strongest emission is centered around

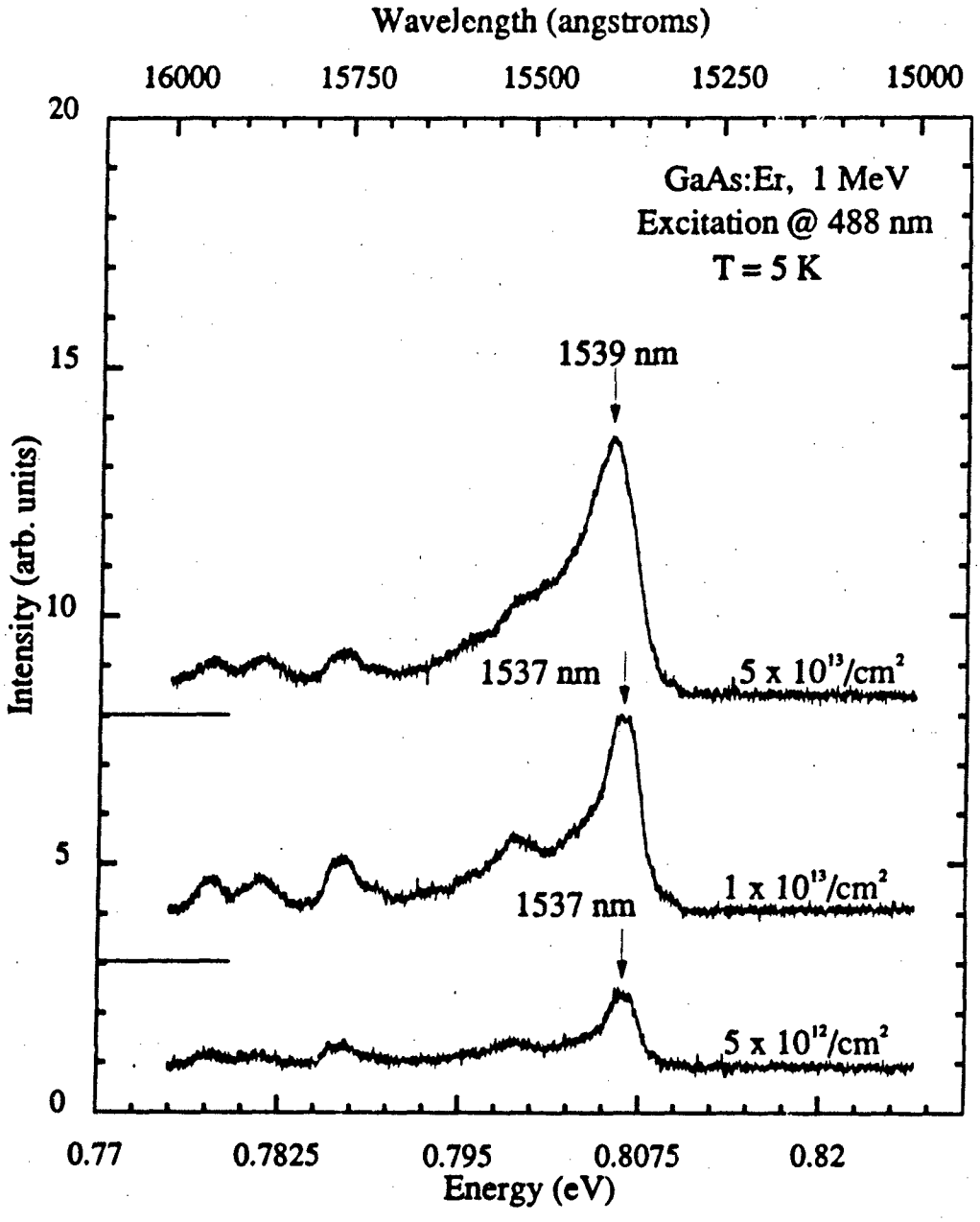

Figure 9 Photoluminescence of SI-GaAs:Er implanted at 1 MeV with different doses and annealed at 750 °C for 15 sec

1.537 μm. Also, both show a series of weaker peaks at the same energy position. An important observation is that the intensity of the Er^{3+} emissions increased by approximately a factor of three when the Er concentration was increased twofold. However, another fivefold increase in the Er dose resulted in only a 30% more increase in the PL intensity of these emissions. This suggests that a big percentage of the Er ions present in the higher dose sample are optically inactive. The most interesting effect shown in figure 9 is the shifting of the strongest emission peak from 1.537 μm for the two lower doses to 1.539 μm for the highest dose which also yields a broader linewidth. All other minor peaks are seen at the same wavelength positions. These results may indicate that at low concentrations, the Er ions will be preferentially incorporated into the center responsible for the emission near 1.537 μm. As the Er concentration increases, this center saturates and then much of the Er will be incorporated into other centers. Some of these centers are optically inactive and others may have slightly different emission wavelengths, thus accounting for the broadening of the signal and the shifting of the peak position. Similar to the center responsible for the 1.537 μm emission, the other optically active centers, for example the center responsible for the emissions near 1.58 μm, also saturate at somewhat low concentrations. This is suggested by the very small increase in the 1.58 μm peak intensity when the Er dose was increased

from 1 x $10^{13}/cm^2$ to 5 x $10^{13}/cm^2$. These results agree with recent TEM studies of MBE GaAs:Er (Poole et al [1992]), which shows a solubility limit of Er in GaAs of only 7 x $10^{17}/cm^3$. Above this concentration Er form microprecipitates, believed to be ErAs, which are optically inactive. Calculation of the Er implantation profiles shows a peak concentration of approximately 5 x $10^{18}/cm^3$ for a dose of 5 x $10^{13}/cm^2$, i.e., well above the solubility limit. Therefore, at this high dose we can expect at least some of the Er ions to be incorporated as microprecipitates.

Some authors have suggested that free carriers are needed to excite the Er^{3+} emissions. In this scheme, the Er^{3+} PL intensity will be stronger in n-type material (Pomrenke [1989]). In order to test this hypothesis, we studied the low temperature PL as a function of n- and p-type doping concentration. Erbium was implanted into various n- and p-type substrates at a dose of 5 x $10^{13}/cm^2$ with an ion energy of 1 MeV. The n-type substrates were Si doped, three micron thick, MOCVD layers with room temperature carrier concentrations of 4.9 x 10^{15}, 3.3 x 10^{17}, and 1 x $10^{18}/cm^3$, respectively. Following Er implantation, the samples were annealed at 750 °C for 15 seconds using RTA. Figure 10 shows the low temperature PL from these samples. The horizontal lines show the offset for the top two spectra. The same emissions are observed in the three samples. Increasing the Si concentration from 4.9 x 10^{15} to 3.3 x $10^{17}/cm^3$ resulted in

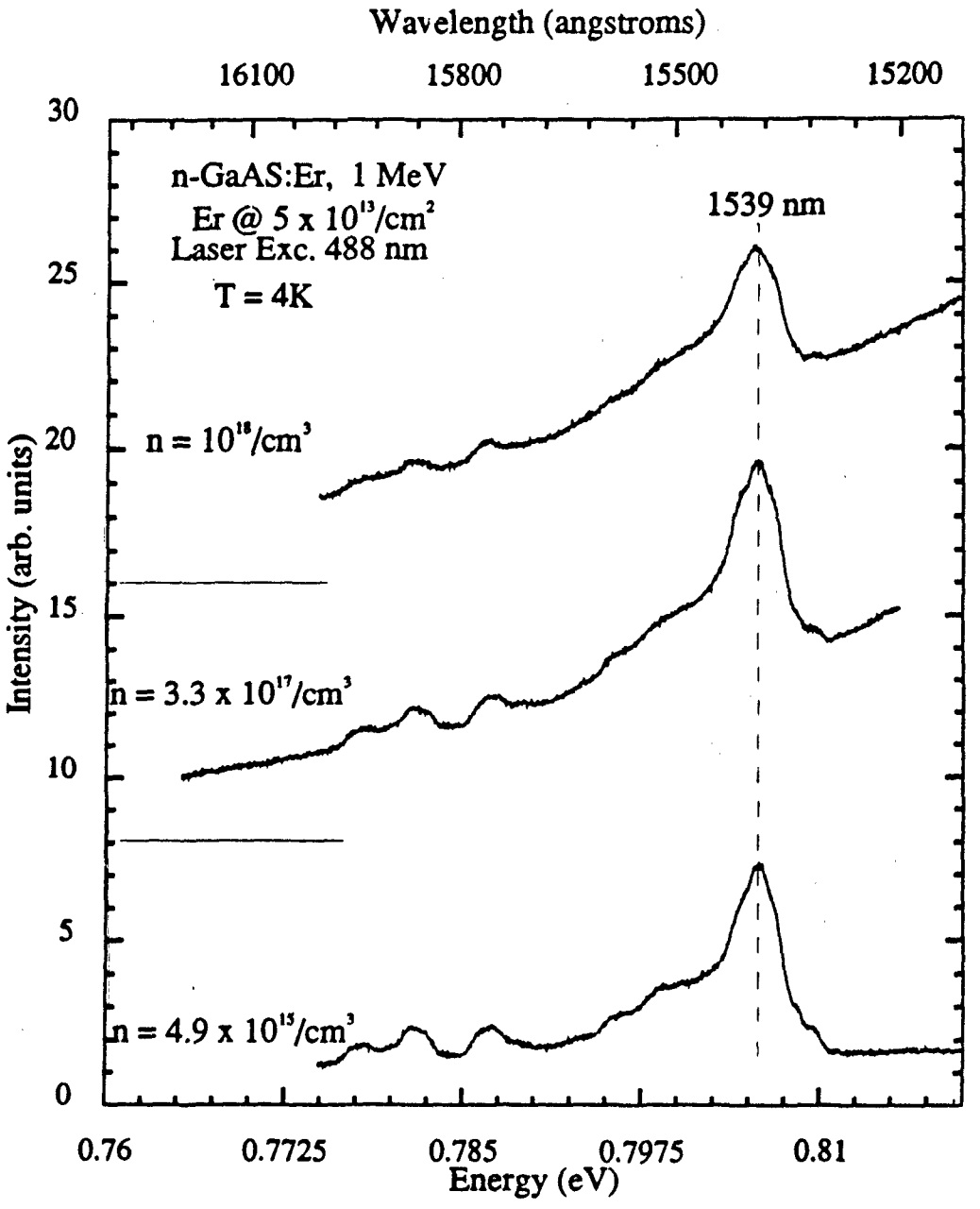

Figure 10 Photoluminescence of GaAs:(Er+Si) implanted with Er at an energy of 1 MeV with a dose of 5 x $10^{13}/cm^2$ into GaAs having various Si doping levels and annealed at 750 °C

somewhat stronger Er^{3+} emissions. The intensity of the underlying bb emission also increased. However, at the highest Si concentration the Er^{3+} PL intensity decreased considerably, although the bb intensity remained about the same as that of the sample with a carrier concentration of $3.3 \times 10^{17}/cm^3$. The p-type samples showed a similar PL behavior as shown in figure 11. In this case, the p-type substrates were prepared by Mg implantation into SI GaAs wafers. Three different implantation energies of 50, 150, and 350 keV with respective doses of 8.3×10^{10}, 2.1×10^{11}, and $6.25 \times 10^{11}/cm^2$ were used to obtain a constant doping profile of $10^{16}/cm^3$ in a one micron layer, and in order to obtain Mg concentrations of 5×10^{16}, 10^{17}, and $5 \times 10^{17}/cm^3$ the same ion energies were used but the Mg doses were increased as needed. After Mg implantation, Er was implanted at a dose of $5 \times 10^{13}/cm^2$ with an ion energy of 1 MeV. Following Er implantation, the samples were annealed at 750°C for 15 seconds using RTA. Hall measurements and CV profiles on control samples, i.e. without Er, confirmed the Mg activation. As the Mg concentration increased from 10^{16} to $5 \times 10^{16}/cm^3$, the PL intensity of the Er^{3+} emissions and the underlying bb emission showed a slight increase. However, for [Mg] = $10^{17}/cm^3$, the intensity of the Er^{3+} emissions decreased by a small factor. For [Mg] = $10^{18}/cm^3$, the background intensity increased considerably, while the Er^{3+} emissions decreased. This dependence on the carrier concentration is closely related to the 4f excitation

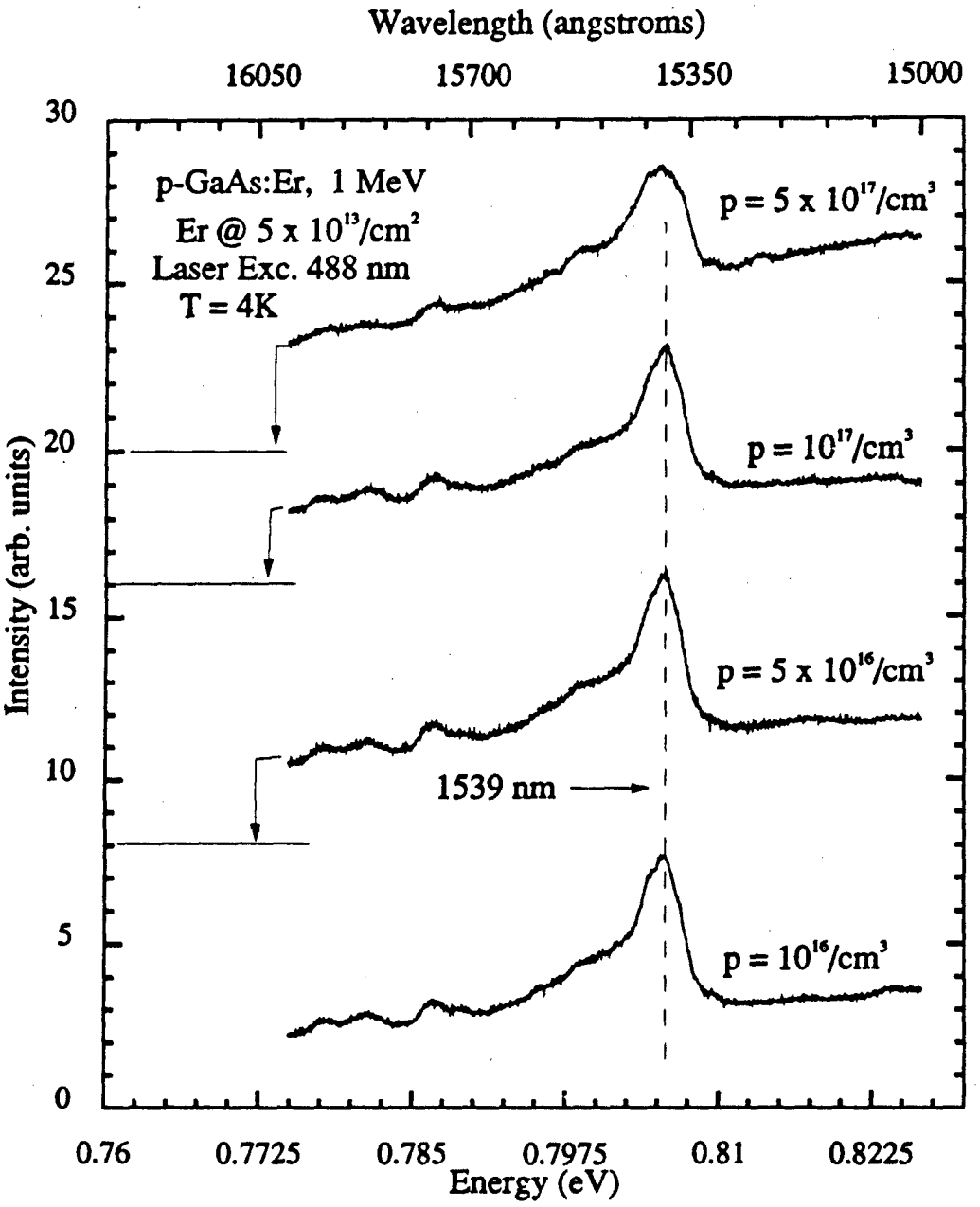

Figure 11 Photoluminescence of GaAs:(Er+Mg) implanted with an Er dose of 5 x $10^{13}/cm^2$ at 1 MeV into GaAs having various Mg doping levels and annealed at 750 °C

mechanism, and a model of the excitation mechanism that can explain this behavior will be proposed in section 4.3.2.

4.1.2 $Al_xGa_{1-x}As$:Er

As in GaAs, Er doping of AlGaAs results in multiple sharp emissions near 1.54 μm. The relative intensity among different peaks show the same dependence on annealing conditions as on the GaAs case. However, it is remarkable that the same emissions can be seen independently of the aluminum mole fraction. This is clearly demonstrated in figure 12. The figure shows the low temperature PL from ion implanted undoped $Al_xGa_{1-x}As$:Er samples with x = 0.1, 0.3, and 0.4. Erbium was implanted at a dose of 5 x $10^{13}/cm^2$ with an ion energy of 1 MeV, and all samples shown here were annealed at 850 °C for 15 seconds using RTA. The 488 nm line of the Ar ion laser was used as the excitation source, and all spectra shown were taken under identical experimental conditions. The resolution used was not good enough to resolve the various Er^{3+} sharp emissions. Therefore, the peaks that can be distinguished from the figure are actually composed of several sharper emissions that have been convoluted. As in ion implanted GaAs:Er, the x = 0.3 and 0.4 samples show a bb emission underlying the sharp Er^{3+} emissions, although the intensity of the underlying bb emission is very weak in the x = 0.1 case. In the present case, it is hard to notice the

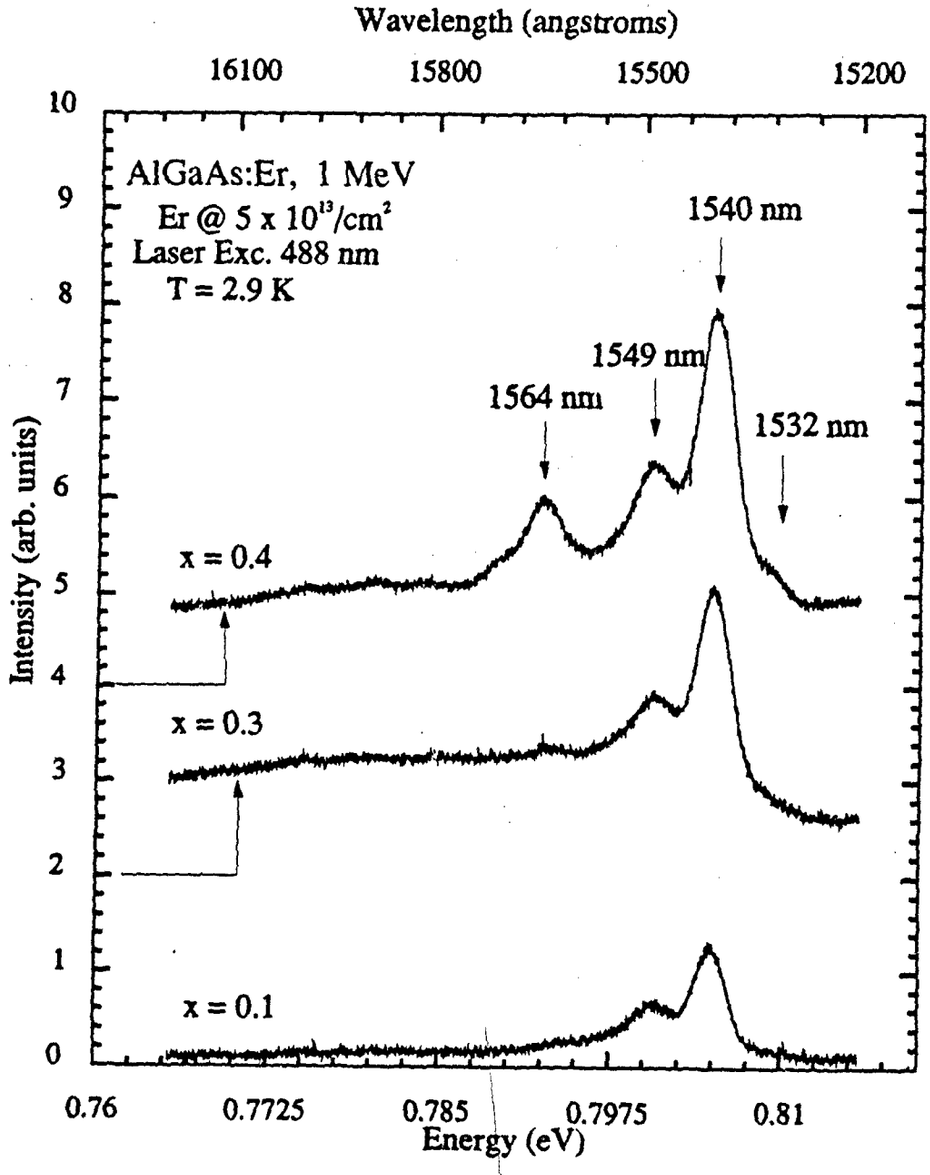

Figure 12 Photoluminescence of undoped $Al_xGa_{1-x}As$:Er implanted at 1 MeV with a dose of 5 x10^{13}/cm² and annealed at 850 °C for 15 sec

bb emission because of the limited spectral range shown in the figure. The local crystalline environment surrounding the Er ions can be expected to vary with the value of x. Also, the emission spectra would normally be expected to change slightly, because of the difference in bandgap. However, the main Er^{3+} emissions, centered around 1.540 and 1.549 μm, are seen in all samples at the same position. This is a good example of the shielding of the 4f-shell from the crystal field, and is indicative of the atomic-like character of these sharp emissions. Also, it is clear from the figure that the strength of the Er^{3+} emissions increases with aluminum mole fraction. Two factors might be contributing to this phenomenon. First, aluminum might help the incorporation of Er ions into the lattice by forming Al-Er complexes that are optically active. A second factor is related to the observation by Favennec et al. [1989] who found a correlation between the bandgap of the semiconducting host material and the temperature quenching of the Er^{3+} emissions. As the bandgap of the host increased, the effect of temperature quenching decreased. In wide band hosts such as ZnS, the strength of the Er^{3+} emissions did not change from 1 to 300 K. Such results were recently verified in GaInPAs:Er (Neuhalfen and Wessels, 1992). Therefore, it seems that in order to have strong Er^{3+} emissions, a wide band semiconducting host must be used even though at present, this effect is not well understood.

The Er^{3+} emissions from $Al_{0.29}Ga_{0.71}As$:Er samples implanted with a dose of 5 x $10^{13}/cm^2$ at an energy of 1 MeV and annealed at 850 °C for 15 sec were also studied as a function of substrate conductivity. The low temperature PL spectra from SI-, n-, and p-type substrates are shown in figure 13. Three micron thick MOCVD layers doped with Si or Zn were used as the n- or p-type substrate, respectively, for Er ion implantation. The carrier concentrations were 3 x 10^{16} and 3.1 x $10^{16}/cm^3$ for the n-type and p-type substrate, respectively. All spectra shown in the figure were taken under the same experimental conditions. Clearly, the strongest emissions are observed from the p-type sample. This enhancement of the Er^{3+} emissions in p-type material is observed not only in $Al_xGa_{1-x}As$ but also in GaAs. Although, as in the case of GaAs, the PL intensity may depend on the Si or Zn doping level in $Al_xGa_{1-x}As$, the results shown in figure 13 are for both samples having nearly the same doping level. Since basically the same emissions are observed in all three samples, this effect is not due to the formation of complexes between Zn and Er ions. Instead, it must be related to the particulars of the 4f-shell excitation mechanism. This is also supported by the fact that for the p-type samples the free carrier concentration did not change after Er implantation and subsequent annealing. On the other hand, for the n-type samples, the free carrier concentration decreased after Er ion implantation and subsequent annealing, and this may be due to the so called

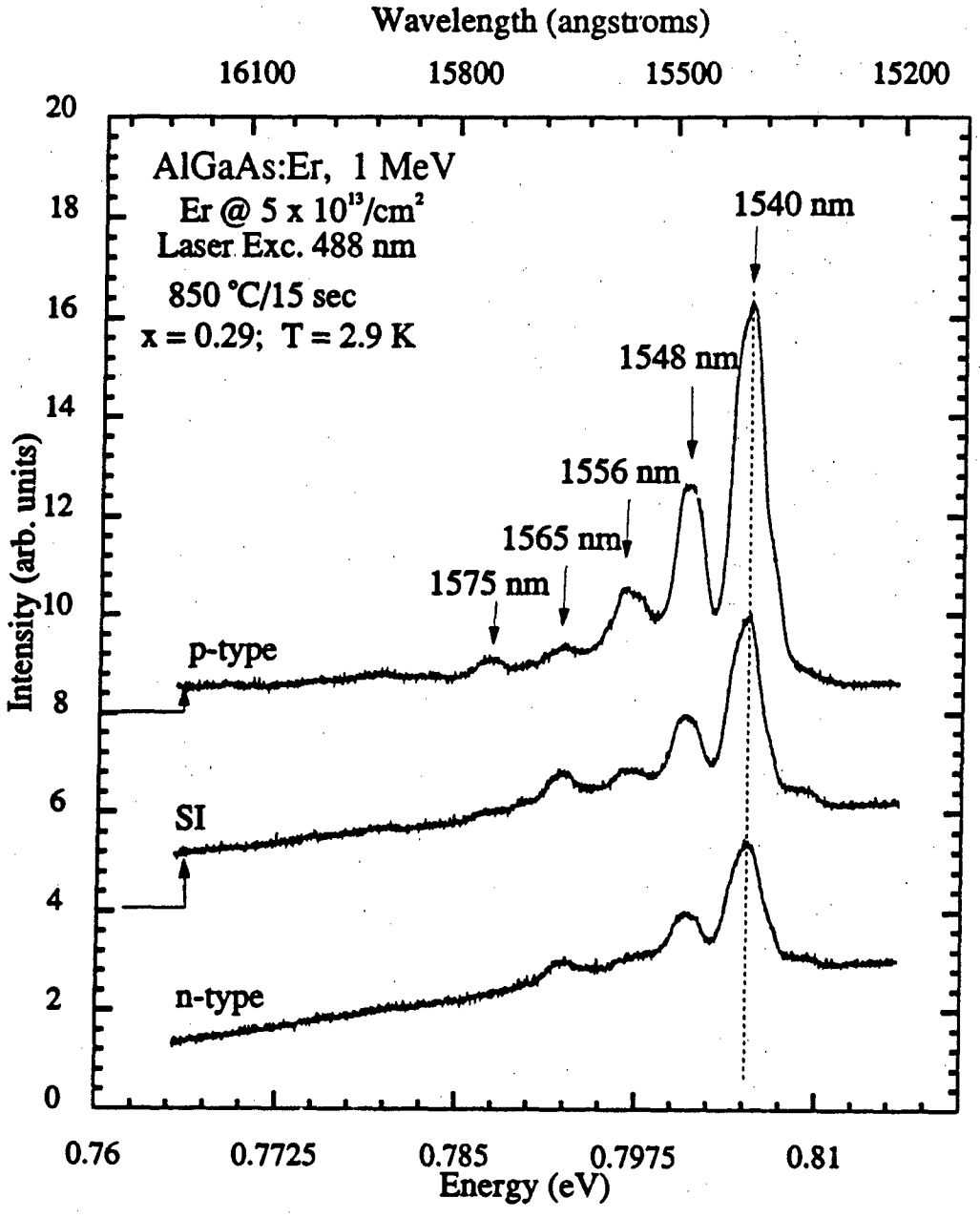

Figure 13 Photoluminescence of $Al_{0.29}Ga_{0.71}As$:Er implanted at an energy of 1 MeV with a dose of 5 x $10^{13}/cm^2$ and annealed at 850 °C for 15 sec from SI-, n-, and p-type substrates

donor gettering effect observed after doping with RE elements (Masterov and Zhakarenkov [1990]). This effect is due to the formation of complexes involving Si and Er ions. Since the PL intensity of the Er^{3+} emissions does not increase in n-type material compared with the PL intensity of the SI-$Al_xGa_{1-x}As$, actually a small decrease is observed in figure 13, and no other differences are observed in the spectra, it seems that these Er-Si complexes are optically inactive. This is also seen in our MBE samples, and it will be discussed in section 4.4.2.

As in the case of GaAs, the strongest Er^{3+} emissions were observed after annealing at 750 °C for 15 sec using RTA. Also, the relative intensity among different emission peaks changed as the annealing conditions and substrate conductivity changed. This is illustrated by figure 14, which shows the low temperature PL from $Al_{.29}Ga_{0.71}As$:Er implanted at 1 MeV with a dose of 5 x $10^{13}/cm^2$ and annealed at 750 °C for 15 seconds. The three spectra shown were taken under the same experimental conditions. Because these emissions were somewhat stronger, the spectra shown in this figure were taken using smaller slit openings. Therefore, these spectra have much higher resolution than the spectra shown on figures 15 and 16. At least 11 sharp emission peaks can be distinguished from the figure. Besides the difference in resolution, essentially the same emissions are seen as in figure 13, but the relative intensities among these peaks have changed. In particular,

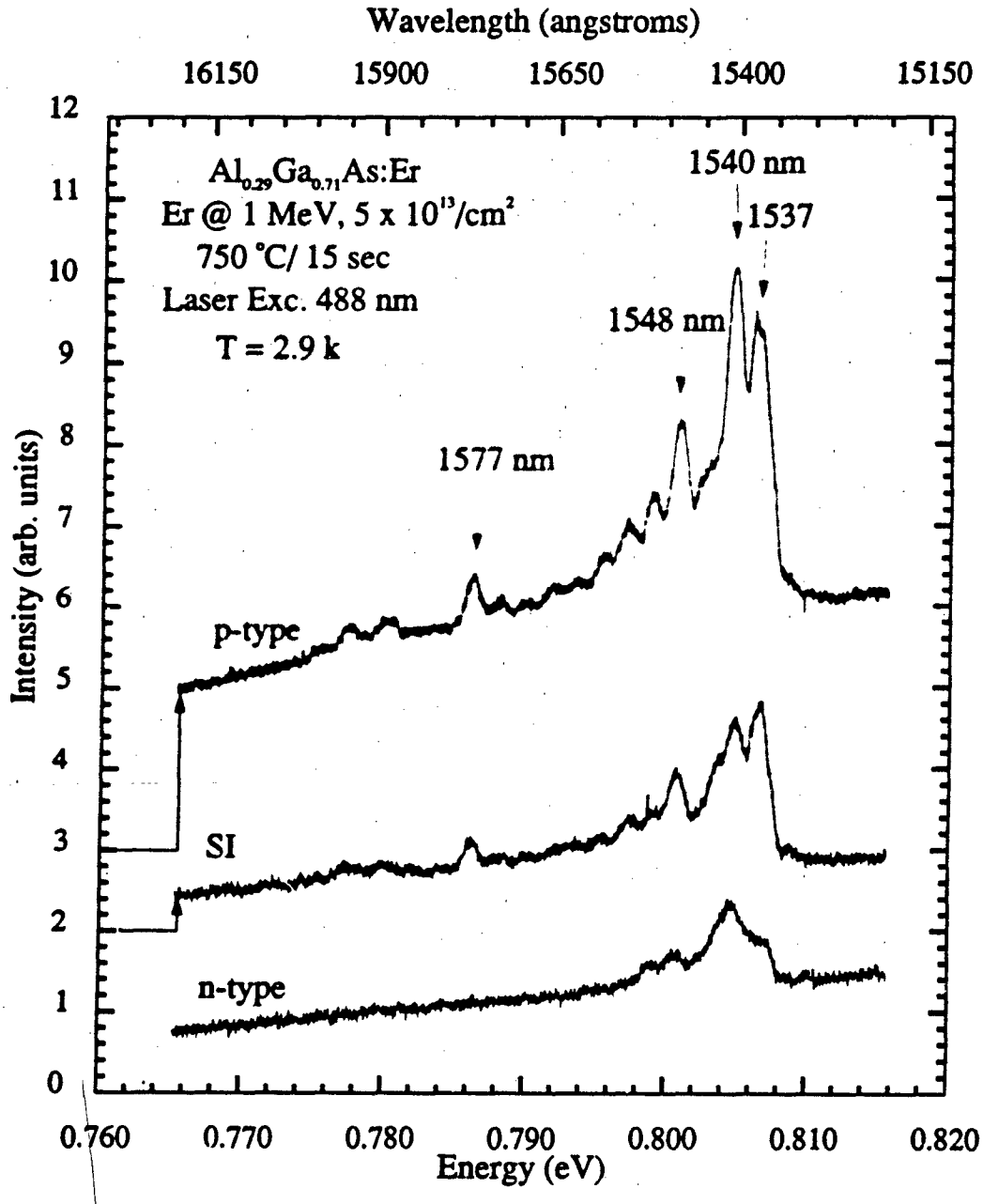

Figure 14 Photoluminescence of $Al_{0.29}Ga_{0.71}As$:Er implanted at an energy of 1 MeV with a dose of 5 x 10^{13}/cm^2 and annealed at 750 °C for 15 sec from SI-, n-, and p-type substrates

the peak at 1.537 μm is obviously much stronger in the present case, and it is the dominant feature in the SI-$Al_{0.29}Ga_{0.71}As$ sample. Changes in the relative intensities among the various Er^{3+} emissions can be realized by noting that the strongest emission shown in figure 13 is centered around 1.54 μm. If the same low resolution had been used in the present case the PL peak would be shifted to somewhere between 1.54 and 1.537 μm, because both emissions have comparable strength. Also, changes in relative intensities among different peaks can be appreciated by comparing the three spectra shown in figure 14. For example, the 1.540 μm peak is the strongest emission from p-type $Al_{0.29}Ga_{0.71}As$, while the 1.537 μm peak is the strongest emission from n-type $Al_{0.29}Ga_{0.71}As$. Clearly, these emissions originate from at least two different luminescent centers.

4.1.3 Separation of Luminescent Centers by Below-bandgap Laser Excitation

In order to understand the physical processes involved in the excitation mechanism of the 4f-shell, it was necessary to separate emissions originating from different luminescent centers. Figure 15 shows the low temperature PL spectra from GaAs:Er implanted at 1 MeV with a dose of 5 x $10^{13}/cm^2$ as a function of substrate conductivity. The 488 nm line of the argon ion laser was used as the excitation source. All

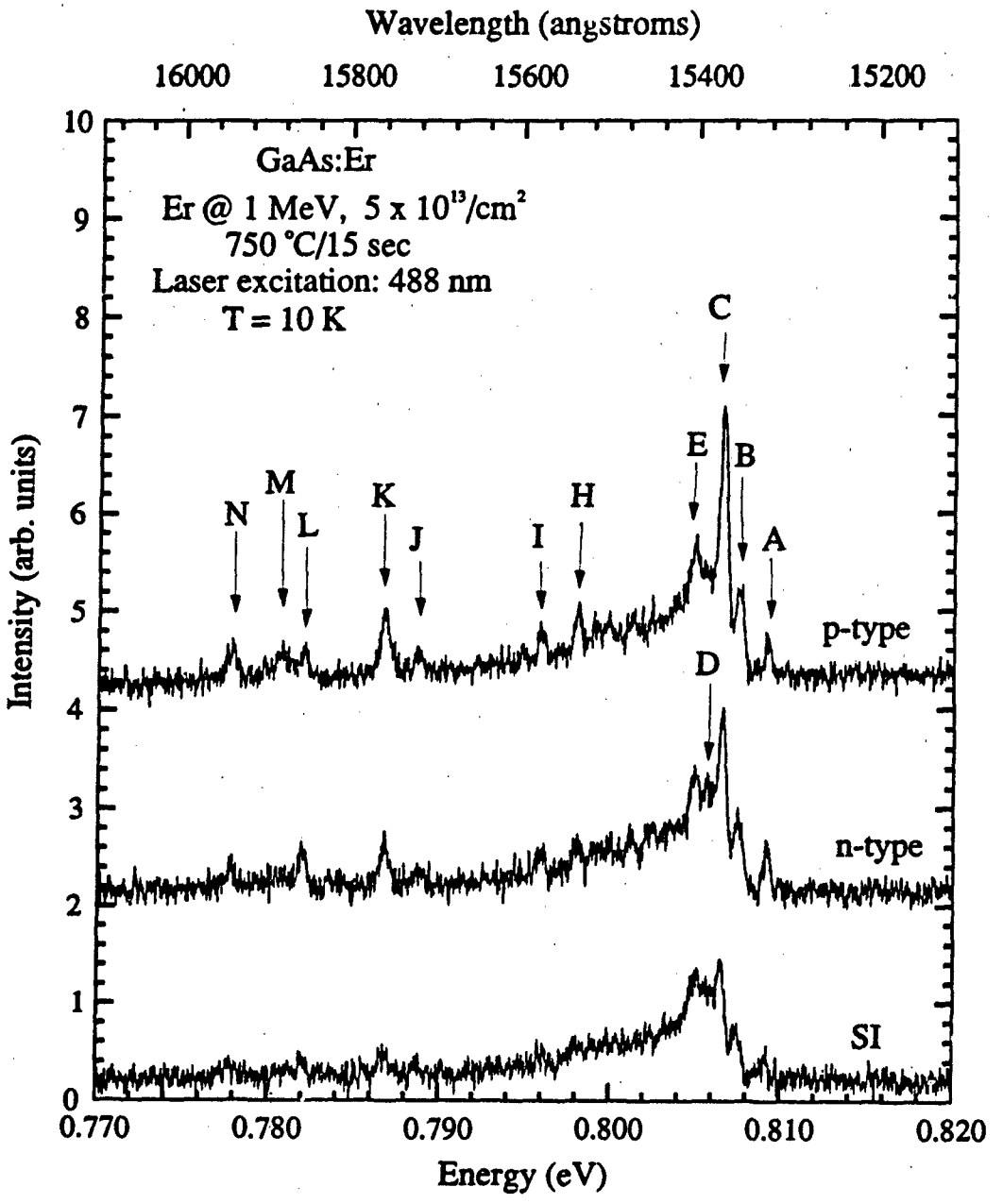

Figure 15 High resolution PL of GaAs:Er implanted at an energy of 1 MeV with a dose of 5 x $10^{13}/cm^2$ and annealed at 750 °C as a function of substrate conductivity

Table II

Er^{3+} Emissions from GaAs:Er

Peak	Wavelength (Angstroms)	Energy (eV)
A	15323	0.8092
B	15354	0.8076
C	15374	0.8065
D	15389	0.8055
E	15403	0.8051
F	15438	0.8031
G	15494	0.8003
H	15535	0.7982
I	15578	0.7960
J	15721	0.7887
K	15760	0.7867
L	15856	0.7819
M	15883	0.7807
N	15939	0.7779
m1 (in Fig. 16)	15403	0.8050
m2 (in Fig. 16)	15419	0.8042

samples shown were annealed at 750 °C for 15 sec using the RTA technique. Table II lists the wavelengths of all the emission peaks that are observed in the high resolution PL spectra shown. At least 12 different emissions can be clearly distinguished, all due to the intra-4f transitions $^4I_{13/2} \rightarrow {}^4I_{15/2}$ of Er^{3+}. However, the multiplicity of lines and the fact that the relative intensity among different peaks changes as the annealing conditions, erbium dose, and substrate conductivity change suggest that these emissions originate from several different luminescent centers. Peaks A, B, and C seem to

originate from the same luminescent center, because the relative intensities among these three peaks remained the same for all three samples. This center will be called C1, and it is the dominant feature in all the samples shown in figure 15. Changes in the relative intensity between emissions from the C1 center and other emission peaks can be seen from the figure. For example, in SI-GaAs peak E is almost as strong as peak C, but in p-type GaAs it's intensity is only half that of peak C. However, the other emissions cannot be classified based on the spectra shown on figure 15 alone. A useful technique to separate different centers is to do annealing studies. However, annealing at temperatures other than 750 °C resulted in weaker emissions, thus making it impossible to observe these emissions with the necessary resolution. Another possible technique is to selectively excite one luminescent center using below-bandgap excitation. The idea is that the excitation mechanism of some centers might be more efficient at a particular excitation energy. The excitation spectra of these samples will be discussed later.

Figures 16 and 17 show the luminescence spectra of the same samples, as in figure 15, upon below-bandgap laser excitation at 1.4377 and 1.3399 eV, respectively. The spectra in both figures were recorded at 10 K using a Ti-sapphire laser as the excitation source. All other experimental conditions were the same as in figure 15. The most striking difference is that in figures 16 and 17 the emission spectra are dominated by peaks

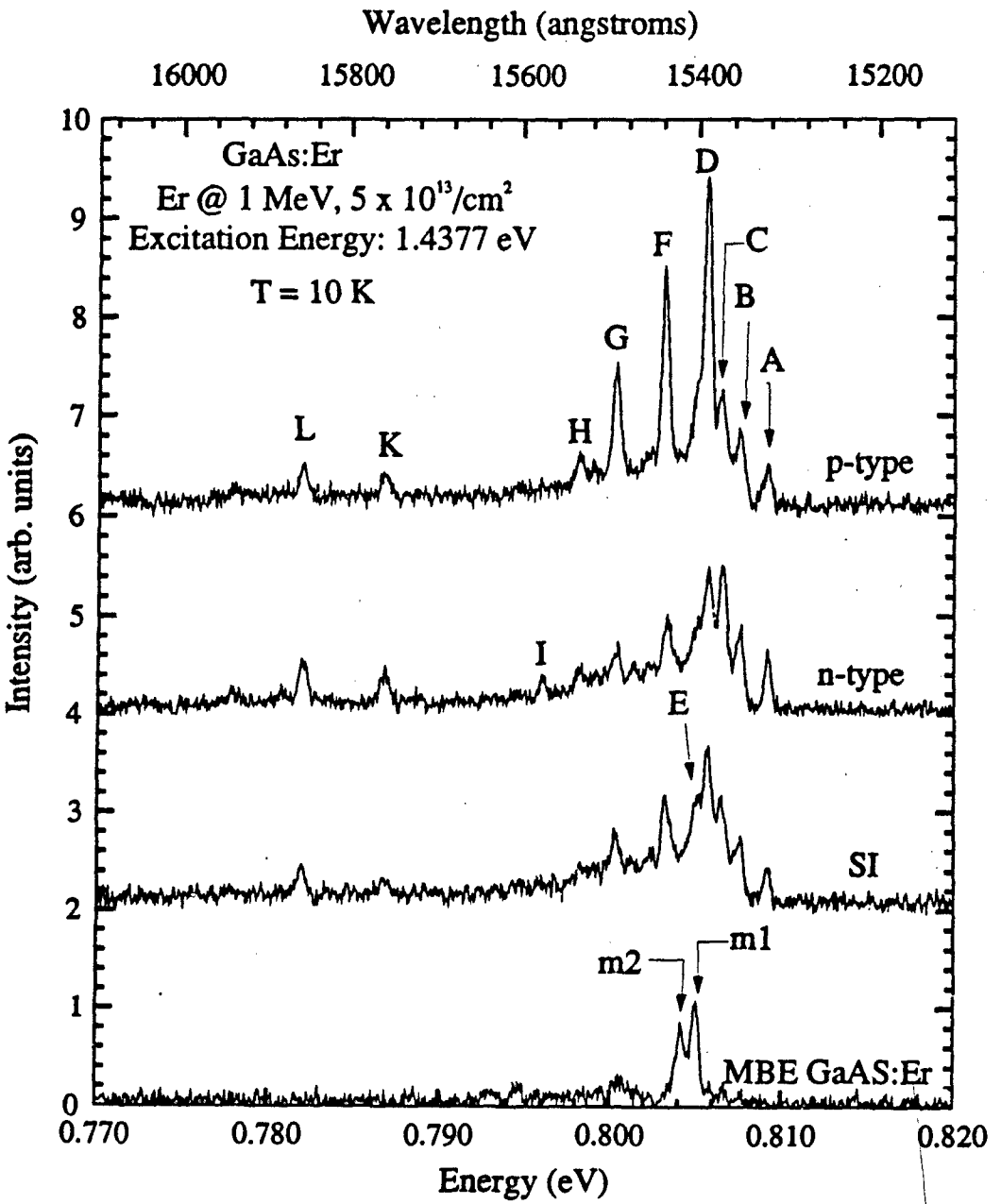

Figure 16 Emission spectra of various GaAs:Er samples implanted at 1 MeV with a dose of 5 x 10^{13}/cm^2 and annealed at 750 °C upon below-bandgap laser excitation at 1.4377 eV

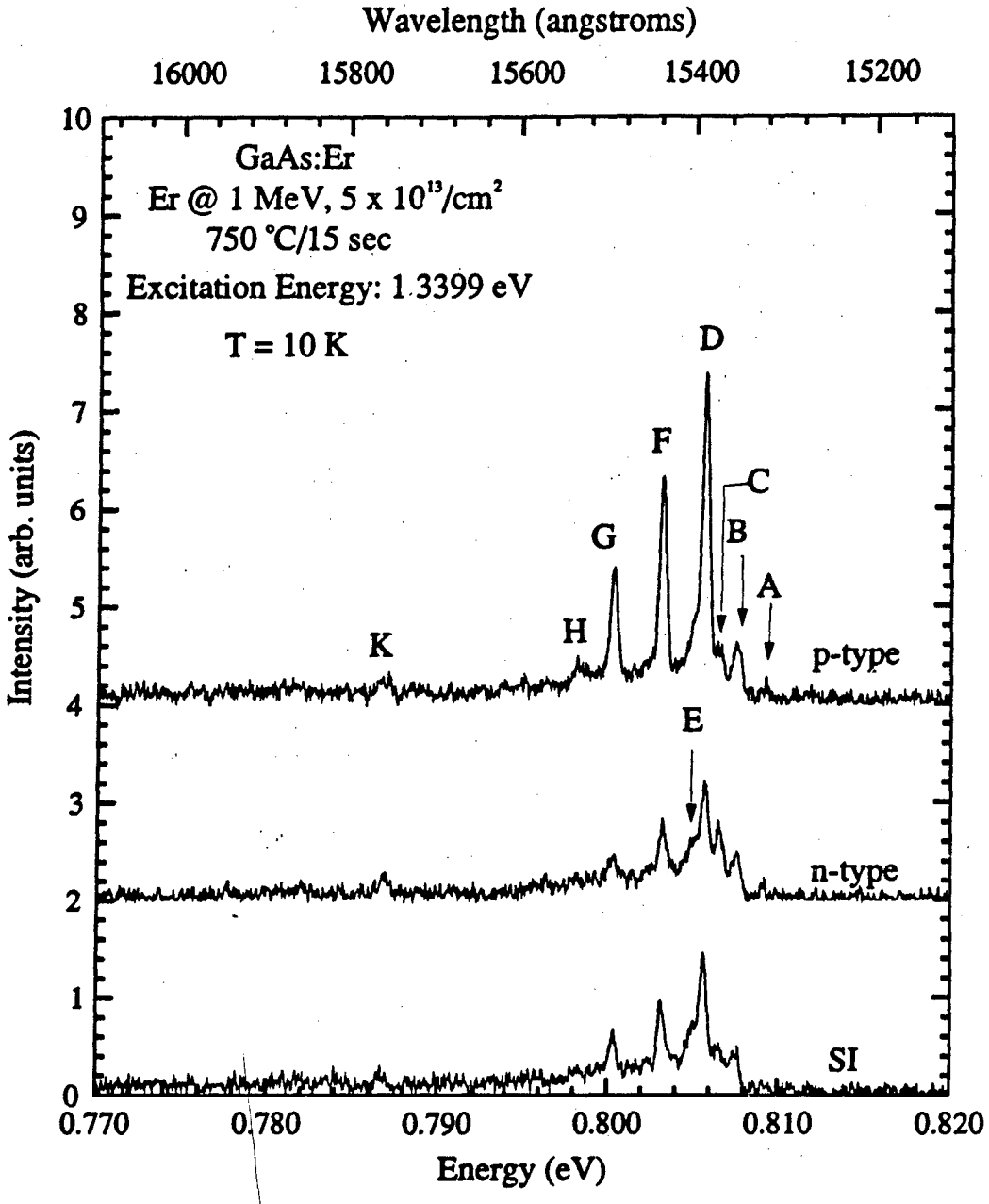

Figure 17 Emission spectra of various GaAs:Er samples implanted at an energy of 1 MeV with a dose of 5 x 10^{13}/cm^2 and annealed at 750 °C upon below-bandgap laser excitation at 1.3399 eV

D, F, and G, while in figure 15, peak D is apparent only in the n-type sample, and it cannot be easily distinguishable in the spectra of the SI and p-type samples. Figures 16 and 17 show that the relative intensity among these peaks is basically the same, independent of the excitation energy and substrate conductivity. Therefore, these emissions most probably originate from the same luminescent center, which will be called C2 in later discussions. We will see that this center plays a very important role in the interpretation of the excitation spectra of these samples. It is very difficult to group the other emissions observed since they are too weak. Because of the differences in relative intensities among them, which can be realized by comparing the spectra shown in figures 15-17, it seems that these peaks originate from at least two different luminescent centers. Among the weak emissions, peak E is of interest because it is the dominant emission from our MBE grown GaAs:Er samples. As shown in the figure, this emission can also be seen in all ion implanted samples. Therefore, it is reasonable to assume that the peak E in the MBE samples originates from the same type of Er complex as in the ion implanted samples. However, there seem to be two different luminescent centers present in our MBE GaAs:Er samples, because the emission m2 (see figure 16) would originate from a different center. It is also possible that both emissions originate from the same luminescent complex, and it just happens that m1 is at the same energy position as

peak E. This point of view is implied by lifetime measurements, which showed the same exponential decay for both peaks, m1 and m2. This point will be discussed later when presenting the results for MBE samples. In order to allow for this second possibility, we will refer to the luminescent center giving rise to the m1 and m2 emissions as M1.

In summary, Er in GaAs forms at least four different luminescent centers which give rise to the Er^{3+} emissions. The PL spectrum of ion implanted samples annealed at 750°C for 15 seconds is dominated by emissions from the C1 center. However, emissions from C2 are the most intense when using below-bandgap excitation. This is especially true for the p-type sample, which shows very strong C2 emissions upon excitation with below-bandgap laser energies. With above-bandgap laser excitation, the p-type sample also shows the strongest emissions, but the C1 emissions are dominant, as mentioned.

4.1.4 Excitation Power Dependence

The behavior of the Er^{3+} emissions as a function of excitation power is strongly related to the excitation and de-excitation mechanisms of the 4f shell. Bantien et al. [1987] and Smith et al. [1987] reported that the intensity of the Er^{3+} emissions in GaAs:Er increased linearly with increasing excitation power, and showed no sign of saturation. This

behavior is similar to the near edge excitonic emissions. Contrary to these results, we have found that the PL intensity exhibits a sublinear dependence on the excitation power. We have observed this behavior in all of our GaAs:Er samples. This can be deduced from figure 18, which shows the PL spectra at different excitation powers. The spectra shown are from a p-type GaAs substrate implanted at an ion energy of 1 MeV with a dose of 5 x $10^{13}/cm^2$ and annealed at 750°C/15 sec using RTA. All spectra in the figure were obtained using the Ti-sapphire laser set at a photon energy of 1.6418 eV. The power densities used were 0.3527, 1.7635 and 3.527 W/cm^2. In the figure, each spectrum is identified with the respective laser output power. Note that when increasing the power density by a factor of five, from 0.3527 to 1.7635 W/cm^2, the intensity of the 1.54 μm emissions increased only by a factor of two. A further increase in excitation power from 50 to 100 mW resulted in only a slight increase in the PL intensity of these emissions. The bb emission underlying the Er^{3+} emissions also showed a sublinear dependence on the excitation power.

When using below-bandgap excitation a sublinear dependence on the excitation power is also observed, as shown in figure 19. The figure shows the PL spectra of the same sample excited at the same power densities as in figure 18 but with a photon energy of 1.4642 eV. In the present case, an increase in the power density by a factor of five from 0.3527

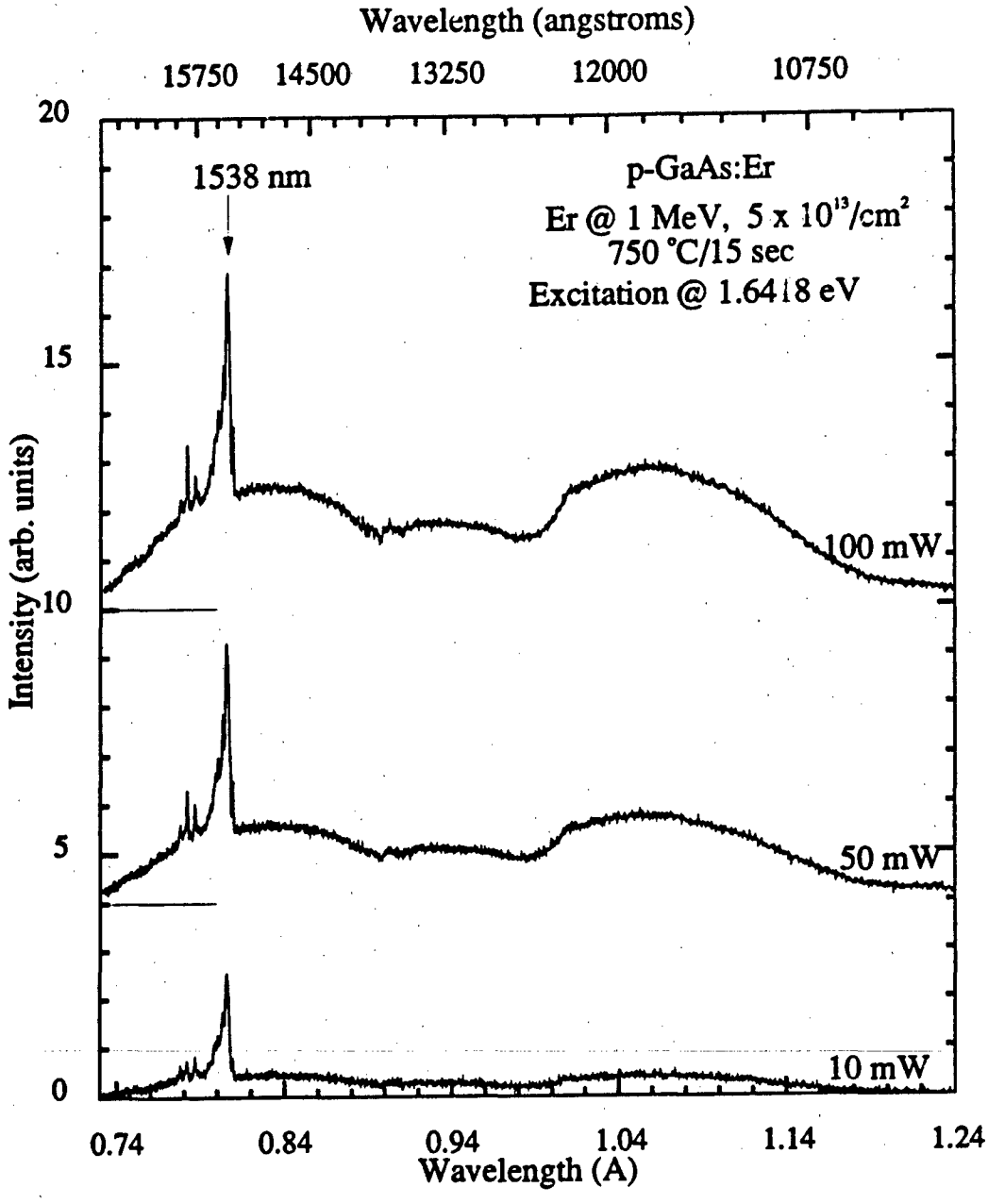

Figure 18 Photoluminescence of p-type GaAs:Er implanted at an energy of 1 MeV with a dose of 5 x $10^{13}/cm^2$ and annealed at 750 °C upon above-bandgap laser excitation at 1.6418 eV with different laser excitation powers .

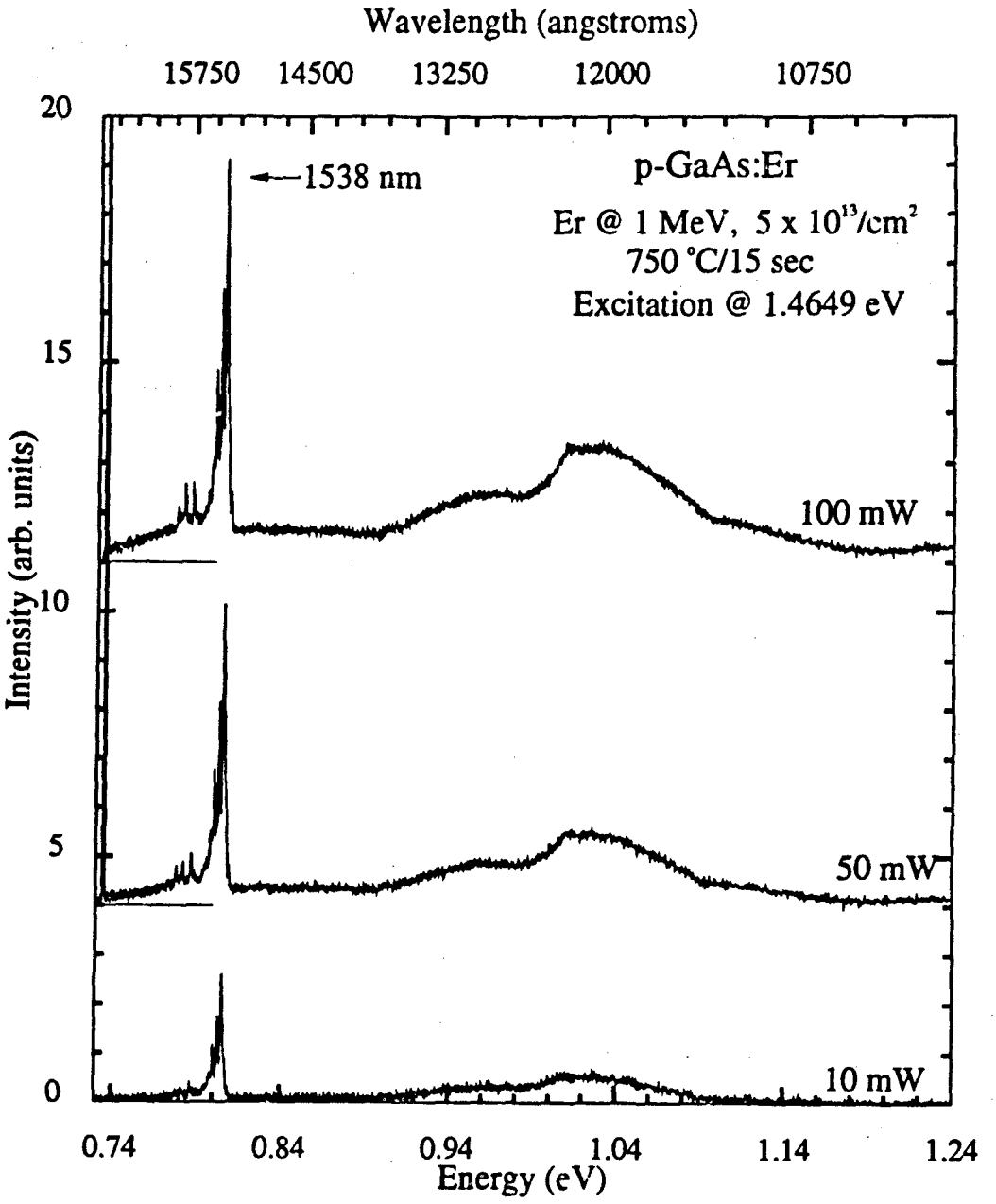

Figure 19 Emission spectra of p-type GaAs:Er implanted at 1 MeV with a dose of 5 x $10^{13}/cm^2$ and annealed at 750 °C upon below-bandgap laser excitation at 1.4649 eV with different laser excitation powers

to 1.7635 W/cm^2 results in an increase in the Er^{3+} PL intensity approximately by a factor of $\sqrt{5}$. The Er^{3+} PL intensity increased by a factor of slightly less than $\sqrt{2}$ when doubling the power density from 1.7635 to 3.527 W/cm^2 if the background signal is subtracted. However, if the peak intensity is measured from the zero level, the PL intensity at 1.54 μm increased by a factor of $\sqrt{2}$.

In summary, when using above bandgap excitation, the PL intensity of the Er^{3+} emissions varies sublinearly as a function of excitation laser power. As the power is increased, more of the excitation power goes into exciting the underlying bb emission and the Er^{3+} emissions saturate, but at a lower excitation power than when using below bandgap excitation. The peak intensity of the Er^{3+} emissions seems to follow a square root dependence on the excitation power, until saturation sets in. Also, the underlying bb emission seems to follow the same behavior. This behavior is observed in all of the ion implanted samples independently of substrate conductivity.

When using below-bandgap laser excitation, the PL intensity of the Er^{3+} emissions also seems to follow a square root dependence on the laser excitation power as shown in figure 20. However, at these excitation energies, the underlying bb emission is not excited very efficiently. In this case, the Ti-sapphire was set at 1.4399 eV, and the same power densities were used as in figures 18 and 19. The spectra shown in this

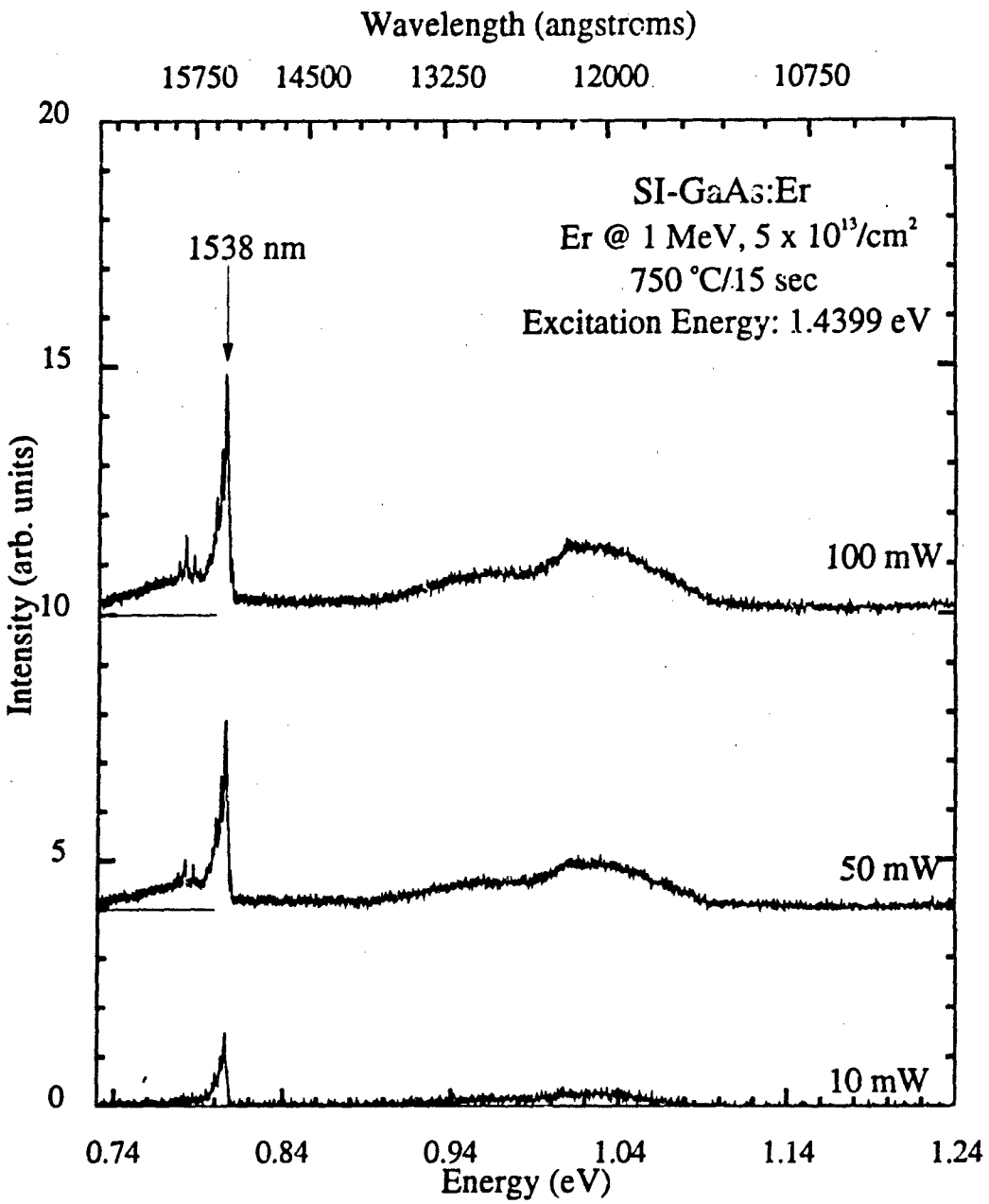

Figure 20 Emission spectra of SI-GaAs:Er implanted at an energy of 1 MeV with a dose of 5 x $10^{13}/cm^2$ and annealed at 750 °C upon laser excitation at 1.4399 eV with different laser excitation powers

figure correspond to a SI-GaAs substrate implanted with Er at a dose of 5 x $10^{13}/cm^2$ with an energy of 1 MeV and annealed at 750 °C/15 sec. Again, a sublinear dependence on the excitation power can be observed, but the intensity of the underlying bb emission is very weak. In section 4.2.4, a model of the excitation mechanism that can explain this behavior will be proposed.

4.2 Selective Excitation Luminescence Study

4.2.1 Selective Excitation Luminescence of GaAs:Er

The excitation spectra of the Er^{3+} emissions from GaAs:Er implanted at an energy of 1 MeV with a dose of 5 x $10^{13}/cm^2$ show very efficient below-bandgap excitation. Of particular interest is the excitation spectrum of the 1.538 μm emission from p-type GaAs:Er that is shown in figure 21. The figure shows three curves as a function of the laser excitation energy, and the topmost curve shows the PL intensity of the 1.538 μm emission, which was the strongest Er emission from that sample. The spectrum was recorded at 10 K by setting the spectrometer at 1.538 μm, and scanning the wavelength of the Ti-sapphire laser. Slit widths of 800 μm were used for both the entrance and exit slits. With these slit openings, the SEL spectrum will include contributions from other adjacent Er^{3+} emissions. The bottom curve corresponds to the excitation spectrum of the underlying background signal. This excitation spectrum was taken by setting the spectrometer at 1.530 μm where there is no Er emission, and under the same conditions as the 1.538 μm excitation spectrum. The middle curve shown in the figure is the difference between these two excitation spectra. Therefore, it is a measure of the "true" intensity of the erbium emission since the background has been subtracted out. The spectra shown have not been corrected for

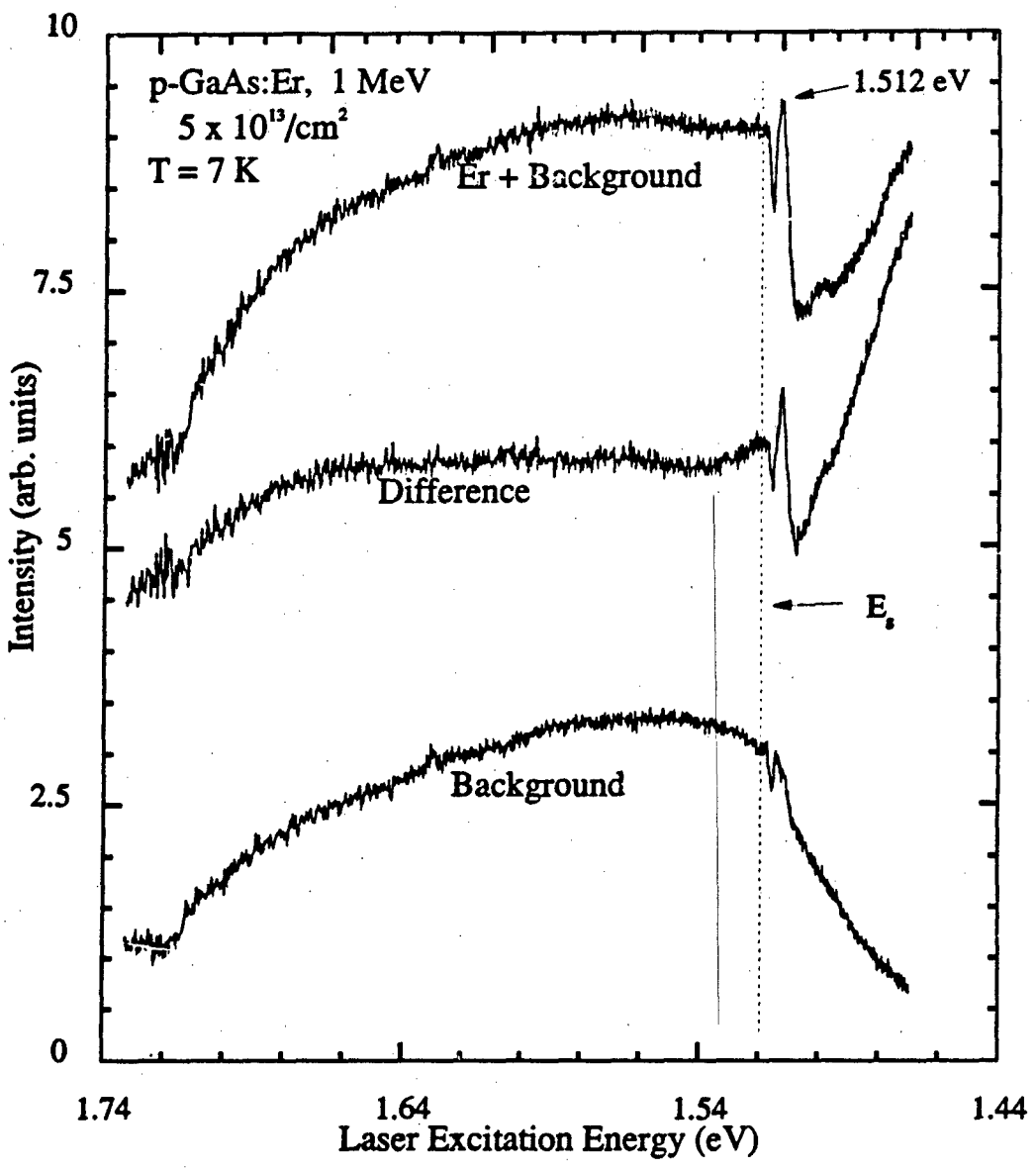

Figure 21 Selective excitation of the 1.538 μm and background emissions from p-type GaAs:Er implanted at an energy of 1 MeV with a dose of 5 x 10^{13}/cm^2 and annealed at 750 °C

changes in the laser excitation power. Therefore, we must keep in mind the intensity variations which depend on the laser excitation power when analyzing the SEL spectrum. Figure 22 shows a plot of the Ti-sapphire laser power as a function of emission energy. The figure shows that the laser excitation power increased as the laser was scanned from 1.72 to approximately 1.59 eV. However, in the same excitation energy range the increase in signal strength is due mostly to an increase in the background intensity. This can be seen by comparing the excitation spectra shown on figure 21. Upon subtracting the background signal, the Er^{3+} PL intensity remained basically constant from 1.67 to 1.53 eV, due in part to the change in the penetration depth with excitation laser energy. As the laser excitation energy is decreased, the light penetrates deeper into the sample, thus exciting other deep centers not related to Er. Since the Er implant layer is very thin, the deeper the beam penetrates the smaller the percentage of the total power used to excite the erbium. However, this is not the only reason for the Er^{3+} intensity remaining constant in the 1.67 to 1.53 eV region, while the excitation laser power increased in the same range. As mentioned in section 4.1.4, the Er^{3+} emissions saturate at some excitation power. After the saturation level is achieved, any increase in the laser excitation power will result in an increase in the background intensity. The origin of the background signal was discussed in section 4.1.1. As

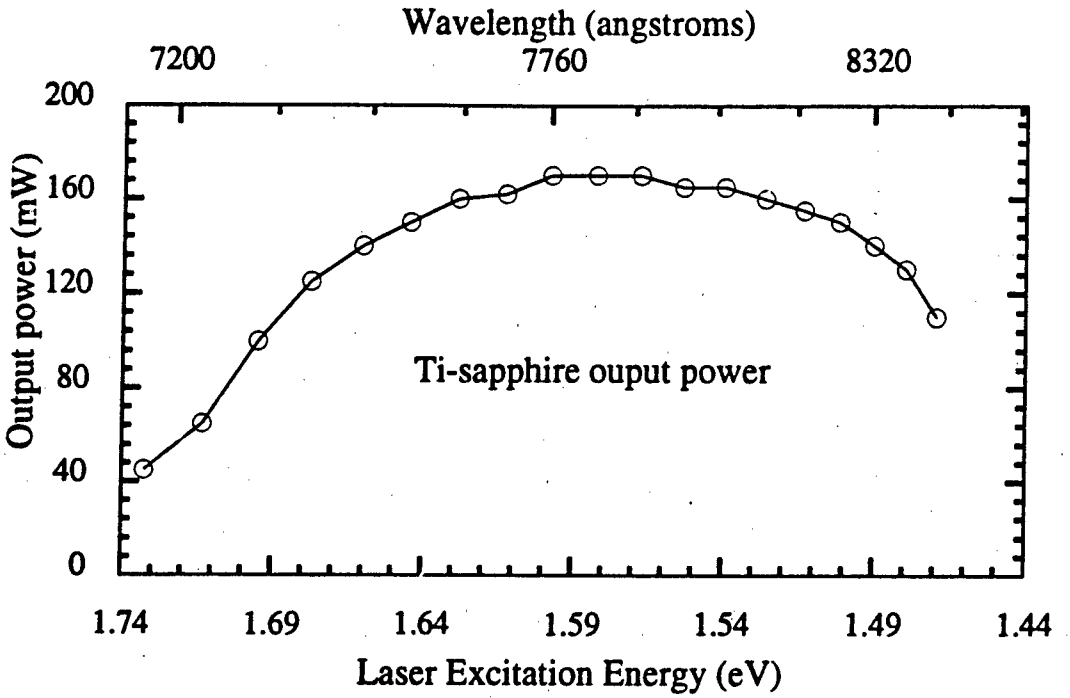

Figure 22 Ti-sapphire's power output as a function of laser energy

shown in figure 21, the Er^{3+} excitation spectrum also shows a small increase in PL intensity near the bandedge at 1.519 eV. As the laser excitation energy decreases below the bandgap, the signal intensity shows a small dip near 1.513 eV. This is followed by a sharp excitation peak centered near 1.512 eV. Below 1.512 eV, the signal intensity decreases, but it starts to increase immediately below 1.507 eV. When the background is subtracted, this effect is more pronounced, and it will show a more dramatic change if we consider that the laser excitation power actually decreased from 1.55 to 1.46 eV (as can be seen from figure 22).

Figure 23 shows the excitation spectrum obtained with laser excitation energies from 1.74 eV to 1.239 eV. Unfortunately, for the excitation energies smaller than 1.46 eV, it was necessary to change the optics in the Ti-sapphire laser. After doing this, the laser tunable range was found to be only from 1.438 to 1.239 eV, and therefore, there is a region in the excitation spectrum that was not covered in this experiment. This is shown in the figure by a discontinuity of line. The first part of the excitation spectrum shown in the figure is the middle curve of figure 21, i.e., the difference between the Er and background signals. Below 1.46 eV, there is little or no background, therefore it wasn't necessary to subtract it. This second part of the excitation spectrum was recorded in three different segments. Although efforts were made to keep the laser excitation power close to 50 mW during most of the experiment, the laser excitation power varied from a maximum of 60 mW to a minimum of 28 mW near the end of the run. No attempt was made to normalize the SEL spectrum because of the saturation effect mentioned above. Since the maximum laser excitation power used in the second part of the SEL experiment was approximately half the power used near the end of the first part, i.e., near 1.438 eV, the intensity of the second part of the SEL spectrum was multiplied by $\sqrt{2}$ in order to correct for the PL intensity dependence on laser power. The figure shows that below 1.46 eV, the PL intensity increases, peaking at approximately 1.416 eV, and then it

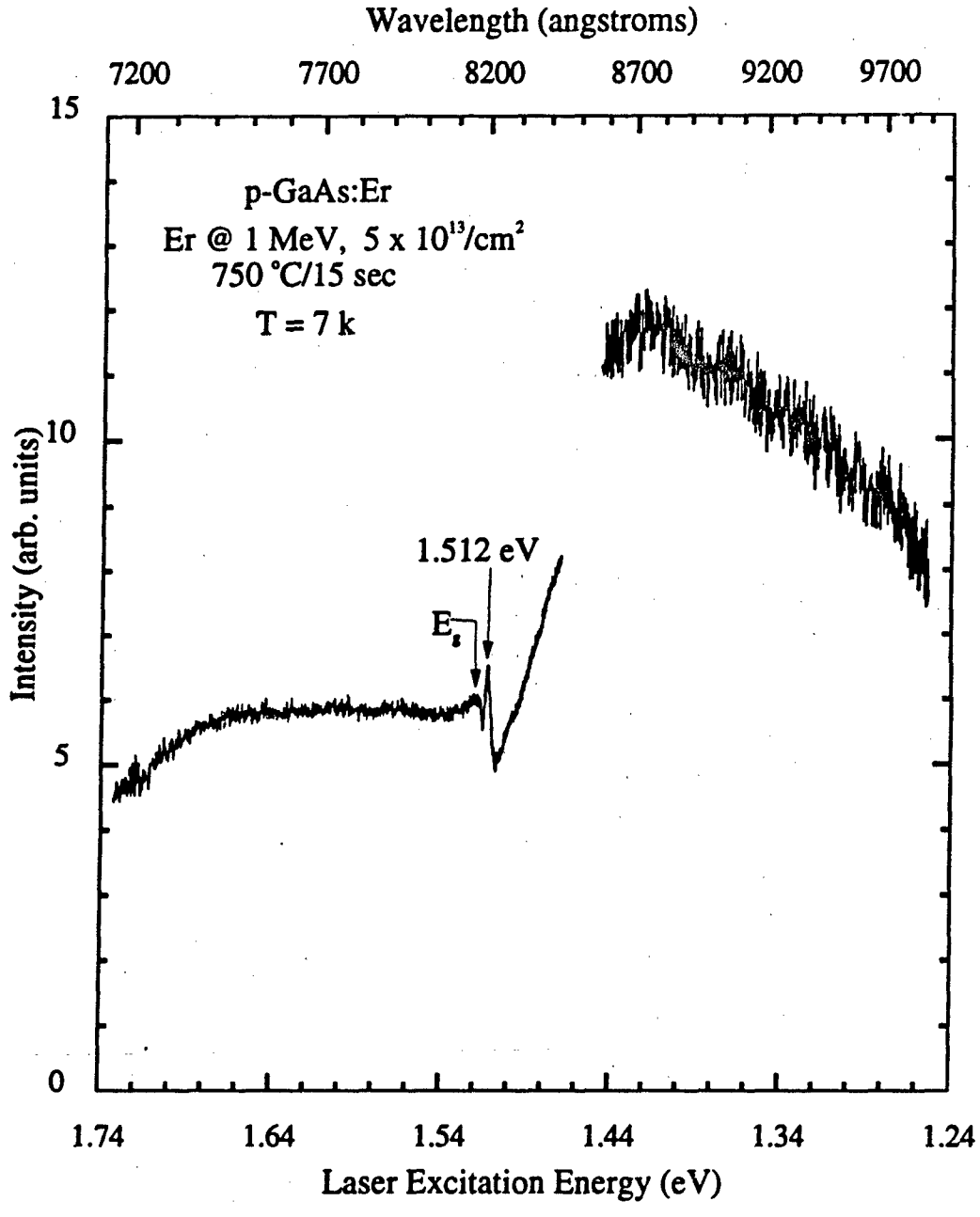

Figure 23 Excitation spectrum of the 1.538 μm emission from p-type GaAs:Er implanted at 1 MeV with a dose of 5 x $10^{13}/cm^2$ and annealed at 750 °C for laser excitation energies from 1.23 to 1.74 eV

decreases very slowly, thus forming a broad excitation band that extends past 1.24 eV.

The dependence of the Er^{3+} emissions on excitation laser energy can be observed from the PL spectra obtained from different laser excitation energies. Figure 24 shows the luminescence spectra resulting from laser excitation at 1.6418, 1.4649, 1.4377, and 1.3399 eV. All spectra shown were taken under the same experimental conditions. The laser excitation power was 100 mW, and the slitwidth was 800 μm for both the entrance and exit slits. As shown in the figure, excitation at 1.6418 eV results in a broadband emission underlying the Er^{3+} emissions. This broadband emission is responsible for the background signal discussed earlier. At least another broad emission, centered near 1.04 eV, can be seen from the figure. The spectra shown were not corrected for the system's response, and this might be responsible for the strange shape of the broad emission near 1.04 eV. Below bandgap excitation at 1.4649 eV results in stronger Er^{3+} emissions with a much weaker bb emission underlying the 4f emissions. If the background is subtracted, the main Er emission for 1.4649 eV is approximately 1.5 times stronger than that for 1.6418 eV. This trend continues as the laser excitation is shifted to 1.4377 eV, that is, the Er^{3+} emissions are twice as strong as those observed with above-bandgap laser excitation of 1.6418 eV, while the broadband emissions are much weaker. As the laser excitation energy is

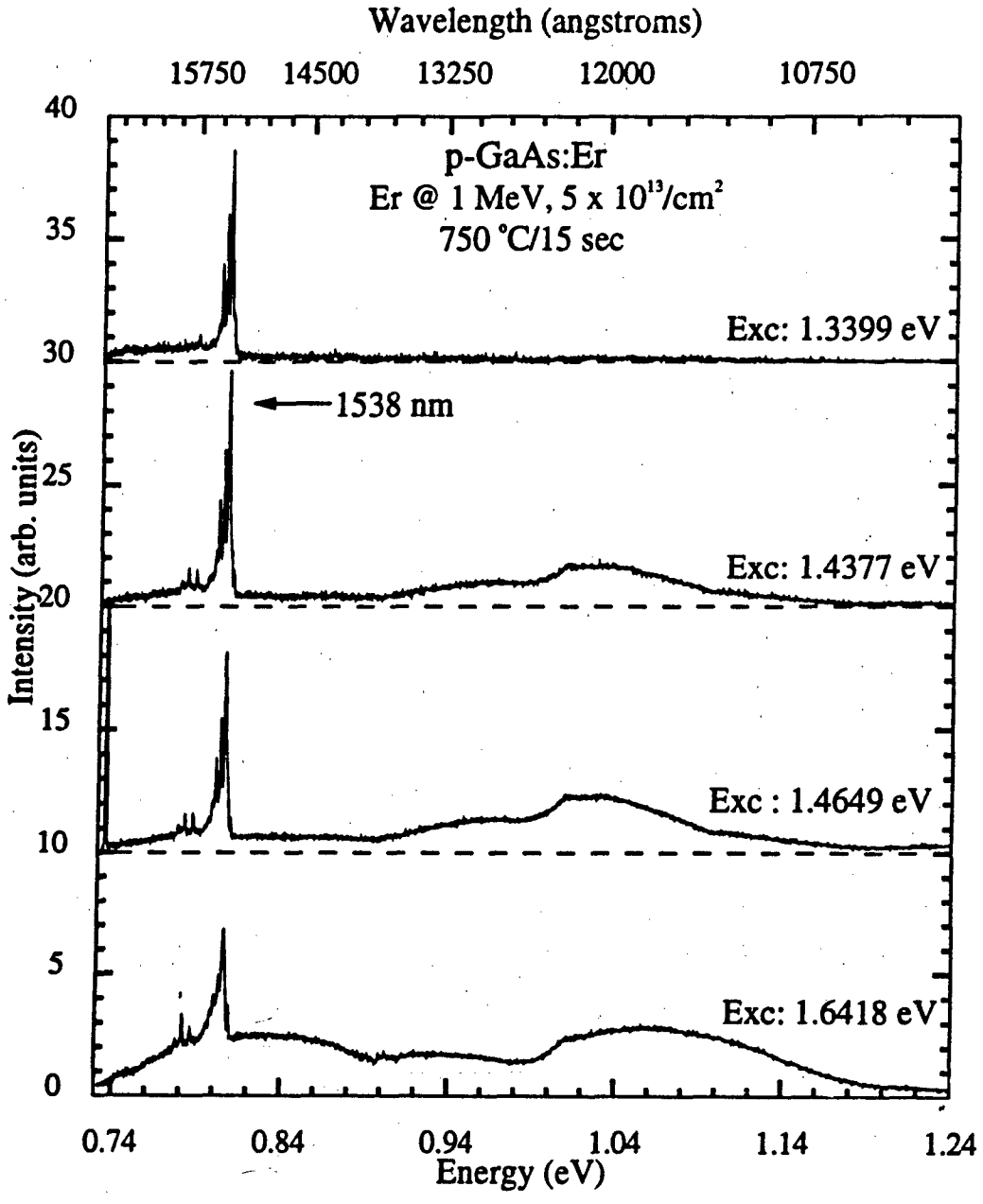

Figure 24 Emission spectra obtained with different laser excitations for p-type GaAs:Er implanted at 1 MeV with a dose of 5 x 10^{13}/cm^2 and annealed at 750 °C for 15 sec

decreased further, the Er^{3+} PL intensity starts to decrease slowly, and the broadband emissions disappear. Because of the low resolution used, it is very difficult to see changes in each of the erbium emissions from figure 24.

Recall that section 4.1.3 discussed the high resolution spectra from SI, n-, and p-type GaAs:Er samples with both the above- and below-bandgap excitations. At this point, it will be useful to compare the PL spectra from the same sample taken at different laser excitation energies. Figure 25 shows the high resolution PL spectra from p-type GaAs:Er upon excitation at 1.6641, 1.4338, and 1.3399 eV. The spectra shown are from the same sample as that used for the spectra of figures 21, 23, and 24. As mentioned previously, when using above-bandgap laser excitation, the emission spectrum is dominated by the C1 emissions (peaks A, B, and C in figures 15-17, and 25). However, when using below-bandgap excitation, the emission spectrum shows much weaker C1 emissions, but dramatically stronger C2 emissions (Peaks D, F, and G in figures 16, 17, and 25). It is this luminescence center, i.e. C2, which is responsible for the strong increase in signal intensity observed in the excitation spectrum below 1.465 eV as is clearly demonstrated in figure 25. This fact explains the apparent discrepancies between current results and those of Klein et al. [1992]. The excitation spectrum of ion implanted GaAs:Er observed by Klein et al. showed a strong decreased in the signal intensity for below-bandgap excitation, although it

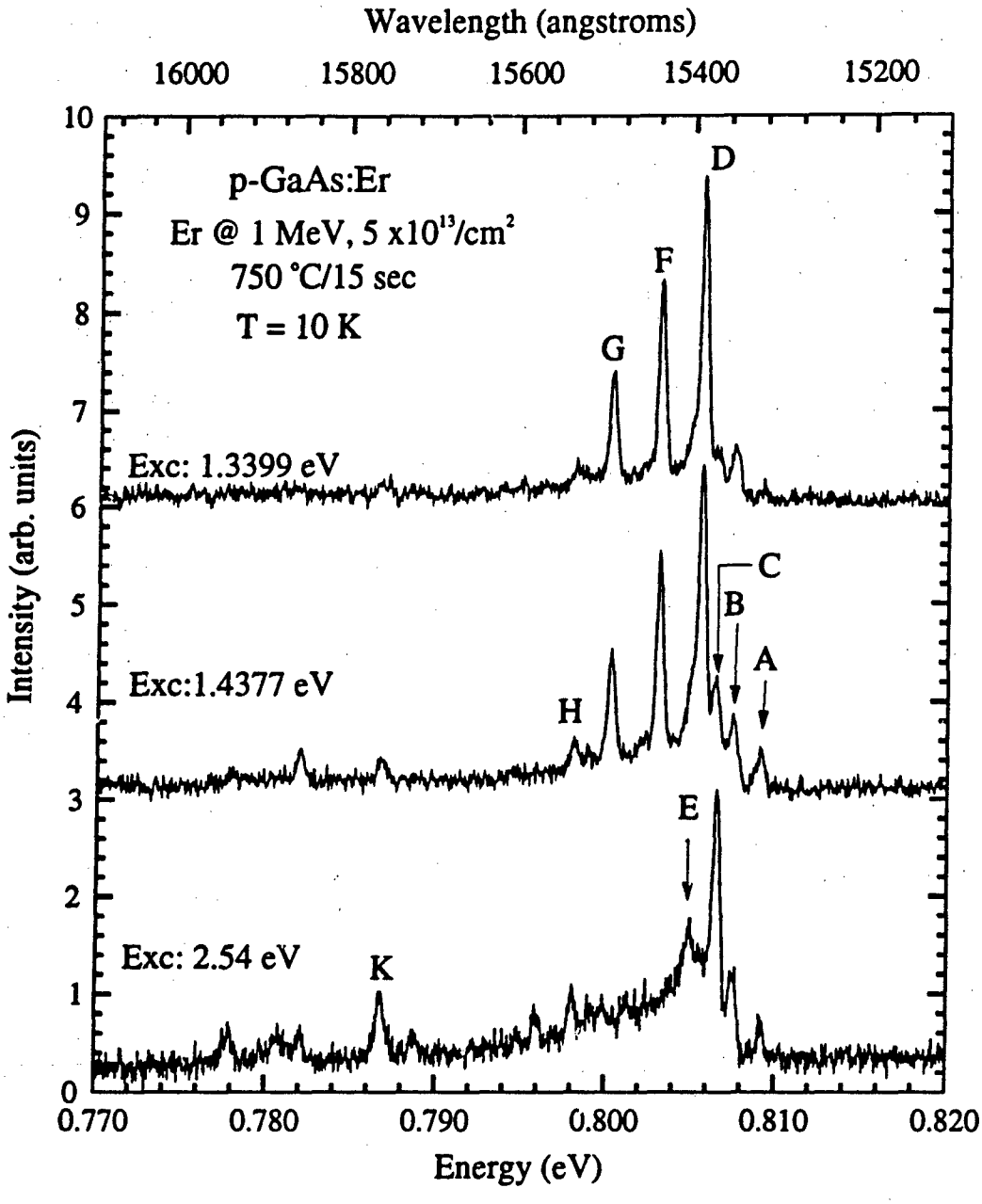

Figure 25 High resolution emission spectra of p-type GaAs:Er implanted at 1 MeV with a dose of 5 x $10^{13}/cm^2$ and annealed at 750 °C with different laser excitation energies

did show a broad excitation band similar to the present case. Strong below-bandgap excitation will be observed only if the Er complex responsible for the C2 emissions is present in that particular sample studied.

The selective excitation spectra of the 1.538 μm emission for Er ion implanted SI or n-type GaAs substrates are very similar to the p-type case, although for these samples the PL intensity does not increase as dramatically as in the p-type case with below-bandgap excitation. Figures 26 and 27 show the selective excitation spectra of the 1.538 μm emission for the SI and n-type samples, respectively. The spectra shown here were taken under the same experimental conditions as the spectra on figure 21. As in figure 21, figures 26 and 27 show the excitation spectra of the total signal which includes the background and the Er^{3+} emissions, the background signal, and the difference between the total and background signals. In the case of the SI sample, figure 26, the excitation spectrum shows the same sharp peak near 1.512 eV as in the p-type case. Also, the peak at 1.512 eV is followed by a broad excitation band as the excitation energy decreases, which can be seen in the excitation spectrum shown in figure 28. As in figure 25, the first part of the excitation spectrum shown in figure 28 is the difference between the 1.538 μm signal and background intensity, and it is not normalized for changes in the laser excitation power. Because the Ti-sapphire output power decreased very rapidly as the lasing energy was decreased, the

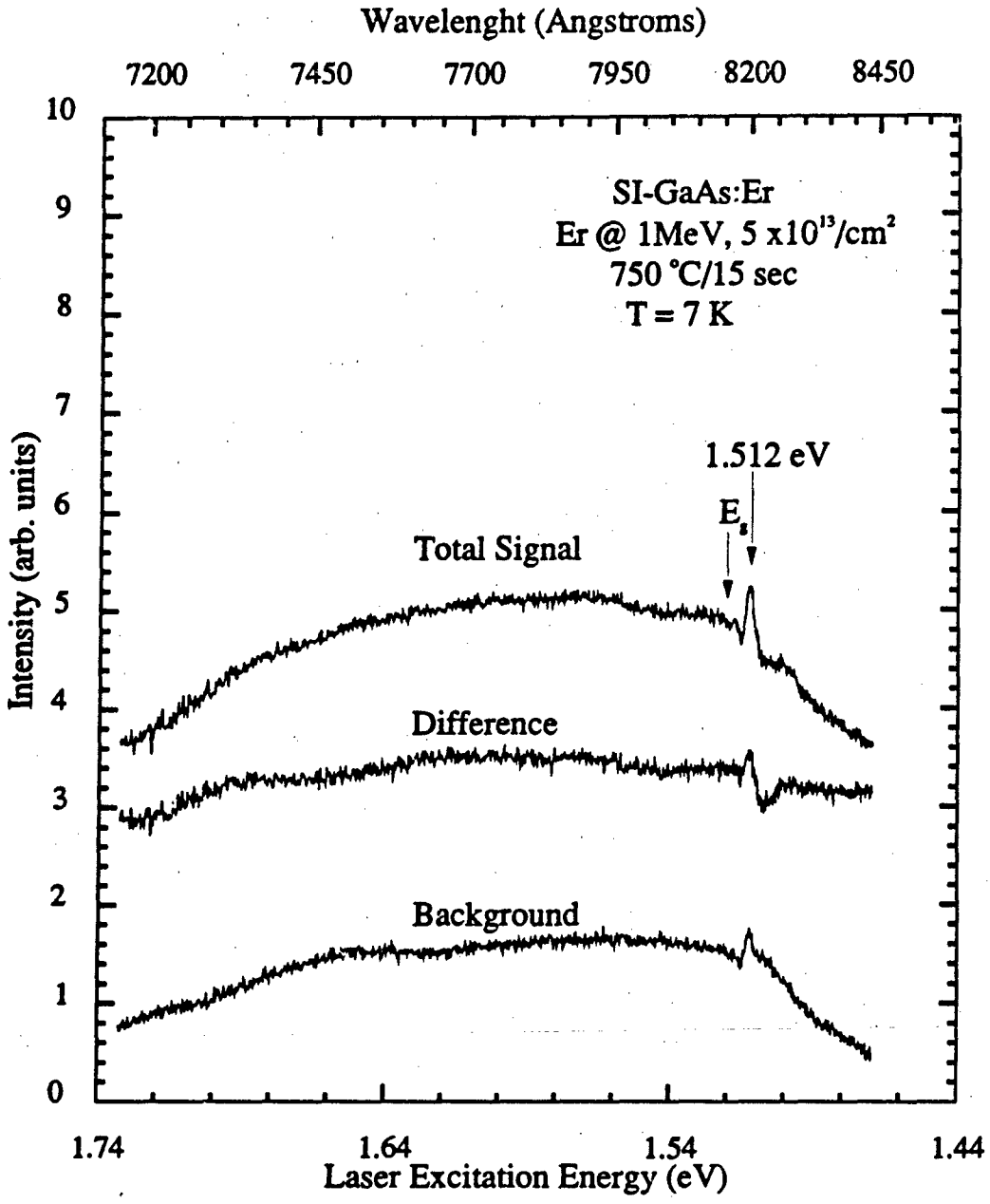

Figure 26 Selective excitation of the 1.538 μm and background emissions from SI-GaAs:Er implanted at 1 MeV with a dose of 5 x 10^{13}/cm^2 and annealed at 750 °C for 15 sec

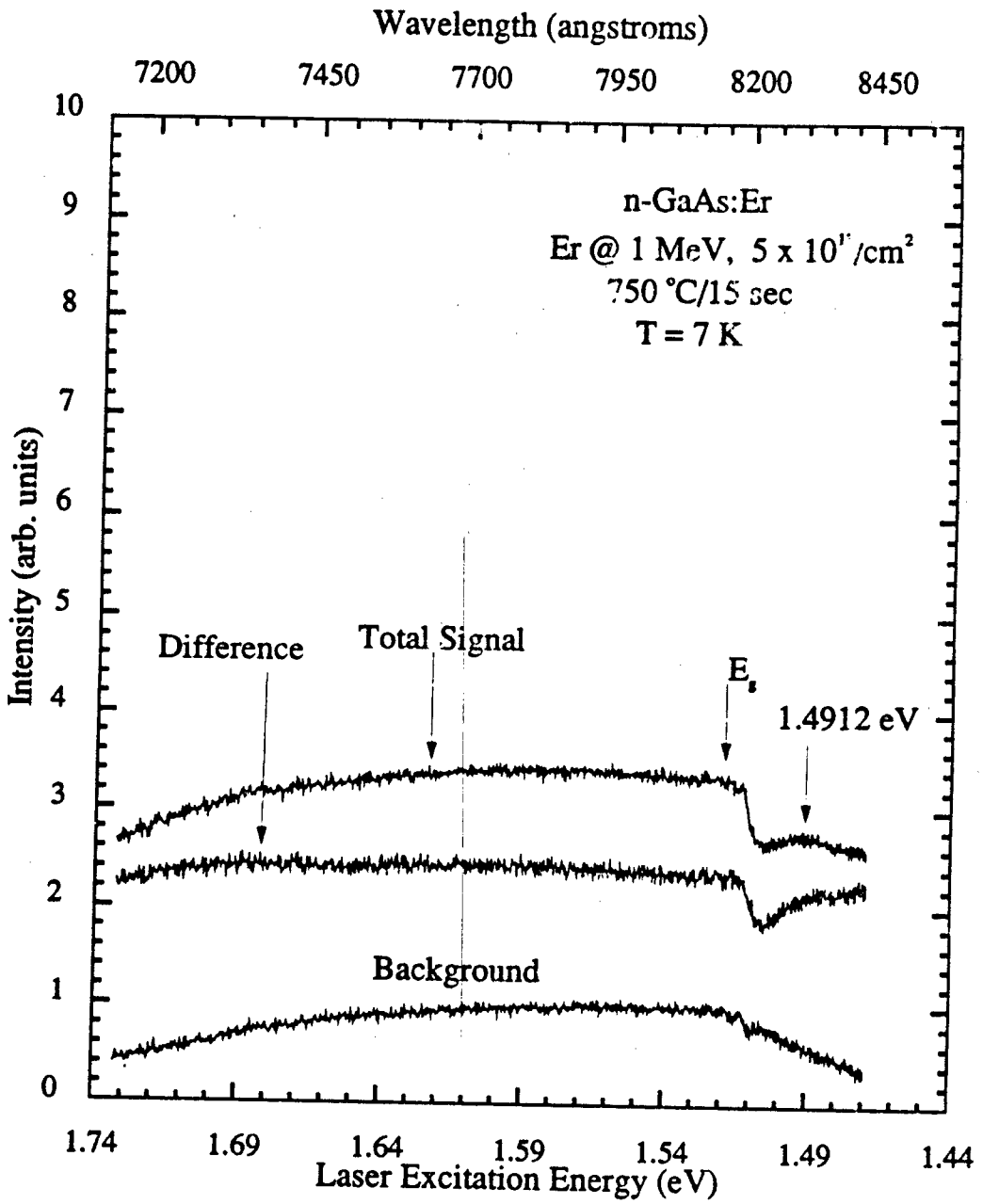

Figure 27 Selective excitation of the 1.538 μm and background emissions from n-type GaAs:Er implanted at 1 MeV with a dose of 5 x 10^{13}/cm² and annealed at 750 °C for 15 sec

SEL spectrum below the 1.465 eV laser energy on figure 28 was recorded in two different runs. An attempt to normalize the second and third parts of the excitation spectrum resulted in distortion of the spectrum, most probably due to the saturation effect, and therefore, it was the un-normalized SEL spectrum which is presented. At laser energies from 1.43 to 1.34 eV the excitation power varied from 100 to 60 mW, while at laser energies from 1.34 to 1.25 eV the power changed from 120 to 20 mW. Figure 28 shows that the strongest PL intensity is obtained near 1.44 eV excitation. This can also be verified from the PL emission spectra taken at different excitation laser energies, which are shown in figure 29. The spectra show the same broad band emission underlying the Er^{3+} emissions that were seen in the p-type case. As in the p-type case, the intensity of the Er^{3+} emissions increases as the excitation energy decreases from 1.6455 to 1.4675 eV, but the intensity of the underlying bb emission decreases. In this case, the intensity of the Er^{3+} emissions does not increase as much as in the p-type case. (Note that different vertical scales were used in figures 24 and 29). Although it is difficult to observed from figure 29, the intensity of the C2 emissions is only increased. This is better illustrated by the high resolution spectra shown in figure 30.

The results for the n-type GaAs:Er sample, figure 27, show some differences from the results of the p-type and SI-GaAs:Er cases. First, the sharp excitation peak near 1.512 eV is not

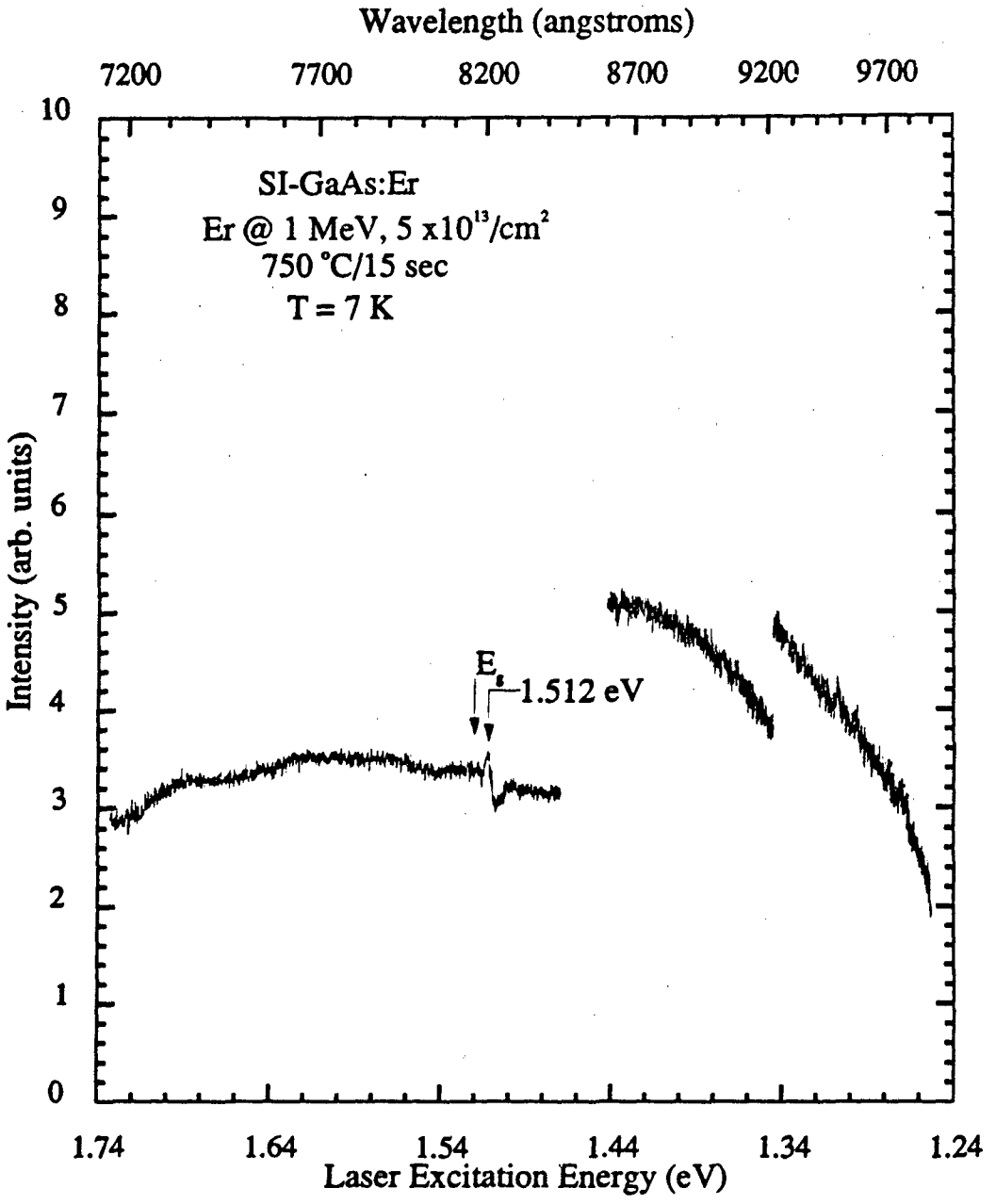

Figure 28 Selective excitation of the 1.538 μm emission from SI-GaAs:Er implanted at 1 MeV with a dose of 5 x 10^{13}/cm^2 for laser excitation energies from 1.24 to 1.74 eV

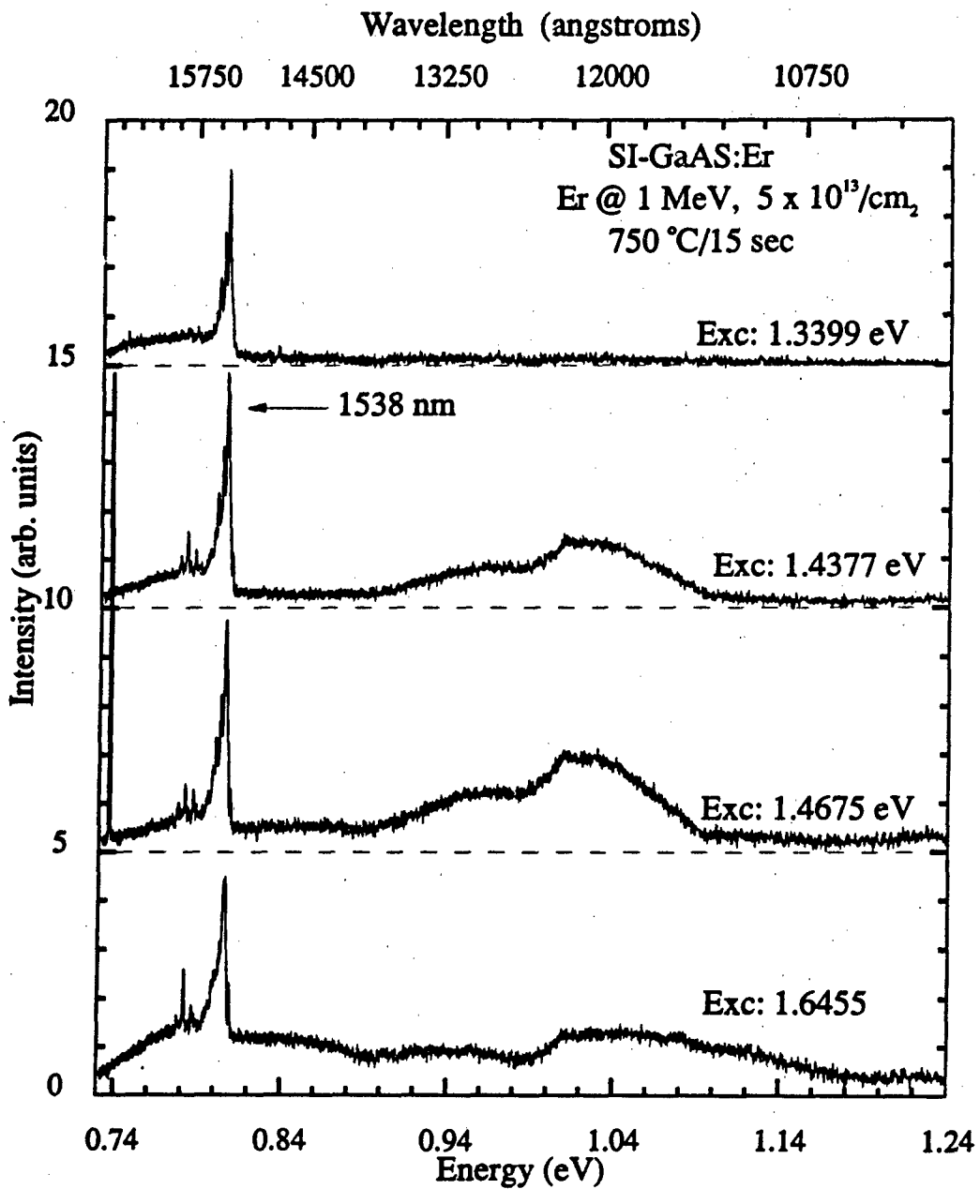

Figure 29 Emission spectra obtained with different laser excitations for SI-GaAs:Er implanted at 1 MeV with a dose of 5 x $10^{13}/cm^2$ and annealed at 750 °C for 15 sec

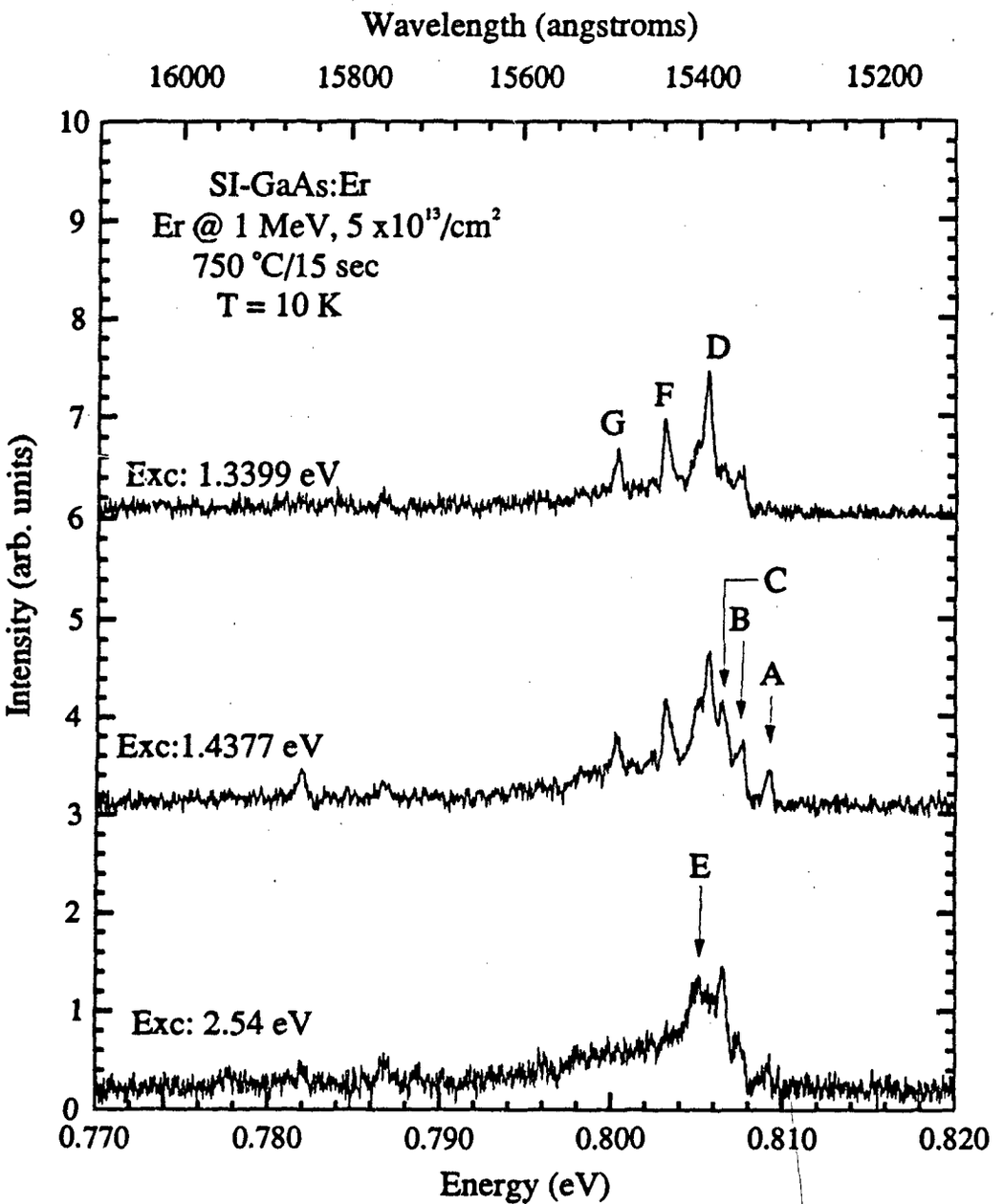

Figure 30 High resolution emission spectra of SI-GaAs:Er implanted at 1 MeV with a dose of 5 x $10^{13}/cm^2$ and annealed at 750 °C for 15 sec with different laser excitation energies

seen in the SEL spectrum and a small bump is observed at 1.4912 eV for n-type GaAs:Er. Second, below-bandgap excitation did not result in much stronger emissions although it is as efficient as above-bandgap excitation. Figure 31 shows the SEL spectrum of the 1.538 μm emission for the laser excitation from 1.73 to 1.23 eV. As with the SI sample, below 1.44 eV the SEL spectrum was recorded in two different runs. In the first part the laser excitation power varied from 100 to 60 mW, while the second part was started with an excitation power of 120 mW, but it decreased to 20 mW near the end of the experiment. Note that the intensity of the broad excitation band decreases more rapidly as the excitation energy decreases than in the two previous cases. Also, the SEL shows weak but sharp excitation peaks near 1.29 eV that were not clearly observed in the SEL spectra of the two other cases. Although these peaks might be due to direct excitation of the 4f-shell from the ground state to the $^4I_{11/2}$ excited state, it can not be ruled out that they might be spikes from the Ti-sapphire laser. The SEL spectrum shown in figure 31 is consistent with the emission spectra taken at various excitation energies that are shown in figure 32. Since the intensity of C2 emissions with below-bandgap laser excitation depends on the presence of C2 centers, the number of C2-type centers in this sample is probably smaller than that in the p-type case. This is consistent with the results from high resolution emission spectra that are shown in figure 33.

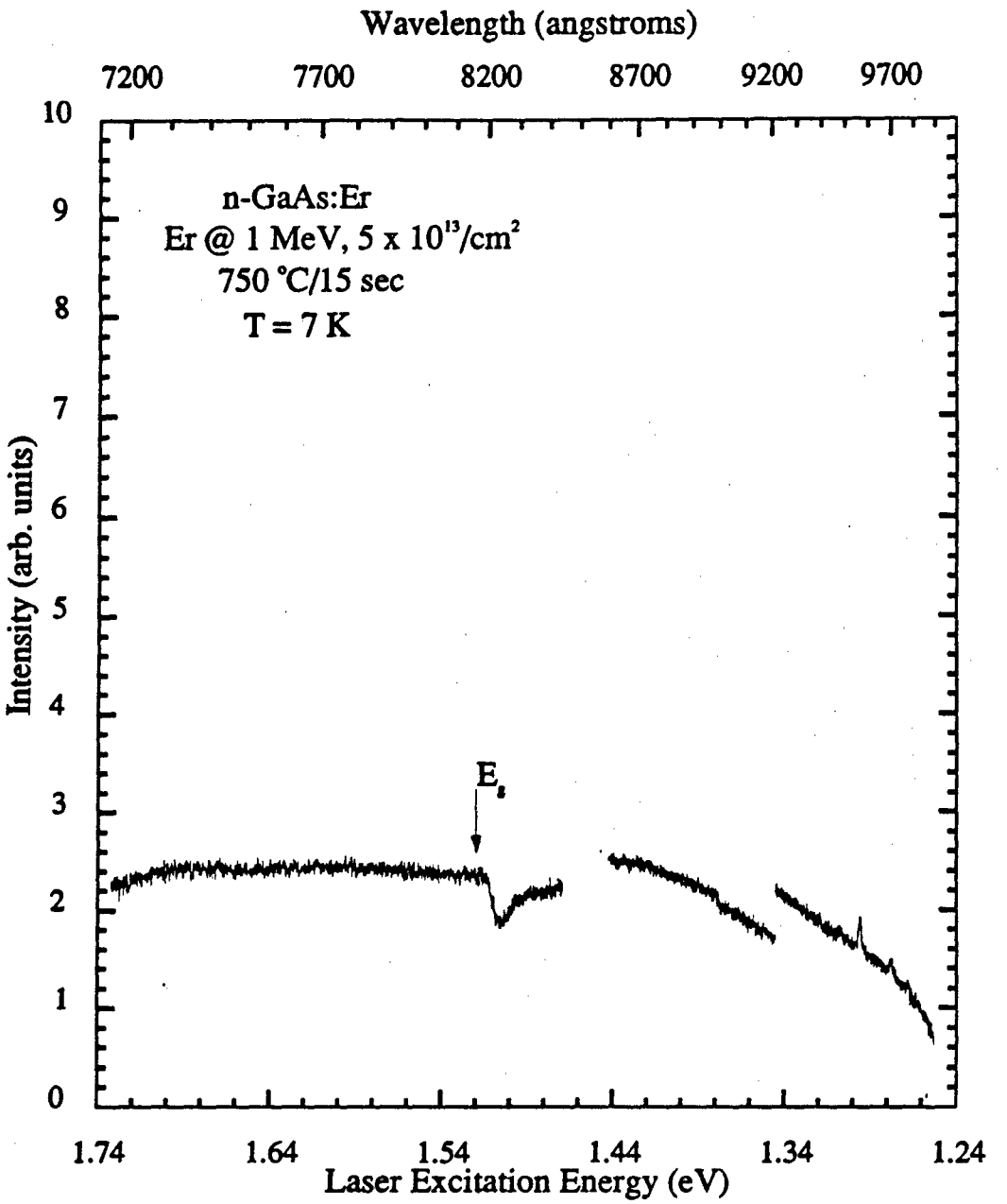

Figure 31 Selective excitation of the 1.538 μm emission from n-type GaAs:Er implanted at 1 MeV with a dose of 5 x $10^{13}/cm^2$ and annealed at 750 °C for 15 sec for laser excitation energies from 1.24 to 1.74 eV

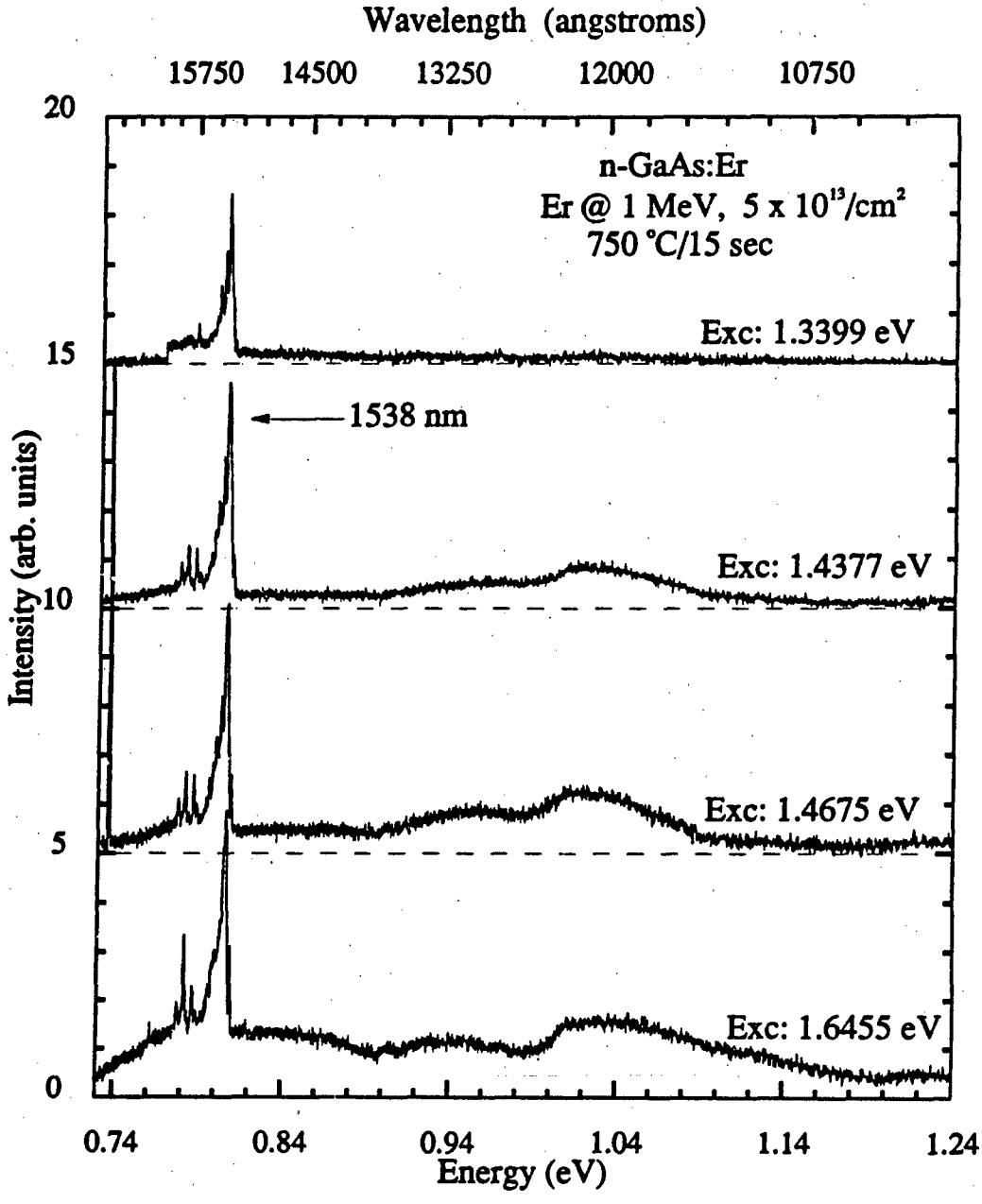

Figure 32 Emission spectra of n-type GaAs:Er implanted at 1 MeV with a dose of 5 x $10^{13}/cm^2$ and annealed at 750 °C for 15 sec obtained with different laser excitation energies

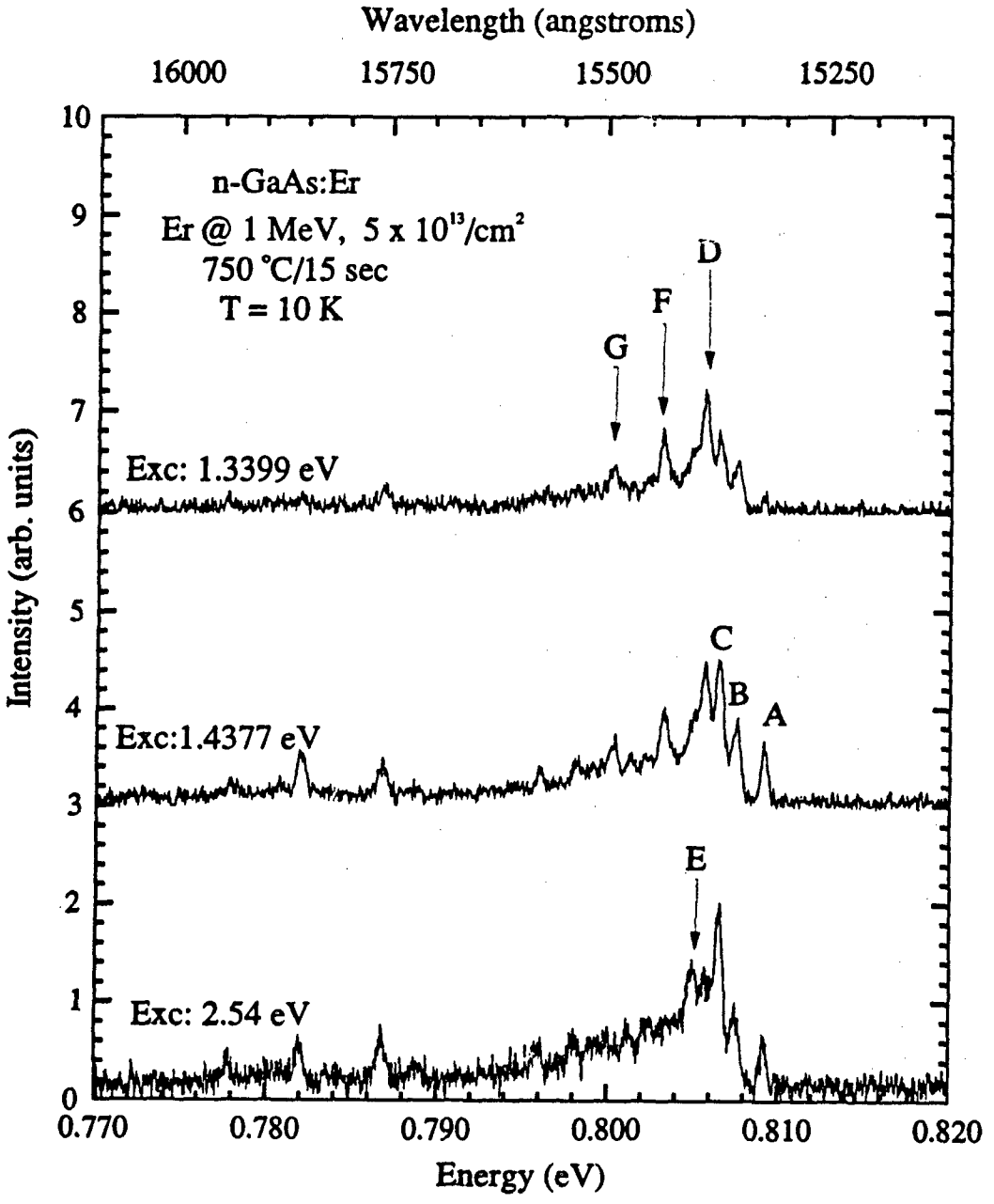

Figure 33 High resolution emission spectra of n-type GaAs:Er implanted at 1 MeV with a dose of 5 x 10^{13}/cm^2 and annealed at 750 °C obtained with different laser excitation energies

4.2.2 Temperature Dependence of the Excitation Spectrum

The selective excitation spectrum of the 1.538 μm emission line for p-type GaAs:Er was also studied as a function of sample temperature, and the results for the Er signal remaining after subtracting the background intensity was recorded at 7, 50, and 100 K as is shown in figure 34. As discussed earlier, the excitation spectrum measured at 7 K shows a sharp excitation peak at 1.512 eV. In addition, there is a small bump near 1.498 eV, i.e., approximately 20 meV below the bandgap. As the temperature increases to 50 K, the sharp excitation peak at 1.512 eV not only disappears, but the PL intensity decreases further as the laser excitation energy is scanned from the bandedge to 1.5 eV. However, below 1.5 eV, the intensity increases sharply as in the T = 7 K case, but there is a clear change in the slope at approximately 1.4856 eV, i.e., approximately 28 meV below the bandedge [E_g(50K) = 1.5137 eV]. This effect is most probably due to the same process responsible for the small bump at 1.498 eV observed at T = 7 K. Also, as the temperature increases to 50 K, the total signal intensity decreases. However, the background intensity, i.e., the intensity of the bb emission underlying the Er^{3+} emissions remained essentially the same. This can be better understood from figure 35, which shows the SEL spectra of the total signal at 1.54 μm and along with the background. As the temperature is increased to 100 K, the PL intensity is

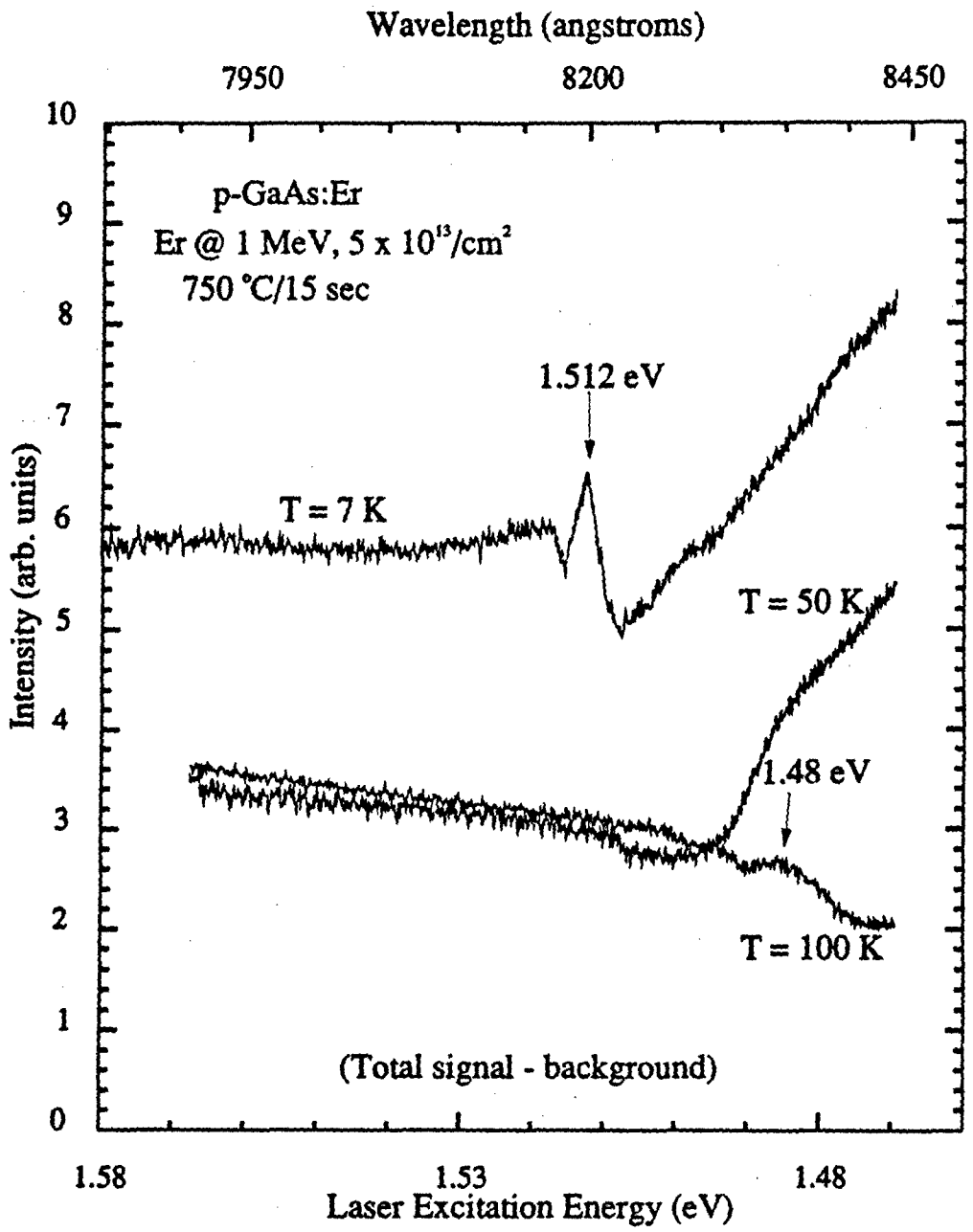

Figure 34 Selective excitation of the 1.538 μm emission from p-type GaAs:Er implanted at 1 MeV with a dose of 5 x $10^{13}/cm^2$ and annealed at 750 °C measured at T = 7, 50, and 100 K

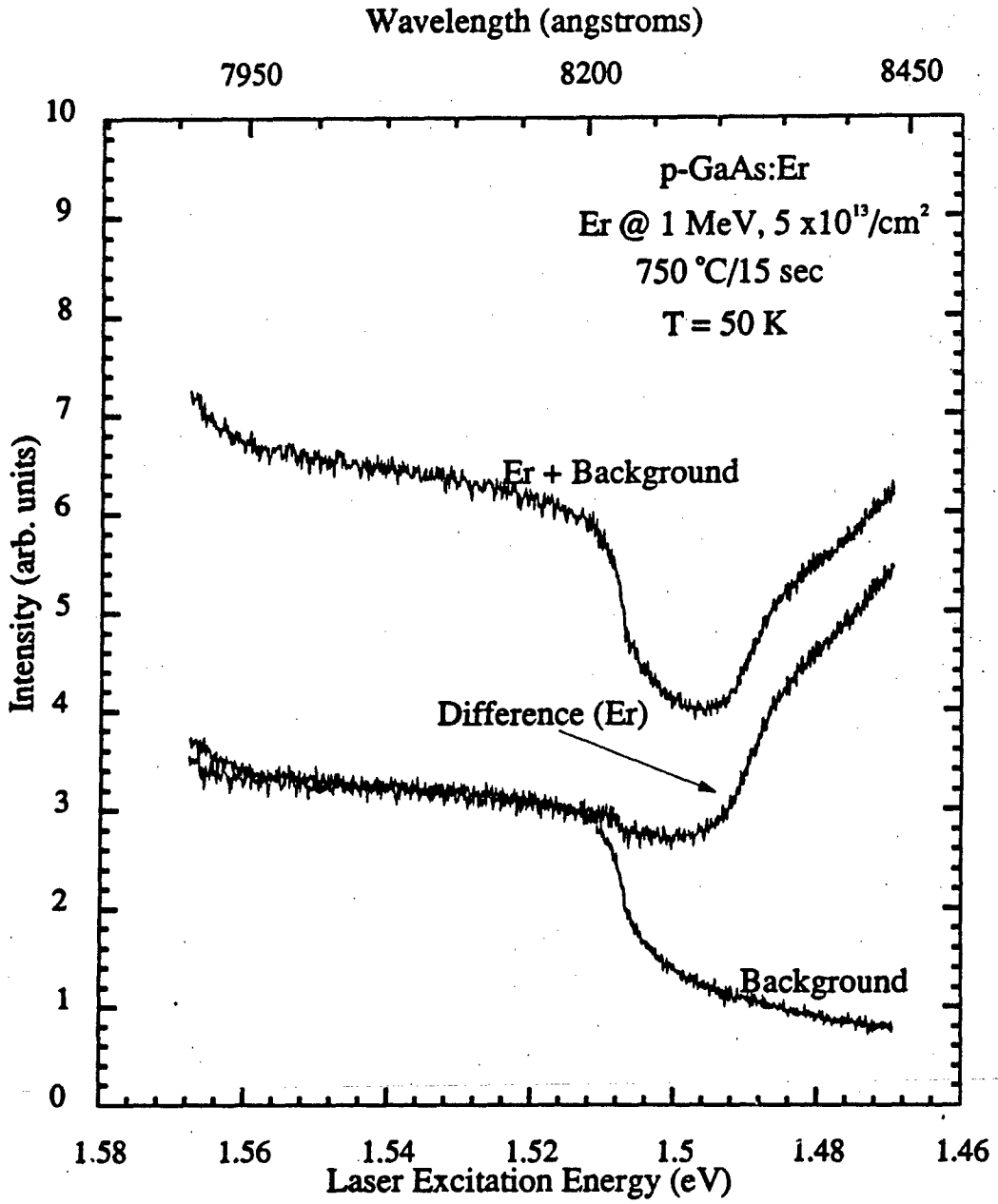

Figure 35 Selective excitation of the 1.538 μm and background emissions from p-GaAs:Er implanted at 1 MeV with a dose of 5 x $10^{13}/cm^2$ and annealed at 750 °C measured at 50 K

decreased almost by a factor of two due solely to the quenching of the bb emission. As shown in the figure, at excitation energies greater than the bandgap energy, the intensity of the Er^{3+} emission was basically the same at 100 and 50 K when the background was subtracted. As the excitation energy decreases below 1.5012 eV, which is the GaAs bandgap at 100 K, a small excitation peak centered around 1.485 eV, i.e. 16 meV below the bandgap, can be observed. We should keep in mind that the values for small bumps obtained at 7 and 50 K, located at 20 and 28 meV, respectively, are somewhat uncertain due to the influence of a stronger excitation band immediately after this peak. Therefore, it can be assumed that the same bump peaks are observed in all three spectra. The nature of this process will be discussed in our model of the excitation mechanism. In contrast to the cases of 7 and 50 K, the intensity of the 1.538 μm emission continues to decrease with the laser excitation below 1.485 eV.

4.2.3 Excitation Power Dependence of the Selective Excitation Spectrum

As discussed in section 4.1.4, the Er^{3+} emissions show a sublinear dependence on the excitation laser power density. In addition, these emissions saturate at low power densities. This saturation effect can be observed from the excitation

spectra of the p-type GaAs:Er sample obtained at a high excitation power of around 375 mW as shown in figure 36. The figure shows the selective excitation spectra of the Er 1.538 μm emission, the background at 1.530 μm, and the difference between them. The output power of the Ti-sapphire for this experiment is also plotted in figure 37 as a function of lasing energy. Note that the excitation power is increasing for laser energies from 1.74 eV to about 1.58 eV. Although there is an increase in the total signal strength, over this energy range, this increase is primarily due to an increase in the background intensity. It can be seen from the figure that if the background is subtracted, the Er^{3+} intensity basically remains constant. As the excitation laser energy is scanned below the GaAs bandgap, the background intensity decreases very rapidly. As with lower excitation power of around 50 mW, strong Er^{3+} emissions are observed with the below-bandgap excitation. Because of the saturation of the Er^{3+} emissions and the sublinear power dependence, most of the excitation spectra presented in this work were not normalized for changes in the power density. Instead, a plot of the excitation power used is presented.

Another example of this saturation effect is shown in figure 38 for the SI-GaAs:Er sample. The spectra shown in the figure are the signal intensities at 1.538 μm obtained after subtracting the background intensity plotted as a function of different excitation power densities. In each

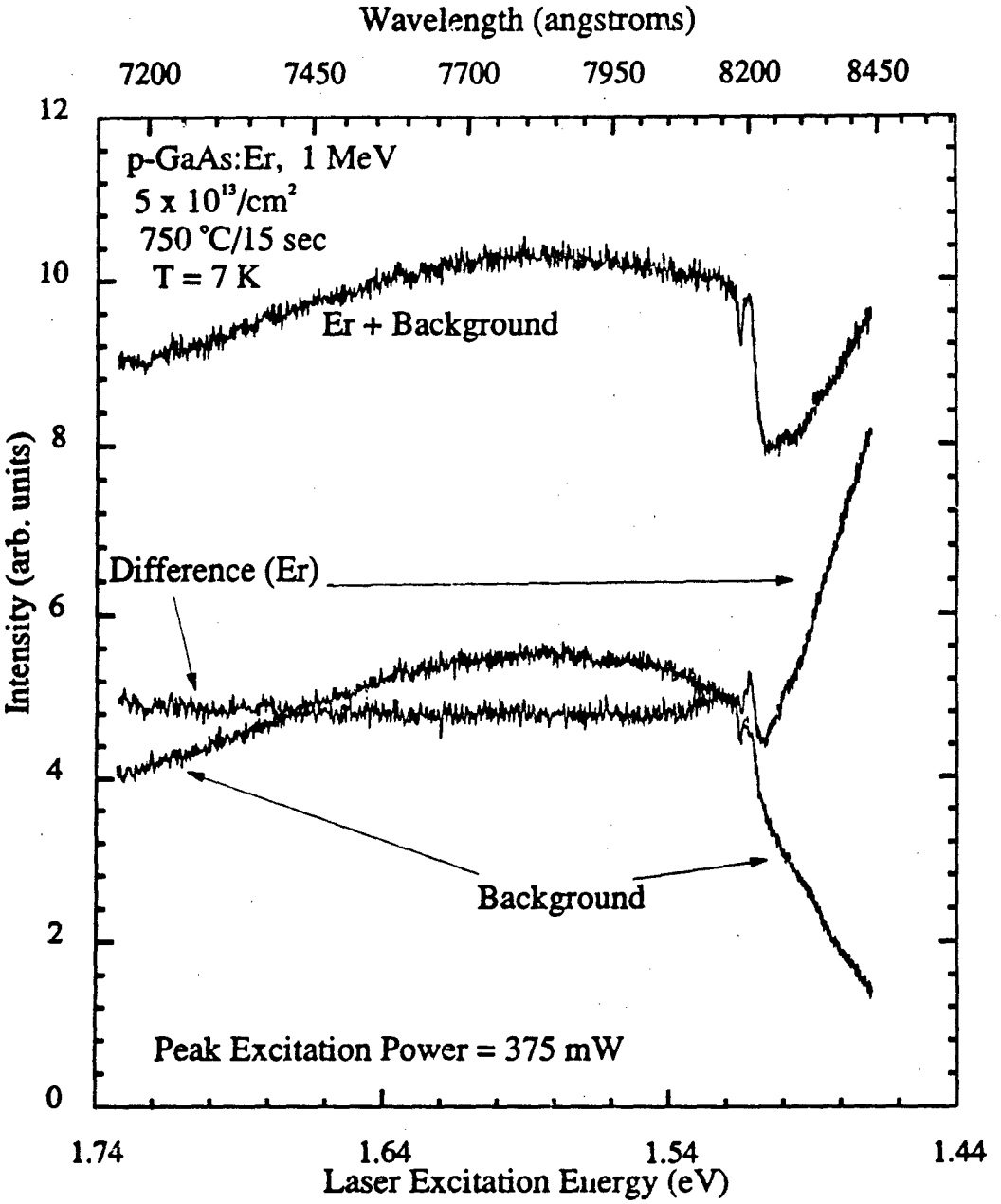

Figure 36 Selective excitation of the 1.538 μm and background emissions from p-type GaAs:Er implanted at 1 MeV with a dose of 5 x $10^{13}/cm^2$ and annealed at 750 °C measured at high laser excitation power of about 375 mW

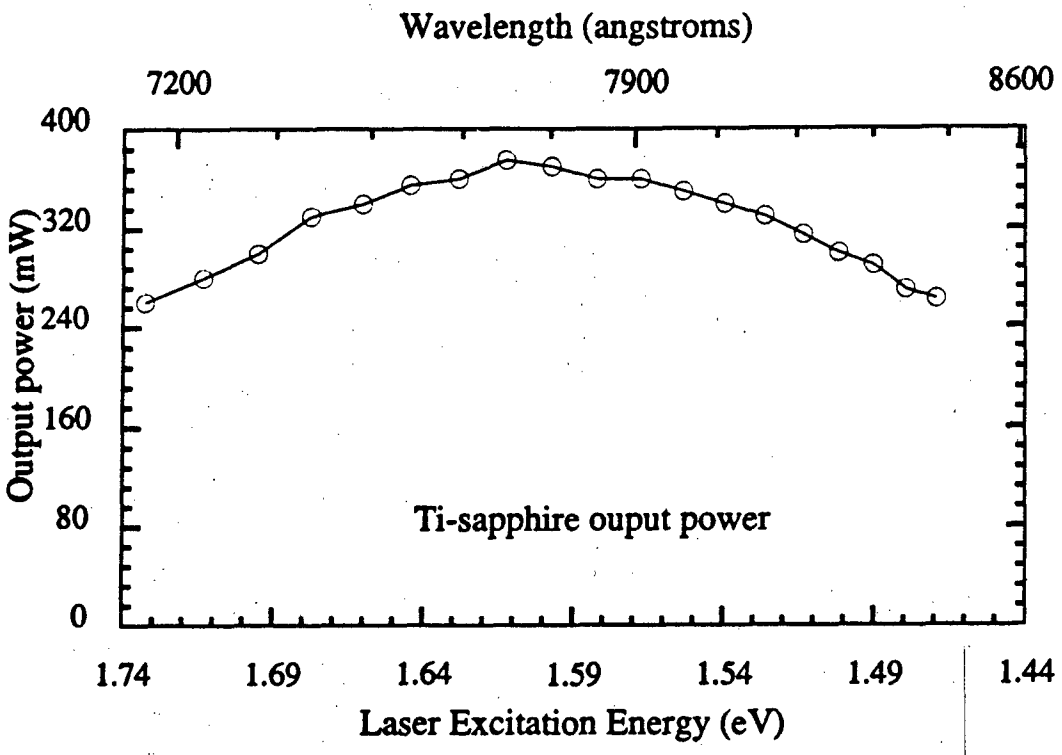

Figure 37 Ti-sapphire power output as a function of laser energy at higher laser power

case, the peak excitation power is shown. Note that the top spectrum have been offset by an arbitrary amount in the up direction, and its zero luminescence line is indicated by the arrow shown in the figure. Comparison of the two topmost spectra shows that the intensity of the Er^{3+} emissions basically remained the same upon increasing the excitation power almost by a factor of three. However, at low excitation power the square root dependence on the excitation power can be deduced by comparing the excitation spectra corresponding to peak excitation powers of 10 and 60 mW. In this case the Er^{3+} intensity increased by a factor of approximately $\sqrt{6}$. Another interesting observation is that the excitation spectra

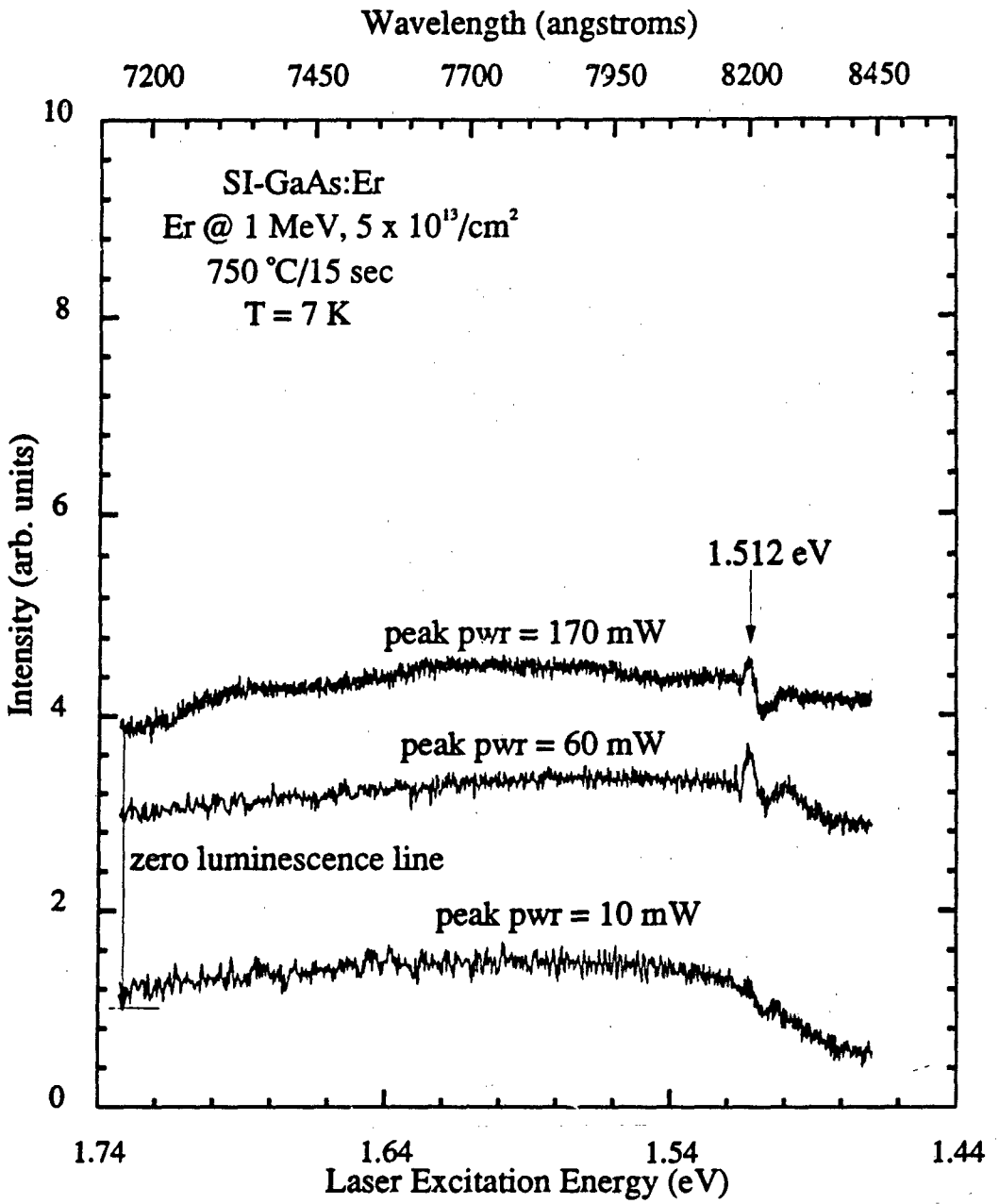

Figure 38 Selective excitation of the 1.538 μm and background emissions from SI-GaAs:Er implanted at 1 MeV with a dose of 5 x 10^{13}/cm^2 and annealed at 750 °C measured at different laser excitation powers.

recorded at excitation powers of 10 and 60 mW show a clear small peak at the same energy position at which the kink was observed in the excitation spectrum of the p-type sample (at approximately 20 meV below the bandgap).

4.2.4 Excitation Mechanism Model

The excitation of the 4f-shell cannot be explained by a resonant energy transfer because of the large energy mismatch between the excitation laser energy and the emission energy. As mentioned above, the selective excitation spectrum of the 1.538 μm emission is characterized by the presence of a broad excitation band with the below-bandgap laser excitation. These broad excitation bands are characteristic of processes involving the excitation of impurity states outside the 4f shell as the primary excitation sources (see the discussion on section 2.3.5). Among these processes, we can discard the possibility of the transfer of energy from sensitizing centers, because the results obtained here seem to be characteristic of a specific Er-related center. That is, this broad selective excitation band is observed in all samples containing the luminescent center that has been identified as C2 (see section 4.1.3). Using Boyn's classification of the rare earth excitation mechanisms, we are left with two possibilities for the primary excitation process:

1. Transitions between external states of the RE centers; or

2. Excitation of donor-acceptor pairs involving the Er ions as either the donor or the acceptor.

The second possibility can be discarded because electrical measurements have shown that Er doping alone does not introduce carriers (Moore et al. [1992]). Changes in carrier concentration have been attributed to either accidental impurities or the gettering effect by the RE elements (Raczyńska et al. [1988], Masterov and Zaharenkov [1990]). Therefore, one is left with the first possibility, i.e. excitation between external states of the RE centers. An example of such a process is the formation of isoelectronic traps similar to the case of Yb in InP. In fact, our results can be explained by assuming that Er introduces a trapping level in the bandgap of GaAs. This idea is supported by the results of Smith et al. [1988] who found an Er-related trap in GaAs. Unfortunately, in that work, the activation energy and the character of the trapping level were not established. Recent results obtained from DLTS measurements at AFIT indicate that Er implantation into GaAs introduces several hole traps in the bandgap (Colón et al. [1991]). By assuming that an Er-related hole trap is involved in the 4f-shell excitation mechanism, a model of the excitation mechanism that is consistent with present experimental results can be constructed.

According to Robins and Dean [1978], a bound exciton state at an isoelectronic trap might be created either by direct

capture of a free exciton or by sequential capture of free carriers. In the first case, illumination of the sample with a laser energy greater than or near E_g results in the creation of free excitons, which can subsequently be trapped by the Er-related hole trap, thus forming a bound exciton. Subsequent recombination of the electron-hole pair at the trap results in a transfer of the recombination energy to the 4f-shell via an Auger energy transfer. Langer [1986] referred to this type of energy transfer as the impurity Auger effect to distinguish it from the more common Auger processes involving free carriers. This process can explain the sharp selective excitation peak with a laser energy of 1.512 eV. Bound excitons can also be formed by sequential trapping of free carriers. In this case, laser illumination of the sample results in the creation of electron and hole pairs. Free holes are subsequently trapped at the Er-related hole trap, and after capturing a hole, the trap will have a slightly electron attractive potential and thus can bind an electron. Recombination of the electron-hole pair at the Er-related trap results in the non-radiative Auger energy transfer of the recombination energy to the 4f shell.

In this model, below-bandgap laser excitation of the 4f shell can be explained as follows:

i. Upon illumination, electrons at the isoelectronic trap can be excited to the conduction band, leaving a hole behind;

ii. The bound hole subsequently recombines with an

electron, transferring its recombination energy to the 4f shell.

In the case of isoelectronic impurities, the attractive potential is a short range potential, and thus, the bound particle is localized around the impurity, causing large lattice distortions around the impurity ion. Consequently, trapping of a particle at this type of center results in large lattice relaxations. This is shown in the configuration coordinate diagram as a horizontal displacement of the parabola representing the energy level. As mentioned in section 2.1, this type of process gives rise to broad excitation bands as observed in the selective excitation spectra of current samples.

The excitation model is illustrated by the configuration coordinate diagram shown in figure 39. The diagram shown is only meant to be a qualitative description of the excitation process, since the various necessary parameters have not all been determined experimentally yet. In the figure, V_b and C_b indicate the valence and conduction band, respectively, while T_{Er} indicates the Er-related isoelectronic trap. As discussed in section 2.1, after trapping a carrier (a hole in this case), the trap is represented by a displaced parabola, T^*_{Er}, which illustrates the lattice relaxation. Two sets of arrows are shown in the figure representing possible transitions involving above- and below-bandgap excitations. Four different steps in the excitation process are illustrated.

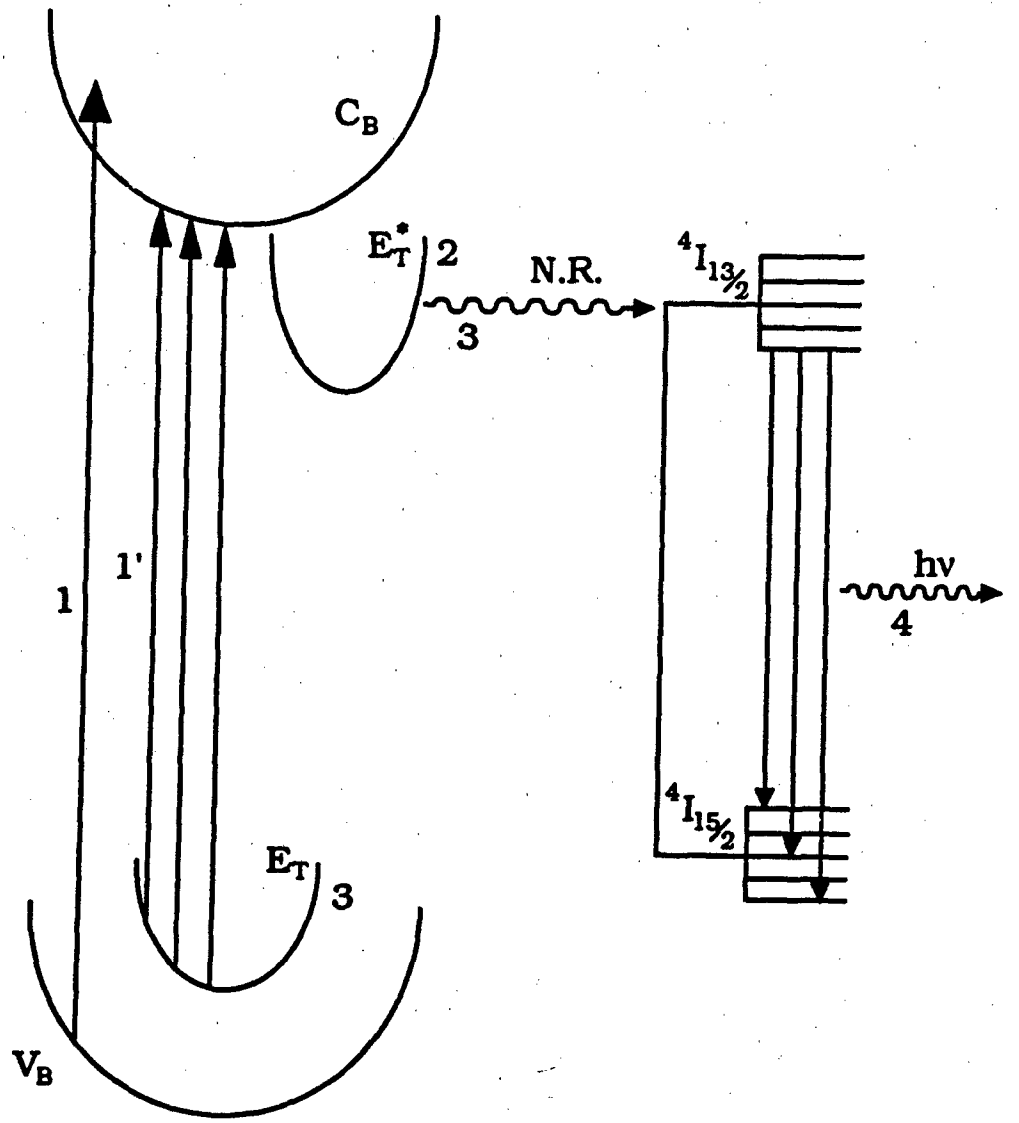

Figure 39 Configuration coordinate diagram illustrating the 4f excitation mechanism in GaAs:Er

Arrow 1 illustrates the excitation of an electron from the valence to the conduction band. In step 2, free holes are trapped, thus raising the energy level to T^{*}_{Er}. In step 3, following electron-hole recombination, this excited level changes back to T_{Er}, while the recombination energy is transferred non-radiatively to the 4f-shell. This will leave the 4f-shell in the $^4I_{13/2}$ excited state. For illustration purposes, the 4f energy levels are arbitrarily placed in the diagram, since the positions of these levels with respect to the GaAs energy bands are not known. Step 4 is the de-excitation process of the 4f shell through a radiative transition to the ground state. Below-bandgap excitation is illustrated by the arrows of primed numbers. Several arrows are shown to illustrate the possibilities of multiple transitions (see section 2.1), which can result in a broad selective excitation band. The exact location of T_{Er} is not known, although DLTS experiments suggest that it might be located just above the valence band. This is consistent with current SEL results, which show a maximum in the selective excitation spectrum with the below-bandgap laser excitation around 60 to 100 meV less than the bandgap energy.

We have consistently observed stronger Er^{3+} emissions from p-type samples than from SI and n-type GaAs substrates. Two processes might contribute to this observed enhancement of the 4f emissions in p-type GaAs:Er. Holes at acceptor levels can be trapped by the Er-related isoelectronic trap. These holes

can subsequently recombine with non-equilibrium free electrons, transferring the recombination energy to the 4f-shell by an Auger type process. Also, holes at the acceptor levels can be excited deep into the valence band. This, in turn, will mean that more free holes are available which can now be trapped at the Er-related hole traps.

One problem that needs to be addressed is the large energy mismatch between the laser excitation energy and the energy of the $^4I_{13/2}$ excited state. In our excitation model, the process $T_{Er} \rightarrow T^*_{Er}$ results in large lattice relaxations with the consequent multiphonon emissions. Two other schemes can be proposed to account for the large energy mismatch, both of which can be consistent with the current excitation model. One possibility is that after the non-radiative energy transfer, step 3, the 4f-shell is left in the $^4I_{11/2}$ excited state with a subsequent decay to the $^4I_{13/2}$ level. The fact that the $^4I_{11/2}$ level should be between 1.3 and 1.24 eV above the $^4I_{15/2}$ ground state, as opposed to approximately 0.8 eV for the $^4I_{13/2}$ level, explains a large portion of the energy mismatch. One problem with this scheme is that it implies a more efficient excitation of the 4f-shell in a narrower gap material, because the excitation would be near resonant. However, the opposite has been observed, that is, intra-4f-shell excitation is more efficient in a wider bandgap material such as AlGaAs and ZnS. For example, Er^{3+} emissions are much stronger in $Al_xGa_{1-x}As$:Er than in GaAs. Also, current SEL results show that the 1.54 μm

emissions can be excited with laser energies smaller than the energy difference between the $^4I_{11/2}$ and the $^4I_{15/2}$ energy levels. Therefore, it seems that the non-radiative energy transfer from electron-hole recombination at the Er-related trap leaves the 4f-shell in the $^4I_{13/2}$ state rather than in the $^4I_{11/2}$ state. Another possibility can be deduced from the results of Klein et al. [1990, 1991], which showed that Er might be originally in the 2+ state. In this scheme, Er is initially in the 2+ state and part of the energy difference is used to ionize the Er^{2+} ions to the 3+ state and most of the remaining energy is used in exciting the 3+ state. However, it is not clear whether Klein's results will apply to all GaAs:Er samples, since Ennen et al. [1987] were able to excite the 1.54 μm emissions resonantly. It should be mentioned that Klein's SEL results differ from the results for the present ion implanted samples, and in fact are similar to results obtained for the MBE samples. Also, current results from temperature dependent lifetime measurements are different to those of Klein et al., which will be discussed in section 4.3. All these suggest that different excitation mechanisms may be involved.

Our excitation model can also account for the excitation power dependence of the Er^{3+} emissions. We have consistently observed a sublinear power dependence. At low excitation power the Er^{3+} PL intensity shows a square root dependence on the excitation power. Benyattou et al. [1991, 1992] observed a similar behavior in $Al_{0.55}Ga_{0.45}As$:Er. These authors argued that

an exciton bound at the Er trap have two different recombination channels: (i) energy transfer to the 4f shell, (ii) energy transfer to free carriers by Auger recombination. The first channel will result in excitation of the 4f shell, while the second is responsible for losses in the excitation process. This model was presented in section 2.3.6. It predicts a square root dependence on the excitation power. In our samples, we also observed a sublinear power dependence for the underlying bb emission. In addition there is a saturation effect, which was discussed in sections 4.1.4 and 4.2.3. When the excitation power exceeds the saturation point a greater percentage of it goes into exciting the bb emission, thus suggesting that these are competing processes. Assuming a model similar to Benyattou's, the Er-related trap is very efficient in trapping free carriers. However, the excitation efficiency of the 4f shell is limited by a competing Auger energy transfer to free carriers. These hot carriers are then available for recombination at other deep centers, such as the EL2 trap. At high excitation powers the Er trap will be almost completely populated, thus resulting in the observed saturation effect. At this point, the excess photogenerated carriers can recombine at other trapping centers. In this model, the rate equation can be written:

$$-\frac{dn_E^*}{dt} = N_{exc}(t)\frac{P_1}{P_1 + Bn} - \frac{n_e^*}{\tau_f}.$$

The symbols used were explained in page 32. Note that the number of bound excitons, $N_{exc}(t)$, will depend on the free carrier concentration since at higher carrier concentrations the probability of trapping a carrier will increase. On the other hand, the probability of energy transfer from the bound exciton to the 4f shell is given by $P_1/(P_1 + Bn)$. This term decreases with increasing carrier concentration. Therefore, we should expect that as the carrier concentration increases the Er^{3+} PL intensity will increase until the decrease of the energy transfer probability offsets the increase in the trapping probability. Beyond this point the PL intensity will decrease. This observation is consistent with the results discussed in section 4.1, on the Er^{3+} PL study for different n- and p-type samples.

4.3 Lifetime Measurements of 4f Excited States of Ion Implanted GaAs:Er

4.3.1 Introduction

Lifetime measurements of excited states can provide important information concerning the de-excitation and excitation mechanisms. In this work, the decay of the Er^{3+} emissions was studied. In particular, information was sought on non-radiative processes affecting these emissions, and on the nature of the observed temperature quenching of these emissions. Decay times of the emissions near 1.54 μm have been measured by other researchers for Er doped GaAs, InP, and $Al_{.45}Ga_{.55}As$. The reported values range from 150 μsec to 1.5 msec [Klein and Pomrenke, 1989]. The decay time depends not only on the host material, but also on the doping method and sample treatment. In this study, the decay time of the main Er^{3+} emission from ion implanted and MBE-grown GaAs:Er and $Al_xGa_{1-x}As$:Er is reported. Erbium was implanted with an ion energy of 1 MeV at a dose of 5 x $10^{13}/cm^2$. For ion implanted samples, the decay rates of the Er^{3+} emissions were studied as a function of substrate conductivity type and for n-type samples as a function of carrier concentration. In addition, for the 1.54 μm emissions, the decay time was also studied as a function of temperature. The MBE-grown $Al_xGa_{1-x}As$:Er sample showed very strong emissions, and thus it was possible to measure the decay times from ten different sharp emissions in

the 1.5 to 1.6 μm region. Also, the lifetimes of various of these emissions were studied as a function of sample temperature. This provided important information on the different luminescent centers present in this sample. Lifetime measurements were also performed on samples co-doped with oxygen. The results for the ion implanted samples will be presented in this section. The results for the MBE-grown samples will be presented in section 4.4, and those for the samples co-doped with O will be discussed in section 4.5.5.

4.3.2 Data Analysis

The experimental setup for the lifetime measurements and the system response were discussed in section 3.3, and the measured system response, τ_s, was found to be approximately 15 μsec. Since most of the measured decay times, τ, were in the order of 1 msec, the condition $\tau_s << \tau$ applies for most of the current measurements. Therefore, it would seem that it is not necessary to consider the system response. However, even with long decay times, the system response does affect the transient being measured, in particular, the rise time. This can be understood by considering that the observed decay is really the convolution of the signal's decay, e(t), and the system's response, i(t). Since the excitation pulse was 9-12 nsec, it can be assumed to be a delta function. Assuming

both decays to be a single exponential, i.e.,

$$i(t) \propto \exp(-\frac{t}{\tau_s}) \quad ; \quad e(t) \propto \exp(-\frac{t}{\tau}),$$

the observed decay will be:

$$D(T) = A(\exp(-\frac{t}{\tau}) - \exp(-\frac{t}{\tau_s})),$$

where A is a constant whose value depends on τ and τ_s. When $\tau_s << \tau$ and at $t >> \tau_s$, the effect of the system response can be ignored. However, at short times the decay will be affected, in particular, the second term in the last equation will introduce a relatively slow rise time, even when assuming an instantaneous excitation pulse. This can be seen by calculating the time, t_m, at which the signal shows a maximum. Taking the derivative of D(t) and equating it to zero:

$$D'(t) = 0 = A(-\frac{1}{\tau}\exp(-\frac{t}{\tau}) + \frac{1}{\tau_s}\exp(-\frac{t}{\tau_s})).$$

Solving this equation yields:

$$\rightarrow \frac{1}{\tau}\exp(-\frac{t}{\tau}) = \frac{1}{\tau_s}\exp(-\frac{t}{\tau_s})$$

$$\rightarrow \frac{\tau_s}{\tau} = \exp(\frac{t}{\tau} - \frac{t}{\tau_s})$$

$$\rightarrow t(\frac{1}{\tau} - \frac{1}{\tau_s}) = \ln\frac{\tau_s}{\tau}$$

$$\rightarrow t_{max} = \frac{1}{\frac{1}{\tau} - \frac{1}{\tau_s}}\ln(\frac{\tau_s}{\tau}) = \frac{\tau\tau_s}{\tau_s - \tau}\ln(\frac{\tau_s}{\tau}).$$

Thus, even with an instantaneous excitation, the transient

will rise relatively slowly, and will show a maximum at t_{max}. For example, for τ_r = 15 μsec and τ = 1000 μsec,

$$t_{max} = \frac{15000}{985}\ln(.015) = 63.95\mu\text{sec}$$

This example is representative of our results. Note that even if the emission signal rises to its maximum at t = 0 after the excitation pulse, the observed decay will take approximately 64 μsec to reach its maximum. Thus it requires caution when trying to obtain information from the rise time of the observed signal. It is particularly omnimious since t_{max} has the same functional form as various proposed excitation mechanisms for the luminescence (Demas [1983], pp. 117-126). For example, it is interesting to note that the delay in the rise of the Yb^{3+} signal from InP:Yb observed by Kasatkin et al. [1985] was fitted to an equation that has the same functional form as t_{max} (see sec 2.3.5.1). Since these authors did not discuss the system response of their experimental setup, their results are somewhat doubtful.

Since in our case $\tau >> \tau_r$, the exponential decay associated with τ_r decreases much faster than the true emission decay itself. Therefore, at long enough times, the decay will be a single exponential with time constant τ. One way to determine τ is to fit the data after a delay time t_d from the signal maximum. In that case τ will have an error that depends on the value of t_d. Demas [1983] summarized the expected errors

Table III

Required delay (in units of τ) past the maximum intensity in order to obtain a given error associated with the system response (Demas [1983], pp. 122)

Error ≤ τ_s/τ	10%	5 %	1%	0.1%
0.05	0.12	0.16	0.24	0.36
0.10	0.25	0.32	0.50	0.76
0.15	0.38	0.50	0.78	1.19
0.20	0.53	0.70	1.10	1.67
0.25	0.68	0.91	1.44	2.21
0.30	0.85	1.14	1.82	2.81
0.35	1.04	1.40	2.25	3.49
0.40	1.24	1.68	2.73	4.27
0.45	1.46	1.99	3.29	5.16
0.50	1.70	2.35	3.92	6.22

in τ for specific t_d values (in units of τ) as shown in table III. The first column on the table indicates the ratio τ_s/τ, and the top line shows the maximum error for a specific value of t_d. For example, if $\tau_s/\tau = 0.1$, and the data is fitted with $t_d = .12\tau$ then the error will be smaller than 10%. But if $t_d = .76\tau$, for the same τ_s, then the error due to the system's response will be smaller than 0.1 %. In our case τ_s/τ is typically on the order of .015, and $t_d \approx .3\tau$ was chosen, therefore the error associated with τ_s will be smaller than 0.1 %. There is a tradeoff between minimizing the effect of τ_s and having a signal strong enough to be able to fit. The longer t_d the weaker the signal will be, thus making the fitting less reliable. This is especially true when studying

the τ dependence on temperature, since τ decreases with increasing T, and the signal strength gets much weaker. So far it was assumed that the decay is a single exponential, but current results show that it is composed of two decay components. This complicates the data analysis, since the lifetime of the fast decay component seems to be even smaller than the system response.

4.3.3 GaAs:Er

Figure 40 shows the low temperature decay of the main Er emission from Er ion implanted SI, n-, and p-type GaAs implanted with an ion dose of 5 x $10^{13}/cm^2$ at an energy of 1 MeV. The p-type substrate was ion implanted with Mg at $10^{16}/cm^3$, while the n-type MOCVD-grown substrate was doped with Si at 4.9 x $10^{15}/cm^3$. In figure 40, the symbols indicate the experimental data, and for the sake of clarity, only one of every 20 data points is plotted. All three decays show fast decay components in the first 300 to 500 μsec after the excitation pulse. This component is most probably due to the underlying bb emission. After 500 μsec, the signal decays much more slowly and it appears to be a single exponential decay. The solid lines show a single exponential fit to the slow component of the decay. The decay times obtained from the least square fit were 1.07, 0.98, and 1.13 msec for the SI, n-, and p-type sample, respectively.

The n-type sample has the shortest lifetime, and the decay

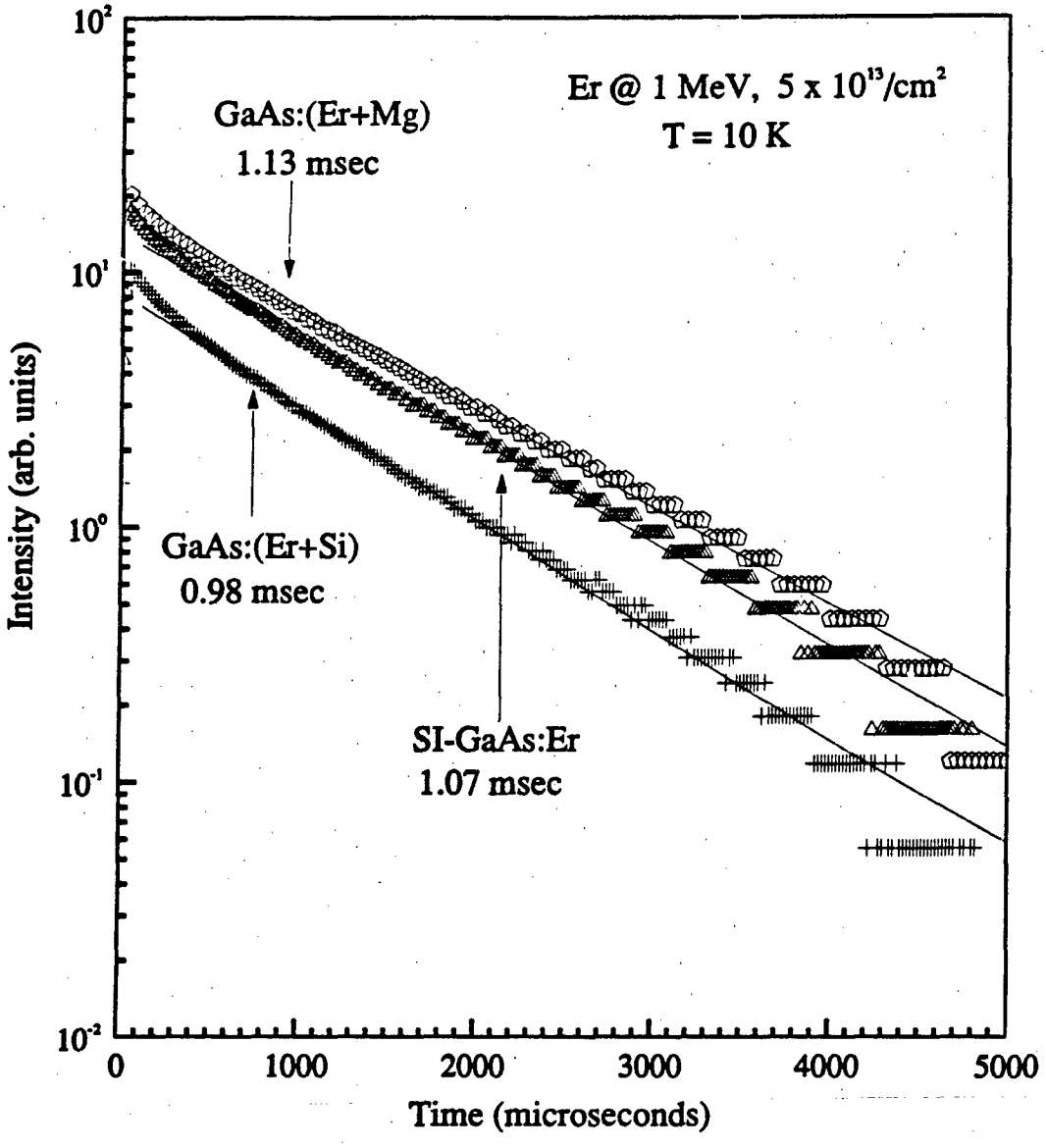

Figure 40 Time decay of the 1.538 μm Er^{3+} emission from SI, n-, and p-type GaAs:Er implanted at an ion energy of 1 MeV with a dose of 5 x $10^{13}/cm^2$

time may depend upon the Si doping level. In order to determine the influence of the Si doping level on the decay of the Er^{3+} emissions, lifetime measurements were made on the three different Si doping levels of n-type samples, and the results are shown in figure 41. The PL spectra from these samples were discussed in section 4.1, and they were plotted in figure 10.

The solid lines show a single exponential fit to the experimental values. As before, the fit was done for the decay curve from 0.5 to 5 msec after the excitation pulse. The sample doped with Si at $4.9 \times 10^{15}/cm^3$ is the same sample used in figure 40. At a higher Si concentration, $3.3 \times 10^{17}/cm^{13}$, the lifetime increases to approximately 1 msec. This sample shows the strongest signal of the three, and also, the initial fast decay is hardly noticeable. The sample with the highest Si concentration shows the weakest signal. In this case, the effect of the initial fast decay is much more pronounced. At 400 μsec after the excitation pulse, the signal strength is decreased by a factor of three. However, the slow component has the longest lifetime of the three samples. That is, the lifetime consistently increased with increasing Si concentration. It is interesting to correlate these results with the low temperature PL, which was shown in figure 10. As the Si concentration increased from 4.4×10^{15} to $3.3 \times 10^{17}/cm^3$, the PL intensity of the Er^{3+} emissions and the underlying bb emission increased. Since the lifetime of

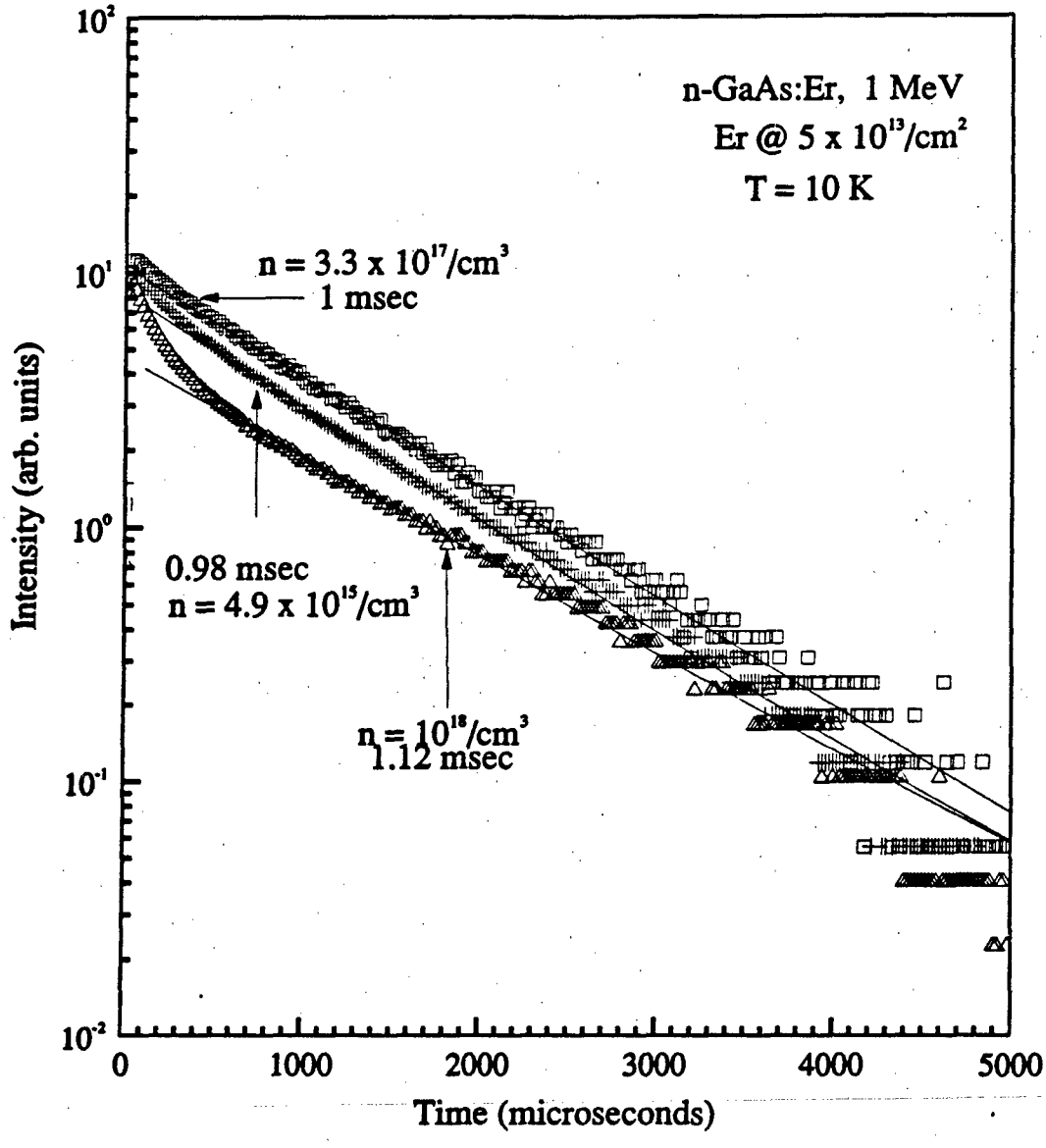

Figure 41: Time decay of the 1.538 μm Er^{3+} emission from n-GaAs:Er implanted at 1 MeV with a dose of 5 x $10^{13}/cm^2$ for different Si doping levels

the bb emission is probably several orders of magnitude smaller, the initial fast decay is most probably due to this bb emission. Also, because the Er^{3+} emissions are much stronger, the decay is mostly dominated by the slow component. On the other hand, the sample having the highest Si concentration shows a small decrease in the intensity of the underlying bb emission, but the intensity of the Er^{3+} emissions decreased considerably. As a result, the initial decay is dominated by the bb emission. The decrease in the Er^{3+} PL intensity at the highest Si doping can be explained by an increased competing Auger energy transfer from the Er-bound exciton to free carriers, such as proposed initially by Benyattou et al. [1990, 1991]. This was discussed in the excitation model presented in section 4.1.3. Upon illumination, hot carriers are created by excitation from the donor level. As discussed previously, increasing the carrier concentration beyond a certain level will result in a smaller probability of energy transfer from the Er-bound exciton to the 4f-shell. Of course this process will only affect the excitation efficiency as indicated by the PL intensity at t = 0, and it should not affect the lifetime. Furthermore, the lifetime increased with Si concentration, and this might be due to the presence of an additional excitation mechanism in the doped samples. One possibility is that holes trapped at the Er-related trap may recombine with electrons at the donor level. This process will be much slower than

recombination with free electrons. It will also depend on the Si concentration. At high Si concentrations, the distance between the Er and Si ions will be smaller, thus increasing the probability of this process. This could also explain the presence of a small peak close to the bandedge in the SEL spectra, since this weak excitation peak could then be interpreted as due to the excitation of electrons from the valence band to the donor states. The presence of a fast and a slow excitation process will affect the decay, resulting in apparently longer decay times.

Temperature dependent lifetime measurements were done on the SI-GaAs sample, and figure 42 shows the Er^{3+} decay at 10, 40, 100, and 160 K. The initial fast component was seen at all temperatures. It is interesting to compare present results with those obtained by Klein et al. [1991]. These authors studied the time decay from ion implanted GaAs:Er, and they found that the Er^{3+} decay consisted of a fast and a slow component. However, the low component was found to be non-exponential, and independent of the sample temperature. Furthermore, the fast component of the decay was attributed to the Er^{3+} emissions. In contrast to these results, current results show the slow component can be considered to be a single exponential decay at all temperatures, as shown in the figure by the solid lines, which represent a single exponential fit to the experimental values. Also, the lifetime decreases as the sample temperature increases, even

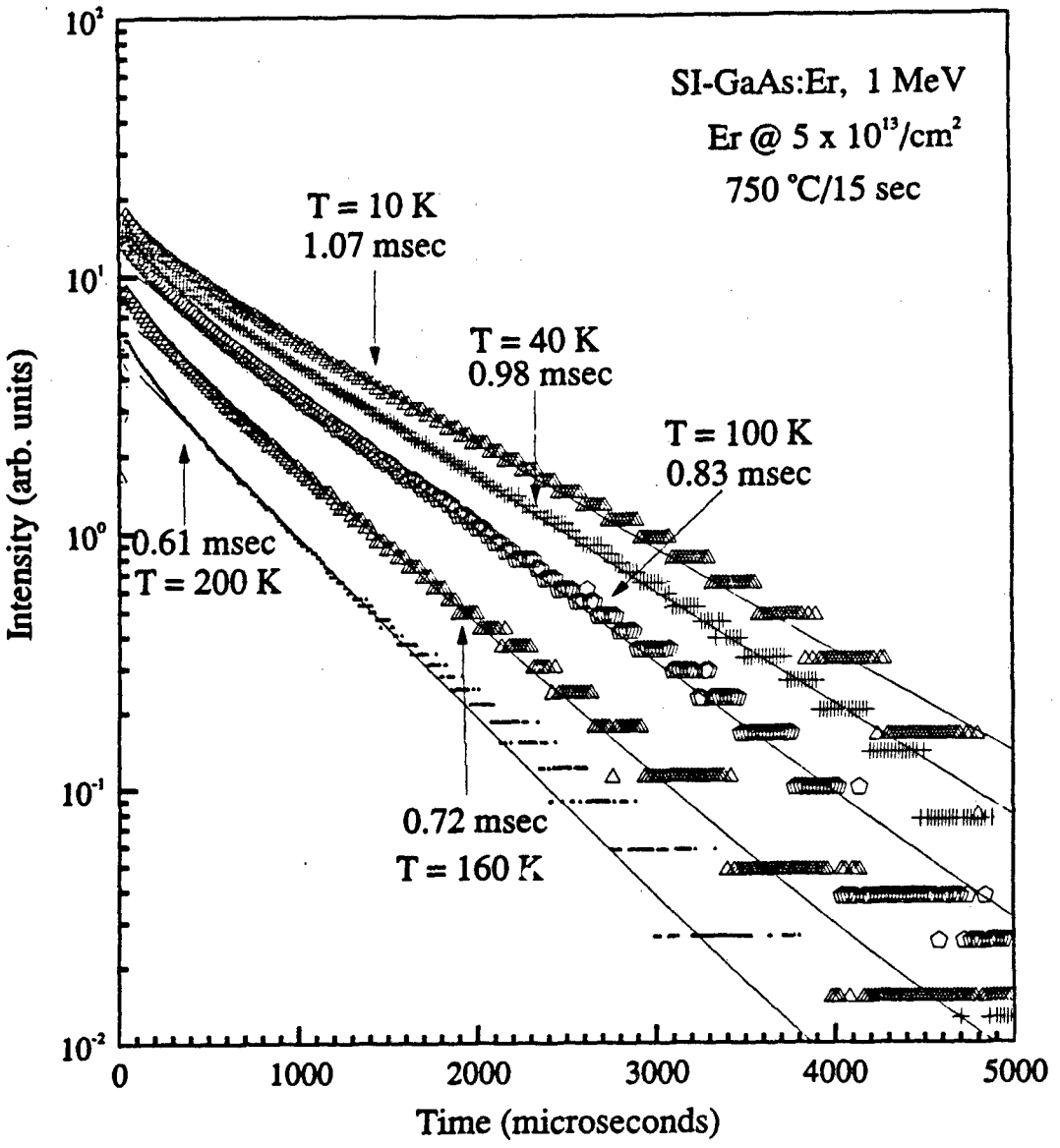

Figure 42 Time decay of the 1.538 μm Er^{3+} emission from SI-GaAs:Er implanted at 1 MeV with a dose of 5 x $10^{13}/cm^2$ at different sample temperatures

at temperatures below 100 K. Finally, we assigned the fast component of the decay as due to the underlying bb emission, while Klein's samples did not show this bb emission.

Figure 43 shows a plot of the lifetime as a function of 1/T. The solid line shows a fit to:

$$\tau(T) = \frac{\tau(0)}{1 + A_1 \exp(-\frac{E_1}{kT}) + A_2 \exp(-\frac{E_2}{kT})}$$

The fitting parameters are $A_1 = 1.05$, $E_1 = 9$ meV, $A_2 = 2959$, and $E_2 = 169$ meV. Although for RE doped III-V materials the integrated PL intensity dependence on temperature is normally fitted to two activation energies, a fit with only one activation energy is expected for the lifetime dependence on temperature (Thonke et al., [1990]). The reason being that in InP:Yb the activation energies obtained from the temperature dependence of the integrated intensity have been interpreted as due to the quenching of the 4f luminescence by thermal emission of the trapped particle to the bands or by dissociation of the exciton bound to the traps. Therefore, in that case one expects to obtain a large activation energy corresponding to the trap energy and a small activation energy corresponding to the binding energy of the exciton to the traps. However, dissociation of the bound exciton will only affect the excitation efficiency and should not affect the lifetime. Therefore, it is surprising that the experimental data for GaAs:Er couldn't be fitted with a single activation

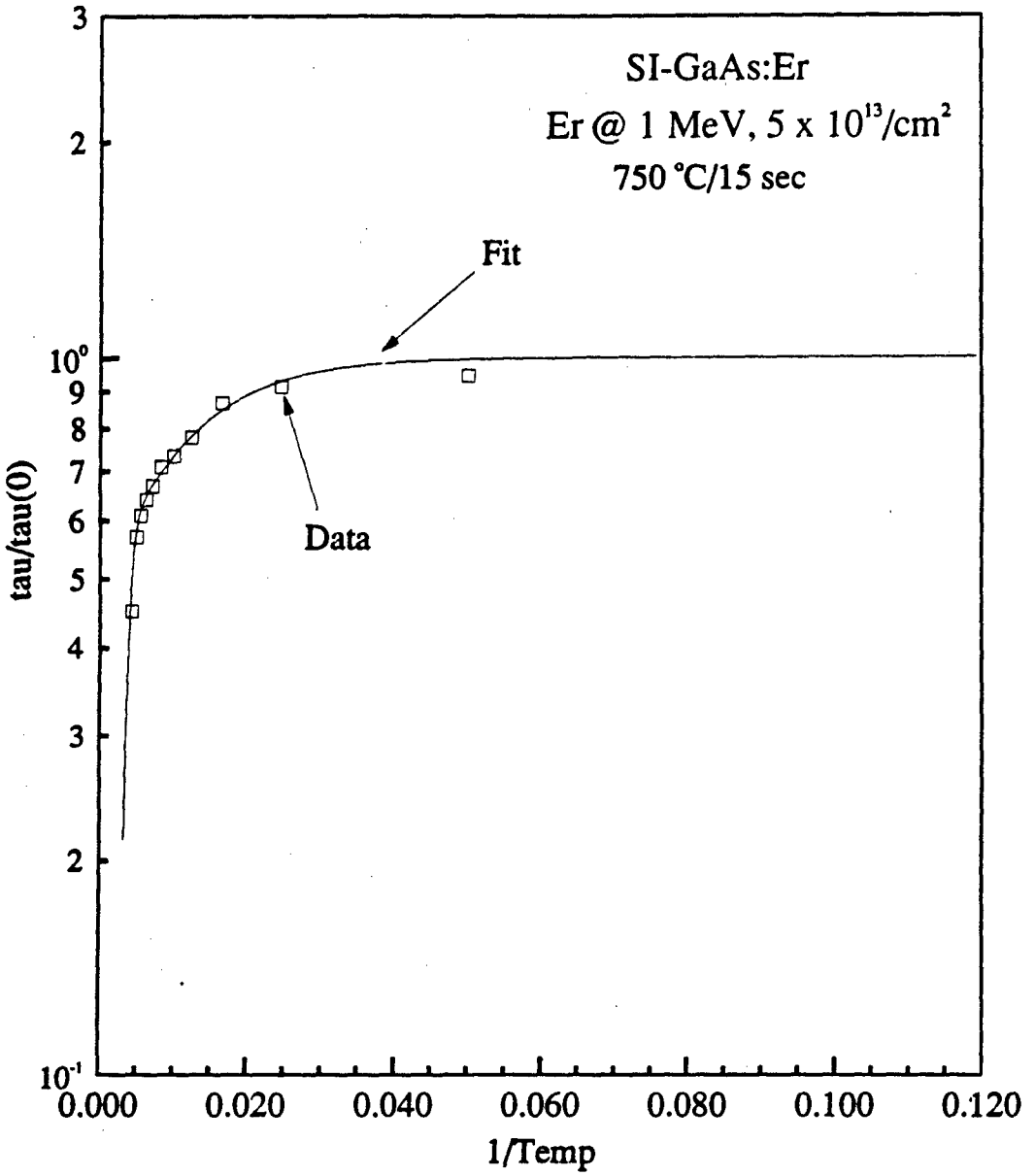

Figure 43 The ratio of lifetimes at T and T = 10 K, $\tau(T)/\tau(0)$, as a function of sample temperature

energy.

At present, E_2 can be interpreted as the sum of the Er-related trap energy and the bound exciton binding energy, however, we do not have a proper interpretation of E_1. The much smaller magnitude of A_1 compared to A_2 suggests that this mechanism is much more inefficient than the mechanism with the larger activation energy. Finally, these values must be interpreted with care, since the temperature quenching is most probably due to a combination of several processes. One of these processes is the de-excitation by energy transfer from the Er^{3+} excited state to free carriers. Thus, in the present case a SI-GaAs sample was used to minimize the effect of this last process. The presence of several quenching processes that affect the temperature dependence of the Er^{3+} emissions reduces the reliability of results obtained from this type of analysis. In order to obtain a better understanding of these processes, it is necessary to do further work.

In conclusion, the results obtained from lifetime measurements can be explained consistently by using our excitation model, although more work in this area is needed in order to obtain a proper interpretation of some of the results obtained such as the small activation energy E_1. There are still some discrepancies between the results reported here and those of other researchers. Two possible reasons for these discrepancies are: (i) the presence of multiple luminescence centers in Er doped GaAs, and, (ii) the fact that the

temperature quenching is most probably due to a combination of various processes. Because of these, the results of lifetime measurements and temperature dependence studies will be sample dependent.

4.4 Intra-4f Emissions from MBE-grown GaAs:Er and $Al_xGa_{1-x}As$:Er

The optical studies of Er doped GaAs and $Al_xGa_{1-x}As$ layers grown by conventional solid source molecular beam epitaxy (MBE) are the subject of this section. $Al_xGa_{1-x}As$:Er and GaAs:Er layers were grown on (001) GaAs substrates, but some layers of GaAs:Er were also grown in other directions. The aluminum mole fraction values used for $Al_xGa_{1-x}As$:Er are $x = 0.33$, 0.5, and 0.7. The Er concentration versus the Er cell flux was calibrated using secondary ion mass spectroscopy (SIMS) measurements. The Er^{3+} emissions were studied as a function of substrate growth temperature and Er concentration. In addition, some Si co-doped samples were also grown.

4.4.1 Growth Characterization: SIMS and RHEED Measurements

The SIMS measurements were calibrated by measuring the profile of an Er ion implanted SI-GaAs sample. In turn, SIMS profile measurements of GaAs:Er grown at a substrate temperature (T_s) of 300 °C were performed to calibrate the Er-cell flux. Erbium doping levels of up to $5 \times 10^{20}/cm^3$ were easily obtained as were sharp concentration profiles. In order to study Er incorporation at different substrate growth temperatures, an Er doped GaAs layer was grown in a square wave fashion while T_s was reduced in steps from 660 to 500 °C. The doping profile of this sample and SIMS profile measurements are shown in figure 44 along with the substrate

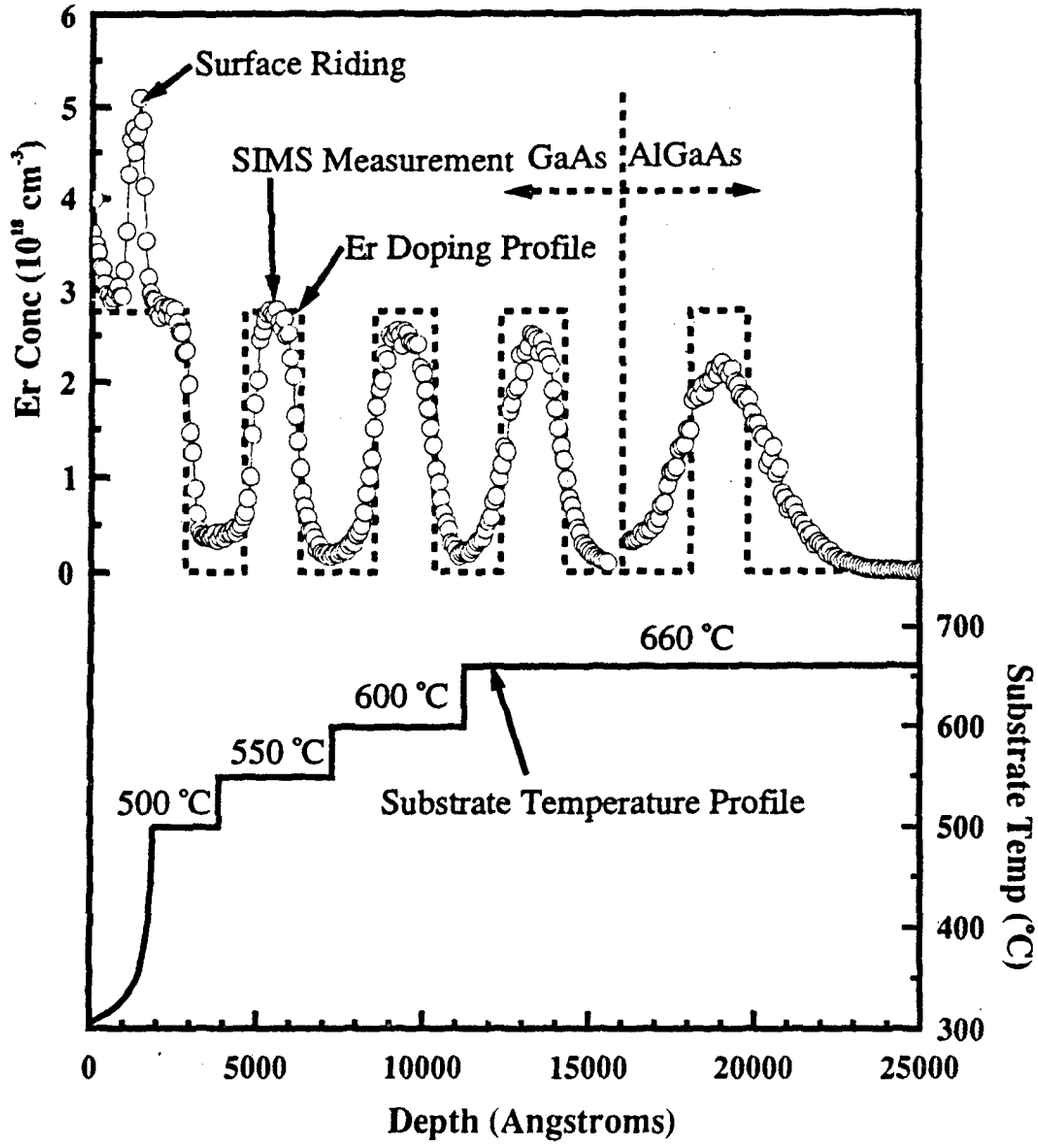

Figure 44 Er doping profile and SIMS profile measurements of MBE GaAs:Er layers grown at various substrate temperatures

growth temperature profile. As can be seen from the figure, the Er peak concentration is independent of T_s from 500 to 660 °C, and is approximately equal to the value expected based on Er-vapor pressure data, thus indicating a 100% Er-incorporation efficiency for $T_s \leq 660$ °C. After growth of 200 nm of GaAs:Er at 500 °C, T_s was ramped to 300 °C, as shown in the figure, while GaAs:Er growth continued. The presence of the spike in [Er] indicates that Er was riding on the surface, and was subsequently incorporated into the lattice when T_s was dropped from 500 °C. The spike represents approximately one Er monolayer. This effect can be important when co-doping with other species, for example Si, since the probability for the second species encountering an Er ion to form a complex will be very high. The steepness of the [Er] profile between undoped GaAs and GaAs:Er layers is reduced for higher T_s values, thus suggesting a thermally activated diffusion mechanism, at least in the growth direction of the substrate. However, in the growth direction, surface riding may be more important than simple thermal diffusion for [Er] profile broadening. Reflective high energy electron diffraction (RHEED) intensity damping and recovery behavior during and upon interrupting the GaAs:Er growth are consistent with the SIMS results, indicating significant surface riding of Er at $T_s \geq 500$ °C. RHEED intensity profiles showed increased damping of the intensity oscillations for [Er] $\geq 4 \times 10^{19}/cm^3$. GaAs:Er growth interruption resulted in

recovery of the RHEED specular beam intensity at a rate that was approximately one order of magnitude slower than that obtained for GaAs growth interruption. Growth of up to ten monolayers of GaAs on the interrupted GaAs:Er surface resulted in very little enhancement of the RHEED intensity recovery rate.

4.4.2 Photoluminescence Measurements

As for the ion implanted samples, MBE-grown GaAs:Er and $Al_xGa_{1-x}As$:Er layers show multiple sharp emissions between 1.53 and 1.6 μm. All of these emissions have been assigned to the intra-4f transitions between the crystal field split states of $^4I_{13/2}$ and $^4I_{15/2}$ of Er^{3+}. The emission spectrum depends strongly on growth conditions, erbium concentration, and co-doping. Figure 45 shows the low temperature PL from GaAs:Er and $Al_xGa_{1-x}As$:Er layers for the values of x = 0, 0.33, 0.5, and 0.7. The spectra shown are for MBE layers grown at T_s = 580 °C with [Er] = 1.5 x $10^{19}/cm^3$. The PL spectra for the x = 0.33 and 0.5 samples were recorded using narrower slit openings than for the two other samples. The emissions from the x = 0.7 sample appear to have wider linewidths because of the difference in resolution. From the figure, two different sets of emissions can be distinguished: a group of very sharp emissions near 1.54 μm and another group near 1.565 μm. The 1.565 μm emissions are only observed in the PL of $Al_xGa_{1-x}As$:Er

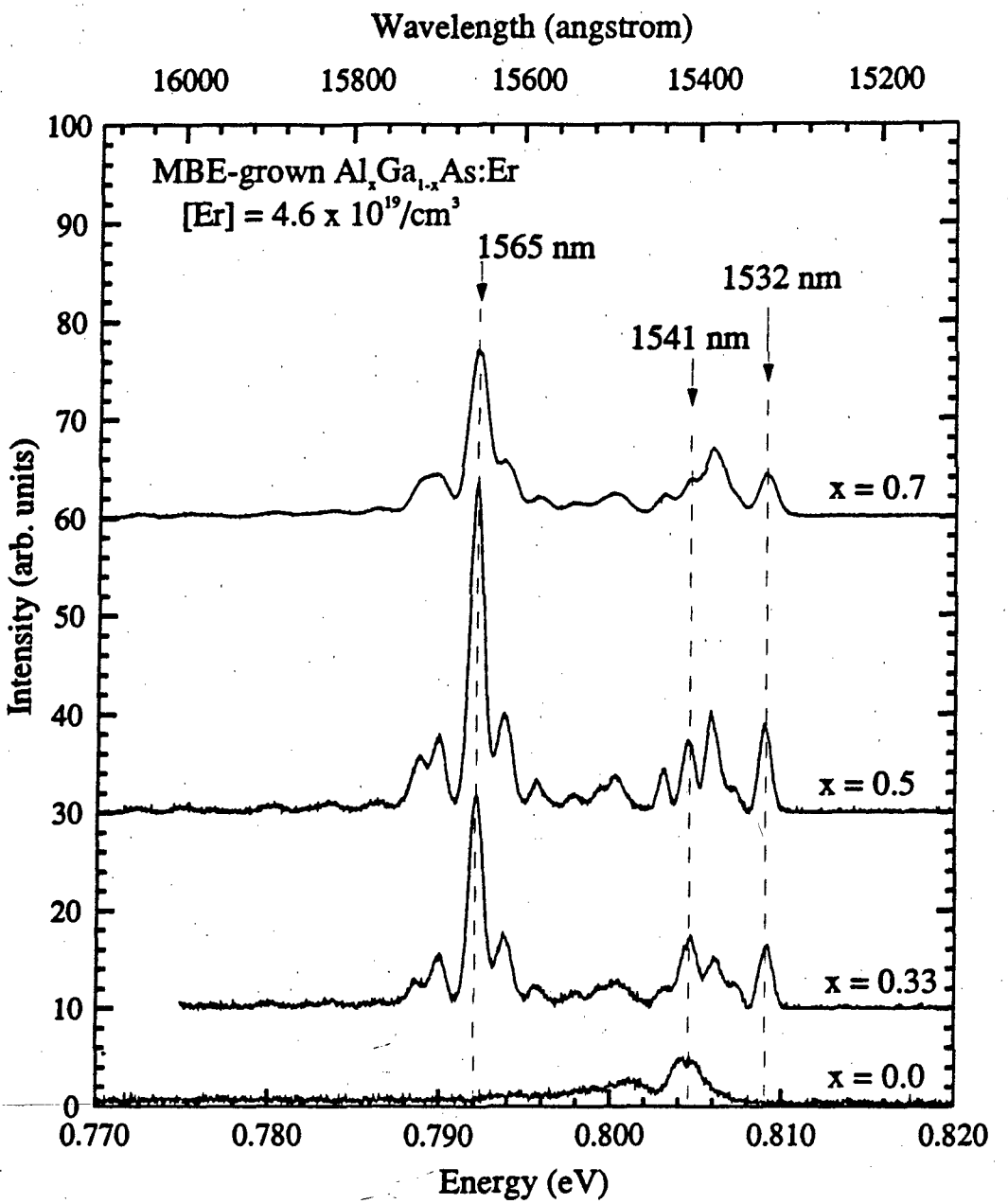

Figure 45 Low temperature PL from MBE grown GaAs:Er and $Al_xGa_{1-x}As$:Er (x = 0.33, 0.5, and 0.7)

samples, and consist of four or more emission peaks. Although the relative intensity among the various peaks changes with x, many of the emissions are observed at the same positions independent of the x value, except for those of GaAs:Er. This is indicative of the atomic nature of these emissions. Furthermore, changes in relative intensities are mostly due to differences in growth conditions and Er concentrations, and not due to the host material itself. This will become evident after discussing the effect of T_s and the Er concentration on the Er^{3+} emissions.

In order to study the effect of T_s on the Er^{3+} luminescence, Er doped GaAs and $Al_{0.33}Ga_{0.67}As$ layers were grown at T_s = 560, 580, 600, and 620 °C on a buffer layer grown on top of the SI-GaAs substrate. A 0.75 μm layer of GaAs:Er with an Er concentration of 4 x $10^{19}/cm^3$ was grown on the buffer layer, followed by a 0.75 μm layer of $Al_{0.33}Ga_{0.67}As$:Er with the same Er concentration. Finally, a 50 Å GaAs layer was grown on the very top. To study the luminescence from the GaAs:Er layers, approximately 9000 Å were etched from each sample. Figure 46 shows the low temperature PL from $Al_{0.33}Ga_{0.67}As$:Er layers grown at different T_s. The PL was excited using the 488 nm line of the Ar ion laser at a sample temperature of 6 K. The dominant feature in the PL from the sample grown at T_s = 560 °C is a doublet structure with peaks at 1.540 and 1.542 μm. At T_s = 580 °C, a weak emission at 1.538 μm begins to show, and it grows in intensity as T_s increases, and dominates the PL

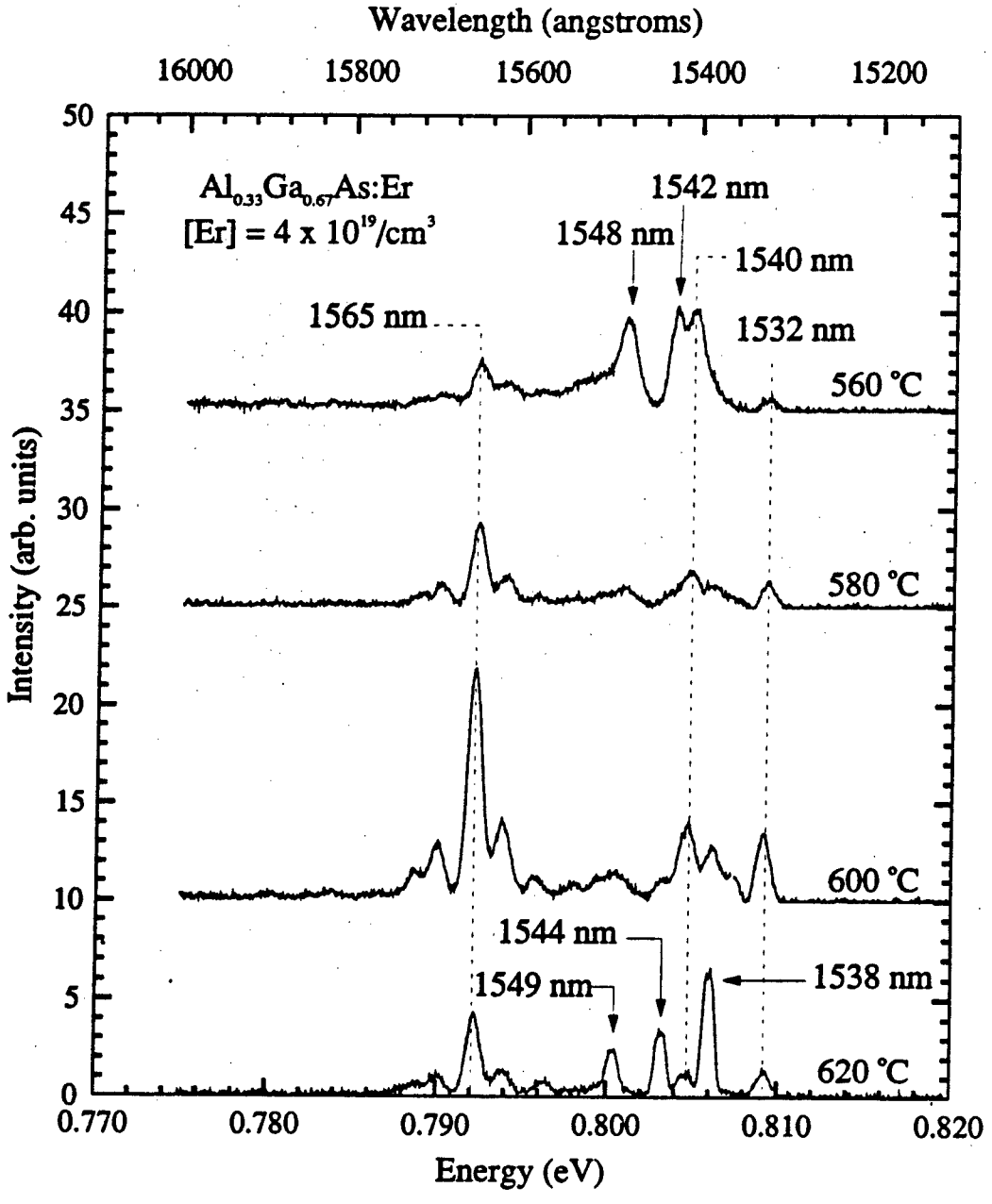

Figure 46 Low temperature PL from $Al_{0.33}Ga_{0.67}As$:Er layers grown by MBE at different substrate temperatures

spectrum at 620 °C. The peaks near 1.56 μm increase fourfold in intensity as T_s increases from 560 to 600 °C, but the intensity decreases at T_s = 620°C. An interesting observation is that the peak centered near 1.532 μm shows the same trend as the 1.565 μm emissions. Therefore, the 1.532 μm emission might originate from the same Er complex center giving rise to the 1.565 μm emissions. Later, we will discuss this point in greater detail. The group of 1.54 μm emissions originate from at least three luminescent centers. This can be deduced by comparing PL intensities of peaks at 1.532, 1.536, 1.538, 1.540, 1.542, and 1.548 μm for each spectrum shown in the figure. Changes in relative intensities among these peaks show that they originate from different luminescent centers.

The effect of T_s on the PL spectrum of GaAs:Er in the 1.5 to 1.6 μm region is shown on figure 47. In all four cases, the Er^{3+} emissions are much weaker than for $Al_{0.33}Ga_{0.67}As$. The sample grown at 620 °C shows the weakest emissions. However, the 1.538 μm peak, which is the strongest emission near 1.54 μm in $Al_xGa_{1-x}As$, is appreciable only at T_s = 620 °C for GaAs. This is consistent with the results discussed previously that the intensity of this peak is very weak at lower T_s as shown in figure 46. In the present case, the strong emissions are centered at 1.5406, 1.5426, and 1.5482 μm. At T_s = 560 °C the PL is dominated by the peaks at 1.5406 and 1.5482 μm, as in $Al_{0.33}Ga_{0.67}As$:Er at 560°C. The main difference between GaAs and $Al_{0.33}Ga_{0.67}As$ is the relative

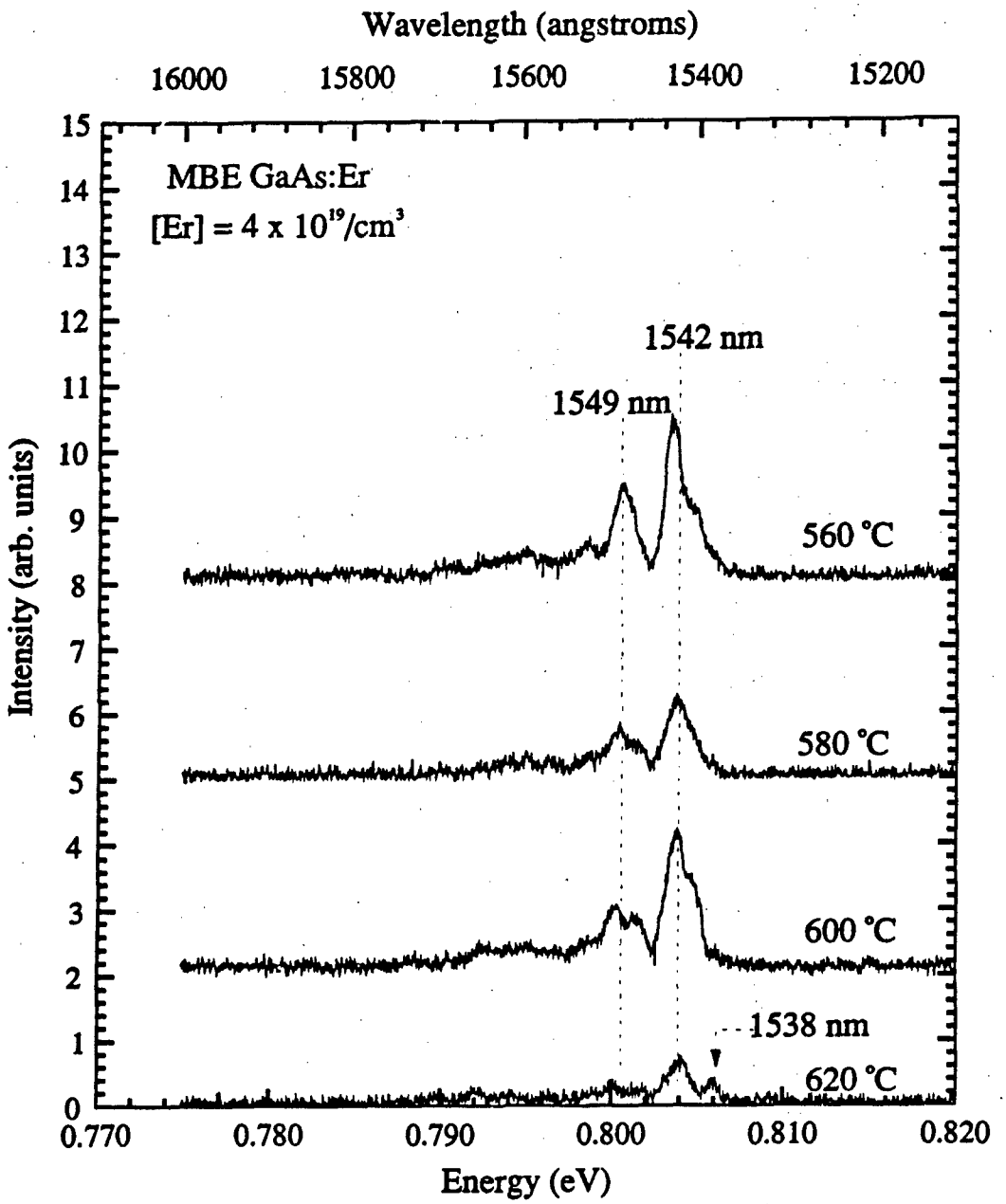

Figure 47 Low temperature PL from GaAs:Er layers grown by MBE at different substrate temperatures

intensity between the 1.5406 and 1.5426 μm peaks, since the 1.5426 μm peak is much stronger in GaAs:Er. Unfortunately, no clear trend can be observed as a function of T_s. However, the intensities of the 1.5406 and 1.5426 μm peaks decrease from 560 to 580 °C, then increase at 600 °C and finally decrease significantly at 620 °C. A careful examination of figure 46 will reveal a similar behavior for the 1.5406 μm emission from $Al_{0.33}Ga_{0.67}As$:Er. However, variations in the PL intensity for the GaAs:Er samples are not significant, since the overall 4f emissions are very weak, and only small intensity changes are observed. The reason for the weak 4f emissions in GaAs:Er is most probably because of the Er concentrations used. Recent studies [Poole, 1992] have shown that the Er solubility limit in GaAs is only $5 \times 10^{17}/cm^3$. Thus, doping at higher concentrations may result in the formation of optically inactive ErAs microparticles. At much higher concentrations, the size of these microparticles increases, causing dislocations and other defects. In the current case, the Er concentration is approximately two orders of magnitude higher than the solubility limit.

In order to study the effect of the Er concentration on the Er^{3+} emissions, the low temperature PL from $Al_{0.5}Ga_{0.5}As$:(Er+Si) and $Al_{0.5}Ga_{0.5}As$:Er samples were studied as a function of Er concentration. The samples were grown at T_s = 580 °C in a similar fashion as the samples used in the T_s study. A 1 μm thick $Al_{0.5}Ga_{0.5}As$:Er layer was grown following a buffer layer on

a SI-GaAs substrate. This layer was followed by another 1 μm thick $Al_{0.5}Ga_{0.5}As$:(Er+Si) layer and a 50 Å GaAs cap layer on top of the structure. Therefore, for the luminescence study of the layers without Si co-doping, approximately 1.1 μm was etched off from the particular structure. The PL spectra of the $Al_{0.5}Ga_{0.5}As$:(Er+Si) and $Al_{0.5}Ga_{0.5}As$:Er samples are presented in figures 48 and 49, respectively. As shown in figure 48 for the case of Si co-doping, at the lowest Er concentration of $1.7 \times 10^{17}/cm^3$, only very weak emissions are observed, both in the 1.54 and 1.56 μm regions. Increasing the Er concentration to $2.7 \times 10^{18}/cm^3$ results in an increase in the PL intensity of the 1.538 μm peak by a factor of 30. However, the 1.538 μm peak intensity decreased slightly upon increasing the Er concentration to $1.5 \times 10^{19}/cm^3$. After a further increase in the Er concentration to $4.6 \times 10^{19}/cm^3$, the Er^{3+} emissions were almost completely quenched, and at [Er] = $2.0 \times 10^{20}/cm^3$, no Er^{3+} emissions can be observed.

The 1.56 μm emissions show a slightly different trend. As the Er concentration was increased from 1.7×10^{17} to $2.7 \times 10^{18}/cm^3$ the PL intensity increased approximately 12 times. At a higher Er concentration of $1.5 \times 10^{19}/cm^3$, the PL intensity of the 1.56 μm emissions was increased further. As with the case of the 1.54 μm emissions the 1.56 μm emissions are quenched at higher Er concentration. Therefore, the optimum Er concentration for these emissions is between 2.7×10^{18} and $1.5 \times 10^{19}/cm^3$. Note that, as with the case of

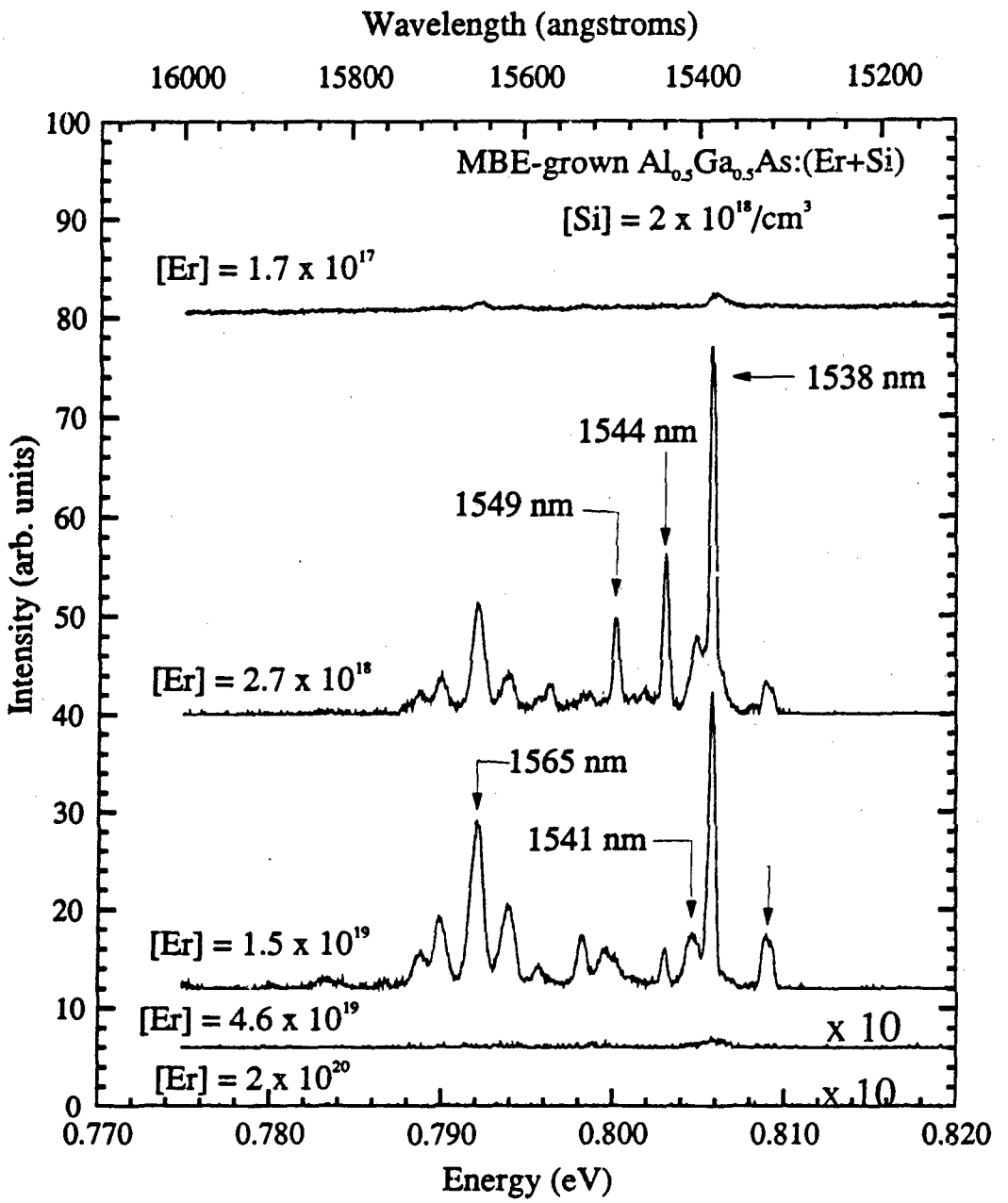

Figure 48 Low Temperature PL of $Al_{0.5}Ga_{0.5}As$:(Er+Si) layers grown by MBE at T_s = 580 °C with various Er concentrations

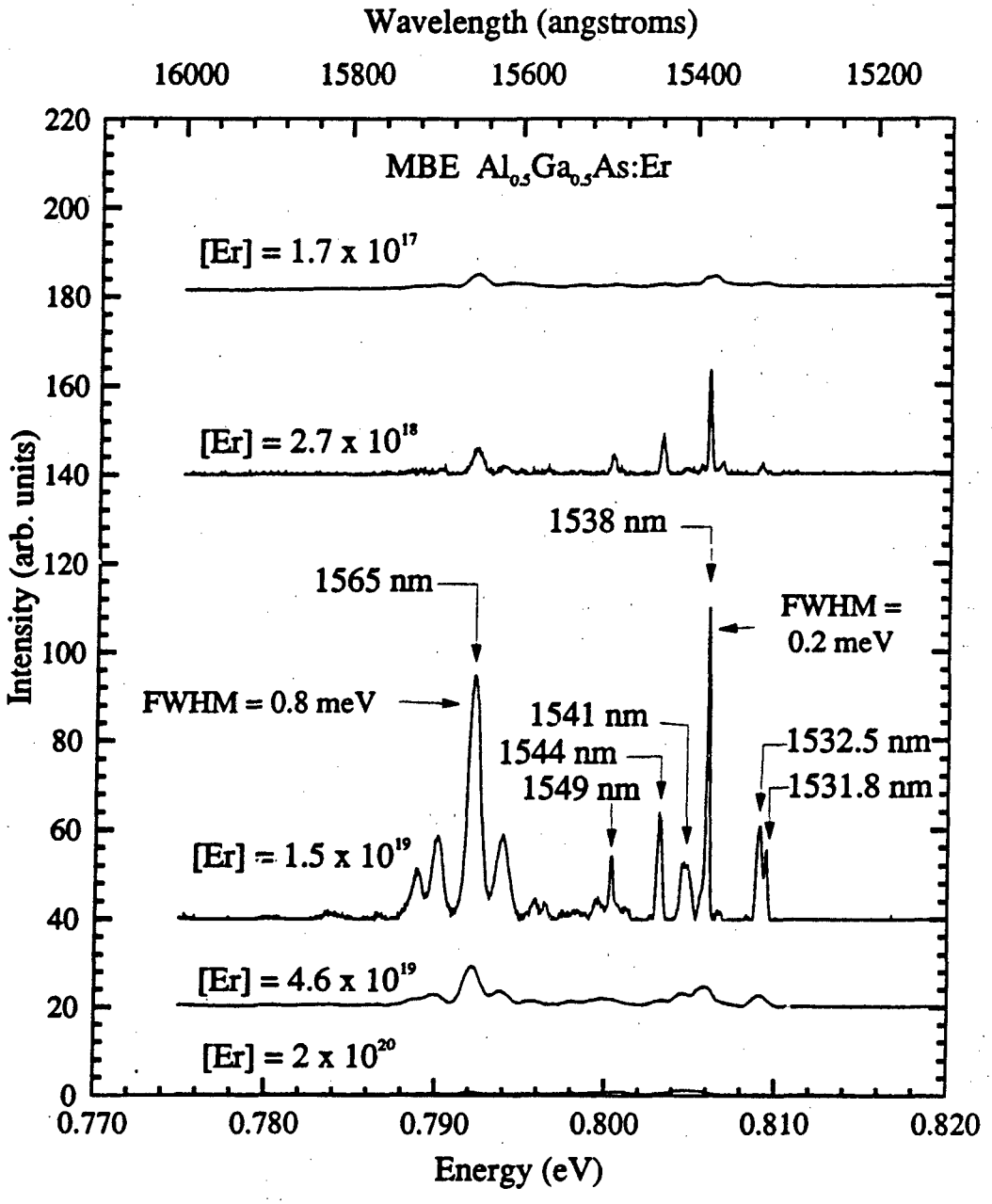

Figure 49 Low temperature PL from $Al_{0.5}Ga_{0.5}As$:Er layers grown by MBE at T_s = 580 °C with different Er concentrations

$Al_xGa_{1-x}As$ grown at different T_s, the intensity variation of the 1.32 μm peak as a function of Er concentration follows the same trend as that of the 1.56 μm emissions.

Figure 49 shows the PL spectra of $Al_{0.5}Ga_{0.5}As$:Er layers grown with different Er concentrations, and similar PL results were obtained as for the samples with Si co-doping. The main difference between the spectra of figure 49 and those shown in figure 48 is the fact that the strongest emissions now occur at 1.5 x $10^{19}/cm^3$, and except for the sample with [Er] = 2.7 x $10^{18}/cm^3$, all other samples show slightly stronger emissions than the corresponding sample co-doped with Si. This is possibly due to the formation of optically inactive Er-Si complexes in the co-doped sample. Since up to one Er monolayer rides on the surface during growth, the probability of Si atoms interacting with Er atoms to form complexes is very high. This interpretation is also supported by the results from electrical measurements.

Figure 50 shows a plot of the PL intensity of the 1.538 μm peak and the carrier concentration as a function of Er concentration. The vertical left axis indicates the PL intensity, and the right axis shows the carrier concentration. Even though all the samples were doped nominally with the same Si concentration, the carrier concentration decreased as the Er concentration increased. It could be argued that Er forms acceptor levels that compensate the donors. However, the results for the ion implanted samples as well as other MBE

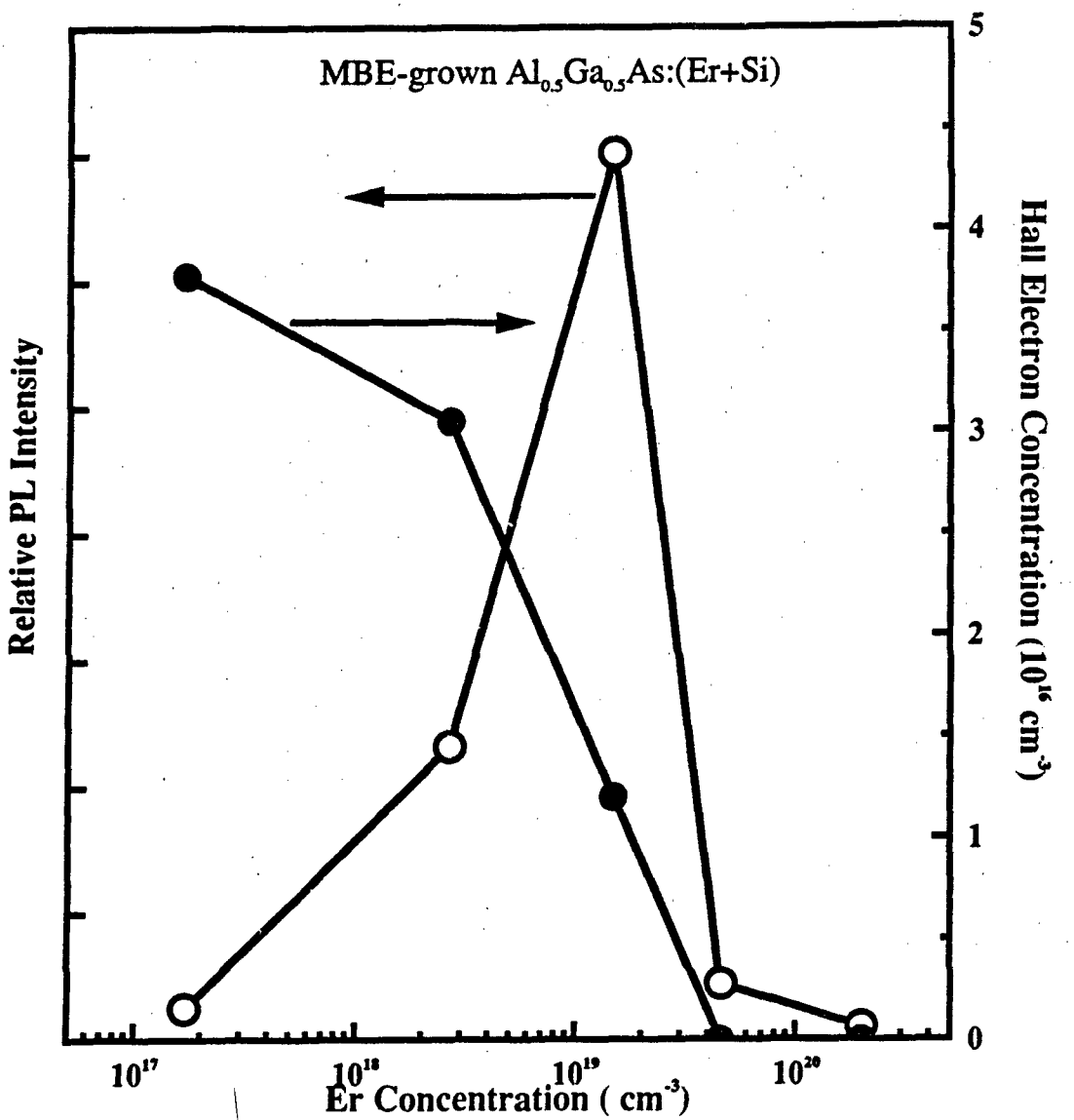

Figure 50 PL intensity of the 1.538 μm emission and carrier concentration obtained from MBE grown $Al_{0.5}Ga_{0.5}As$:(Er+Si) as a function of Er concentration

samples indicate that Er doping does not introduce carriers. This has been verified not only by our own results but also by other researchers in the field (Moore et al, [1992]). Therefore, the decrease in the carrier concentration may be due to the formation of Er-Si complexes. This is the well known "donor gettering" effect, which is observed when doping III-V semiconductors with RE elements during crystal growth (Raczyńska et al. [1988], Lagvilava et al. [1990]). These complexes appear to be optically inactive, because the low temperature PL intensity decreases upon co-doping with Si.

Since the samples doped with Er at 2.7 x 10^{18} and 1.9 x $10^{19}/cm^3$ showed very strong emissions, it was possible to used much narrower slit openings to record their spectra. The slit openings were 100 and 200 μm for the entrance and exit slits, respectively. This represents the best resolution in the 1.5 μm emission region for all the spectra shown in this work. It can be seen from these spectra that the FWHM of the 1.538 μm peak is $\approx$ 0.2 meV, and that of the 1.565 μm peak is $\approx$ 0.8 meV. Also, note that the 1.532 μm peak is really a doublet with peaks at 1.5318 and 1.5325 μm. Note also that the intensity variation of this doublet as well as that of the 1.544 μm peak follow the same trend as a function of Er concentration as that of the 1.56 μm peaks. This correlation, observed in several different samples, is a strong indication that the 1.5318 and 1.5325 μm peaks originate from the same luminescent center as that of the 1.56 μm emissions. The

results from lifetime experiments present further proof of the above relationship between these emissions. Such results will be presented in section 4.4.3.

In summary, low temperature PL studies of $Al_{0.33}Ga_{0.67}As$:Er and GaAs:Er as a function of substrate temperature, and those of $Al_{0.5}Ga_{0.5}As$:Er with and without Si co-doping suggest the presence of at least three different Er-related luminescent centers. The relative strength among peaks originated from different centers varies differently for each sample, depending upon T_s and [Er]. At present, there is no specific knowledge as to the nature of the particular Er complexes giving rise to these emissions. In addition, it should be pointed out that the PL from different regions of the same wafer showed different relative intensities among the various emission peaks, thus indicating that these complexes are not homogeneously distributed across the wafer.

As mentioned above, the Er^{3+} emissions seem to originate mostly from non-substitutional Er and Er-related complexes. This was also suggested by RBS measurements on RE implanted III-V semiconductors (Kozanecki et al. [1992]) as discussed in section 4.1. Therefore, it is of interest to see whether growing the Er doped layers at different crystal orientations would favor the formation of such optical active complexes, thus enhancing the Er^{3+} emissions. To determine this, GaAs:Er layers were grown along the <100>, <211>, <111>, and <311> directions. Another set of GaAs:Er layers were grown on

slightly misoriented substrates. The low temperature PL of these samples is shown in figures 51 and 52. The samples grown along the <100> direction showed the strongest emissions. Other than the PL intensity of the various peaks, the spectra from the samples grown along different orientations showed no differences.

The Er^{3+} energy level diagram shown in figure 2 shows that various excited states of the 4f levels could be accommodated by the bandgap of III-V semiconductors under the right conditions. Specifically, the $^4I_{11/2}$ and the $^4I_{9/2}$ levels are approximately 1.25 and 1.5 eV above the $^4I_{15/2}$ ground state, respectively. Optical transitions from these levels should be observable in the low temperature PL. However, in GaAs:Er, the $^4I_{11/2} \rightarrow {}^4I_{13/2}$ transition has been observed in the electroluminescence (EL) spectra, but not in PL. The reason for this discrepancy between EL and PL might be that the excitation mechanism is different in the two cases. In $Al_xGa_{1-x}As$:Er, sharp peaks around 988 nm that were assigned to the $^4I_{11/2} \rightarrow {}^4I_{13/2}$ transition, have been observed in the low temperature PL of $Al_{0.55}Ga_{0.45}As$:Er (Benyattou et al. [1992]). The 988 nm emissions haven't been observed in the PL of current ion implanted or MBE-grown GaAs:Er samples. However, a series of sharp emissions have been observed from some of our MBE-grown $Al_xGa_{1-x}As$:Er layers with x = 0.33 and 0.5, and the results are shown in figure 53. The wavelength of all the peaks near 988 nm are shown in table IV. The samples are

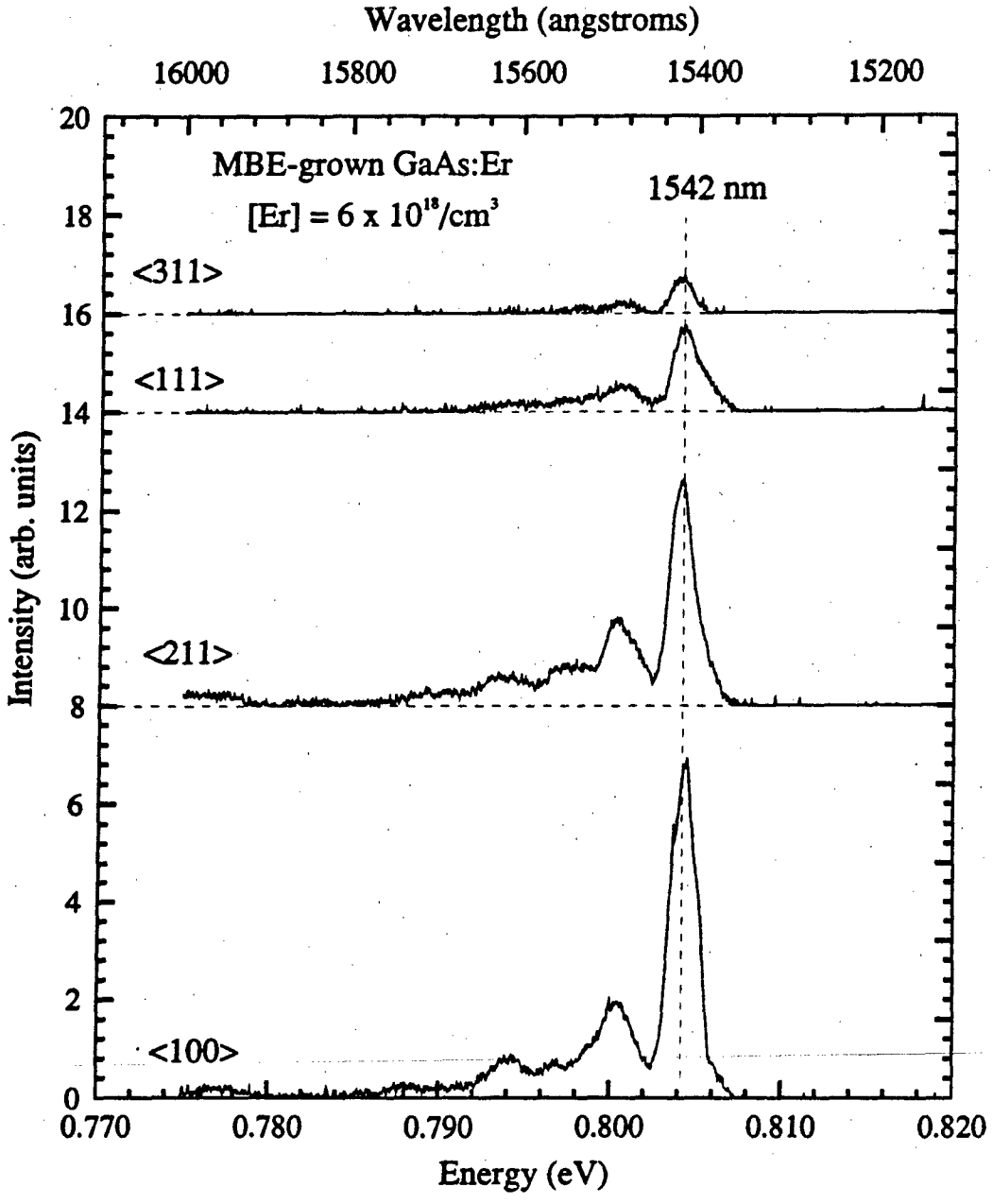

Figure 51 Low temperature PL for GaAs:Er grown by MBE along the <100>, <211>, <111>, and <311> crystal directions

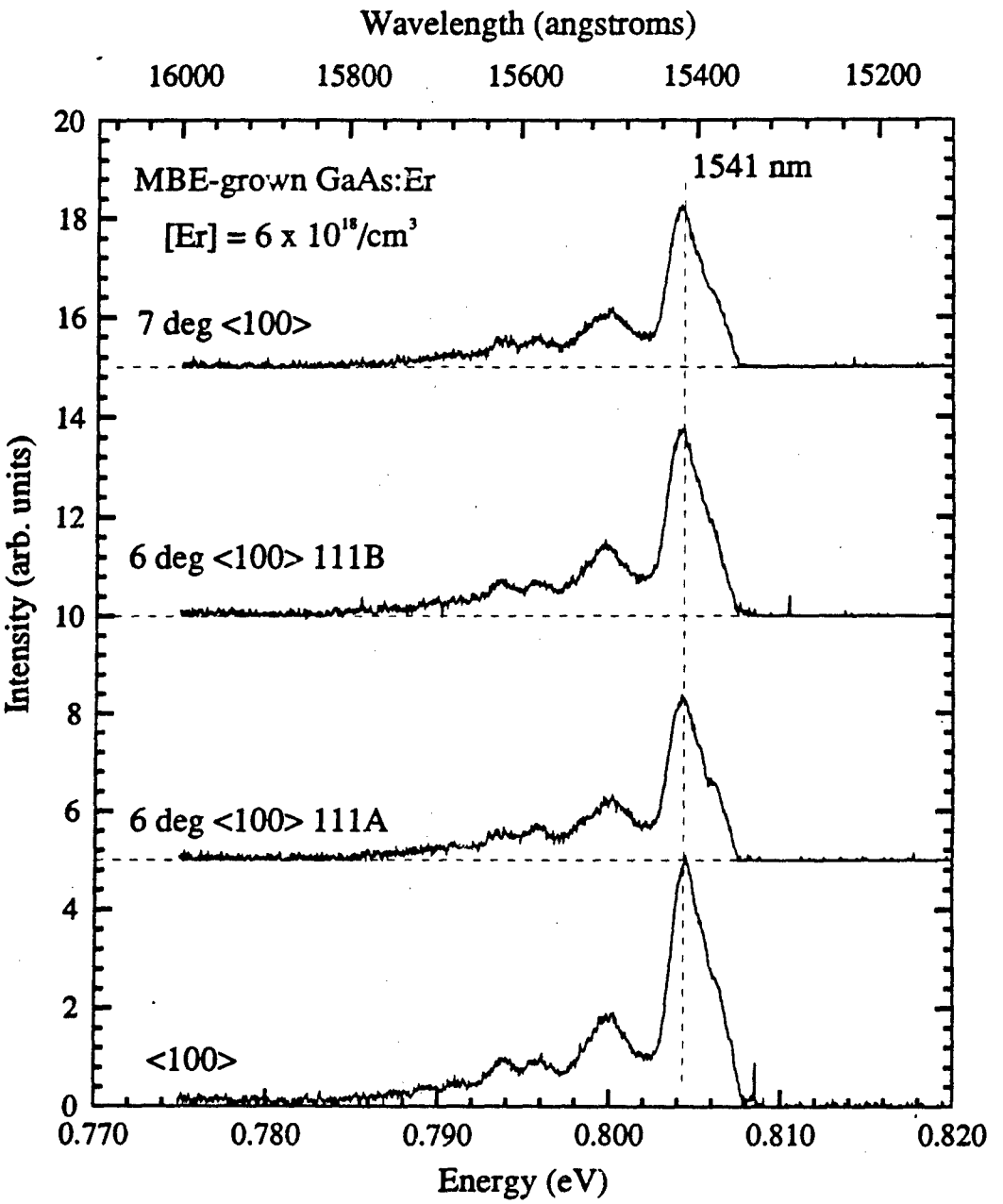

Figure 52 Low Temperature PL for GaAs:Er layers grown by MBE on slightly misoriented substrates

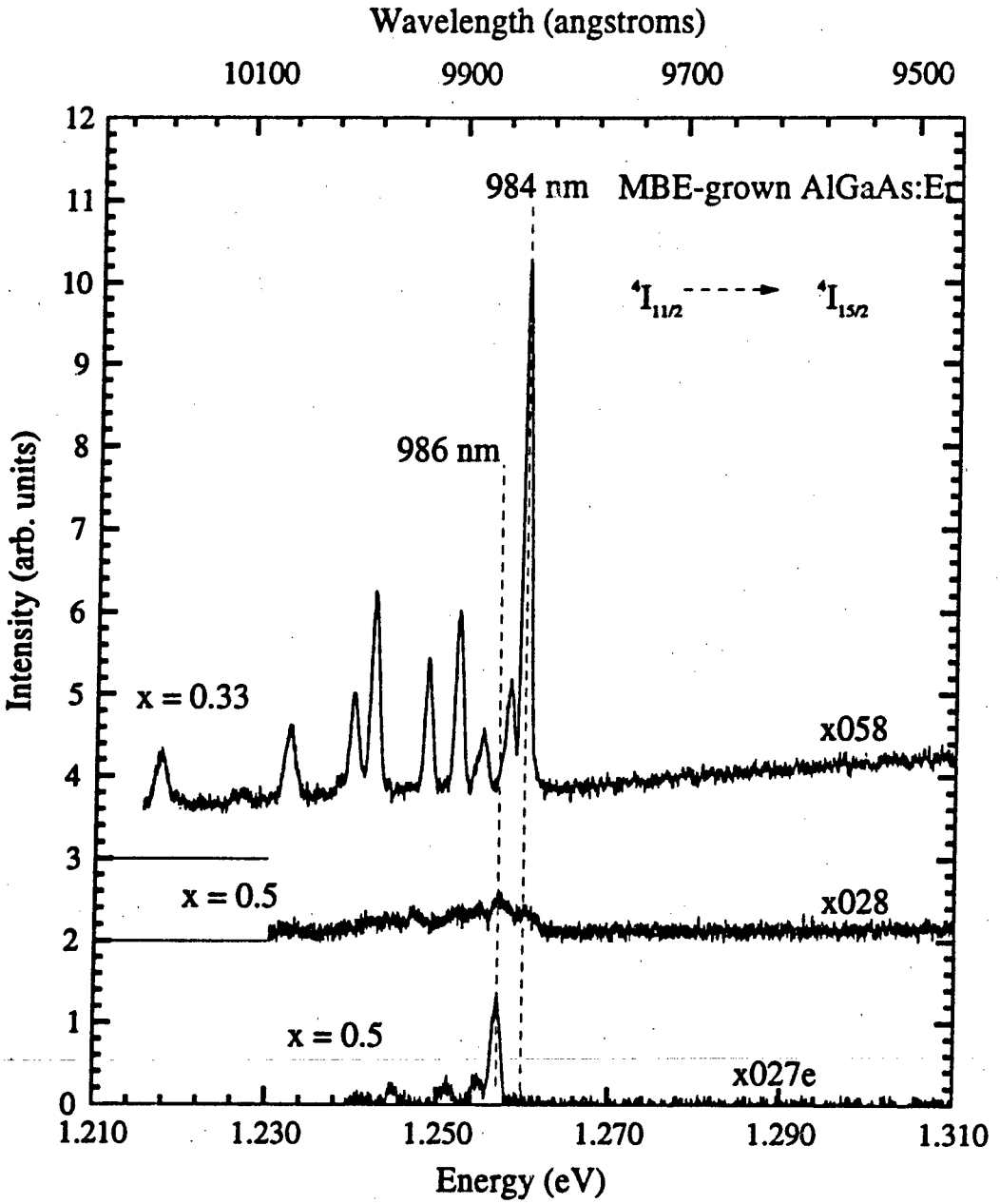

Figure 53 0.988 μm emissions from MBE grown $Al_xGa_{1-x}As$:Er (x = 0.33, 0.5) grown with different Er concentrations

Table IV

Er^{3+} emissions near 1.0 μm

	Wavelength (Angstroms)	Energy (eV)
x058		
	9841	1.2599
	9854	1.2582
	9879	1.2550
	9902	1.2521
	9930	1.2486
	9980	1.2326
	10000	1.2399
	10060	1.2325
	10184	1.2175
x028		
	9840	1.2600
	9863	1.2571
	9880	1.2549
	9941	1.2472
x027e		

labeled as x051, x028, and x027e. The sample x051 is an $Al_{0.33}Ga_{0.67}As$.Er layer grown at T_s = 580 °C with [Er] = 5 x $10^{18}/cm^3$, the sample x028 is $Al_{0.5}Ga_{0.5}As$:(Er+Si) grown at T_s = 620 °C with [Er] = 2.7 x $10^{18}/cm^3$, and the sample x027e is an $Al_{0.5}Ga_{0.5}As$:Er layer grown at T_s = 620 °C with [Er] = 1.5 x $10^{19}/cm^3$ but after etching the (Er+Si) layer. The PL of the 1.5 to 1.6 μm region for samples x028 and x027e, were shown in figures 48 and 49, respectively. Note from figure 53 that the relative intensity among different peaks is different for each sample and not all the peaks are observed in all the samples. This suggests that these emissions originate from at least two

different luminescent centers. In addition, there is no correlation between the strength of the 988 nm emissions and the emissions near 1.54 and 1.56 μm. This can be observed by comparing figure 53 to figure 54, which shows the PL spectra in the 1.5 μm region for the same samples as in figure 53. Note from figure 54 that the samples x027e and x028 showed the strongest emissions in the 1.54 and 1.56 μm regions, while the sample x058 showed much stronger emissions near 988 nm. Previous reports (Benyattou et al. [1992]) argued that these emissions have the same behavior as a function of temperature as the 1.56 μm emissions. However, a comparison of these two sets of emissions, from figures 53 and 54, indicates that the 1.56 μm and the 988 nm emissions originate from different luminescence centers. This also implies that different excitation mechanisms are involved in the excitation of the 988 nm emissions and that of the 1.5 μm emissions.

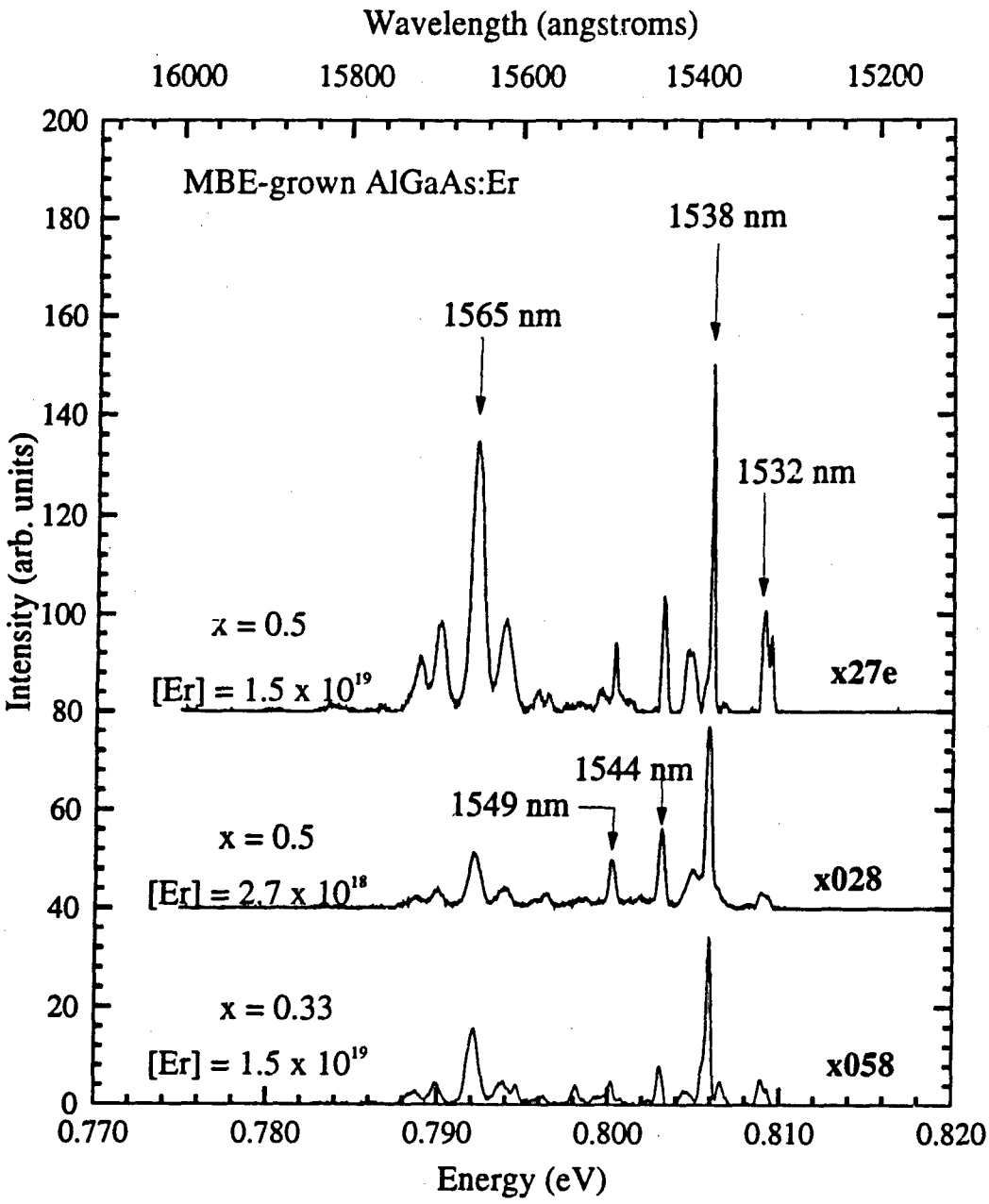

Figure 54 Emission spectra of MBE-grown $Al_xGa_{1-x}As$:Er with x = 0.33 and 0.5 in the 1.5-1.6 μm emission region

4.4.3 Lifetime Measurements and Its' Temperature Dependence

Lifetime measurements of the Er^{3+} emissions from MBE-grown GaAs:Er and $Al_{0.5}Ga_{0.5}As$:Er were performed in order to study the kinetics of the intra-4f emissions. Figure 55 shows the time decay of the main Er^{3+} emission from GaAs:Er measured at T = 10, 55, and 200 K. The PL spectrum of the sample studied was shown in figure 47, and it show that the main emission near 1.54 μm consists of a doublet with peaks at 1.540 and 1.542 μm. Due to the weak intensity of the signal, lifetime measurements on this sample were done using slit openings of 1 mm for both the entrance and exit slits, therefore, the observed signal is really a convolution of the double peaks. However, the observed decay is mostly fitted with a single exponential, as shown in the figure by the solid lines. This would suggest that both emissions originate from the same luminescent center. The initial fast component that was observed in the ion implanted samples is not apparent for the MBE samples until high sample temperatures and even at high temperatures, the initial fast component only affects the decay during first 200 μsec, or less, after the excitation pulse. Since at these high temperatures the Er^{3+} lifetime is much shorter, the initial fast component might be due to both the system response and emission lifetime. At 10 K, the lifetime was found to be 940 μsec, and it is of the same order of magnitude as that obtained for the ion implanted samples. Further information concerning the kinetics of these emissions

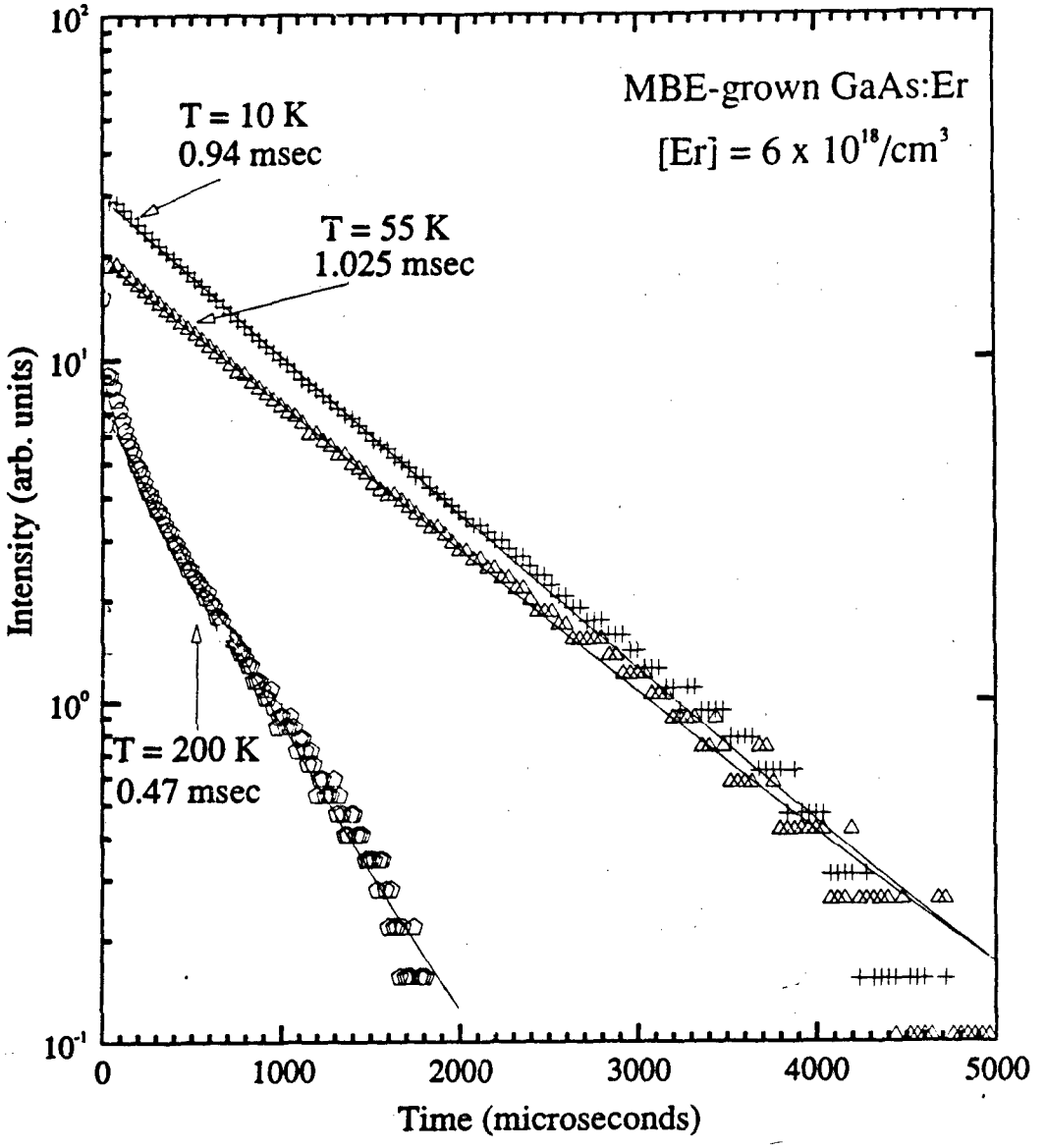

Figure 55 Time decay of the 1.540 μm Er^{3+} emission from MBE-grown GaAs:Er measured at T = 10, 55, and 200 K

Table V
Decay times of the 1.54 μm emission from MBE GaAs:Er as a function of sample temperature

Temp. (K)	τ (μsec)
9.8	944
12	970
16.3	982
23	995
28.7	1002
35.6	1014
45.2	1023
54.9	1029
64.5	1039
74.1	1096
83.9	1076
96.9	1054
108.8	1021
118.8	1000
129.5	955
143.3	901
156.1	809
168.9	699
182.9	516
198.7	466
215.5	360
232.6	229
246.6	195
261.1	132
275.7	57

can be obtained from the temperature dependence of the decay time. Note in figure 55 that the Er^{3+} decay at 55 K is slower than that at 10 K, which is an unexpected result. The lifetimes at various sample temperatures, T, are listed in table V. Note that at low T, the decay time increases unexpectedly as T increases. This is also illustrated in figure 56, which shows the ratio $\tau(T)/\tau(0)$ as a function of 1/T, where $\tau(0)$ was chosen as the decay time at 10 K. For comparison purposes, the figure also shows the same data for

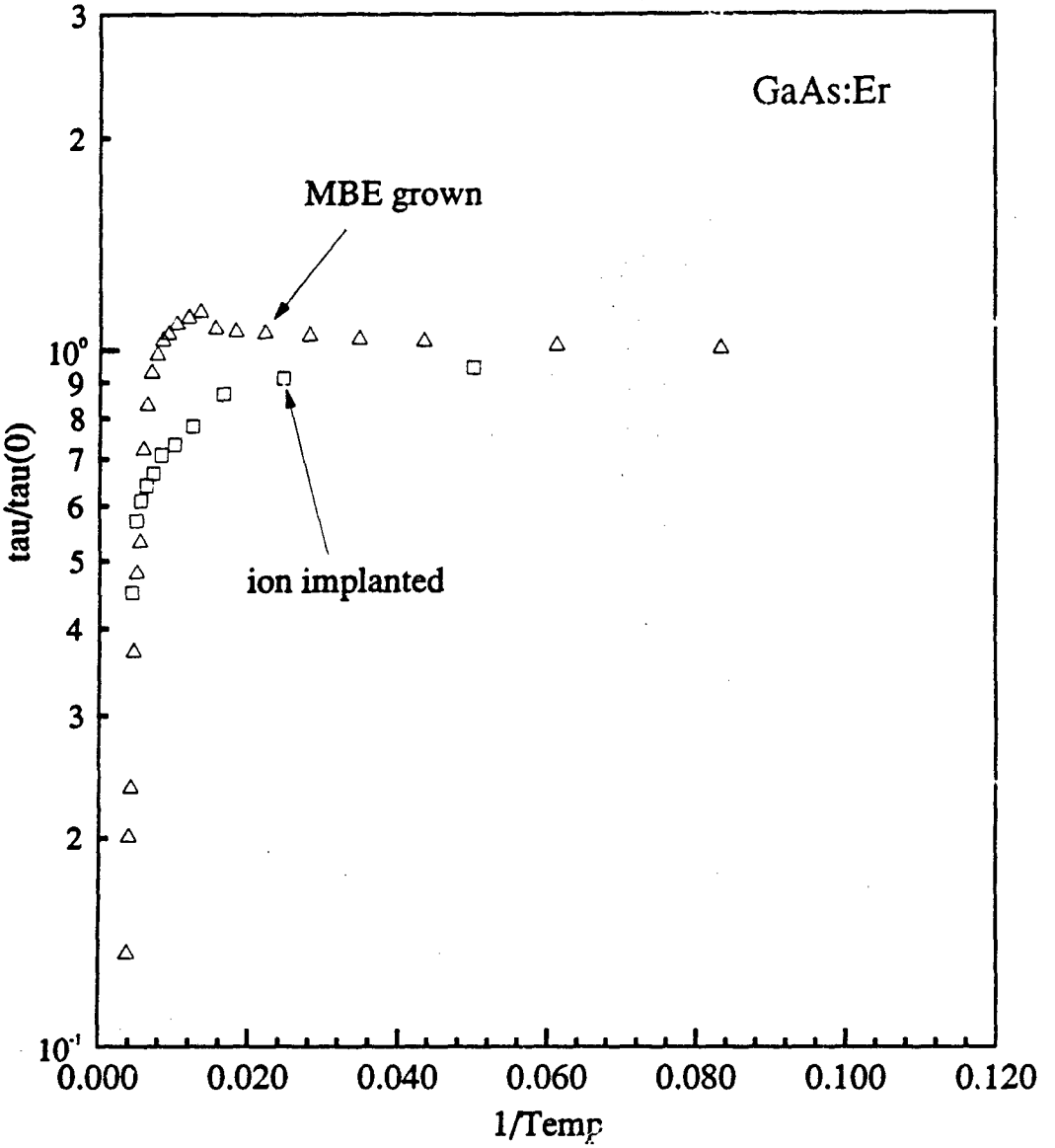

Figure 56 Lifetime ratio $\tau(T)/\tau(0)$ as a function of 1/T for the main 1.540 μm Er^{3+} emission from MBE-grown and ion implanted GaAs:Er

the ion implanted sample. In the case of the ion implanted sample τ decreases monotonically as T increases, while in the case of the MBE sample case τ increases slightly as T increases, from 940 μsec at 10 K to approximately 1.1 msec at 74 K. At higher temperatures for T > 74 K, τ decreases slowly as T increases, but when the sample temperature increases beyond 120 K, τ decreases very rapidly, approaching 60 μsec at 276 K. It is reminded that for these small time constants, the error due to the system response is higher than for the long time constants, therefore the values at high T are less reliable. It is obvious that the experimental values cannot be fitted to an expression of the form:

$$\frac{\tau(T)}{\tau(0)} = \frac{1}{1 + A\exp(-\frac{E}{kT})}$$

In order to determine an activation energy, a fit of the experimental values to this equation for T > 120 K was attempted, but no satisfactory fit could be obtained. Thus, even at high T, the decay time does not follow this functional form, indicating that more complicated nonradiative mechanisms than the one discussed in section 4.3.3 are responsible for the temperature quenching. It is pointed out that the increase in τ with increasing T, at low temperatures, was not observed in other lifetime studies (Klein [1990]). Although the lifetime increased with T, from 10 to 74 K, the initial signal intensity decreased, indicating that the excitation efficiency decreased with increasing T. The increase in

lifetime as T increases is difficult to understand. One possible explanation is that there might be an additional excitation path that can be thermally activated. This new excitation mechanism must be much slower than the main mechanism. The presence of a fast and a slow excitation process will result in apparently longer decay times. However, more work is necessary before the significance of these results can be understood. Also, this behavior was not observed in present ion implanted samples, therefore it appears to be characteristic of a particular Er related center present in current MBE sample. In light of these results, it would be worthwhile to measure the Er^{3+} decay originating from different Er-related centers from the same sample. Although this study for GaAs:Er could not be done due to the weak intensity of the signal, but was done for $Al_{0.5}Ga_{0.5}As$:Er.

Lifetime measurements were also performed on $Al_{0.5}Ga_{0.5}As$:Er having an Er concentration of 1.5 x $10^{19}/cm^3$. The low temperature PL spectrum of this sample is shown in figure 57, and the main features were discussed in section 4.2.2. Since this sample shows the strongest Er^{3+} emissions, much narrower slit openings could be used in this study, and thus it was possible to measure the decay of nine different emissions from this sample. Figures 58 and 59 show the low temperature time decay of various of these emissions, all of which were fitted to a single exponential decay, and the respective fits are

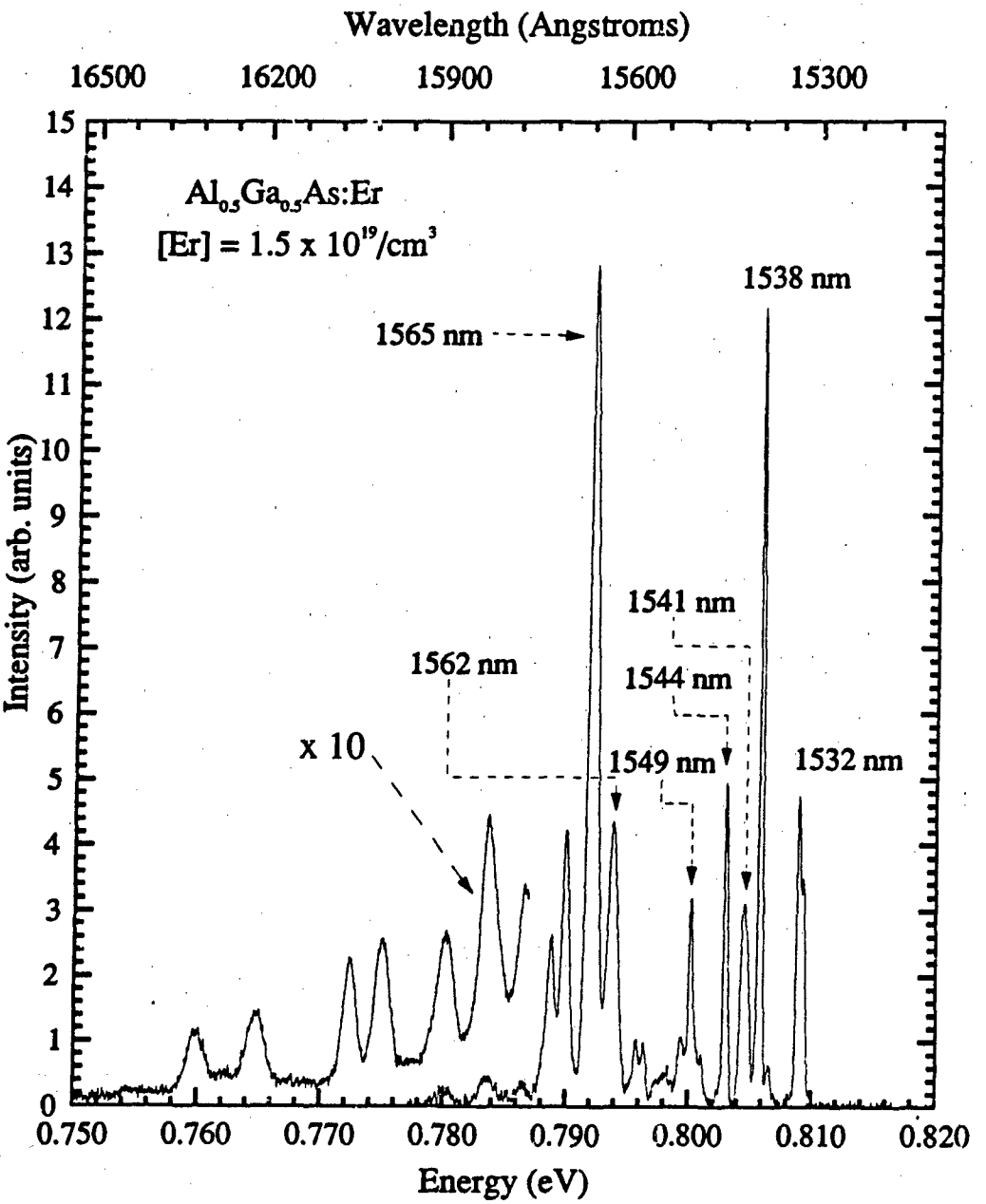

Figure 57 Low temperature PL of the $Al_{0.5}Ga_{0.5}As$:Er sample used in the temperature dependent lifetime measurements

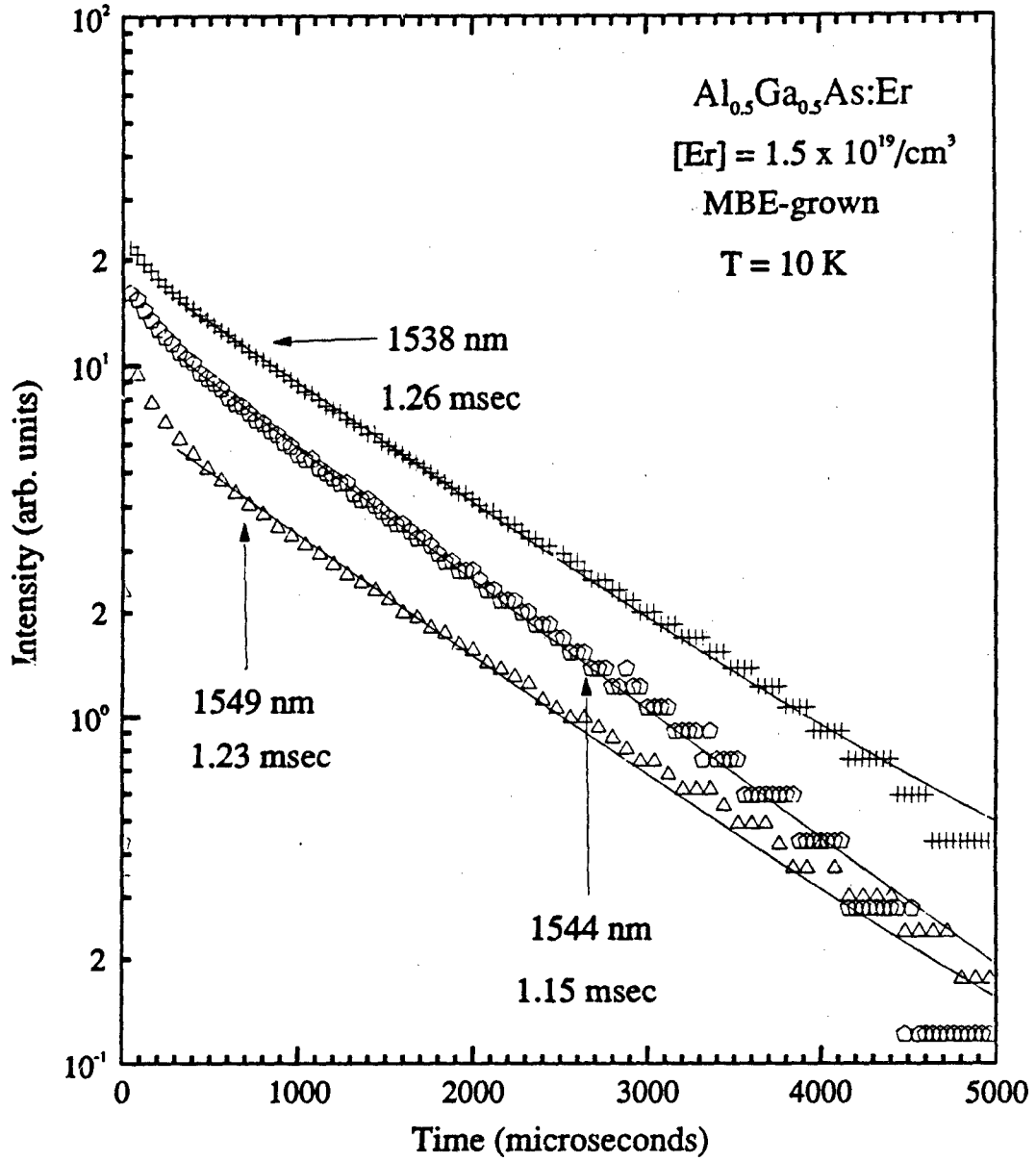

Figure 58 Low temperature time decay of the 1.538, 1.544, and 1.549 μm emissions from $Al_{0.5}Ga_{0.5}As$:Er

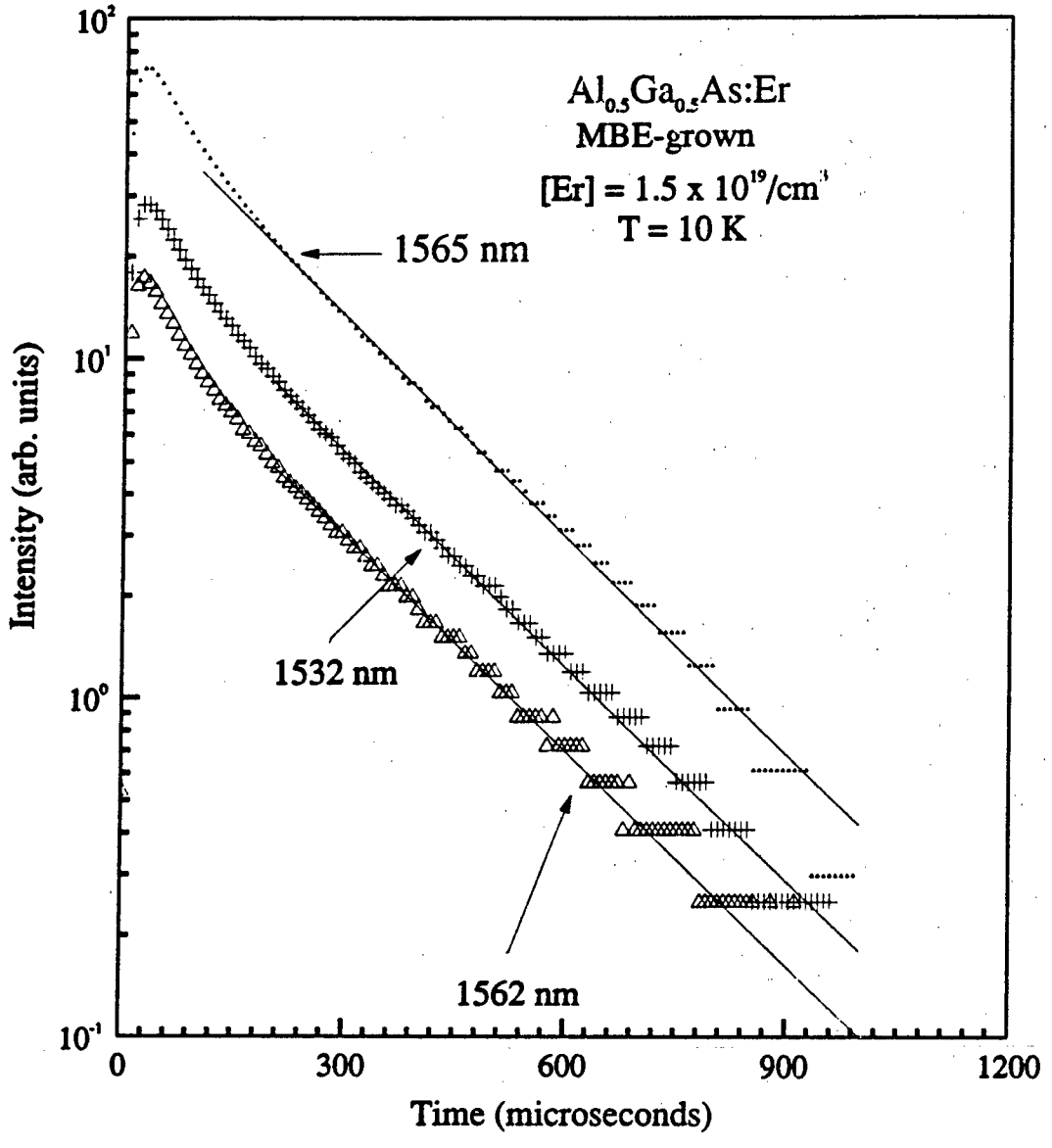

Figure 59 Low temperature time decay of the 1.532, 1.562, and 1.565 μm emissions from $Al_{0.5}Ga_{0.5}As$:Er

shown as solid lines. Note that the emissions studied can be divided into two groups having time constants in the order of 1.1 msec and 200 μsec. These results are consistent with the results from previous measurements on MBE-grown $Al_{0.45}Ga_{0.55}As$:Er (Benyattou et al. [1990], [1991]) which showed a double exponential decay for the Er^{3+} emissions with time constants of 1.2 msec and 360 μsec. In that particular study, the signal was not dispersed with a spectrometer, instead an interference filter with a bandpass of 1.54 ± .024 μm was used. Therefore, the observed decay corresponds to the sum of all the Er^{3+} emissions. Our results show that the 1.538 μm emission has a low temperature decay time constant of 1.28 msec, while the 1.565 μm emissions have time constants of approximately 200 μsec. In addition, two of the other 1.54 μm emissions were found to have short time constants, that is, the 1.532 μm doublet and the peak at 1.541 μm have low T decay times of 200 and 270 μsec, respectively. It should be mentioned that the result for the 1.541 μm peak might have been influenced by the 1.538 and 1.544 μm emissions, which have long time constants, thus giving an apparently longer decay time. In section 4.4.2, a correlation between the intensity of the 1.532 μm doublet and the 1.565 μm emissions was noticed. The lifetime measurements results confirm that these emissions are indeed related. However, the correlation between the 1.541 μm and the 1.565 μm emissions is not as clear. From figure 57, it can be seen that the 1.541 μm peak

has a broader linewidth than the 1.538 μm emission and the other peaks with long time constants, and has a broader linewidth similar to that of the 1.565 μm emission. Thus it seems that the 1.532 and 1.541 emissions originate from the same center as the 1.565 μm emissions.

The decay time dependence on the sample temperature was studied for six different emissions from $Al_{0.5}Ga_{0.5}As$:Er, and the results are listed in table VI. Also, the ratio $\tau(T)/\tau(0)$ is plotted as a function of 1/T is plotted in figures 60 and 61. Figure 62 shows the decay of the 1.538 μm emission measured at temperatures of 10, 98, and 173 K. Although it is less noticeable at low temperatures, the time decay shows an initial fast decay component at all temperatures. At T > 143 K, in figure 62, the fast component dominates the decay, and this is clearly shown for the decay at 173 K. In this case, the decay is clearly fitted to a double exponential, as shown by the solid line, with time constants of 70 and 620 μsec. The nature of this fast component of the decay is not understood at present. The fast component observed from our ion implanted samples could be correlated with a bb emission underlying the Er^{3+} emissions. However, in the present case, the bb emission is absent. Recall that Klein et al. [1991] observed a fast component in ion implanted GaAs:Er, but his sample did not show the bb emission. One possible explanation is that this component is due to the presence of a "hot" line, i.e., an emission originating from

Table VI

Lifetimes of various Er^{3+} emissions from $Al_{0.5}Ga_{0.5}As$:Er as a function of sample temperature

λ = 1.532 μm		λ = 1.538 μm		λ = 1.541 μm	
T (K)	τ (μsec)	T (K)	τ (μsec)	T (K)	τ (μsec)
9.5	205	12.3	1275	9	188
11.1	204	18.5	1291	10.4	192
18.5	187	28	1278	19.1	197
27.8	203	37.7	1282	28.7	201
38.4	224	47.4	1256	38.4	207
48.2	244	58.1	1242	47.9	210
57.9	252	67.8	1240	57.7	206
67.9	253	77.2	1242	67.5	191
77.5	260	87.2	1242	77.1	167
87.7	402	97.5	1233	87	76
107.5	838	114	709	97.4	72
		143.2	770	107	26
		173	618		
		192.9	366		

λ = 1.544 μm		λ = 1.562 μm		λ = 1.565 μm	
T	τ	T	τ	T	τ
13.2	1150	9	188	9.7	200
18.5	1139	10.4	192	18.4	204
28.2	1140	19.1	197	28.1	210
37.8	1136	28.7	201	39	212
47.5	1127	38.4	207	48.8	211
57.2	1129	47.9	210	58.5	206
67	1154	57.7	206	68.4	190
77.5	1187	67.5	191	77.8	163
87.5	1226	77.1	167	87.5	94
97.5	1204	87	76	97.8	31
114.5	1134	97	72	107.5	21.6
129.2	946	107.1	26		
144.3	553				
158.9	235				
173.5	190				

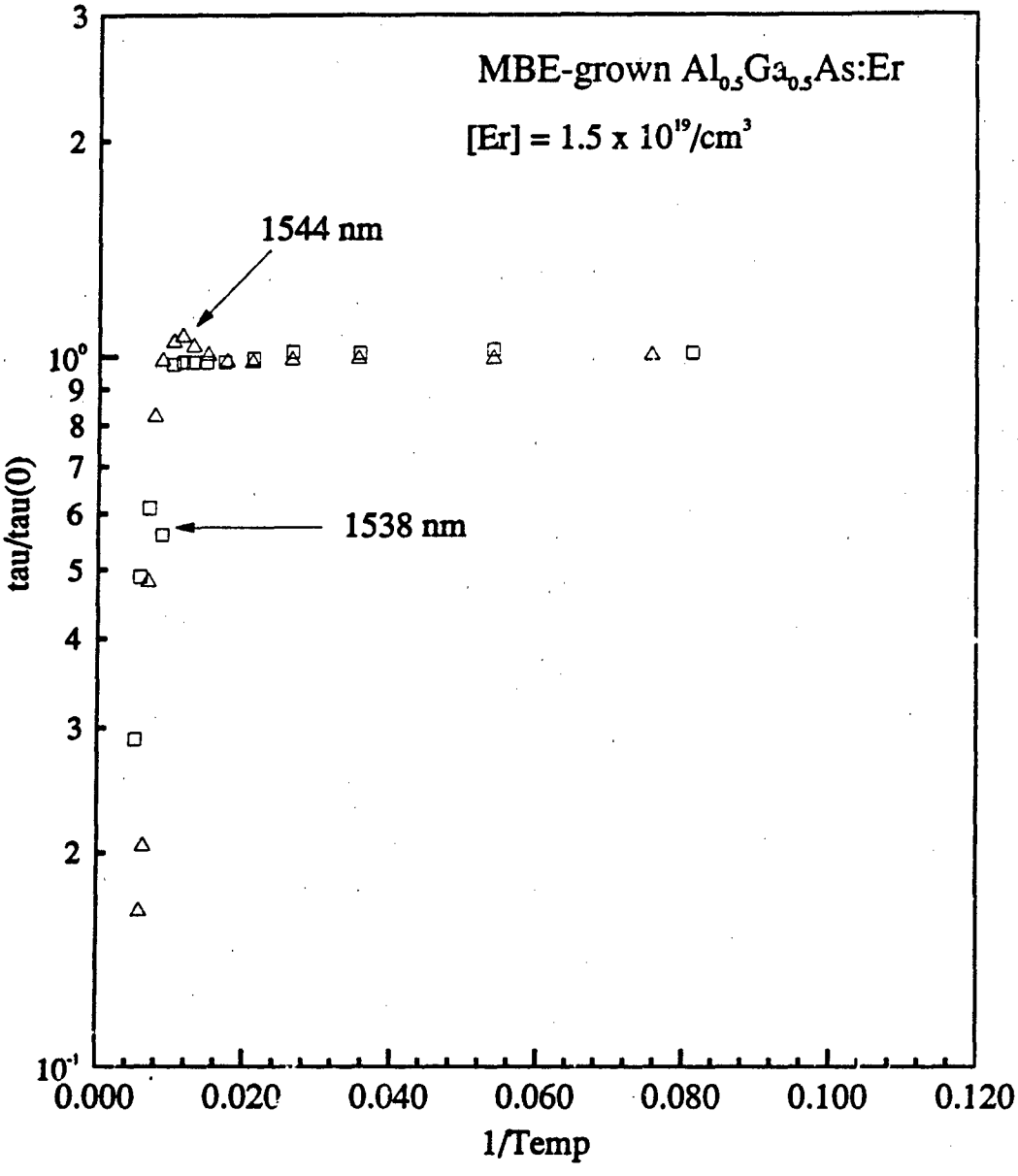

Figure 60 Lifetime ratio $\tau(T)/\tau(0)$ for the 1.538 and 1.544 μm emissions for the MBE-grown $Al_{0.5}Ga_{0.5}As$:Er sample as a function of 1/T

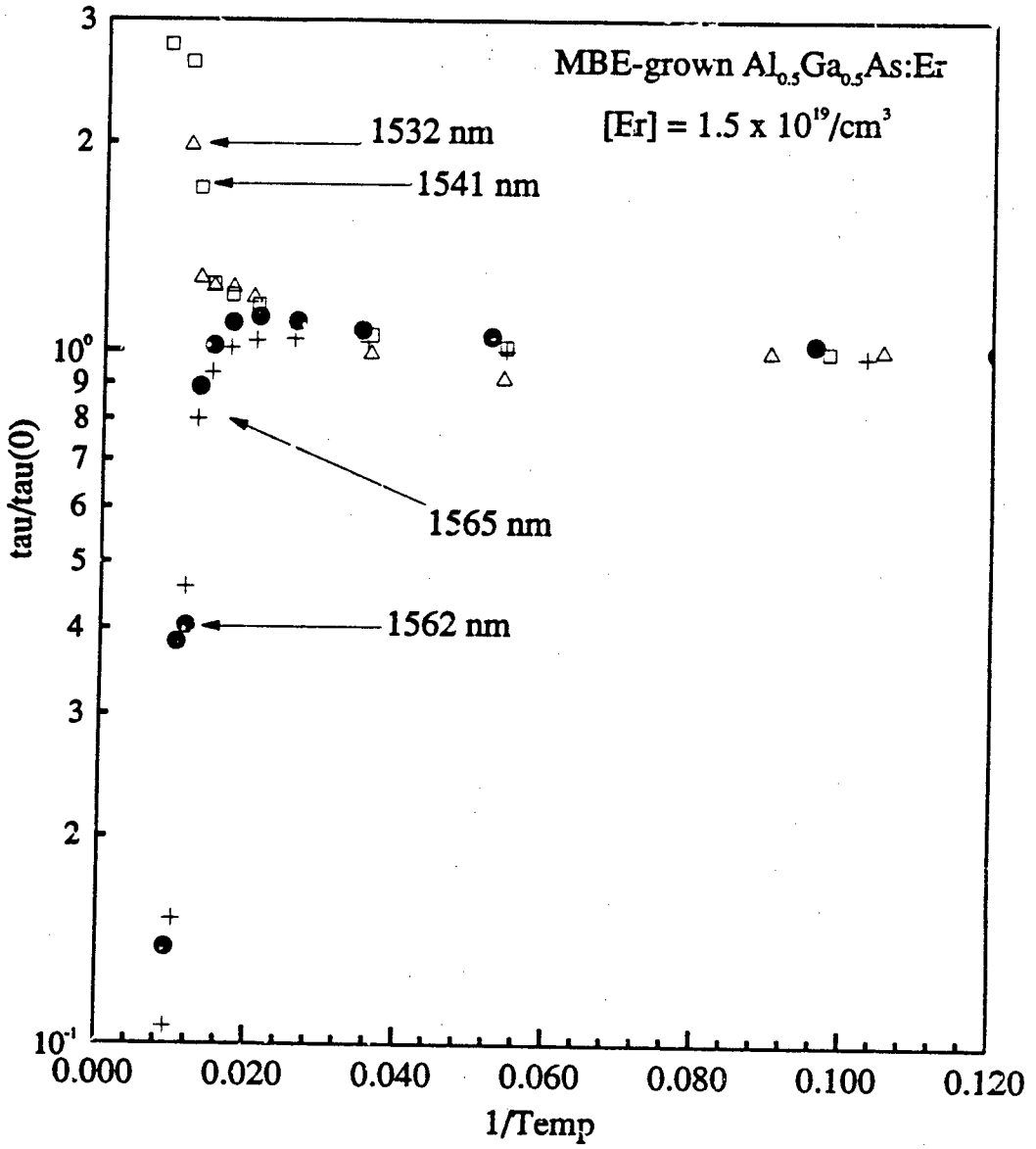

Figure 61 Lifetime ratio $\tau(T)/\tau(0)$ for the 1.532, 1.541, 1.562, and 1.565 μm emissions from the MBE grown $Al_{0.5}Ga_{0.5}As$:Er sample as a function of 1/T

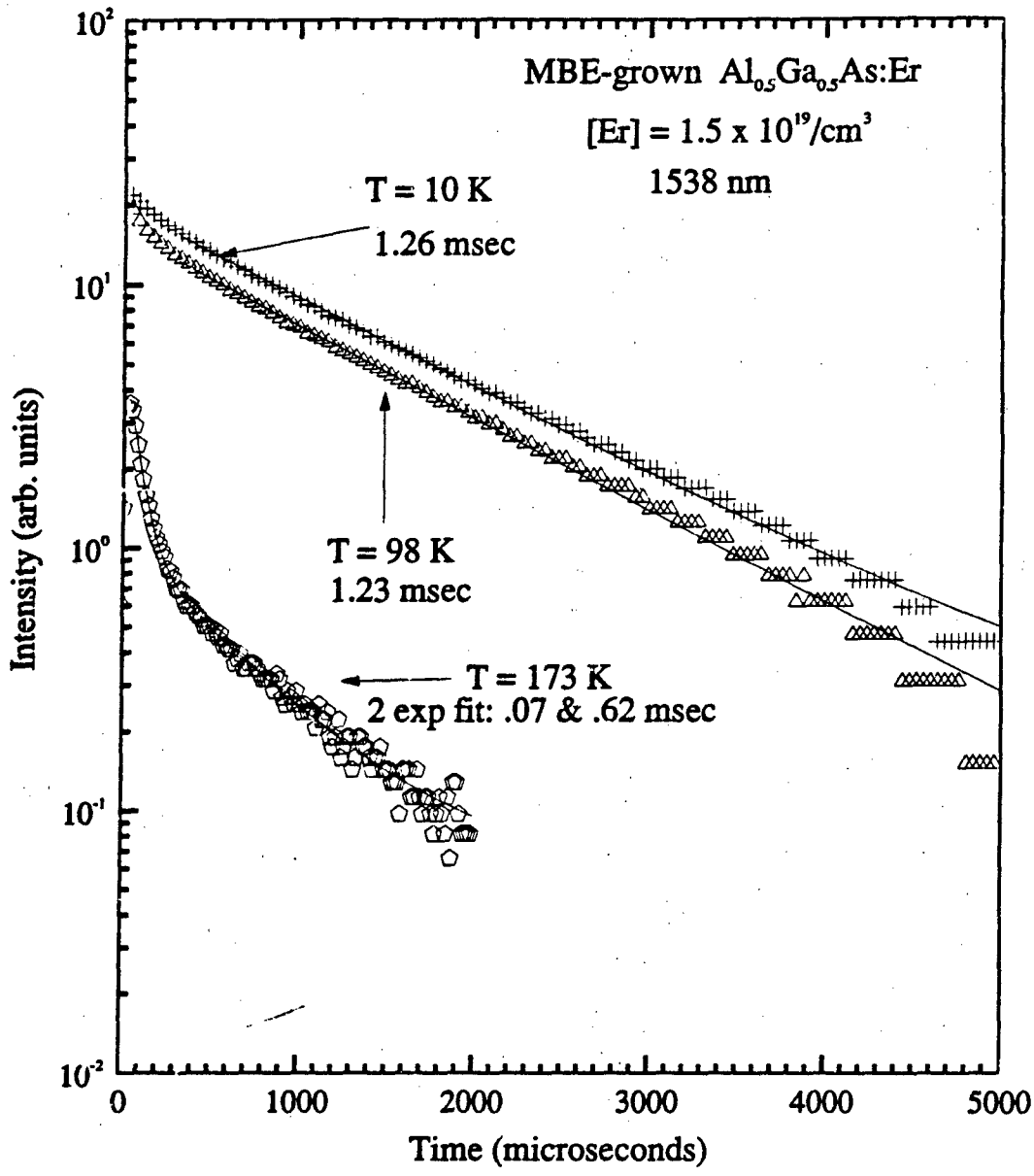

Figure 62 Time decay of the 1.538 μm emission from MBE-grown $Al_{0.5}Ga_{0.5}As$:Er measured at sample temperatures of 10, 98, and 173 K

a higher level in the $^4I_{13/2}$ multiplet, at nearly the same position. This "hot" line would originate from a different luminescent center whose emissions have a much shorter lifetime. It is also possible that the fast component is due to the particular excitation and de-excitation mechanism of the 4f shell. At present, there is no kinetic model which accounts for this effect. For T = 10 and 98 K, the solid lines shown in figure 62 indicate a single exponential fit to the slow component of the decay, with respective time constants of 1.26 and 1.23 msec. This long component of the decay remains as a single exponential independent of T, and the lifetime is basically constant up to T = 90 K. At higher temperatures it decreases very quickly.

From table VI and figure 60, it can be seen that the lifetime of the 1.544 μm peak as a function of temperature behaves differently compared to the 1.538 μm emission. As T was increased from 13 to $\approx$ 60 K, the decay time decreased so slightly that it can be considered constant in this range. However, for T > 60 K, the decay time increased with increasing T, reaching a maximum around 90 K. Then at T > 115 K, it decreased very rapidly with increasing temperature. At T = 173.5 K the decay time of the 1.544 μm emission was only 190 μsec, compared to approximately 600 μsec for the 1.538 μm emission. This drastic difference in the kinetics of these two peaks indicates that they originate from different luminescent centers. The behavior of the 1.544 μm

peak is similar to that observed in MBE-grown GaAs:Er. Figure 63 shows the decay of the 1.565 μm emission at T = 10, 49, 88, and 100 K. Although the decay shows again an initial fast component it might be mostly due to the system's response, because the time scale in this case is much smaller than in the previous cases. The slow component appears to be a single exponential, independent of the sample temperature. In figure 61 the ratios $\tau(T)/\tau(0)$ for the 1.532, 1.541, 1.562 μm and 1.565 peaks are plotted as a function of 1/T. As mentioned above, all these emissions have low temperature time constants of roughly 200 μsec. The lifetimes of the 1.562 and 1.565 μm emissions show the same behavior as a function of temperature. For T < 48 K, the lifetime increases slightly with increasing temperature. However, at higher temperatures, it starts to decrease slowly, and then for T > 77 K, the time constant decreases rapidly with increasing T. On the other hand, the 1.532 and 1.541 μm emissions show a very interesting behavior. As T increases, the decay time of the 1.541 μm peak increases dramatically, i.e., at T = 108 K, the decay time increased threefold from the low temperature value. A similar phenomenon was observed for the 1.532 μm doublet. As shown in figure 64, at higher temperature the decay changes into a single exponential decay, and the decay is mostly dominated by the long time component. In order to understand this behavior, it is useful to look at the temperature dependence of the PL spectra shown in figures 65 to 67.

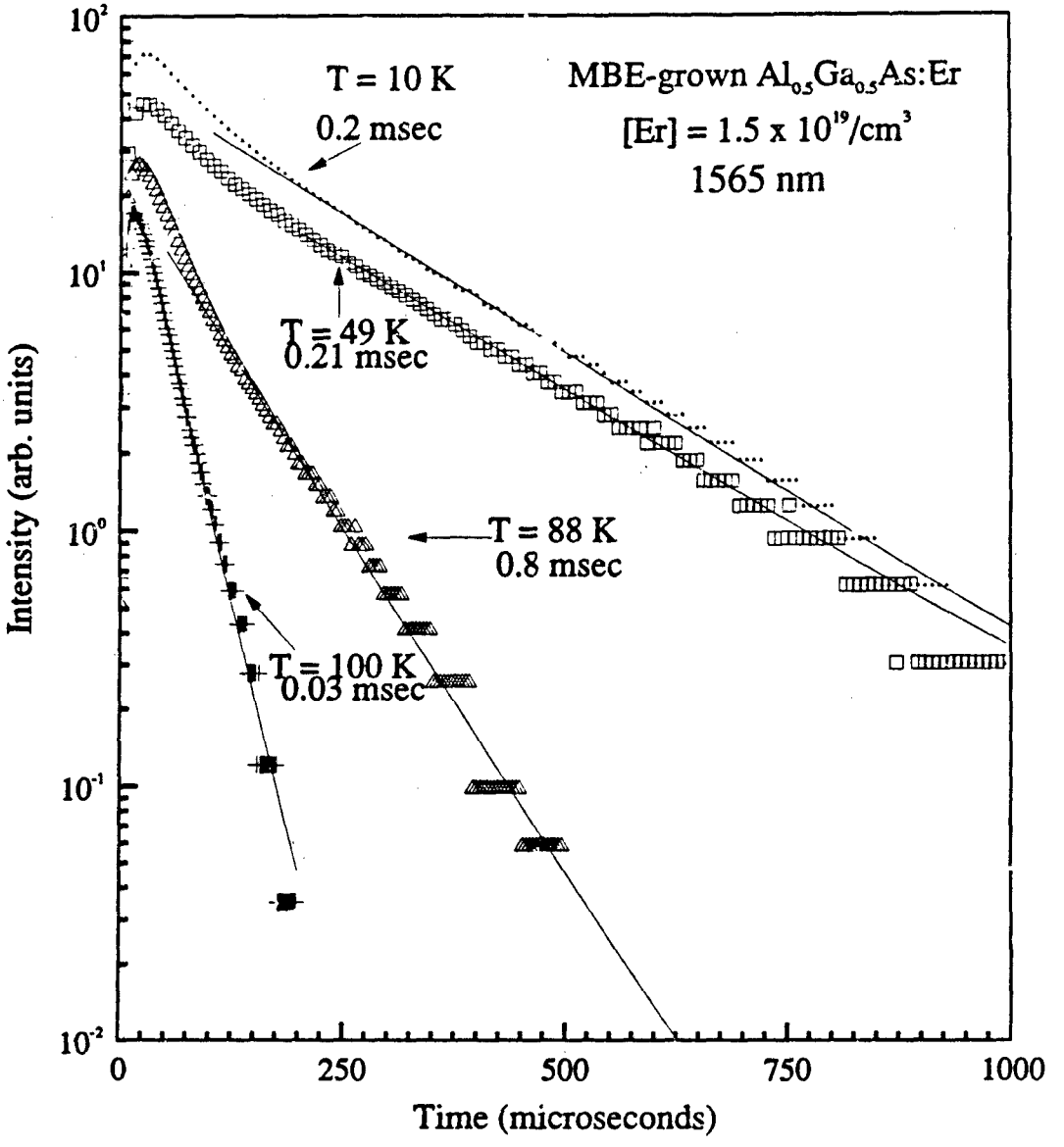

Figure 63 Time decay of the 1.565 μm emission from MBE-grown $Al_{0.5}Ga_{0.5}As$:Er measured at 10, 49, 88, and 100 K

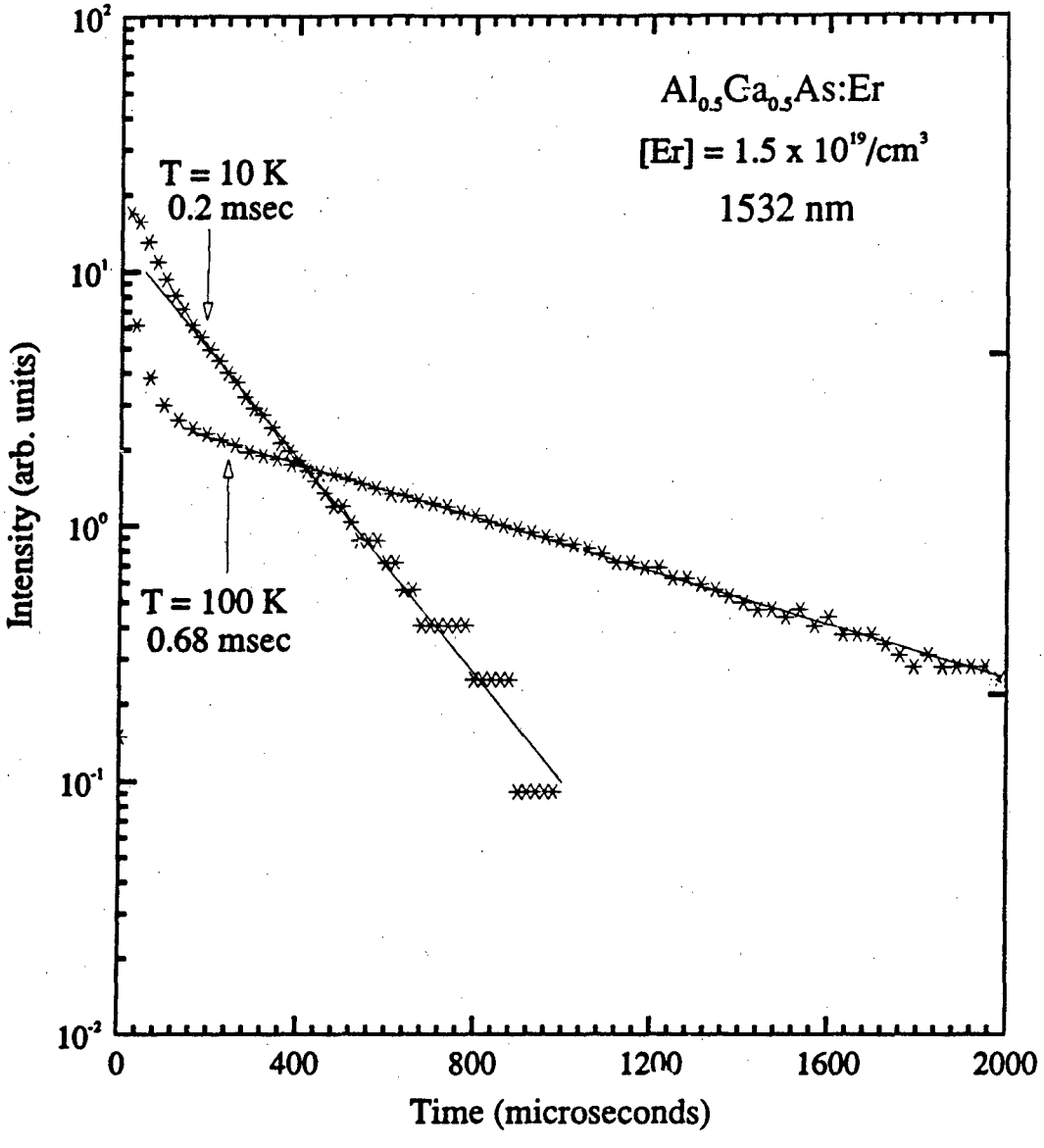

Figure 64 Time Decay of the 1.532 μm emission from MBE-grown $Al_{0.5}Ga_{0.5}As$:Er measured at sample temperatures of 10 and 100 K

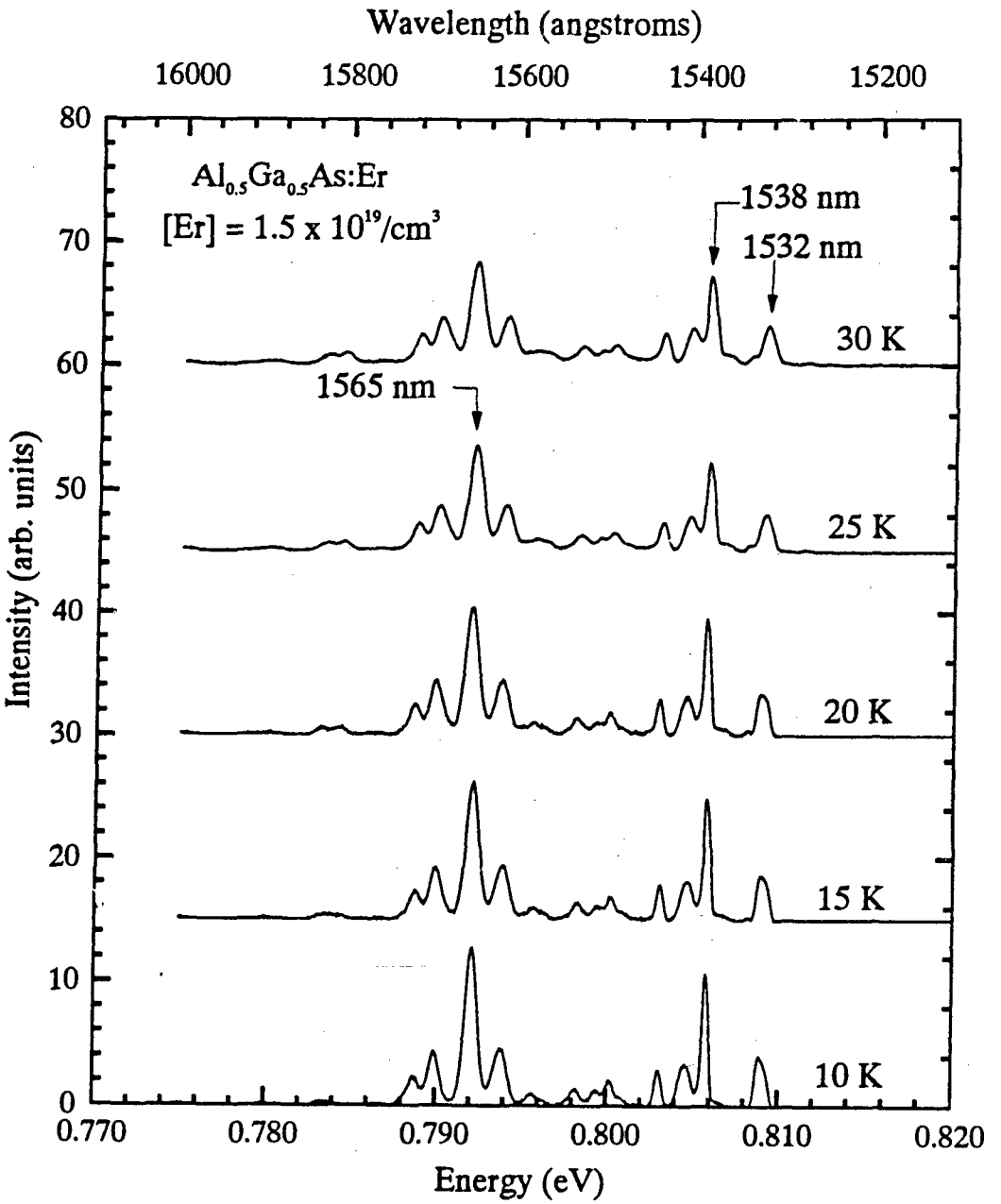

Figure 65 Photoluminescence of MBE grown $Al_{0.5}Ga_{0.5}As:Er$ measured at T = 10, 15, 20, 25, and 30 K

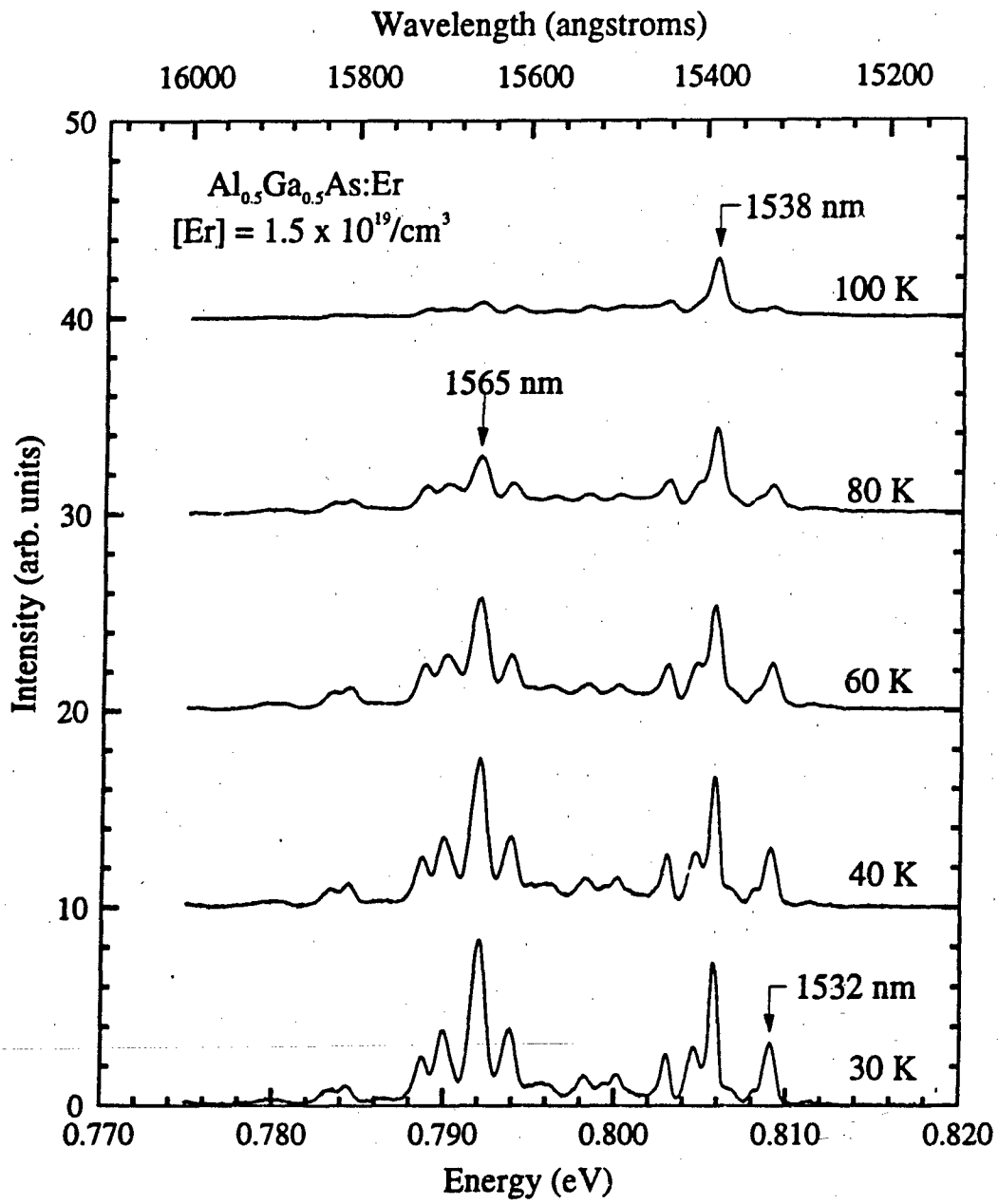

Figure 66 Photoluminescence of MBE grown $Al_{0.5}Ga_{0.5}As$:Er measured at T = 30, 40, 60, 80, and 100 K

As can be seen from figures 65 and 66, the intensities of both sets of emissions near 1.540 and 1.565 μm decreased gradually roughly at the same rate as T increased from 10 to 60 K. However, at a higher temperature, the intensity of the 1.565 μm emission quenches quickly with increasing temperature. For instance, upon increasing the temperature from 60 to 80 K, the intensity of the 1.565 μm emissions decreased by more than 50%, while the intensity of the 1.538 μm emission decreased by less than 20%. An even more drastic difference can be observed at 100 K, and at T > 100 K, the 1.565 μm emissions are completely quenched.

The 1.532 and 1.541 μm peaks seem to follow the same trend as the 1.565 μm emissions rather than the 1.538 μm emission. However, note that the 1.532 μm peak shows a weak shoulder emission on its low energy side. The intensity of this shoulder emission decreases much slower than that of the 1.532 μm emission, similar to the 1.538 μm emission. At T > 60 K, both emissions gradually become of comparable strengths. Thus, it is reasonable to assume that this shoulder emission is responsible for the long decay time component in figure 64 at high T. This is especially true since the lifetime measurements were done using wider slit openings than those used in PL measurements shown in figures 65 and 66, and thus have lower resolution. At low T, the intensity of this shoulder emission is much weaker than that of the 1.532 μm emission. Therefore, the decay will be mostly

a single exponential with a short time constant corresponding to the decay time of the 1.532 μm emission. A similar argument can be applied to the longer decay time observed for the 1.541 μm emission with increasing temperature. Note that at high T the intensity of this peak decreases very quickly, and it appears only as a shoulder on the 1.538 μm emission peak.

In order to conclude the discussion on the temperature dependence of the PL of $Al_{0.5}Ga_{0.5}As$:Er, consider the PL results shown in figure 67, which were measured at T = 165, 200, 250, and 300 K. At these high temperatures, the emissions are much weaker, and it was necessary to use lower resolution. Although some peaks can be seen on the lower energy side of the 1.538 μm peak, the 1.565 μm emissions are completely quenched. Note that the 1.538 μm emission retains its sharpness even at 300 K. The apparent broadening observed in the spectra is mostly due to the poor resolution. Also, there is no shift of the peak position as the sample temperature increases, which is an indication of the atomic nature of these emissions.

4.4.4 Excitation Measurements

Figure 68 shows the selective excitation spectrum of the 1.54 μm emission from MBE-grown GaAs:Er, and this was obtained by setting the spectrometer at 1.54 μm, while scanning the laser excitation energy. From 1.74 to approximately 1.47 eV,

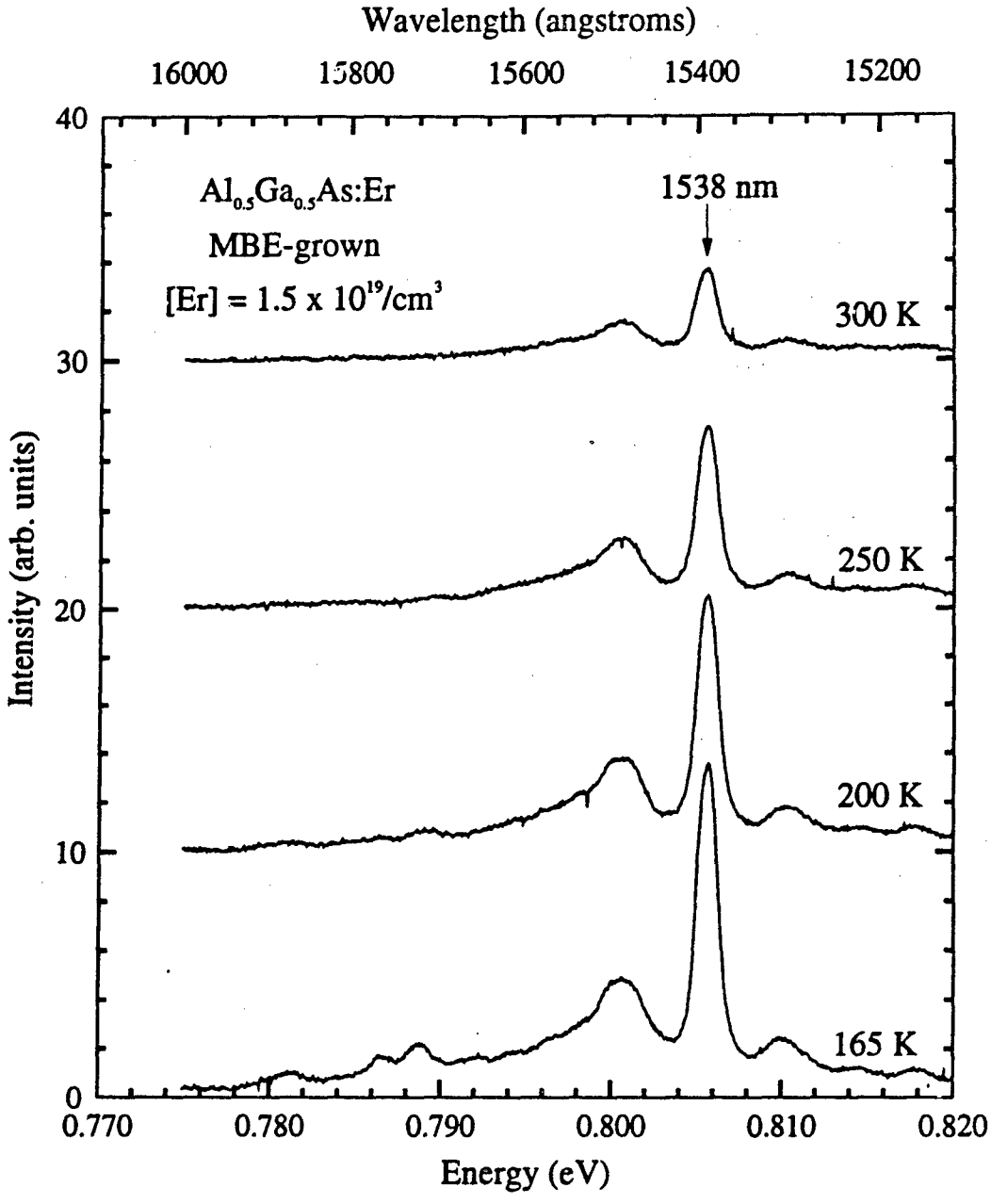

Figure 67 Photoluminescence of MBE-grown $Al_{0.5}Ga_{0.5}As:Er$ measured at T = 165, 200, 250, and 300 K

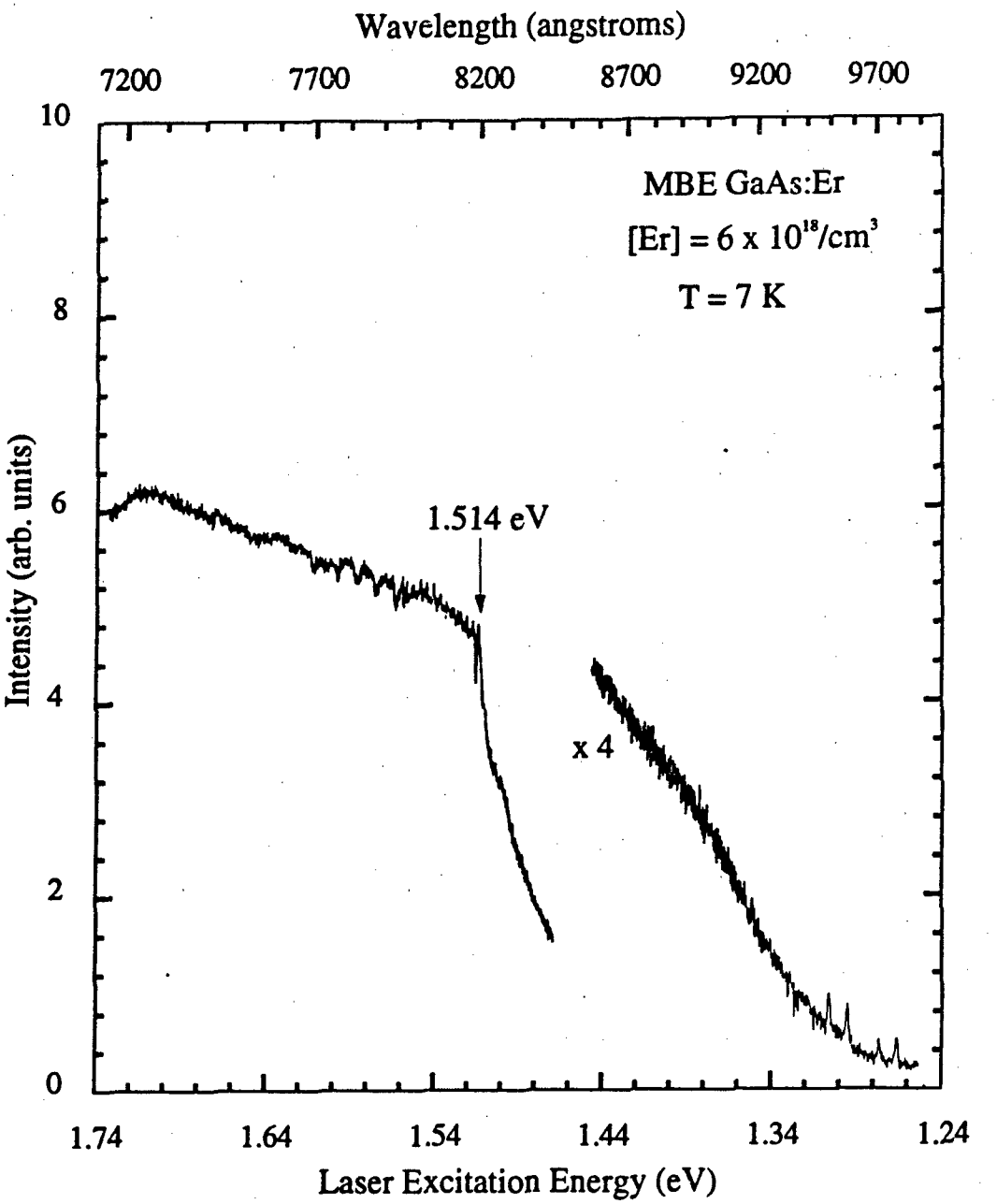

Figure 68 Selective excitation spectrum of the 1.540 μm emission from MBE-grown GaAs:Er with a laser excitation energy from 1.74 to 1.24 eV

the Ti-sapphire power output was same as shown in figure 22, while from 1.47 to 1.25 eV, the excitation power varied from 100 to 70 mW. As shown in figure 68, the second part of the selective excitation spectrum was magnified by a factor of 4. When the excitation laser energy decreases from 1.72 to 1.52 eV, the signal strength decreases. However, this is mainly due to the decrease in the excitation power. Decreasing the laser excitation energy below 1.519 eV results in a very sharp decrease in the signal intensity. Although it is hard to notice from the figure because of the wide energy scale used in the plot, there is a sharp excitation peak centered at 1.514 eV. Recall that the selective excitation spectra of the 1.538 μm emission from ion implanted p-type and SI-GaAs:Er samples showed a sharp excitation peak at 1.512 eV, as shown in figures 21 and 26, respectively. In the present case, the 1.514 eV peak is much sharper due probably to the fact that narrower slit openings were used to record the spectrum shown in figure 68 than that used to record the spectra shown in figures 21 and 26. In section 4.2.4, the 1.512 eV excitation peak observed for the ion implanted sample was interpreted as due to the capture of free excitons by an Er-related trap. It is reasonable to assume that in the present case, the 1.514 eV excitation peak has the same origin.

In section 4.2.1, it was noted that the strong Er^{3+} emissions observed from the ion implanted samples with the below-bandgap laser excitation could be correlated with the

presence of a particular group of emissions labeled as C2 emissions, i.e., peaks D, C, and F in figures 15, 16, and 17. These emissions are not observed for the MBE samples, as can be seen from the emission spectra shown in figure 69. Note that in both the above- and below-bandgap laser excitations, the spectra are dominated by a doublet with peaks at 1.5403 and 1.5419 μm. The absence of these C2 emissions can be correlated to why the signal strength decreases very rapidly as the laser excitation energy is decreased below 1.519 eV in the selective excitation spectrum shown in figure 68. That is, strong Er^{3+} emissions with below-bandgap excitation have been observed only from the samples showing the C2 emissions.

In figure 68, four very weak sharp excitation peaks are observed between 1.3 and 1.24 eV laser excitation. These could be due to resonant excitation of the 4f-shell from the ground state to the $^4I_{11/2}$ excited state, but the intensity is very weak. Thus it may be concluded that the direct excitation of the 4f-shell to the $^4I_{11/2}$ state does not become a significant process in the excitation mechanism of the 1.54 μm emissions. Thefore, the main excitation process is still the model proposed in section 4.2.4. The main difference between the selective excitation spectra of the main Er^{3+} emission from ion implanted samples and that of the MBE sample is that the 1.54 μm emission with the below-bandgap excitation of is much less efficient for the MBE sample. However, there is still a broad excitation band for the MBE samples which

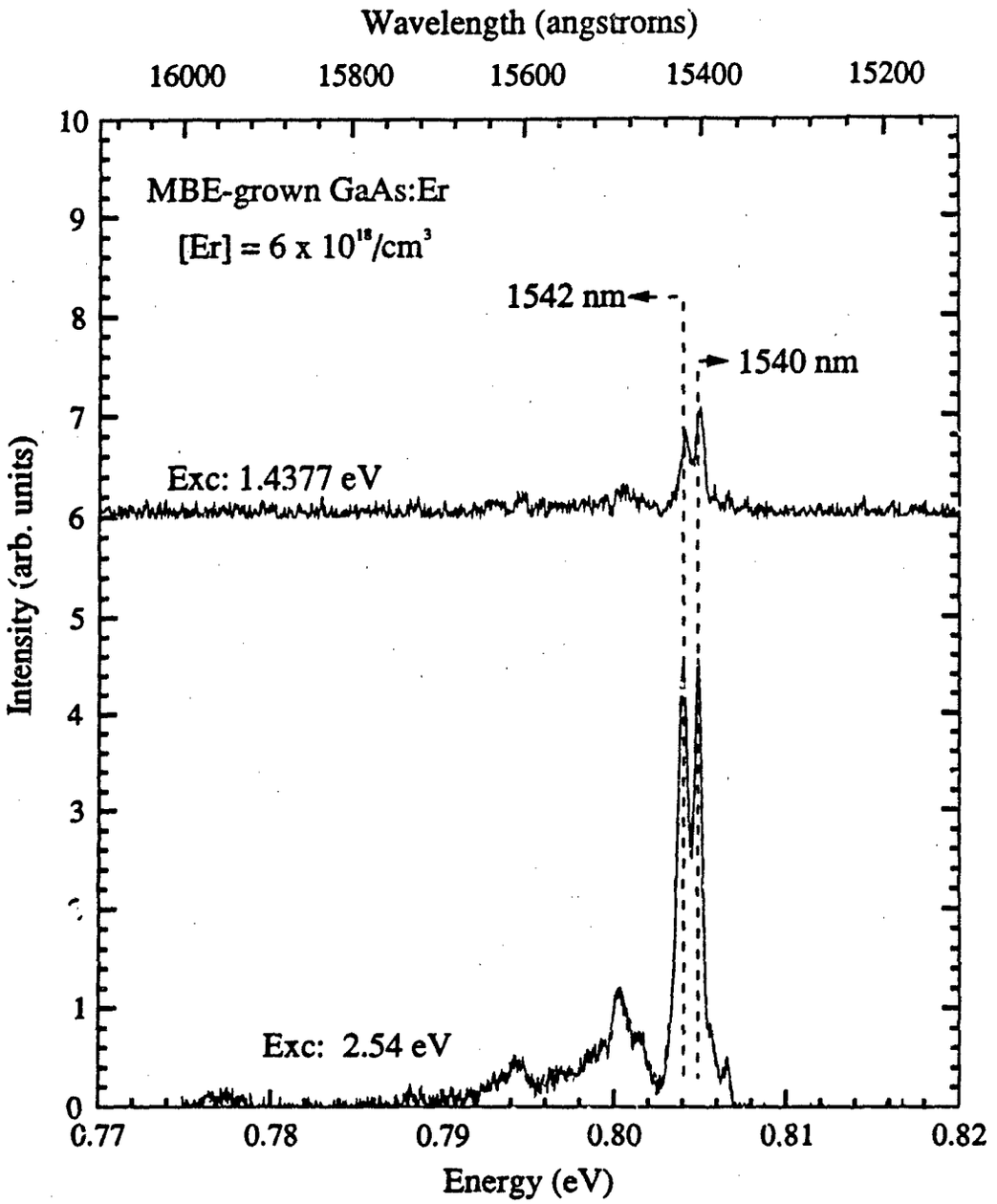

Figure 69 Photoluminescence spectra of MBE-grown GaAs:Er obtained with above- and below-bandgap laser excitation of 2.54 and 1.4377 eV, respectively

extends from the laser excitation energies near 1.51 eV to below 1.24 eV. In addition, the intensity of 1.54 μm emissions from the MBE samples showed the same sublinear dependence on the excitation power as those from the ion implanted samples, thus suggesting that a similar mechanism is responsible for the losses in the excitation process for both the ion-implanted and MBE-grown samples.

4.5 Oxygen Co-doping

4.5.1 Introduction

Currently, the nature of the luminescent centers giving rise to the 1.54 μm emissions is not well understood. The results discussed so far have pointed out that Er tends to form multiple types of centers in III-V semiconductors. Therefore, it is expected that it may react with any other impurities present in the material, thus forming various types of complexes. In particular, it is known that RE elements have strong affinity for oxygen. In a theoretical paper by Auzel et al. [1989] it was suggested that in III-V semiconductors Er is introduced with some oxygen impurity, leading to ionic bonding. As a basis for their assertion these authors used the results published previously by Ennen et al. [1985] on the luminescence from MBE GaAs:Er. Auzel et al. argued that in Er-doped III-V semiconductors the Stark splitting of the $^4I_{13/2}$ state is much larger than expected for covalent bonding. It should be pointed out this large crystal field splitting mentioned by Auzel et al. has not been observed by other researchers nor was it observed in current ion implanted or MBE samples, but this idea of an Er-O complex seemed to agree with the results obtained by Favennec et al. [1989], who studied the cathodoluminescence from GaAs:Er under an electron microscope and found that the 4f luminescence did

not originate homogeneously from the sample, but instead that the sample surface showed a series of bright and dark spots. In order to explain this result, it was suggested that Er was incorporated into GaAs as microparticles, most probably with O as a component. There have been other suggestions of an Er-O complex in III-V semiconductors. For example, Galtier et al. [1989] concluded that in their MBE samples the Er^{3+} emissions from AlGaAs are stronger than those from GaAs due to the presence of oxygen in the AlGaAs samples. If these ideas are right, then it is to be expected that oxygen co-doping will result in the enhancement of the 4f emissions. In fact, it has been found that the addition of certain impurities, such as O, enhanced the Er^{3+} emissions from Si:Er (Favennec et al. [1990] and Benton et al. [1991]). Furthermore, without the presence of these impurities, very weak or no Er luminescence was observed in Si (Benton et al. [1991]).

In order to test whether Er is incorporated in the form of oxygen complexes and if the 4f luminescence originates from these Er-O complexes, we studied the low temperature PL of GaAs and AlGaAs co-implanted with O and Er. In addition, oxygen was also implanted into MBE grown AlGaAs:Er samples. In the preliminary stage of this study, two criteria were used to select the O implantation energy and doses: (i) to have a maximum overlap between the O and Er implantation profiles; and (ii) to try different ratios of the O to Er concentrations. An implantation energy of 110 keV was used

for oxygen implantation to obtain a maximum overlap profile with the Er implanted at 1 MeV. The doses of O were selected such that the peak oxygen concentration was approximately half, the same, and five times that of the peak Er concentration. In this initial stage of the study, oxygen was implanted into n-, and p- type GaAs and $Al_xGa_{1-x}As$ samples with x = 0.2, 0.4, which were previously implanted with Er with a dose of 5 x $10^{13}/cm^2$ at 1 MeV. Oxygen was also implanted into SI, n-, and p-type GaAs samples that were previously implanted with an Er dose of 1 x $10^{13}/cm^2$ at 1 MeV. The doses of oxygen used were 4.9 x 10^{13}, 8.5 x 10^{13}, and 4.5 x $10^{14}/cm^2$ for the samples implanted with an Er dose of 5 x $10^{13}/cm^2$, and 5.3 x 10^{12}, 1.7 x 10^{13}, and 3.4 x $10^{13}/cm^2$ for the samples implanted with an Er dose of 1 x $10^{x3}/cm^2$. Based on the results from the preliminary study, it was decided to include the oxygen doses of 10^{13}, 10^{14}, and $10^{15}/cm^2$.

4.5.2 Luminescence of GaAs:(Er+O).

The results from the preliminary study indicated that O co-implantation into GaAs:Er did not enhance the Er^{3+} emissions, and the results are illustrated in figures 70 and 71, which show the low temperature PL from the SI and n-type GaAs:(Er+O) samples, and the O dose used is shown next to each spectrum, and the arrows on the left axis indicate the zero luminescence line of each spectrum. All spectra shown in these figures

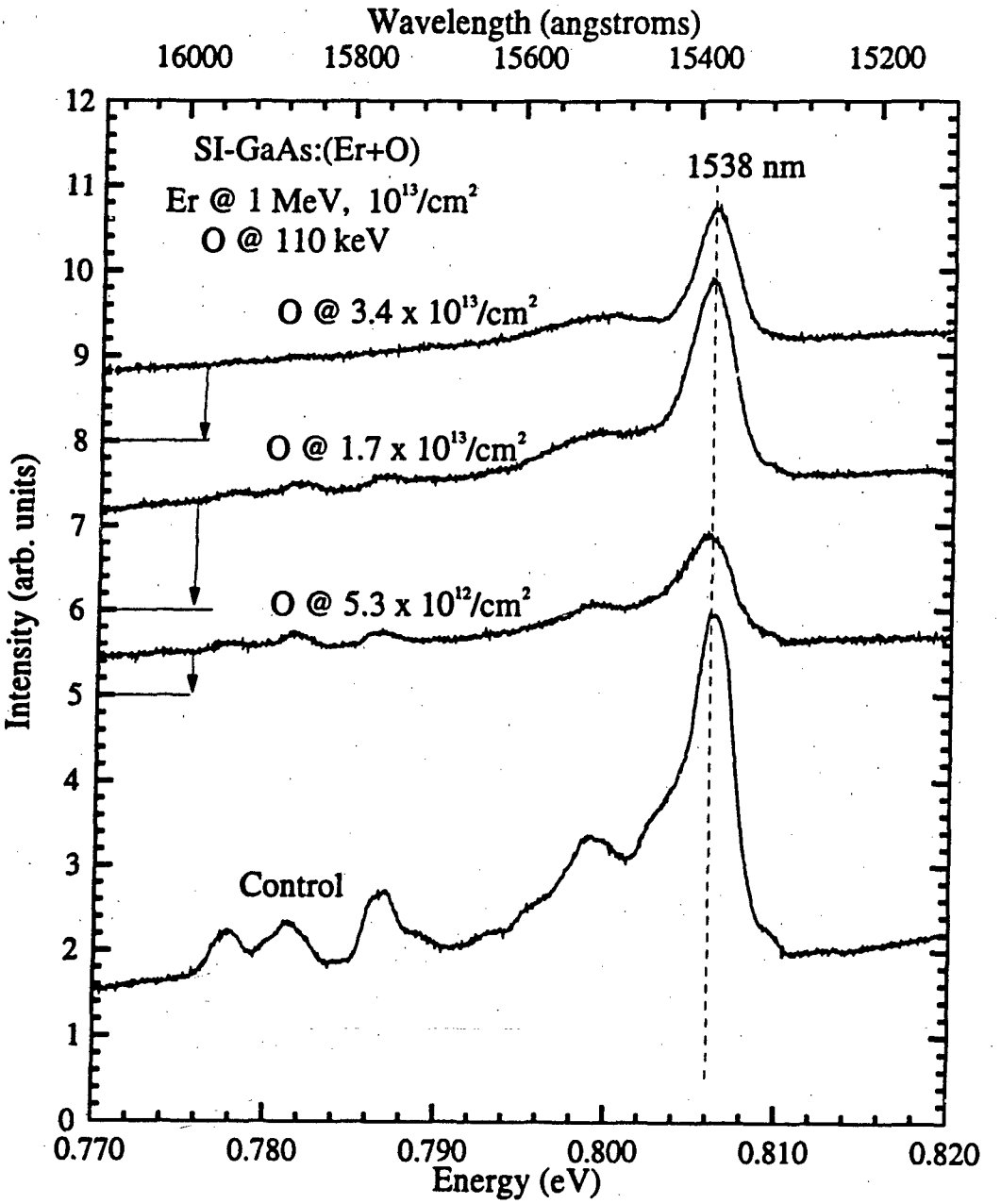

Figure 70 Photoluminescence emission spectra of SI-GaAs:(Er+O) for various O doses implanted at an energy of 110 keV

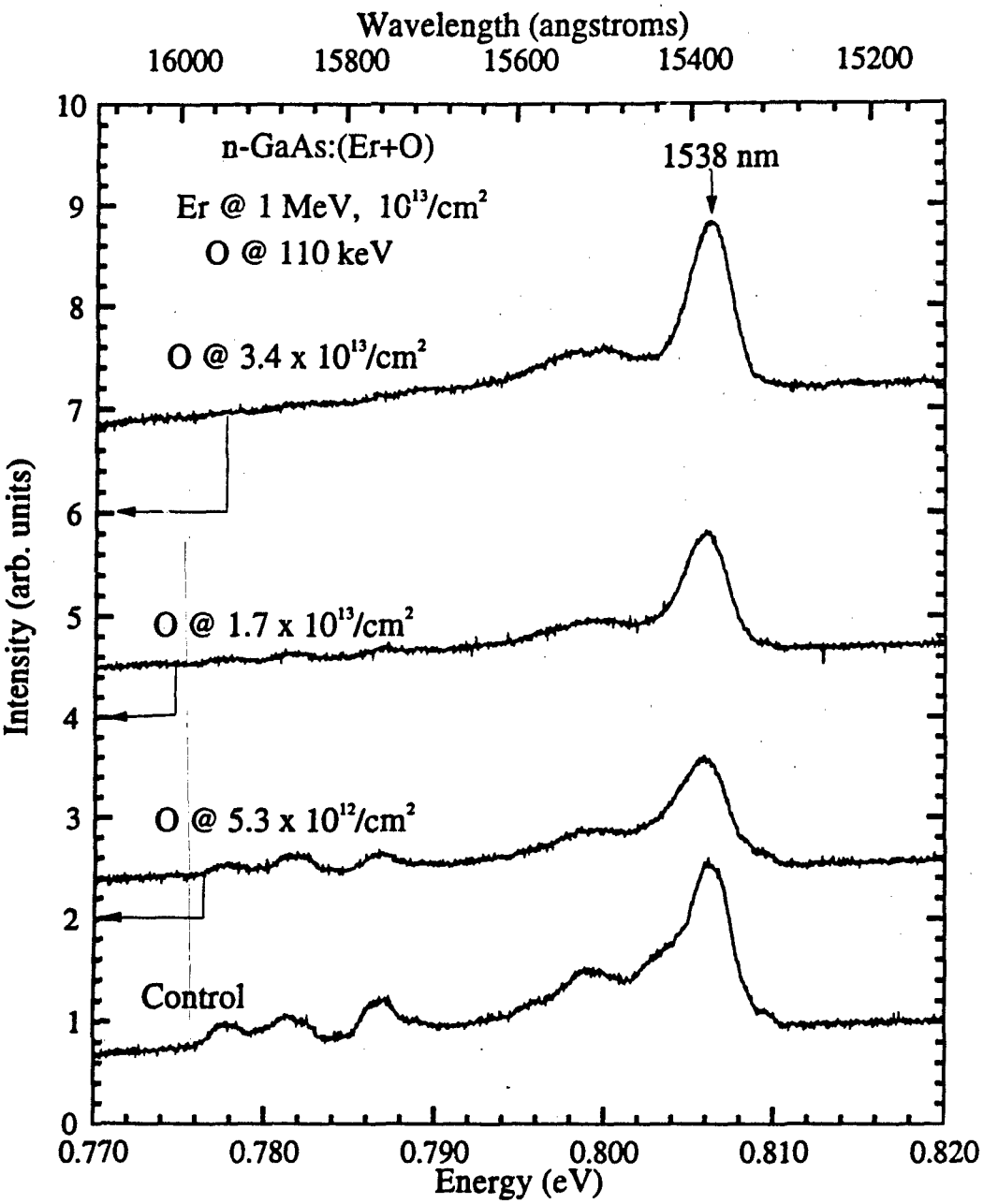

Figure 71 Photoluminescence emission spectra of n-GaAs:(Er+O) at various O doses implanted at an energy of a 110 keV

were taken using wide slit openings of 1000 and 2000 μm for the entrance and exit slits, respectively, because of the low intensity of the emissions near 1.54 μm from these samples. The samples were first implanted with an Er dose of 1 x 10^{13}/cm^2 at 1 MeV, followed by the O implantation at an energy of 110 keV and then annealing at 750 °C for 15 seconds using the RTA method. Among the SI-GaAs samples, the control sample implanted with Er but not implanted with O showed the most intense Er^{3+} emissions, as shown in figure 70. The PL intensity of the Er^{3+} emissions decreased at least threefold upon O co-implantation at the lowest O dose of 5.35 x 10^{12}/cm^2. At a higher O dose, the PL intensity increased approximately twofold compared to that of the sample co-implanted with the lowest O dose, but it decreased again at the highest O dose of 3.4 x 10^{13}/cm^2. For the n-type samples, the PL intensity also decreased upon co-doping with the lowest O dose as shown in figure 71. As the O dose was increased to 3.4 x 10^{13}/cm^2 the intensity increased to approximately the same strength as that in the control sample. Similar results were obtained for the p-type samples.

4.5.3 Luminescence of AlGaAs:(Er+O)

In contrast to the results discussed above, it has been consistently observed that the 4f emissions from ion implanted $Al_xGa_{1-x}As$ are enhance upon oxygen co-implantation at an energy

of 110 keV. A preliminary study involved oxygen implantation into samples of $Al_xGa_{1-x}As$:Er with x = 0.2 and 0.4, and the results of the low temperature PL from these samples are shown in figures 72 and 73. The Er dose used was 5 x $10^{13}/cm^2$, and all the samples were annealed at 750 °C using RTA following O implantation. As shown in figure 72, oxygen implantation at a dose of 4.2 x $10^{13}/cm^2$ resulted in an twofold increase in the PL intensity of the main Er^{3+} emissions from that of the $Al_{0.2}Ga_{0.8}As$:Er sample. Also, the PL emission spectrum of the co-doped sample shows some new peaks that are not seen in the control sample. As the oxygen dose increases, the Er^{3+} emissions become stronger, and the strongest Er^{3+} emissions were observed for the sample implanted with the highest O dose of 4.25 x $10^{14}/cm^2$. In that case, the PL intensity of the main Er^{3+} emission at 1.5375 μm increased approximately by a factor of 3.5 compared to that of the control sample. The same trend was observed for the x = 0.4 samples as can be seen from figure 73. For these samples, the PL intensity of the 1.5375 μm emission was approximately five times stronger after O implantation at 4.25 x $10^{14}/cm^2$.

Further studies of Er and O co-implantation into $Al_xGa_{1-x}As$ with x = 0.1, 0.2, 0.3, and 0.4 yielded very similar results to those discussed above. As the O dose increased, the intensity of the main Er^{3+} emission increased by a factor of ten in the best case (for x = 0.1). Figures 74 to 77 show the low temperature PL from the $Al_xGa_{1-x}As$ samples with x = 0.1,

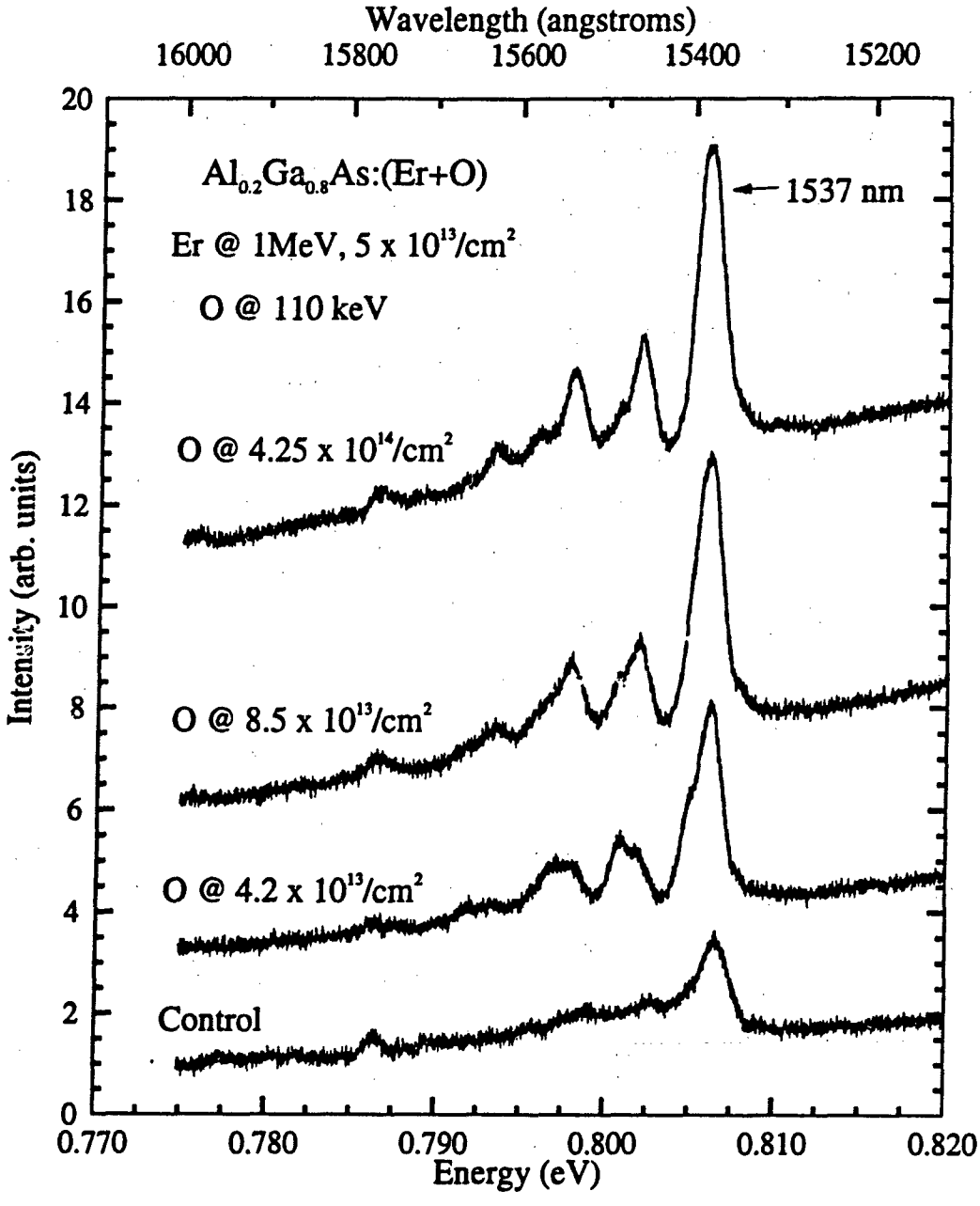

Figure 72 Photoluminescence emission spectra of $Al_{0.2}Ga_{0.8}As$:(Er+O) for various O doses implanted at an energy of 110 keV

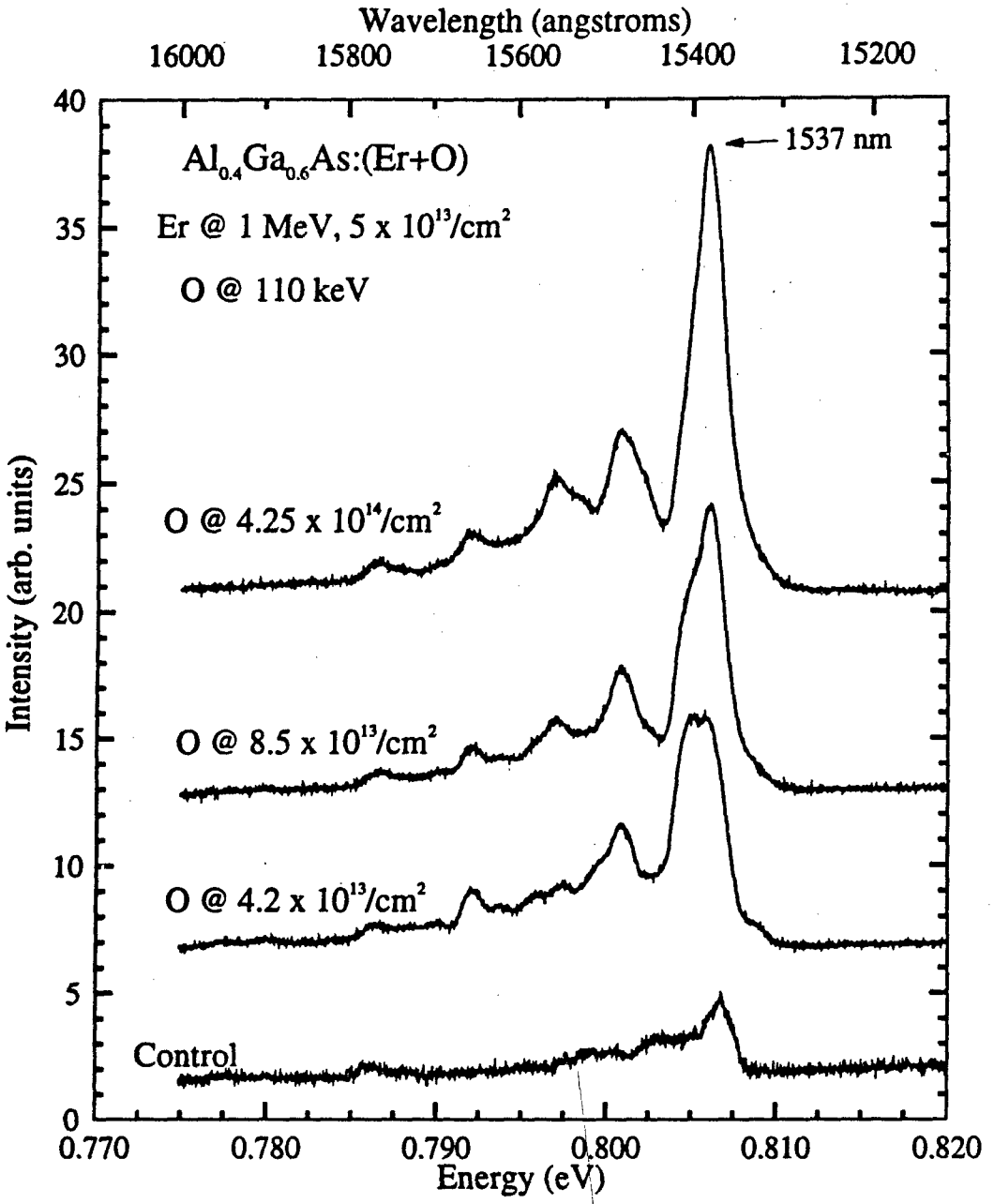

Figure 73 Photoluminescence emission spectra of $Al_{0.4}Ga_{0.6}As$:(Er+O) for various O doses implanted at an energy of 110 keV

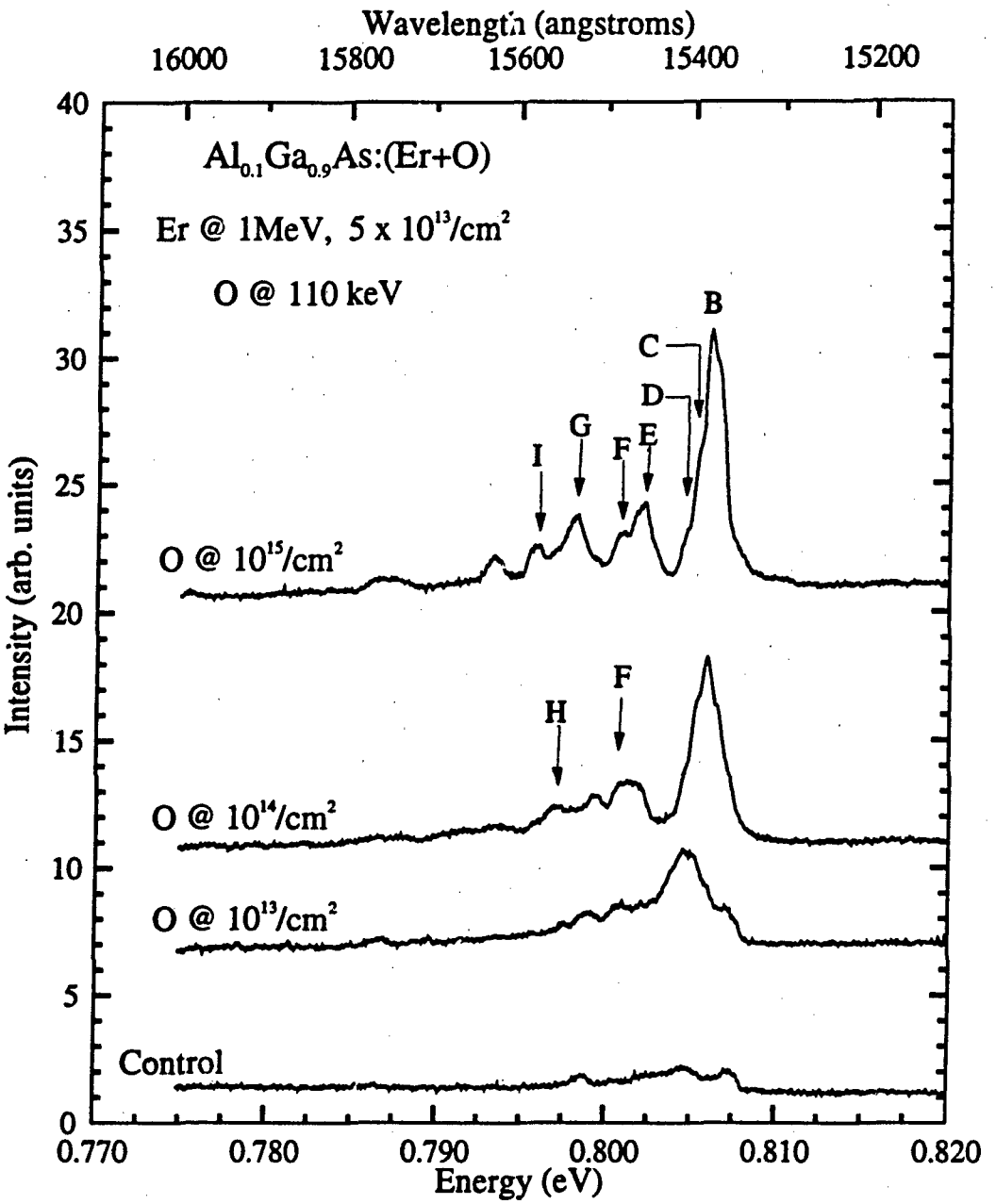

Figure 74 Photoluminescence of $Al_{0.1}Ga_{0.9}As$:(Er+O) for O doses of 10^{13}, 10^{14}, and 10^{15}/cm^2 implanted at 110 keV

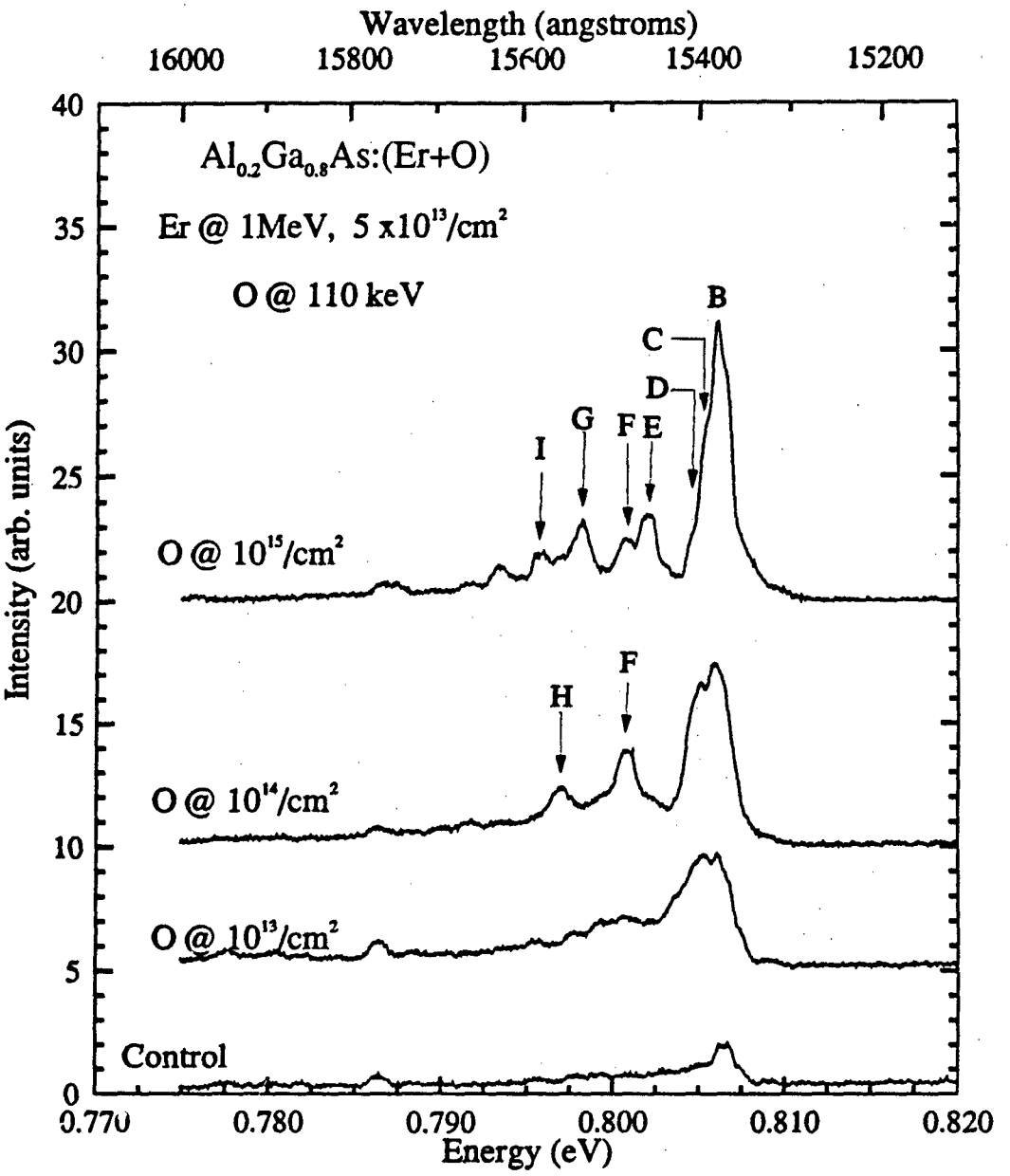

Figure 75 Photoluminescence of $Al_{0.2}Ga_{0.8}As$:(Er,O) for O doses of 10^{13}, 10^{14}, and 10^{15}/cm^2 implanted at 110 keV

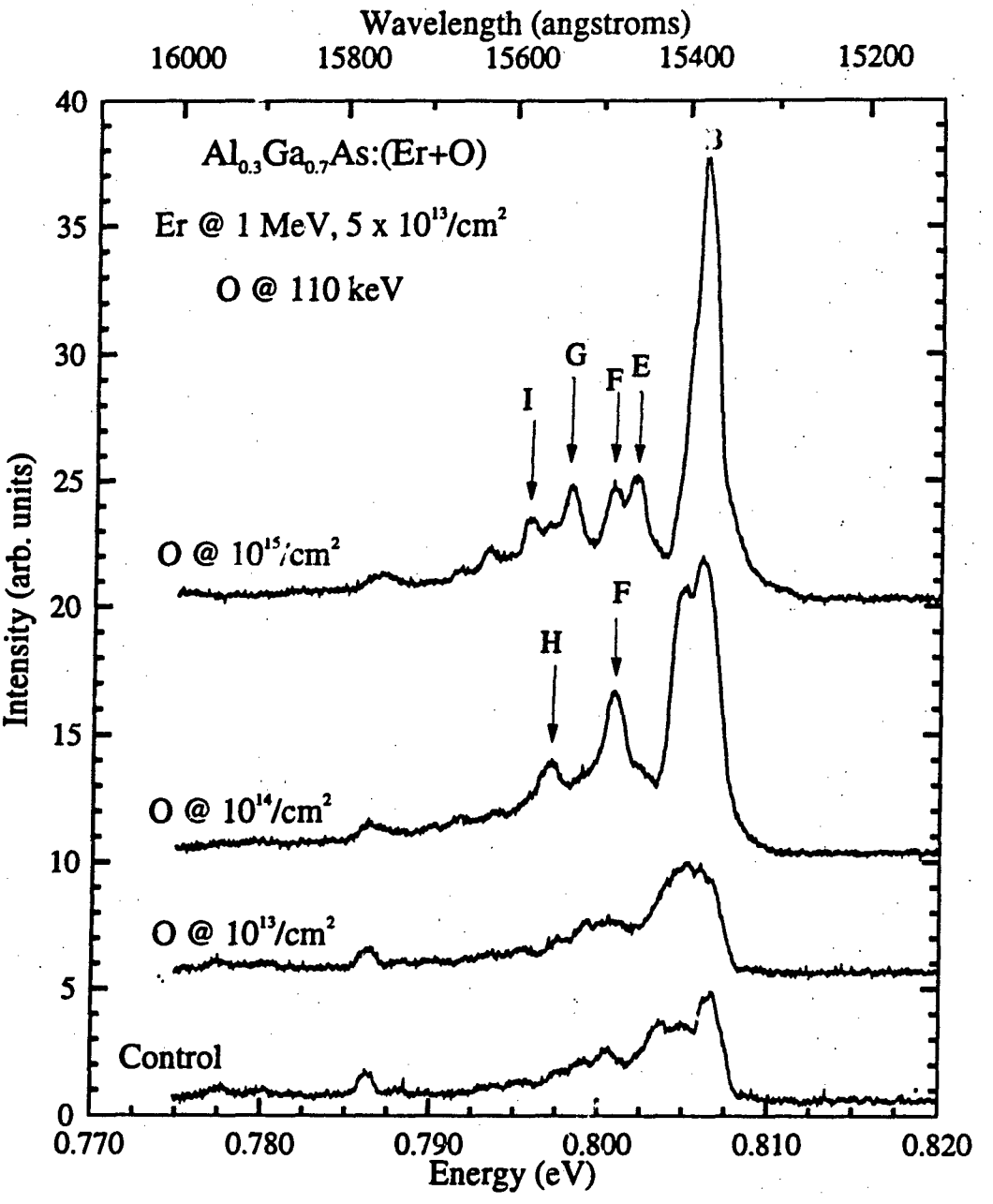

Figure 76 Photoluminescence of $Al_{0.3}Ga_{0.7}As$:(Er,O) for O doses of 10^{13}, 10^{14}, and 10^{15}/cm^2 implanted at 110 keV

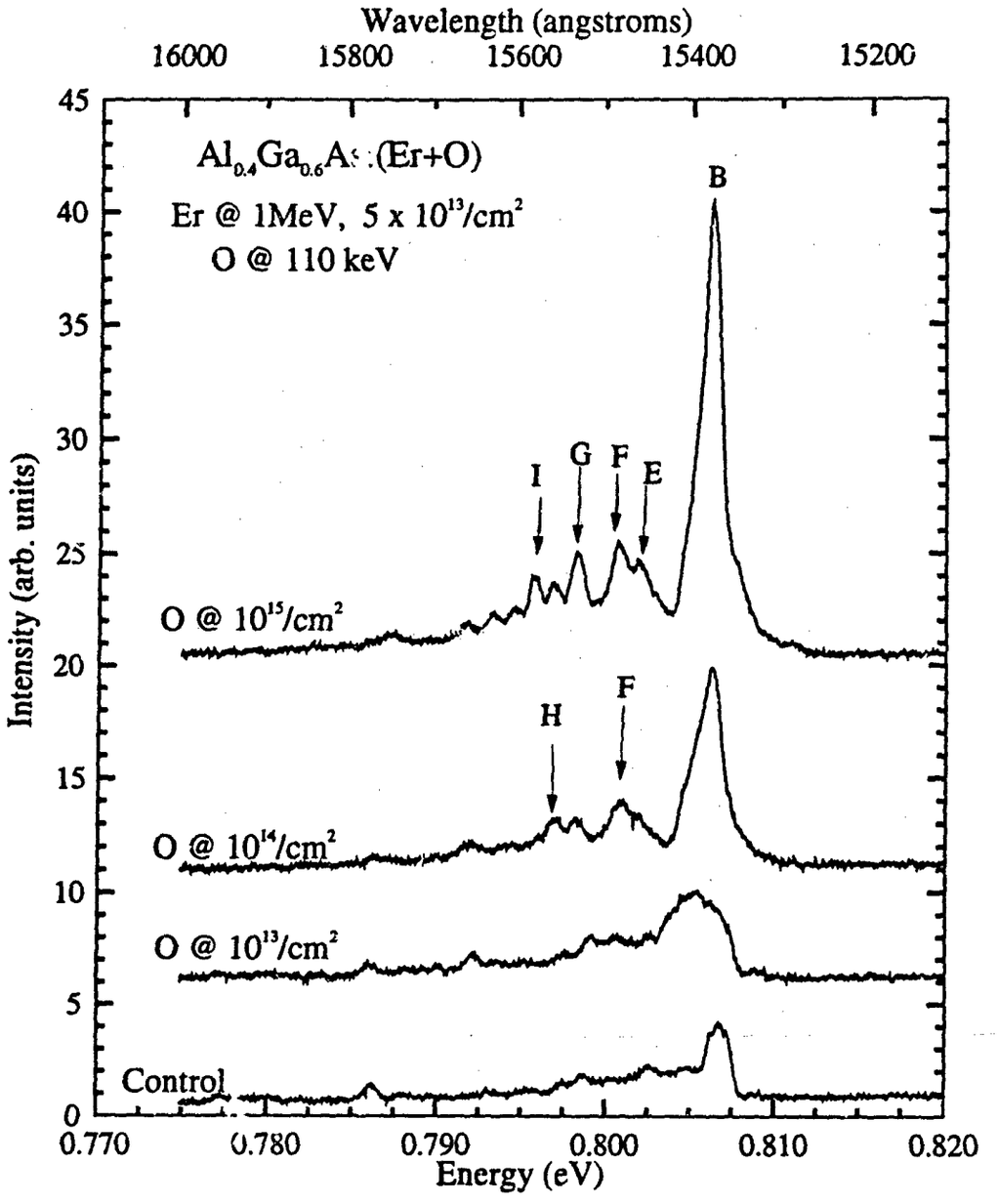

Figure 77 Photoluminescence of $Al_{0.4}Ga_{0.6}As$:(Er+O) for O doses of 10^{13}, 10^{14}, and 10^{15}/cm^2 implanted at 110 keV

0.2, 0.3, and 0.4 co-implanted with Er at 1 MeV with a dose of 5 x $10^{13}/cm^2$ and with O at 110 keV with doses of $10^{13}/cm^2$, $10^{14}/cm^2$, and $10^{15}/cm^2$. All the samples shown were annealed at 750 °C for 15 seconds using the RTA method. Table VII lists the wavelengths of the emission peaks marked with letters in the figures. The results showed a slight PL intensity dependence on the aluminum mole fraction.

Oxygen implantation at a low dose of $10^{13}/cm^2$ resulted in an increase in the PL intensity of the Er^{3+} emissions by a factor of four for the x = 0.1 sample shown in figure 74, and a threefold increase in the emission intensity for the x = 0.2 sample, as shown in figure 75. However, note that not all peaks were enhanced by the same factor. As a result, the relative intensities among different peaks changed after oxygen co-implantation. For both sets of samples, with x = 0.1 and 0.2, oxygen implantation at a higher dose of $10^{14}/cm^2$ resulted in stronger 4f emissions along with further changes in relative intensities among different peaks. Also, in both cases, the samples implanted with the highest O dose of $10^{15}/cm^2$ showed the strongest Er^{3+} emissions. However, only the peak at 1.5375 μm was strongly enhanced while the intensities of other peaks actually were decreased.

The x = 0.3 and 0.4 samples showed a strong enhancement of the Er^{3+} emissions after O co-implantation at 10^{14} and $10^{15}/cm^2$, while O implantation at the lowest dose of $10^{13}/cm^2$ did not change both the emission intensity and spectrum significantly.

Table VII

Main emissions from $Al_xGa_{1-x}As$:(Er,O)

Peak	Wavelength (nm)	Energy (eV)
A	1536	0.8071
B	1537	0.8064
C	1539	0.8055
D	1541	0.8046
E	1546	0.8020
F	1549	0.8006
G	1553	0.7983
H	1556	0.7969
I	1558	0.7958

These results are shown in figures 76 and 77. A comparison of figures 74 to 77 shows that O co-implantation at 10^{13} and $10^{14}/cm^2$ resulted in slightly different relative intensities among the various peaks and different emission peaks depending on the value of x. However, the PL spectra of the samples co-implanted with O at $10^{15}/cm^2$ show the same emission peaks and basically the same relative intensities among different peaks, independent of the aluminum concentration. Therefore, it seems that at low O doses, the PL is dominated by various emissions originating from different luminescent centers whose concentrations are sample dependent. On the other hand, the emission spectra from the co-doped samples at high O concentrations are dominated by an Er-O complex formed upon

co-doping. This can be understood by noting that the probability of an Er ion encountering an O ion is much lower in the samples with low O concentrations, while the formation of Er and O complexes is more probable in samples implanted with the high O doses.

Oxygen and Er were also co-implanted into different conductivity (SI-, n, and p-type) $Al_{0.29}Ga_{0.71}As$ samples, and the results of the PL spectra for these samples are shown in figures 78 to 80. Basically, the same trend of PL spectra was observed as a function of O dose, independent of the substrate conductivity. Although the emission spectra of the samples co-implanted with oxygen at $10^{13}/cm^3$ varied slightly for each sample, these samples essentially showed the same emission spectra as the corresponding control sample without oxygen implantation, however, at higher O doses each emission spectrum changed significantly from that of each control sample. In spite of that, the emission spectra obtained for O doses of 10^{14} and $10^{15}/cm^2$ are all identical except for the PL intensity for all three different conductivity $Al_xGa_{1-x}As$ samples. Since the results are the same in all three cases, only the samples of SI substrate, which are shown in figure 78, will be discussed. As in the previous cases, the addition of oxygen resulted in the creation of new peaks as well as changes in the relative intensities among various peaks. Although the sample implanted at the lowest O dose of $10^{13}/cm^2$ did not show much change in the PL intensity of the Er^{3+}

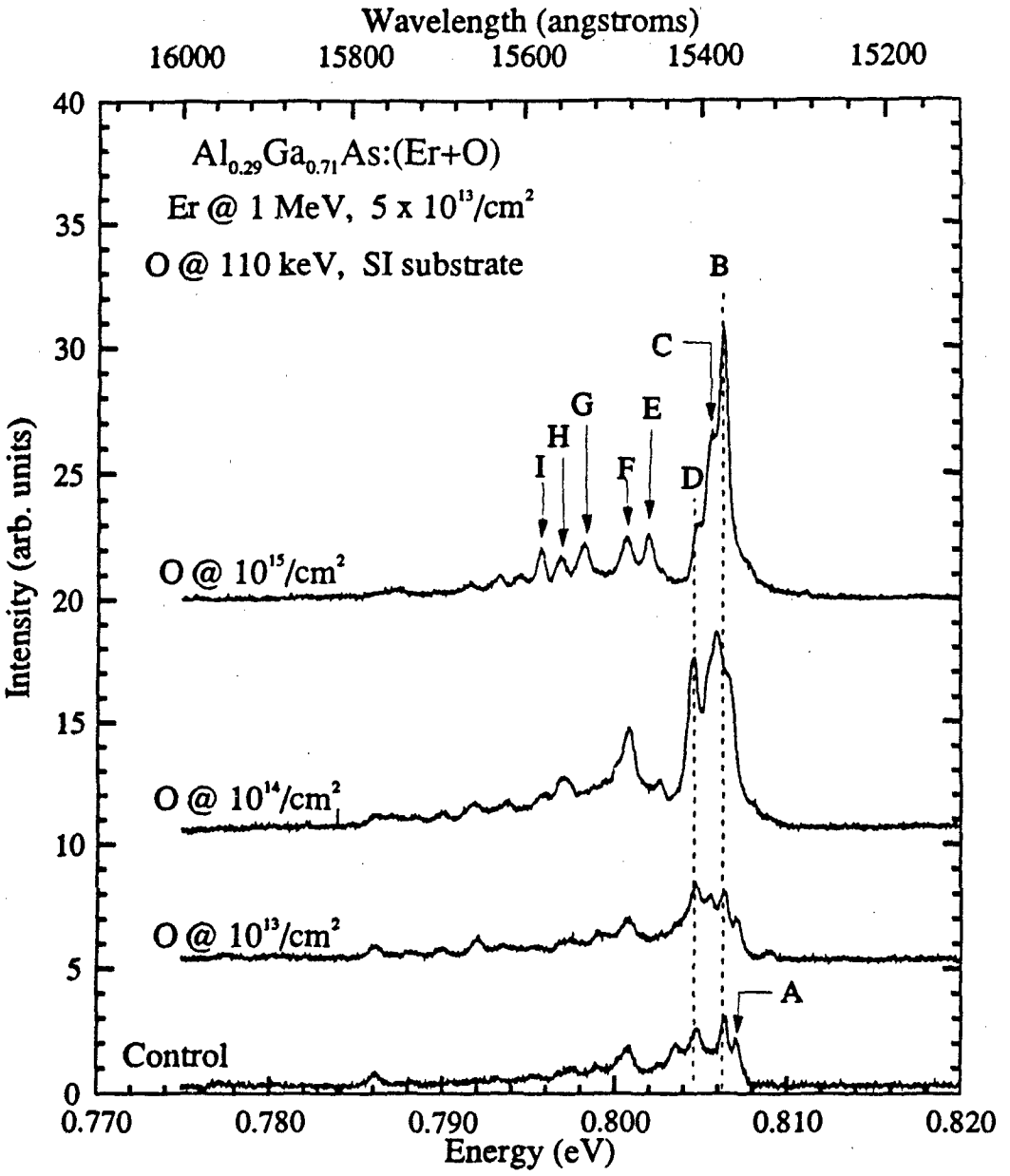

Figure 78 Photoluminescence of SI-$Al_{0.29}Ga_{0.71}As$:(Er+O) for various O doses implanted at 110 keV

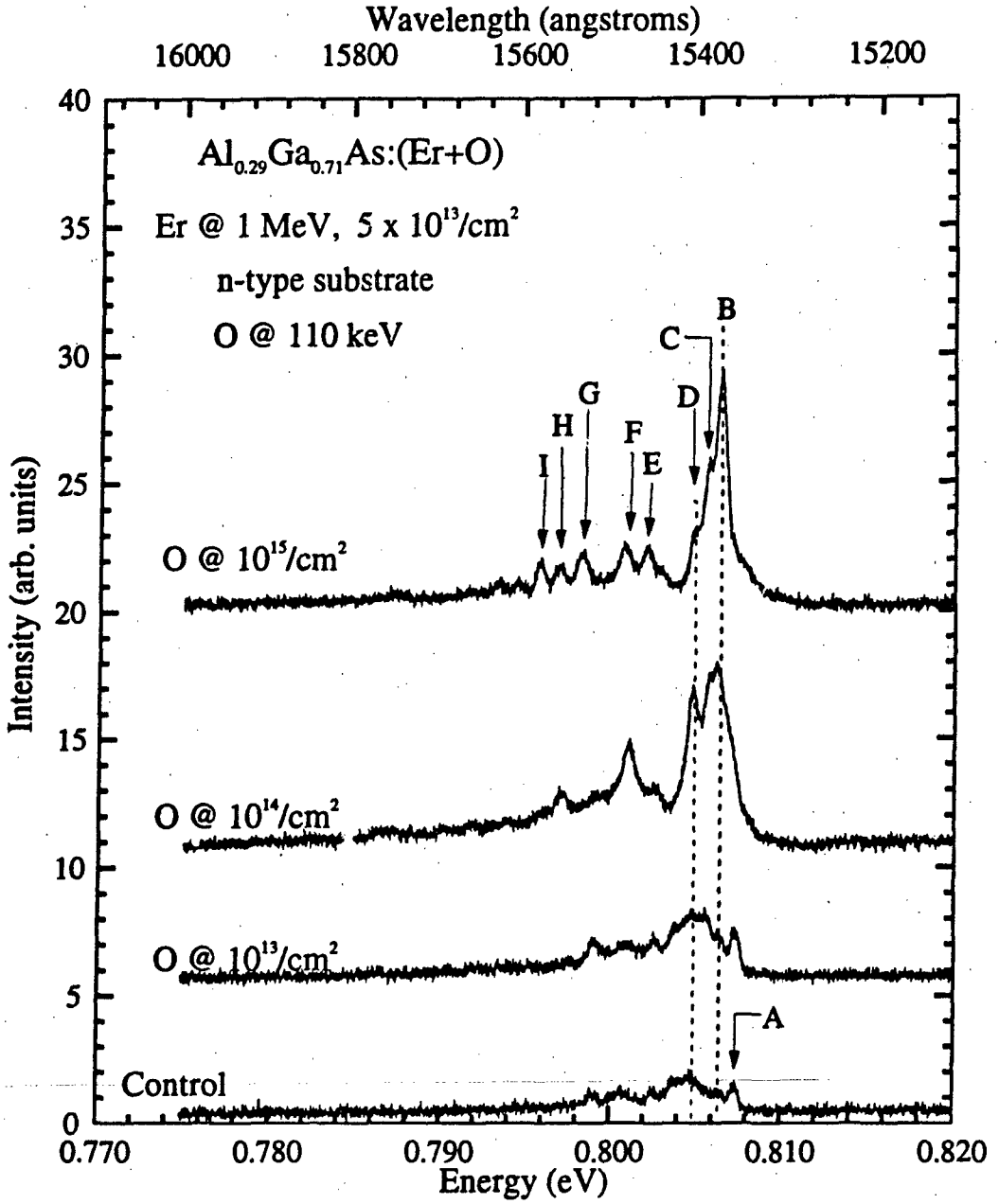

Figure 79 Photoluminescence of n-$Al_{0.29}Ga_{0.71}As$:(Er+O) for various O doses implanted at 110 keV

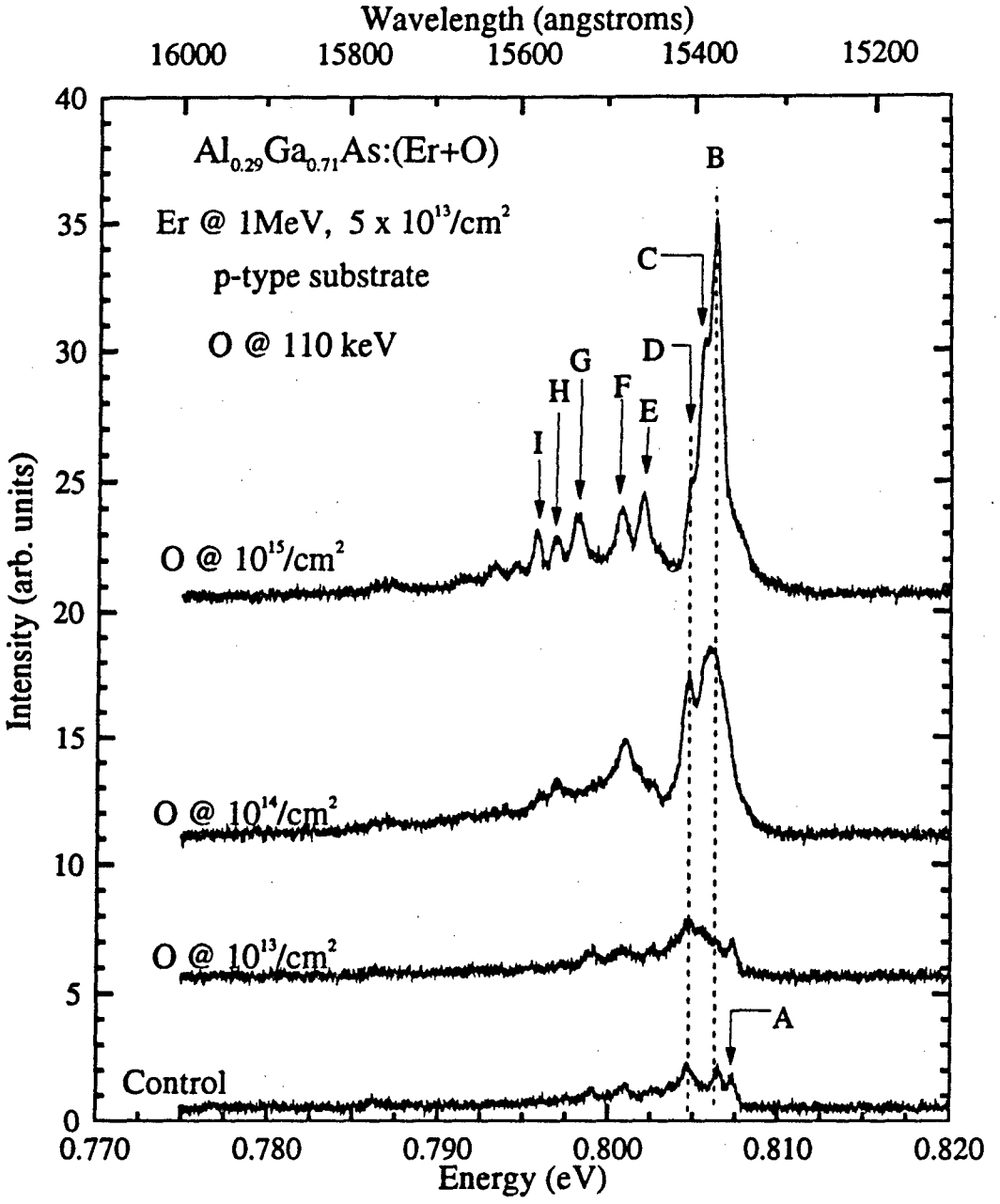

Figure 80 Photoluminescence of p-$Al_{0.29}Ga_{0.71}As$:(Er+O) for various O doses implanted at 110 keV

emissions from that of only Er-doped control sample, the relative intensity of each peak was changed. For instance, the strongest emission from the co-doped sample is at 1.5406 μm, while in the control sample the strongest peak is at 1.5375 μm. For the sample implanted with O at $10^{14}/cm^2$, the main emission at 1.5388 μm is approximately 2.5 times stronger than the main emission at 1.5375 μm from the control sample. Oxygen implantation at a dose of $10^{15}/cm^2$ resulted in further enhancement of the 1.5375 μm emission. Its intensity is approximately 3.5 times stronger than that in the control sample.

In order to study the PL dependence on the Er concentration, oxygen was also implanted into $Al_xGa_{1-x}As$ ($x = 0.1$ and 0.3) samples that were implanted with Er at a dose of $1 \times 10^{13}/cm^2$. Since the Er concentration was five times smaller than that in the previous cases, it was expected that the strongest Er emissions would be achieved at smaller O doses. Figure 81 shows the PL spectra for the $x = 0.3$ samples and the peaks are identified using the same symbols listed on Table VII. As in the previous cases of higher Er concentrations, implantation of O at $10^{13}/cm^2$ resulted in very little enhancement of the Er emissions. However, the sample implanted with an O dose of $10^{14}/cm^2$ showed very strong enhancement of the Er^{3+} emissions, and the spectra showed basically the same emissions that are observed for the samples implanted at an O dose of $10^{15}/cm^2$ and an Er dose of

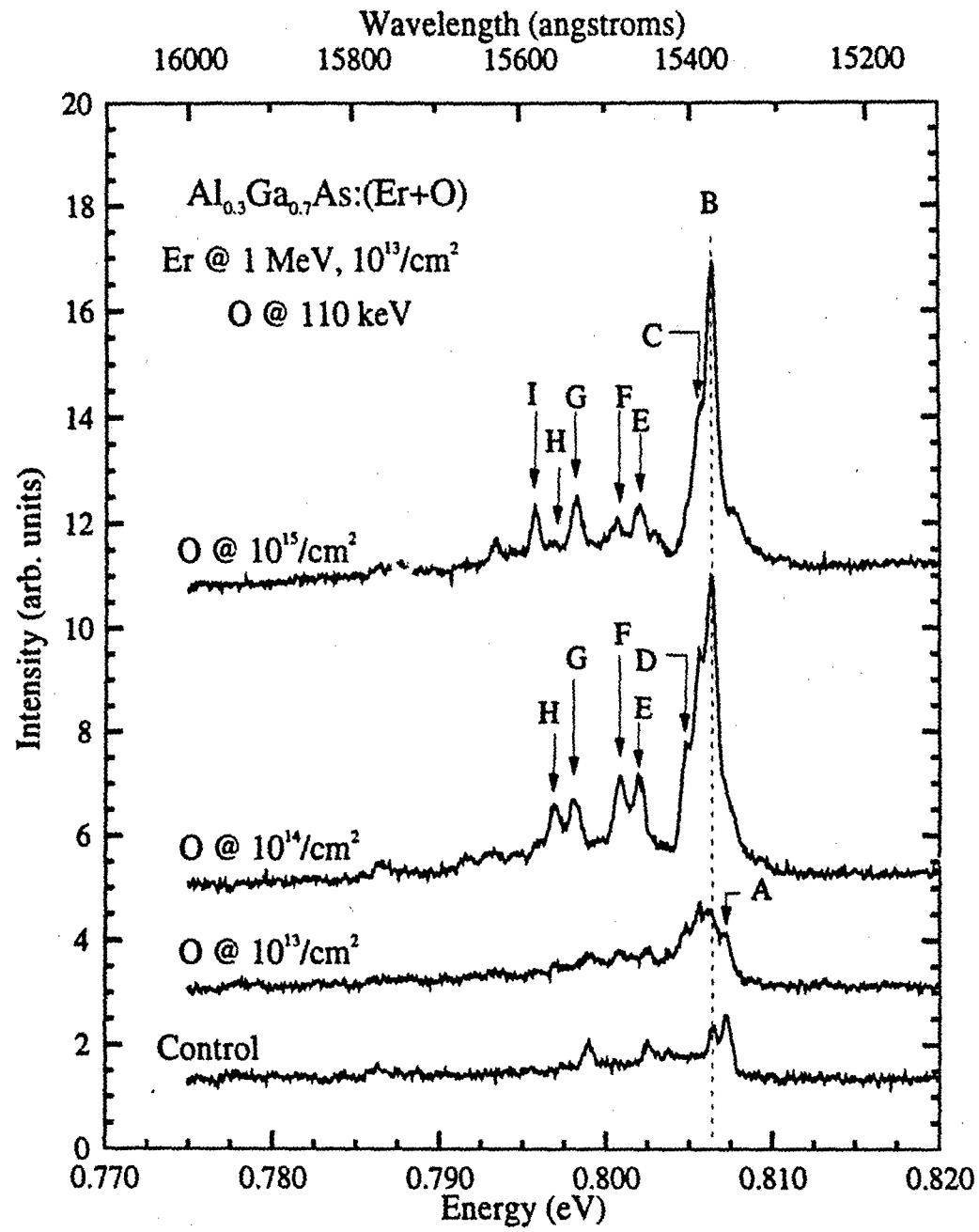

Figure 81 Photoluminescence of $Al_{0.3}Ga_{0.7}As$:(Er+O) implanted with Er at 1 MeV with a dose of 10^{13}/cm^2 for various O doses implanted at 110 keV

5 x $10^{13}/cm^2$, except for the absence of peak I at 1.558 μm. Increasing the O dose to $10^{15}/cm^2$ did not result in the increase of the intensity of the main Er^{3+} emissions any further, while the intensity of the secondary peaks rather decreased. It seems that for an Er dose of $10^{13}/cm^2$, the optimum O dose is between 10^{14} and $10^{15}/cm^2$. As shown in figure 82, similar results were obtained for the x = 0.1 samples. For these samples, the intensity of the Er^{3+} emissions increased by a small factor when co-implanting O at the lowest dose. Upon increasing further the O dose to 10^{14} and $10^{15}/cm^2$, the PL intensity increased by a factor of two. Comparing figure 81 with figure 82, it can be seen that the PL spectra for the x = 0.1 and 0.3 samples implanted with O at $10^{14}/cm^2$ are very similar, thus suggesting the presence of the same type of complexes in both samples. Also, it can be seen that for the samples implanted with O at $10^{15}/cm^2$ the ratio between the intensity of the main emission peak at 1.5375 μm (peak B) and that of peaks D, E, F, G, H, and I changed, thus suggesting that these emissions originate from a different luminescent center than peak B. Clearly, for the x = 0.1 samples, the optimum O dose is smaller than $10^{15}/cm^2$, but possibly slightly greater than $10^{14}/cm^2$.

4.5.4 Temperature Dependence

Temperature dependent photoluminescence experiments on $Al_{0.29}Ga_{0.71}As$:(Er+O) were also carried out. The samples used

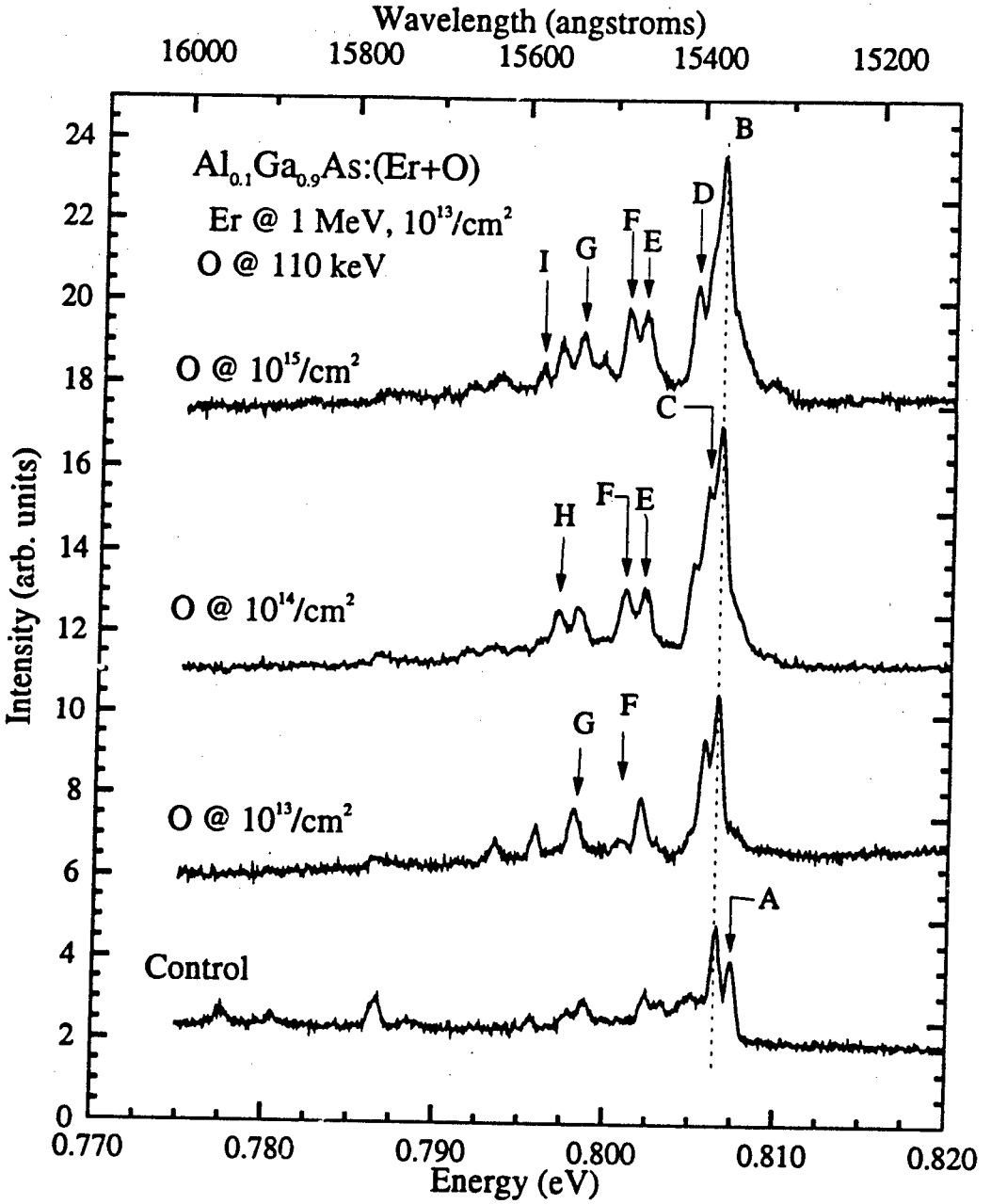

Figure 82 Photoluminescence of $Al_{0.1}Ga_{0.9}As$:(Er+O) implanted with Er at 1 MeV with a dose of 10^{13}/cm^2 for different O doses implanted at 110 keV

were implanted with an Er dose of 5 x $10^{13}/cm^2$ at 1 MeV and with an O dose of $10^{15}/cm^2$ at 110 keV followed by annealing at 750 °C for 15 sec. The PL intensity of the Er^{3+} emissions decreases with increasing sample temperature as shown in figures 83, 84, and 85. However, sharp Er^{3+} emissions can be seen even at room temperature, as shown in figure 86. As can be seen from figure 83, at T ≥ 60 K peak C cannot be distinguished clearly, and the main emission peak at 1.5375 μm has a broader linewidth, which is possibly due to fact that the observed peak is really a convolution of peaks B and C. The temperature dependence of peak E is different from that of the other emission peaks, i.e., as T increases from 20 to 125 K its intensity increases slightly, thus suggesting that this peak might be a "hot line", i.e., it is probably due to a transition from a higher level in the $^4I_{13/2}$ multiplet. New "hot lines" can also be seen at T ≥ 80 K such as the peaks labeled h1, h2, and h3 in figure 84. Although in figure 86 the Er^{3+} emissions seem to have a broader linewidth, this is due to the fact that this spectrum was recorded using wider slit openings than those used in figures 83 to 85. The spectra of the control samples is not shown in the figures, but it was observed that the integrated intensity of the Er^{3+} from the co-doped samples decreased with increasing T at approximately the same rate as the Er^{3+} emissions from the sample implanted with only Er. However, the emissions from the control sample were much weaker than those from the co-

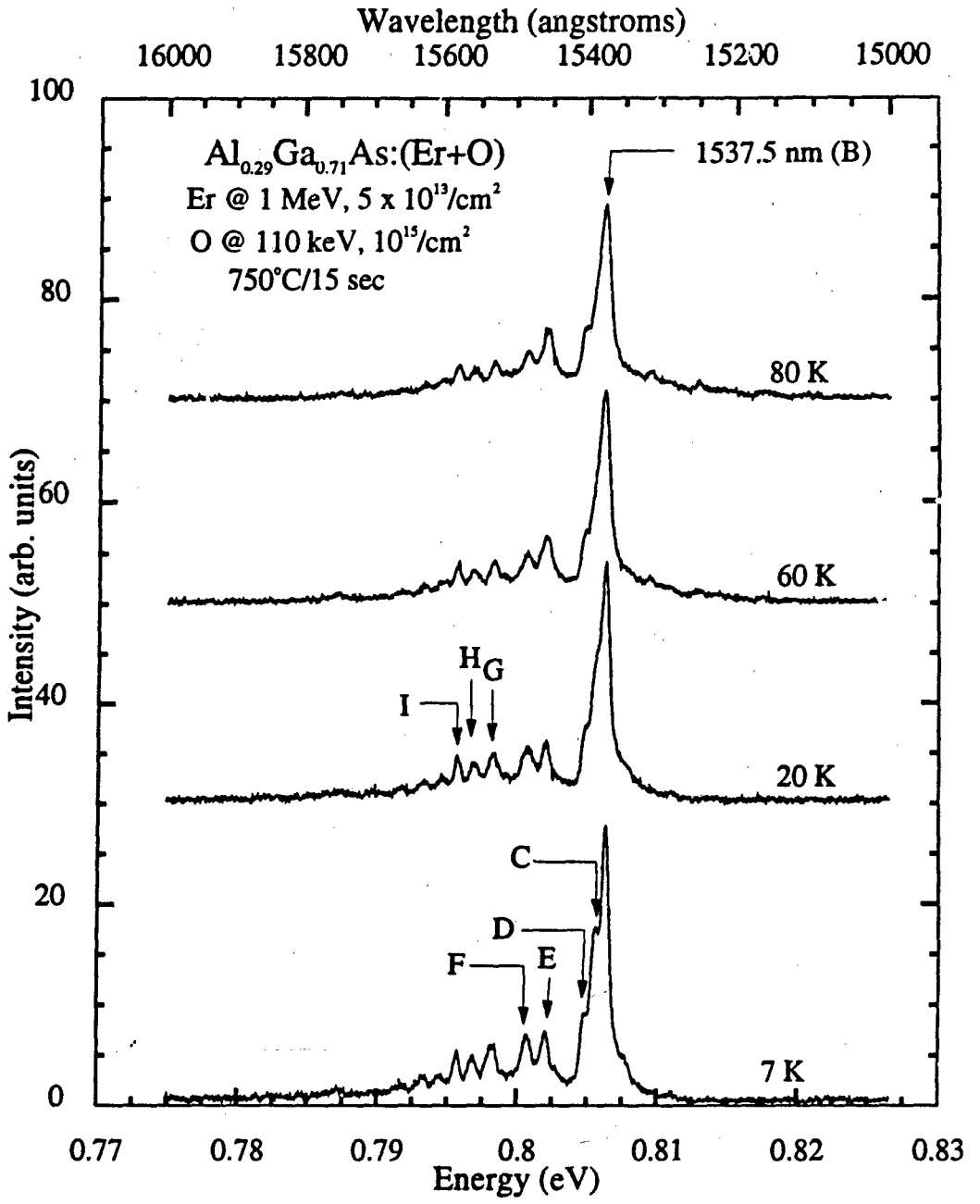

Figure 83 Photoluminescence of SI-$Al_{0.29}Ga_{0.71}As$:(Er+O) taken at various sample temperatures from 7 to 80 K

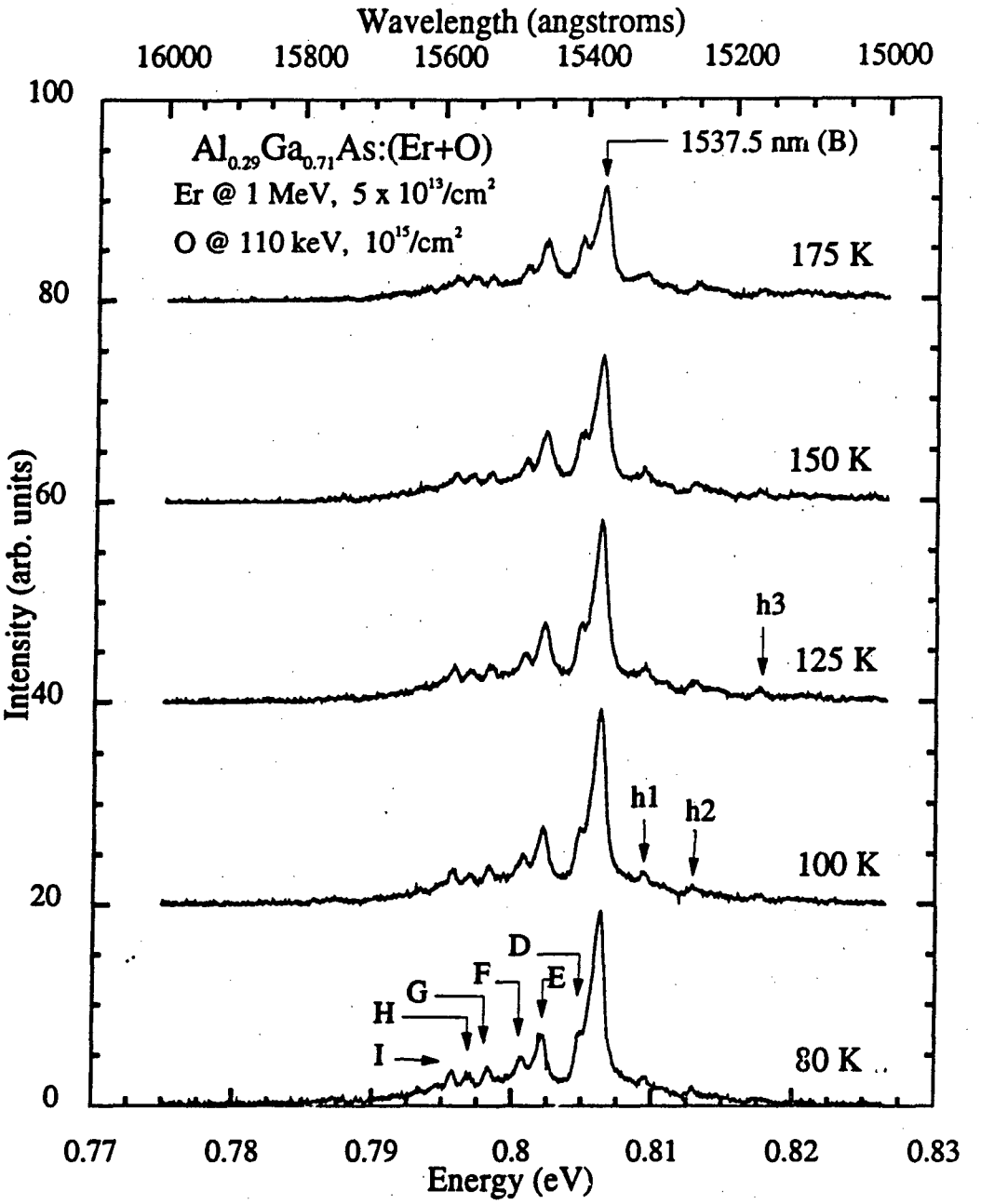

Figure 84 Photoluminescence of SI-$Al_{0.29}Ga_{0.71}As$:(Er+O) taken at various sample temperatures from 80 to 175 K

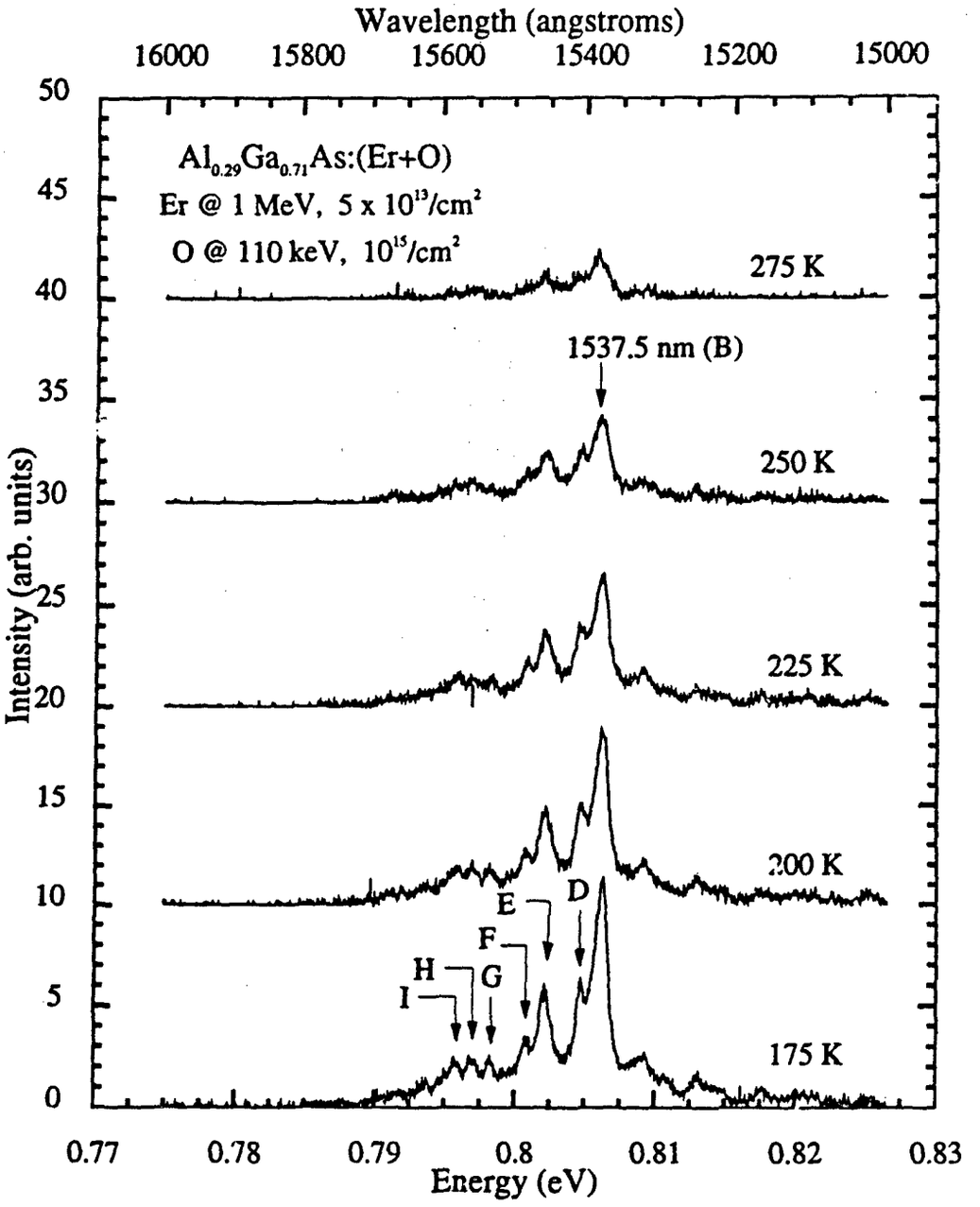

Figure 85 Photoluminescence of SI-$Al_{0.29}Ga_{0.71}As$:(Er+O) taken at various sample temperatures from 175 to 275 K

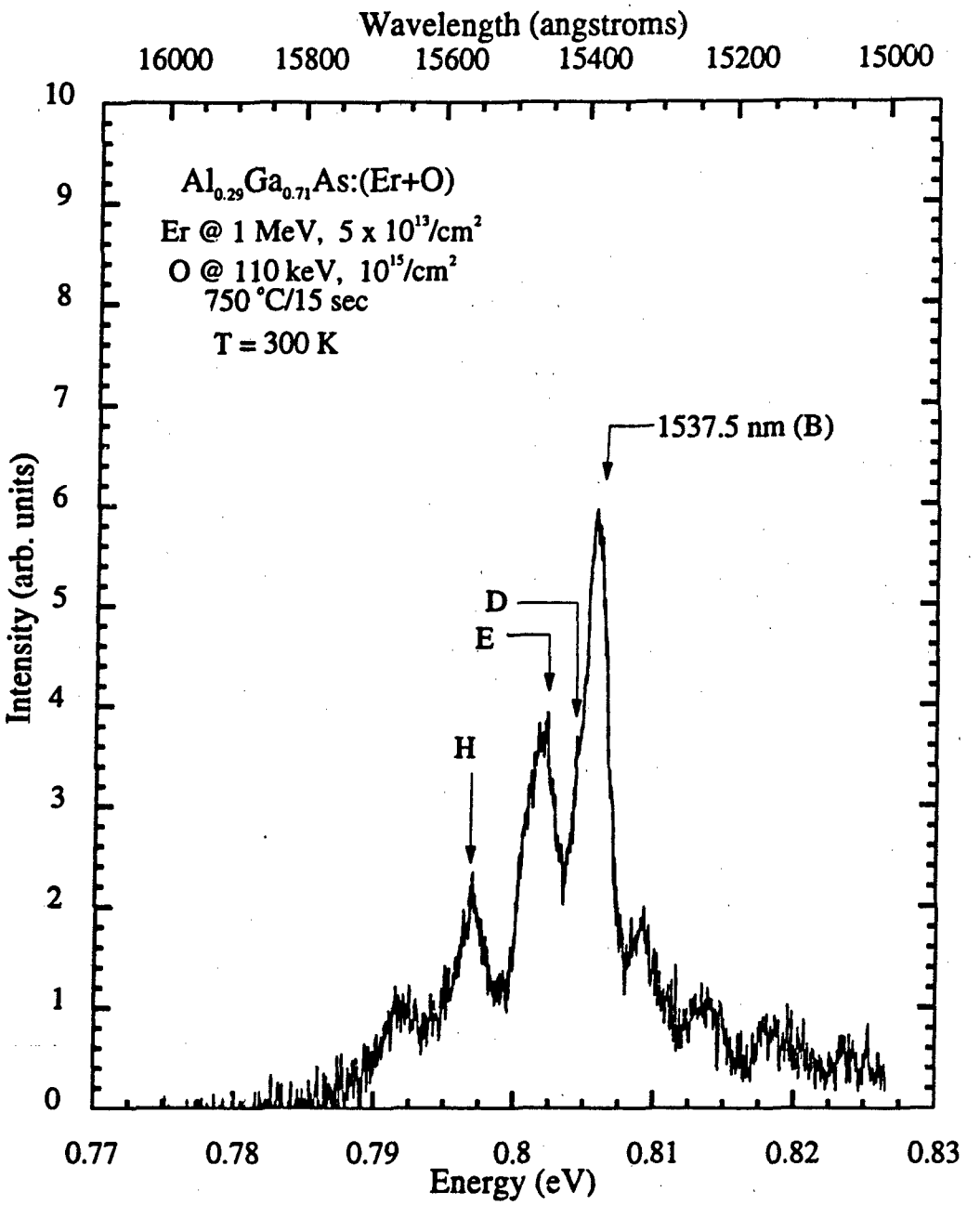

Figure 86 Room temperature photoluminescence from SI-$Al_{0.29}Ga_{0.71}As$:(Er+O) implanted with Er at 1 MeV with a dose of 5 x 10^{13}/cm^2 and with O at 110 keV with a dose of 10^{15}/cm^2

doped sample and could not be monitored at T > 225 K. For both the control and the co-doped samples the integrated intensity did not follow a simple trend and could not be fitted even with two activation energies.

4.5.5 Annealing Behavior

The low temperature PL of $Al_{0.3}Ga_{0.7}As$ co-implanted with Er at 1 MeV with a dose of 5 x $10^{13}/cm^2$ and with O at 110 keV with a dose of $10^{15}/cm^2$ was studied as a function of annealing temperature. It is interesting to compare the annealing behavior of the co-doped samples with the samples without oxygen doping. Figure 87 shows the PL spectra of AlGaAs:Er samples annealed at 750 and 850 °C for 15 sec and AlGaAs:(Er+O) samples annealed at 750, 800, and 850 °C. The PL of the sample with no oxygen doping but annealed at 750 °C is dominated by a main peak near 1.537 μm. However, the sample annealed at 850 °C does not show this peak or it is very weak at best, but instead the emission spectrum is dominated by another peak near 1.54 μm. As discussed in section 4.1, this annealing behavior is typical of the AlGaAs:Er and GaAs:Er samples. On the other hand, samples co-doped with oxygen showed stronger Er^{3+} emissions as the annealing temperature was increased from 700 to 850 °C. The sample annealed at 700 °C showed very weak emissions (not shown in the figure), but as the annealing temperature increased to 750 °C, the intensity increased at least by a

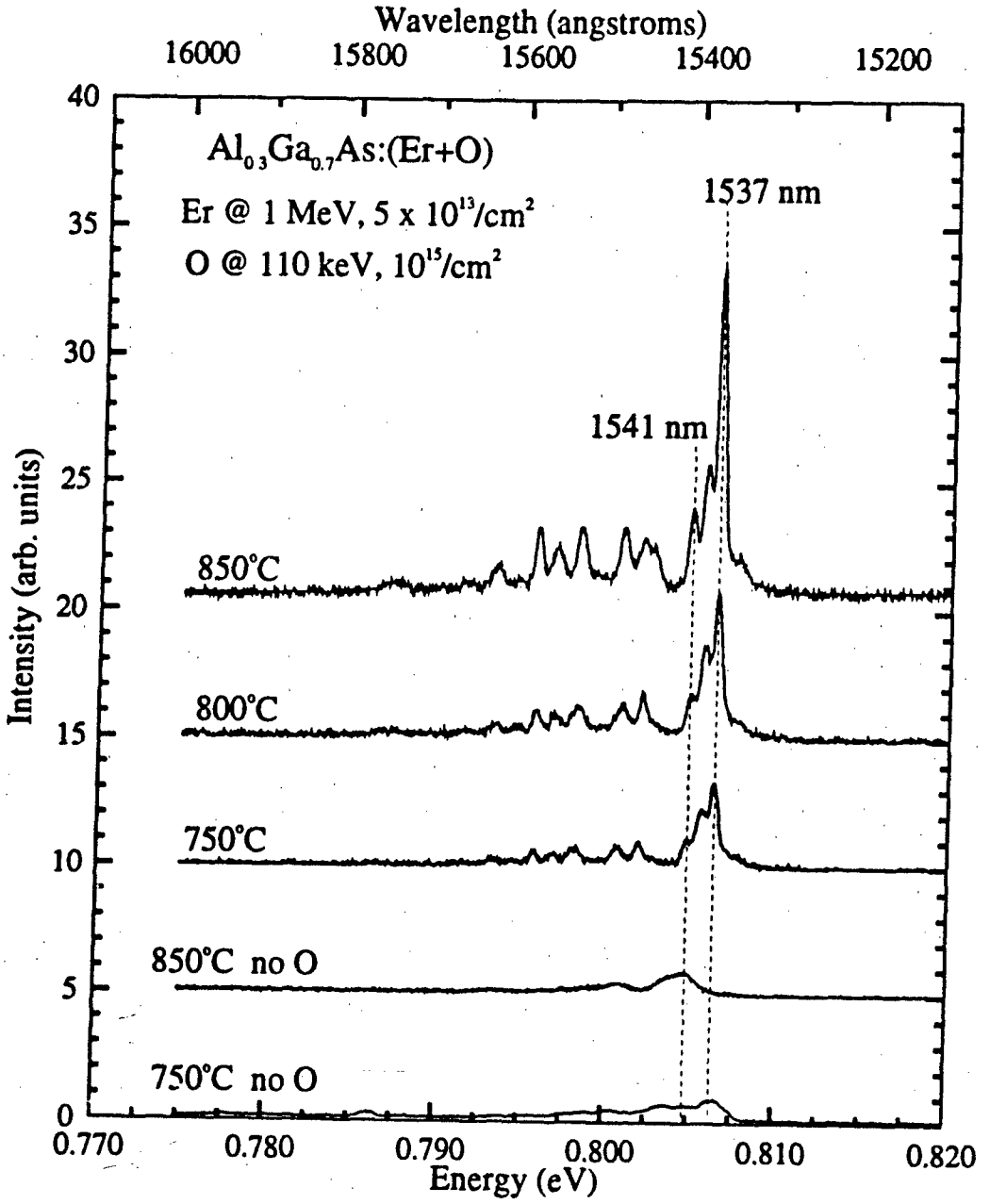

Figure 87 Photoluminescence dependence on annealing temperature for $Al_{0.3}Ga_{0.7}As$:Er and $Al_{0.3}Ga_{0.7}As$:(Er+O)

factor of 10. Furthermore, the PL intensity of the main peak near 1.5375 μm increased drastically as the annealing temperature increased to 850 °C. However, note that not all the peaks were enhanced by the same factor.

These results can be explained in the following manner. For the samples without oxygen doping, the Er^{3+} emissions originate from Er atoms located at interstitial sites or Er complexes formed with other defects. At higher annealing temperatures, the Er moves to substitutional sites, or the defect forming a complex with the Er diffuses thus breaking the complex giving rise to the Er^{3+} emissions. For the case of the samples co-implanted with O, it seems that oxygen forms a complex with Er that is more stable and requires higher annealing temperatures to break. Furthermore, at higher annealing temperatures, it is expected that the O atoms that did not formed complexes with Er may diffuse, thus increasing the probability of forming a complex with Er.

4.5.6 Lifetime Measurements

Lifetime measurements were performed on two of the co-implanted samples and the corresponding control samples. Figure 88 shows the time decay of the 1.5375 μm emission from $Al_{0.29}Ga_{0.71}As$:(Er+O) and $Al_{0.29}Ga_{0.71}As$:Er samples annealed at 750 °C. Both samples shown in figure 88 were implanted with Er at 1 MeV with a dose of 5 x $10^{13}/cm^2$, and the co-doped sample was implanted with O at 110 keV with a dose of 1 x $10^{15}/cm^2$. The

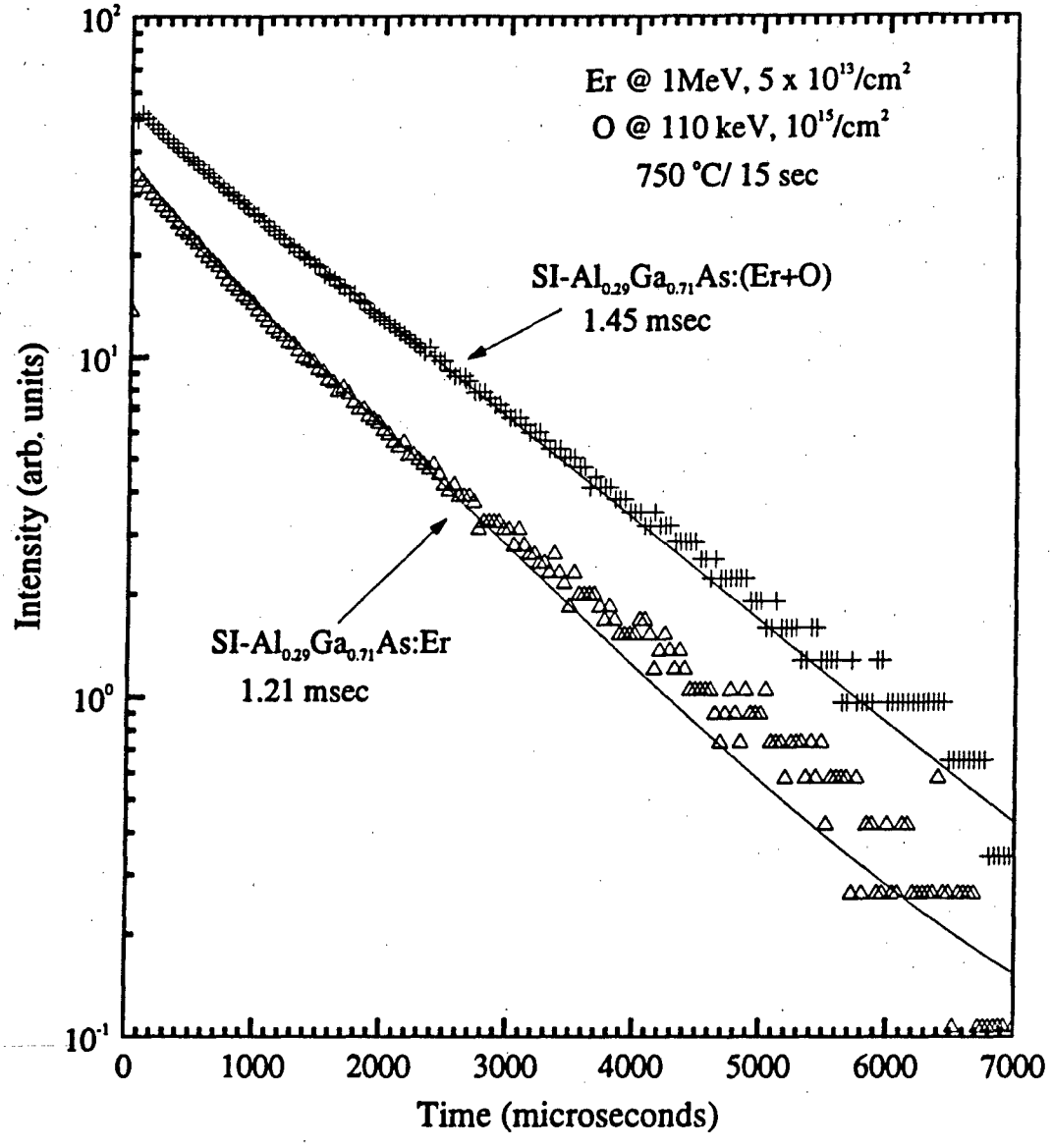

Figure 88 Time decay of the 1.537 μm emission from $Al_{0.29}Ga_{0.71}As$:Er and $Al_{0.29}Ga_{0.71}As$:(Er+O) samples annealed at 750 °C

decays were recorded using wide slit openings of 1 mm for both the entrance and exit slits, and thus, the decays will include contributions from other nearby peaks. In the figure, the solid lines show least square fits to a single exponential. The lifetimes are 1.22 and 1.46 msec for the control and co-doped samples, respectively, showing a slower decay for the co-doped sample.

This is consistent with the results obtained for $Al_{0.3}Ga_{0.7}As$:(Er+O) and $Al_{0.3}Ga_{0.7}As$:Er samples annealed at 850 °C for 15 sec as shown in figure 89. The Er and O doses for these samples were the same as for the two above samples. In this case, the main emission from the control sample occurs at 1.54 μm, as mentioned previously. Therefore, the figure shows the decay of the main 1.537 μm Er^{3+} emission from the co-doped sample and that of the 1.540 μm emission from the control sample. The co-doped sample shows a slower decay with a time constant of 1.7 msec, while the control sample has a lifetime of 1.3 msec. In both cases the data was fitted to a single exponential as shown with solid lines in the figure. These results suggest that oxygen co-doping reduces the losses due to nonradiative processes.

The lifetime of the samples annealed at 850 °C was studied as a function of sample temperature and the result of $\tau(T)/\tau(0)$ is plotted in figure 90, where $\tau(0)$ is the low temperature decay time. Table VIII lists the decay times at various temperatures. For the co-doped sample, the decay time

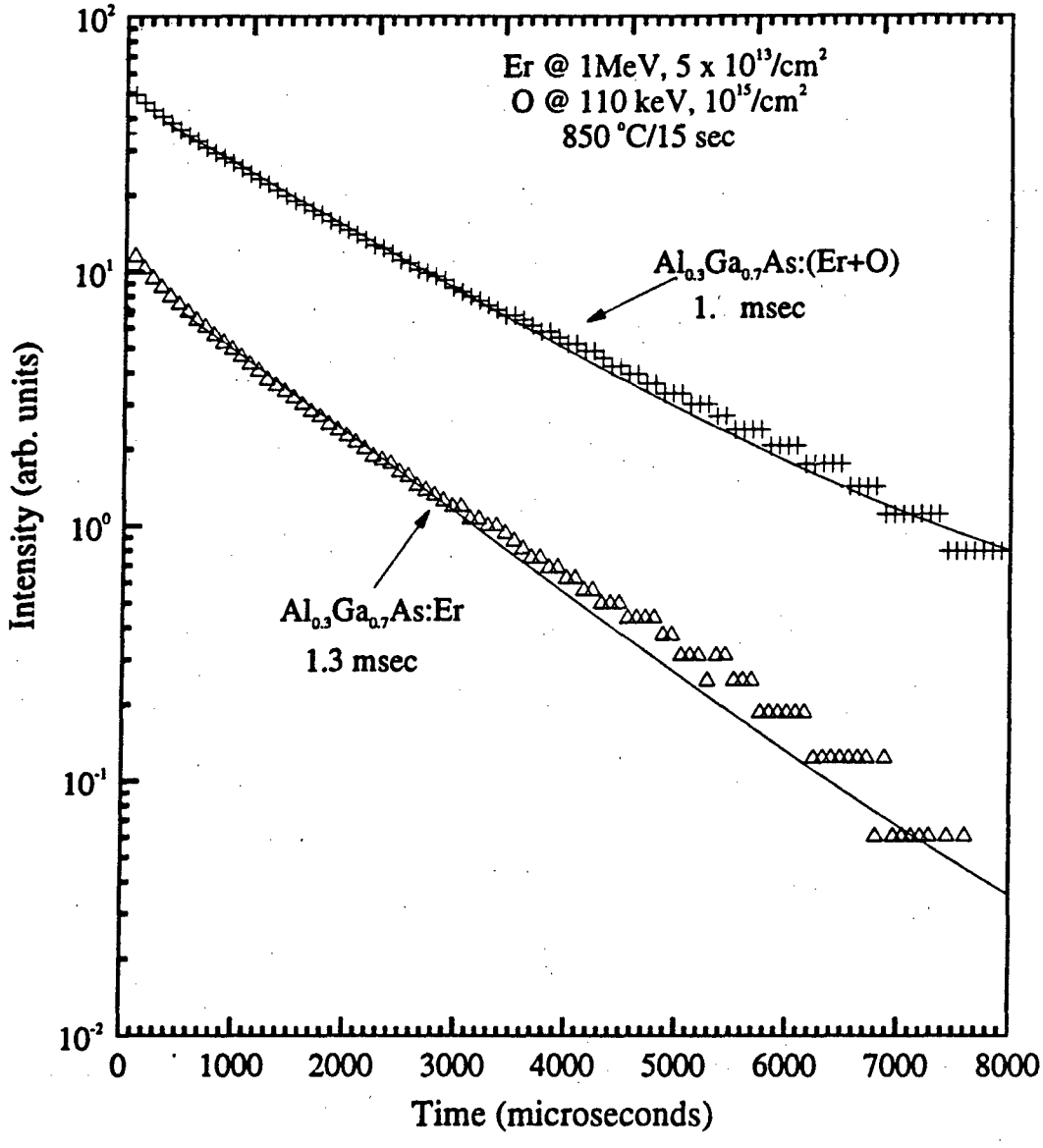

Figure 39 Time decay of the main Er^{3+} emission from $Al_{0.3}Ga_{0.7}As$:Er and $Al_{0.3}Ga_{0.7}As$:(Er+O) samples annealed at 850 °C

Table VIII

Decay times of the main Er^{3+} emissions from $Al_{0.3}Ga_{0.7}As$:(Er+O) and $Al_{0.3}Ga_{0.7}As$:Er samples as a function of sample temperature

$Al_{0.3}Ga_{0.7}As$:(Er+O) Temp (K)	Decay Time (μsec)	$Al_{0.3}Ga_{0.7}As$:Er Temp (K)	Decay Time (μsec)
9.0	1706	8.0	1301
16.3	1702	19.3	1353
25.5	1700	50.6	1201
45.4	1689	74.0	1123
70.2	1665	99.7	1054
95.4	1630	119.4	1003
120.0	1592	139.0	966
149.4	1561	160.0	714
173.3	1499	179.3	672
198.3	1311	199.7	631
222.7	1164	223.1	593
247.0	995	248.6	546
271.1	993	278.7	509
297.0	972	298.8	406

decreases slowly as T increases, and it is still close to 1 msec at room temperature. The decay time decreased by less than 50% when the temperature increased from 9 to 297 K. However, a steeper decrease was observed for the control sample. In this case, the decay time decreased by approximately 70% of its low temperature value of 1.3 msec to approximately 400 μsec at room temperature. The difference between the decay times at low and high temperatures is a measure of the de-excitation rate of the excited state by nonradiative processes. Therefore, we may conclude that nonradiative de-excitation of the 4f shell is much less for the O and Er co-doped samples. An interesting observation is

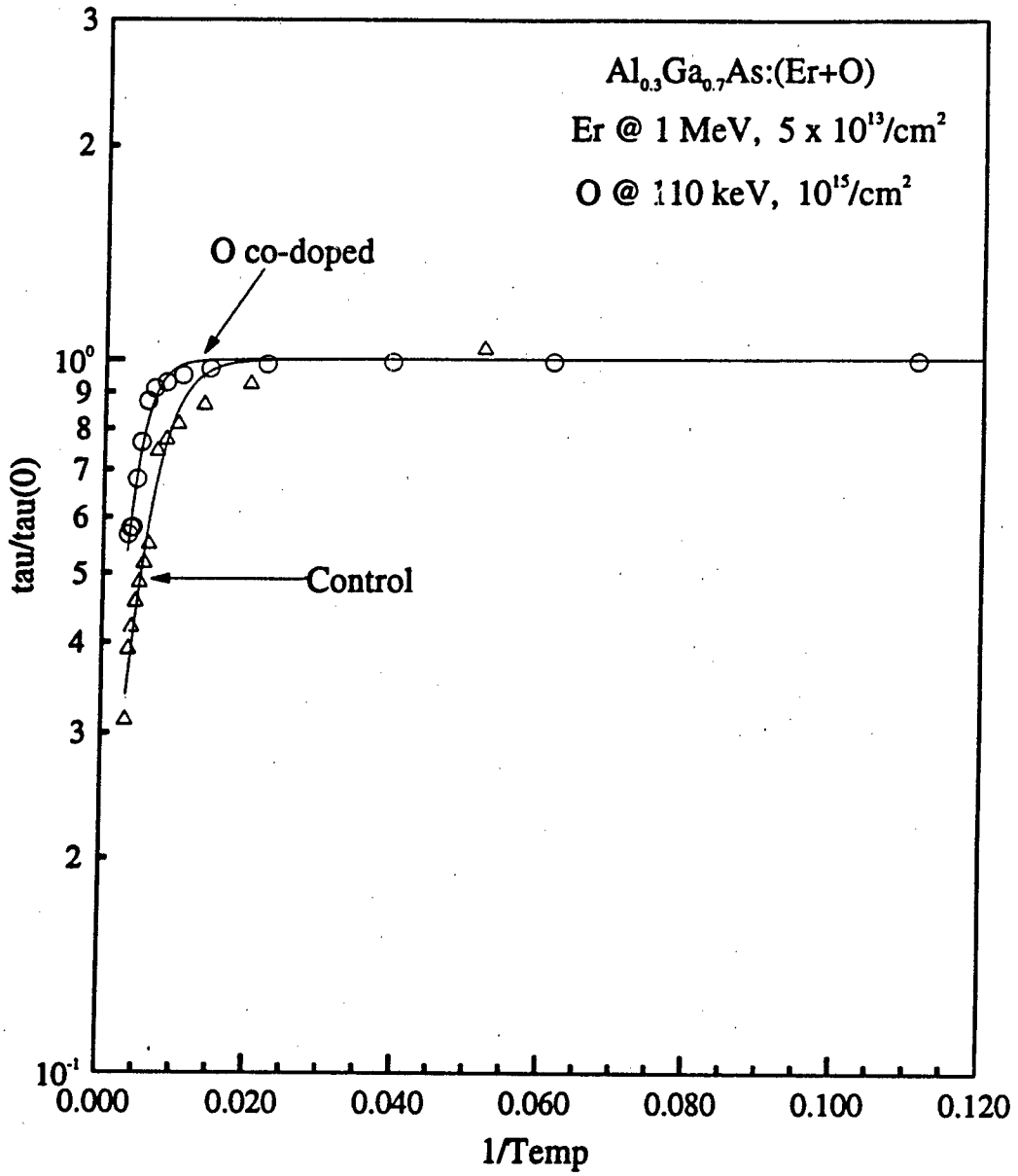

Figure 90 Lifetime ratio, $\tau(T)/\tau(0)$, of the main Er^{3+} emission from $Al_{0.3}Ga_{0.7}As$:Er and $Al_{0.3}Ga_{0.7}As$:(Er+O) samples annealed at 850 °C

that for both the control and the co-doped samples the initial PL intensity showed a much greater decrease with increasing T than the lifetime. Since this decrease in the intensity is not reflected in the lifetime, it is mostly due to a decrease in the excitation efficiency, as opposed to nonradiative de-excitation of the $^4I_{13/2}$ excited state.

As with GaAs:Er, a fit of this lifetime data to an expression of the form

$$\tau(T) = \frac{\tau(0)}{1 + A\exp(-\frac{E}{k}T)}.$$

was attempted, however, a satisfactory fit could not be obtained, even with two activation energies. The decay time follows this equation only at high temperatures, which implies that a different type of process is responsible for the decrease in the lifetime at lower temperatures. Therefore, only the values for $T > 100$ K were fitted to this equation. The solid lines in the figure show this fit. The fitting values for the co-doped sample were $A = 5.36 \pm 1.21$ and $E = 0.047 \pm 0.0049$ eV and for the control sample were $A = 6.5 \pm 0.98$ and $E = 0.031 \pm 0.0031$ eV. Since these results show comparable values of A for both samples, the smaller decrease in the decay time with increasing T observed for the co-doped sample, is due solely to a larger activation energy. In the excitation model proposed in section 4.2.2, the activation energy E can be interpreted as the sum of the Er-

related trap energy and the bound exciton binding energy, therefore the energy of the Er-related trap in the co-doped samples is different from that of the samples doped with Er alone in agreement with the idea of an Er-O complex.

4.5.7 Concluding Remarks

The addition of oxygen to GaAs:Er and AlGaAs:Er results in the enhancement of the Er^{3+} emissions from AlGaAs:Er but not from GaAs:Er. These results can be explained by the formation of an Er-Al-O complex. Interestingly, the growth of a new material $Al_xEr_yO_z$ on Si has recently been reported (Salvi et al. [1991]), however, the PL presented in that report was too weak to allow a comparison with the PL from our samples. In our model of the excitation mechanism, the excitation of Er in III-V semiconductors proceed through the binding of excitons at an Er-related trap (either electron or hole trap). Therefore, it may be concluded that the enhancement of the 4f emissions is due to the formation of a new complex that binds excitons much more efficiently than the other complexes formed for only Er implantation. It has also been found that the main Er^{3+} emission from the co-doped samples has longer lifetimes, which suggests smaller losses due to nonradiative processes. Also, annealing studies suggest that luminescence centers formed through co-implantation of Er and O are more stable than those formed when through Er implantation only. In fact, when only Er is implanted, an increase in the

annealing temperature from 750 to 850 °C results in weaker 4f emissions, a fact possibly due to the dissociation of the complex giving rise to the Er^{3+} luminescence or to the formation of new optically inactive complexes. However, samples co-implanted with O at the highest dose of $10^{15}/cm^2$ showed an increase in the signal strength upon increasing the annealing temperature in the same range of 750 to 850 °C.

Current study also shows that fairly high concentrations of oxygen are needed to enhance the Er emissions. The best results were consistently obtained when the oxygen peak concentration was more than ten times greater than the Er peak concentration. However, since only three oxygen doses were used in this study the optimum concentration of O is not known, possibly somewhere between 10^{14} and $10^{15}/cm^2$. At least this is certainly true for the samples with smaller Er concentrations.

In view of the results obtained in present study, it is very doubtful that the 4f luminescence normally observed from GaAs:Er and AlGaAs:Er originates from a complex involving oxygen, as suggested by Auzel et al [1989]. First, the large crystal field splitting quoted by Auzel has only been observed in a few samples. Results from other researchers and current results for ion implanted and MBE grown GaAs:Er and AlGaAs:Er samples indicate a much smaller crystal field energy separation between the Er emissions. Second, current results show that the addition of oxygen does not enhance the Er

emissions from GaAs:Er, and even for AlGaAs very high O concentrations are needed to enhance the Er emissions. The high oxygen concentration doping always produced a characteristic PL spectrum, independent of x and the annealing temperature. However, ion implanted and MBE grown AlGaAs:Er generally shows a different emission spectrum. Therefore, it may be concluded that stronger emissions from AlGaAs:Er as compare to those from GaAs:Er are not necessarily due to a high concentration of oxygen in the AlGaAs samples as suggested by Favennec et al [1989].

v. Conclusions and Recommendations

This investigation represents an extensive study of the spectroscopic properties of Er doped GaAs:Er and $Al_xGa_{1-x}As$:Er. The main objective of this work was to study the excitation and de-excitation mechanisms of the Er-4f shell. In order to accomplish this, the effect of various parameters on the Er^{3+} emissions was first investigated for the Er ion implanted samples. These emissions were studied as a function of substrate conductivity (SI, n- and p-type), aluminum mole fraction, Er concentration, and annealing temperature. An effort was made to identify emissions originating from different centers. This is important to an understanding of the excitation mechanism, because emissions originating from different centers might have different excitation mechanisms. In fact, this is responsible for a series of contrasting reports in the literature. Based on the results obtained, through current study a model of the excitation mechanism was proposed. The Er^{3+} emissions from MBE-grown GaAs:Er and $Al_xGa_{1-x}As$:Er were also studied. These emissions were studied as a function of Er concentration, substrate growth temperature, and substrate orientation. Lifetime measurement studies of the 1.54 μm emissions from GaAs:Er and ten different emissions from $Al_{0.5}Ga_{0.5}As$:Er were performed, and their kinetics were compared. The excitation spectrum of the 1.54 μm emission from the MBE-grown GaAs:Er was found to be signifi-

cantly different from that of the ion implanted samples. Finally, a study was made on the effects of O co-doping on the Er^{3+} emissions. A practical reason for this study was to find whether the addition of O would enhance the Er^{3+} emissions. A more fundamental reason was to test if the Er^{3+} luminescence from Er-doped III-V semiconductors originates from some type of Er-O complex as suggested by various authors. The important results from this work include the followings.

i. The PL intensity of Er^{3+} emission increases with the aluminum mole fraction, x.

ii. Although the detailed emission spectrum over the 1.5 to 1.6 μm region depends on the particular sample and annealing conditions, the same emissions were seen at the same wavelength position, independent of x. This was also true for the MBE samples, where x varied from 0 to 0.7. This remarkable effect shows the atomic nature of these emissions.

iii. Photoluminescence and selective excitation photoluminescence measurements showed the presence of multiple luminescence centers in Er-doped samples. In particular, it can be distinguished at least three different centers in our ion implanted GaAs:Er samples. One of these, labeled C2 in the discussion in section 4.1, can be excited very efficiently with laser energies well below the bandgap. Efficient below-bandgap laser excitation of the Er^{3+} emissions was observed only in those samples containing the C2 center.

iv. The p-type samples showed stronger Er^{3+} emissions for both

GaAs:Er and $Al_xGa_{1-x}As$:Er. In GaAs:Er, it was demonstrated that the PL intensity of the Er^{3+} emissions increased with n- or p-type doping level up to a certain concentration. However, at high concentrations on the order of $10^{18}/cm^3$, the intensity of the Er^{3+} emissions decreases while the intensity of an underlying broadband emission increases, and the lifetime of the 4f emissions increased with the doping level. This suggests that the decrease in intensity is due to a decrease in the excitation efficiency rather than due to nonradiative de-excitation of the 4f excited state. This phenomenon was explained in our excitation model as due to a competing Auger energy transfer from the Er-bound exciton to a hot carrier.

v. The excitation spectra of an ion implanted GaAs:Er show a broad excitation band extending from the bandedge to at least 1.24 eV. For the ion implanted samples, below-bandgap laser excitation was at least as efficient as above-bandgap laser excitation, and for the p-type sample, it was rather much more efficient than the above-bandgap laser excitation. This was explained with an excitation model that involved electron-hole recombination at an Er-related hole trap with subsequent transfer of the recombination energy to the 4f shell.

vi. Temperature dependent lifetime measurements revealed that the lifetime decreases with increasing sample temperature. An activation energy of 169 meV was determined for the ion implanted GaAs:Er sample. The MBE sample showed a peculiar behavior, i.e., at T < 100 K, the lifetime showed a small

increase as T increased. The reason for this is not well understood at this point. A similar behavior was also observed for some of the Er^{3+} emissions from MBE grown $Al_{0.5}Ga_{0.5}As:Er$.

vii. The lifetimes of ten different emissions from MBE-grown $Al_{0.5}Ga_{0.5}As:Er$ were determined. It was demonstrated that the emissions near 1.56 μm and the peaks at 1.532 and 1.5404 μm originate from the same center. These emissions have a short lifetime of approximately 200 μsec.

vii. A series of sharp emissions near 988 nm was attributed to the intra-4f-shell transition from the $^4I_{11/2}$ excited state to the $^4I_{15/2}$ ground state of Er^{3+}.

viii. Oxygen co-implantation showed consistently a strong enhancement of the Er^{3+} emissions from $Al_xGa_{1-x}As:(Er+O)$. The annealing behavior of the O co-doped sample was found to be different from that of the Er only implanted sample. No enhancement of the Er^{3+} emissions from GaAs:(Er+O) was observed with O co-doping. The enhancement of the Er^{3+} emissions from $Al_xGa_{1-x}As:(Er+O)$ was attributed to the formation of an Er-Al-O complex.

ix. Er^{3+} emissions from the samples co-implanted with O have longer lifetimes, thus suggesting smaller losses due to nonradiative processes. Temperature dependence of the lifetime showed larger activation energy for the O co-implanted samples.

Although, this work contributes to further understanding of the

excitation mechanism of the 4f shell, there are still many questions that will require further research. The following is a list of suggestions for further work.

1. A selective excitation luminescence study of $Al_xGa_{1-x}As$:Er: Our preliminary results showed that the Er^{3+} emissions from the ion implanted and MBE-grown samples could be efficiently excited with below-bandgap laser excitation as for the ion implanted GaAs:Er samples. Therefore, a systematic study over the whole range of x values from 0 to 1 will provide very important information on the excitation mechanism.

2. A selective excitation luminescence study of oxygen co-doped samples as well as a study of O co-doping where the doping is introduced via another technique such as MOCVD.

3. It is necessary to do SIMS, RBS, and/or TEM studies on the samples co-doped with O in order to understand how O and Er are incorporated.

4. Electrical measurements on the samples co-doped with O: Although O doping into III-V semiconductors generally makes the sample semi-insulating, preliminary Hall measurements have shown that the Er and O co-implantation do not change the carrier concentration.

5. Systematic study of n- and p-type MBE-grown samples: This study should yield very interesting information concerning the excitation study. This study has shown that the p-type samples consistently yield stronger emissions and is important to see whether the C2 emissions can also be observed on these

samples.

6. Erbium doping of wide bandgap semiconductors: The results have been reported that the Er^{3+} emissions are stronger and the effect of temperature quenching is smaller in wider gap materials. Also, it will be interesting to see whether transitions from other excited states of Er^{3+} can be observed.

7. Copper and lithium co-doping: In II-VI compounds these elements are used to enhance the 4f emissions. It would be of great practical interest to study their effect on RE doped III-V semiconductors.

8. Other RE systems: Excitation studies of Nd, Pr, and Tm are necessary in order to obtain a better understanding of the 4f excitation mechanisms. Oxygen co-doping of Nd- and Pr-doped samples will be of particular interest.

9. Electroluminescence studies: The excitation mechanism of the 4f shell may be different in devices with carrier injection. Although there are some reported studies, there is a great need to do further work on this area.

The study of RE-doped III-V semiconductors has been motivated by the desired to develop a rare-earth injection laser, however current results suggest that the development of such a device is not feasible in the near future. In the case of Er-doped GaAs and $Al_xGa_{1-x}As$, the major obstacle is the weak intensity of the Er^{3+} emissions and the quenching of these emissions at room temperature. Current results have demonstrated the enhancement of the Er^{3+} emissions when co-

implanting Er and O and these emissions where observed even at room temperature, however the intensity of the Er^{3+} emissions is still too weak. Further work on Er and O co-doping might lead to a significant enhancement of the 1.54 μm emissions that would made an Er-injection laser feasible, also an electroluminescence study of the co-doped samples will provide important information concerning the feasibility of such a device.

References

F. Auzel, A. M. Jean-Louis, and Y. Toudic. "Oscillator Strength, Quantum Efficiencies, and Laser Cross Sections of Yb^{3+} and Er^{3+} in III-V Semiconductors," J. Appl. Phys. 66 (8): 3952-3955 (October 1989).

F. Auzel, B. W. Zhou, D. Meichenin, and A. M. Jean-Louis. "Passive Wavelength Stabilization in the 1.54 μm Region of Wide Gain Spectrum lasers by Er^{3+} Doped Materials," J. Appl. Phys. 69 (10): 7310-7312 (May 1991).

M. Baeumler, J. Schneider, F. Könl, and E. Tomzig. "Electron Spin Resonance of Erbium in Gallium Arsenide," J. Phys. C:Solid State Phys. 20: L963-L965 (1987).

N. T. Bagraev, L. S. Vlasenko, K. A. Gatsoev, A. T. Gorelenok, A. V. Kamanin, V. V. Mamutin, B. V. Pushnyl, Yu P. Tolparov, and A. E. Shubin. "Influence of Rare-Earth Elements on the Carrier Mobility in Epitaxial InP and InGaAs Films," Sov. Phys. Semicond. 18 (1): 49-50 (January 1984).

B. Kh. Bairamov, L. F. Zakharenkov, G. V. Il'menkov, V. F. Masterov, and V. V. Toporov. "Influence of Rare-Earth Elements on the Properties of Bulk InP Single Crystals," Sov. Phys. Semicond. 23 (8): 927-929 (August 1989).

F. Bantien, E. Bauser, and J. Weber. "Incorporation of Erbium by Liquid-phase Epitaxy," J. Appl. Phys. 61 (8): 2803-2806 (April 1987).

J. L. Benton, J. Michel, L. C. Kimerling, D. C. Jacobsson, Y. -H. Xie, D. J. Eaglesham, E. A. fitzgerald, and J. M. Poate. "The Electrical and Defect properties of Erbium-Implanted Silicon," J. Appl. Phys. 70 (5): 2667-2671 (September 1991).

T. Benyattou, D. Seghier, G. Guillot, R. Moncorge, P. Galtier, and M. N. Charasse. "Time-resolved Pholuminescence Spectroscopy from Erbium-doped $Ga_{0.55}Al_{0.45}As$" Appl. Phys. Lett., 58 (19): 2132-2134 (May 1991).

T. Benyattou, D. Seghier, G. Guillot, R. Moncorge, P. Galtier, and M. N. Charasse. "Optical Studies of Erbium Excited States in $Ga_{0.55}Al_{0.45}As$" Appl. Phys. Lett., 60 (3): 350-352 (January 1992).

Karl W. Boer. Survey of Semiconductor Physics, volume 1. Van Nostrand Reinhold, New York, 1990.

R. Boyn. "4f-4f Luminescence of Rare-Earth Centers in II-VI

Compounds" Phys. Stat. Sol. (b) 148 (11): 11-47 (November 1988).

C. Delerue and M. Lannoo. "Theory of Substitutional Rare Earth Impurities in Semiconductors," In Gordon Davies, Gary G. DeLeo, and Michael Stavola, editors, Proceedings of the 16th International Conference on Defects in Semiconductors, Materials Science Forum, vol. 83-87: 659-664. Trans Tech Publications, 1992.

J. N. Demas. Excited State Lifetime Measurements, Academic Press, New York, 1983.

J. F. Donegan. "Observation of Non-radiative Transfer in the Excitation of Nd^{3+} Luminescence in GaP," Physical Review B, 41 (14): 10254-10256 (May 1990).

D. J. Eaglesham, J. Michel, E. A. Fitzgerald, D. C. Jacobson, J. M. Poate, J. L. Benton, A. Polman, Y. H. Xie, and L. C. Kimerling. "Microstructure of Erbium-Implanted Silicon,"Appl. Phys. Lett. 58 (24): 2797-2799 (June 1991).

H. Ennen and J. Schneider. "Luminescence of Rare Earth Ions in III-V Semiconductors," Proceedings of the 13th International Conference on Defects in Semiconductors: 115-127 (August 1984)

H. Ennen, G. Pomrenke, A. Axmann, K. Eisele, W. Haydl, and J. Schneider. "1.54-μm Electroluminescence of Erbium-Doped Silicon Grown by Molecular Beam Epitaxy,"Appl. Phys. Lett. 46 (4): 381-383 (February 1985).

H. Ennen, G. Pomrenke, and A. Axmann. "Luminescence of the Rare-Earth Ion Ytterbium in InP,GaP, and GaAs,"J. Appl. Phys. 57 (6): 2182-2185 (March 1985).

H. Ennen, J. Wagner, H. D. Muller, and R. S. Smith. "Photoluminescence Excitation Measurements on GaAs:Er Grown by Molecular Beam Epitaxy,"J. Appl Phys. 61 (10): 4877-4879 (May 1987).

K. R. Evans, E. N. Taylor, C. E. Stutz, D. W. Elsaesser, J. E. Colon, Y. K. Yeo, R. L. Hengehold, J. S. Solomon. "Molecular-beam Epitaxial Growth and Characterization of Erbium-doped GaAs and AlGaAs," J. Vac. Sci. Technol. B 10 (2): 870-872 (Mar/Apr 1992).

L. K. Ermakov, V. A. Kasatkin, and L. P. Pasechnik. "Luminescence of Ytterbium in Gallium and Indium Phosphides," Opt. Spectrosc. (USSR) 57 (1): 6-7 (July 1984).

P. N. Favennec, H. L'Harridon, M. Salvi, D. Moutonnet, and Y. Le Guillou. "Luminescence of Erbium Implanted in Various Semiconductors: IV, III-V, and II-VI Materials," Electronics Letters 25 (11): 718-719 (May 1989).

P. N. Favennec, H. L'Harridon, D. Moutonnet, M. Salvi, and M. Gauneau. "Optical Activation of Er^{3+} Implanted in Silicon by Oxygen Impurities," Japanese J. of Appl. Phys. 29 (4): L524-L526 (April 1990).

P. Galtier, M. N. Charasse, J. Chazelas, A. M. Huber, C. Grattepain, J. Siejka, and J. P. Hirtz. "Erbium-Doping of GaAs, AlGaAs, and GaAs/AlGaAs Quantum Wells by Molecular Beam Epitaxy, "In Gallium Arsenide and Related Compounds 1988, number 96 in Inst. Phys. Conf. Ser.: 61-64 (1988).

P. Galtier, T. Benyattou, J. P. Pocholle, M. N. Charasse, G. guillot, and J. P. Hirtz. "1.54 μm Photoluminescence and Electroluminescence of Erbium Doped GaAs and GaAlAs grown by Molecular Beam Epitaxy, "In Gallium Arsenide and Related Compounds 1988, number 106 in Inst. Phys. Conf. Ser.: 327-331 (1989).

K. A. Gatsoev, A. T. Gorelenok, S. L. Karpenko, V. V. Mamutin, and R. P. Seisayan. "Effects of Doping with Rare Earth Elements on the Low Temperature Edge Luminescence of InP," Sov. Phys. Semicond. 17 (12): 1373-1375 (December 1984).

A. A. Gippius, V. V. Ushakov, V. N. Yakimkin, and V. S. Vavilov. "Transition and Rare Earth Elements Used as Luminescent Probes in Studying Ion-Implanted III-V and II-VI Semiconductors," Nuclear Instruments and Methods in Physics Research B39: 492-495 (1989). (December 1984).

M. Godlewski, K. Światek, A. Suchocki, and J. M. Langer. "Excitonic Mechanism of Luminescence Excitation of Rare-Earths and Transition Metals in Solids,"Journal of Luminescence 48 & 49: 23-28 (1991).

L. A. Hemstreet. "The Electronic States of a substitutional Ytterbium Impurity in Indium Phosphide," Materials Science Forum, Defects in semiconductors Vol 10-12 85-90 (1986).

B. J. Heijmink Liesert, M. Godlweski, A. Stapor, T. Gregrokiewicz, C. A. Ammerlaan, J. Weber, M. Moser, and F. Scholz. "Optically Detected Microwave-Induced Impact Ionization of Ytterbium Bound Excitons in InP," Appl. Phys. Lett. 58 (20): 2237-2239 (May 1991).

Hideo Isshiki, Hitoshi Kobayashi, Shigemi Yugo, Riichiro Saito, Tadamasa Kimura, and Toshiaki Ikoma. "Emmision of the

1.54 μm Er-Related Peaks by Impact Excitation of Er atoms in InP and its Characteristics," SPIE Vol. 1361 Physical Concepts of Materials for Novel Optoelectronic Decice Applications I: 223-227 (1990).

Hideo Isshiki, Riichiro Saito, Tadamasa Kimura, and Toshiaki Ikoma. "Characteristics of the Electroluminescence and Photoluminescence Emission of Erbium Ions Doped in InP and the Energy Transfer Mechanism," J. Appl. Phys., 70 (11): 6993-6998 (December 1991).

V. A. Kasatkin, F. P. Kesamanly, and B. E. Samorukov. "Luminescence of Dysprosium-Doped Gallium Phosphide," Sov. Phys. Semicond. 12 (8): 974-975 (August 1978).

V. A. Kasatkin, F. P. Kesamanly, V. G. Makarenko, and B. E. Samorukov. "Luminescence of Epitaxial GaP Films Doped with Lanthanide Impurities," Sov. Phys. Semicond. 13 (10): 1207-1208 (October 1979).

V. A. Kasatkin, F. P. Kesamanly, V. G. Makarenko, V. F. Masterov, and B. E. Samorukov. "Intracenter Transitions in Yb^{3+} Impurities in Gallium Phosphide," Sov. Phys. Semicond. 14 (9): 1092 (September 1980).

V. A. Kasatkin, F. P. Kesamanly, and B. E. Samorukov. "Photoluminescence of Heat Treated Gallium Phosphide Doped with Praseodymium and Ytterbium," Sov. Phys. Semicond. 15 (3): 352-353 (March 1981).

V. A. Kasatkin and V. P. Savel'ev. "Excitation of Ytterbium Luminescence in Gallium and Indium Phosphides," Sov. Phys. Semicond. 18 (9): 1022-1023 (September 1984).

V. A. Kasatkin. "Instability of Low-Symmetry Yb^{3+} and Pr^{3+} Luminescence Centers in Gallium Phosphide," Sov. Phys. Semicond., 19 (10)3: 1174-1175 (October 1985).

V. A. Kasatkin and V. N. Romanov. "Influence of the Charge State of Ytterbium on the Conductivity of InP:Yb," Sov. Phys. Semicond. 19 (10): 1177-1178 (October 1985).

P. B. Klein. "Time Resolved Photoluminescence from Yb^{3+} Centers in InP:Yb," Solid State Commun. 65 (10): 1097-1101 (1988).

P. B. Klein and G. S. Pomrenke. "Photoluminescence Decay of 1.54 μm Er^{3+} emission in Si and III-V Semiconductors," Elect. Letters 24 (24): 502-502 (November 1988).

P. B. Klein, F. G. Moore, and H. B. Dietrich. "1.54μm

Electroluminescence in MeV Ion-Implanted Er-Doped GaAs," Electronics Letters 26 (16): 1299-1300 (August 1990).

Korber and Hangleiter. "Excitation and decay Mechanisms of the Intra-4f Luminescence or Yb^{3+} in Epitaxial InP:Yb Layers," Appl. Lett. 52 (2): 114-116 (January 1988).

A. Kozanecki and R. Groetzschel. "On the Location Of Ytterbium in GaP and GaAs Laticces," J. appl. Phys. 64 (6): 3315-3317 (September 1988).

A. Kozanecki and R. Groetzschel. "Ytterbium as a Probe of the Local Lattice Environment in $Ga_xIn_{1-x}P$ Crystals," J. appl. Phys. 66 (7): 3202-3206 (October 1989).

A. Kozanecki and R. Groetzschel. "Lattice Location and Optical Activity of Yb in III-V Semiconducting Compounds," J. Appl. Phys. 68 (2): 517-522 (July 1990).

A. Kozanecki, M. Chan, C. Jaynes, B. Sealy, and K. Homewood. "Lattice Location of Erbium Implanted into GaAs," Solid State Commun. 69 (8): 763-766 (1991).

A. Kozanecki and R. Groetzschel. "Rutherford Backscattering and Luminescence Characteristics of Neodymium Implanted GaP, GaAs, and AlGaAs," J. Appl. Phys. 69 (3): 1300-1303 (February 1991).

T. A. Lagvilava, M. G. Mil'vidskii, and E. V Solov'eva. "Influence of Yb on Residual Donor and Acceptor Impurities in GaP," Sov. Phys. Semicond. 24 (8): 858-860 (August 1990).

B. Lambert, Y. Toudic, G. Grandpierre, A. Rupert, A. Le Corre. "Electrical Activity of Ytterbium in InP," Electr. Lett. 24 (33): 1446-1447 (1989).

B. Lambert, A. Le Corre, Y. Toudic, C. Lhomer, G. Grandpierre, and M. Gauneau. "Electrical and Optical Properties of Rare Earth Dopants (Yb,Er) in n-type III-V (InP) Semiconductors," J. Phys.: Condens. Matter 2: 479-483 (1989).

J. M. Langer, A. Suchocki, Le Van Hong, P. Ciepielewski, and W. Walukiewicz. "Auger Effect at Localized Impurities in Semiconductors," Physica 117 & 118B: 152-154 (1983).

C. Lhomer, B. Lambert, Y. Toudic, A. Le Corre, M. Gauneau, F. Clerot, and B. Sermage. "Excitation Mechanisms of Rarre Earth (Yb) Luminescence in III-V Semiconductors (InP)," Semicond. Sci. Technol., 6: 916-923 (June 1991).

V. F. Masterov, V. V. Romanov, and K. F. Shtel'makh.

"Paramagnetic Resonance and Relaxation of Trivalent Ytterbium in Indium Phosphide," Sov. Phys. Solid State 25 (5): 824-826 (May 1983).

V. F. Masterov, V. P. Savel'ev, K. F. Shtel'makh, and L. F. Zakharenkov. "Properties of Heavily Doped InP:Yb and InP:Er Crystals," Sov. Phys. Semicond. 23 (12): 1381-1382 (December 1989).

V. F. Masterov and L. F. Zakharenkov. "Rare-earth elements in III-V semiconductors (review)," Sov. Phys. Semicond. 24 (4): 383-396 (April 1990).

V. F. Masterov, K. F. Shtel'makh, L. F. Zakharenkov, I. L. Likhilit, and I. A. Terletskii. "Electron Spin Resonance of an axial ytterbium Center in InP," Sov. Phys. Semicond. 25 (8): 830-833 (August 1991).

F. G. Moore, P. B. Klein, and H. B. Dietrich. "Type Conversion of Epitaxial GaAs Layers After Heavy Ion MeV Implantation and Annealing," Nuclear Instr. and Methods in Phys. Research B59/60: 1103-1105 (1991).

H. D. Muller, H. Ennen, J. Schneider, and A. Axmann. "Photoluminescence of Neodymium Implanted Gallium Phosphide and Gallium Arsenide," J. Appl. Phys., 59 (6): 2210-2212 (March 1986).

H. Nakagome, K. Takahei, and Y. Homma. "Liquid Phase Epitaxy and Characterization of Rare Earth Ion (Yb,Er) Doped InP," Journal of Crystal Growth 85: 345-356 (1987).

H. Nakagome, K. Uwai, and K. Takahei. "Extremely Sharp Erbium Related Intra 4f-shell Photoluminescence of Erbium Doped GaAs Grown by Metalorganic Chemical Vapor Deposition," Appl. Phys. Lett., 53 (18): 1726-1728 (October 1988).

Hiroshi Nakagome and Kenichiro Takahei. "MOCVD Growth and PL-Characteristics of Nd Doped GaAs," Extended Abstracts of the 21st Conference on Solid State Devices and Materials, Tokyo: 325-328 (1989).

A. J. Neuhalfen and B. W. Wessels. "Thermal Quenching of Er^{3+}-Related Luminescence in $In_{1-x}Ga_xP$," Appl. Phys. Lett. 60 (21): 2657-2659 (May 1992).

V. V. Petrov, V. S.Prolsolovich, V. D. Tkachev, G.S. Tsyrul'kevich, and Yu A. Karpov. "Thermal Donors in Erbium Doped Silicon," Sov. Phys. Semicond., 19 (4): 474-475 (April 1985).

Gernot S. Pomrenke, H. Ennen, and W. Haydl.

"Photoluminescence Optimization and Characteristics of the Rare-Earth Element Erbium Implanted in GaAs, InP, and GaP," J. Appl. Phys., 59 (2): 601-610 (January 1986).

Gernot S. Pomrenke. Luminescence of Lanthanides and Actinides into Binary III-V Semiconductors and AlGaAs, Doctoral Dissertation, AFIT/DS/ENP/89-4, (December 1989).

I. Poole, K. E. Singer, A. R. Peaker. "Growth and Structural Characterization of Molecular Beam Epitaxial Erbium-doped GaAs." Journal of Crystal Growth, 121: 121-131 (1992).

H. Przybylinska, K. Swiatek, A. Stapor, A. Suchocki, and M. Godlewski. "Recombination Processes in Yb-Activated ZnS," Phys. Rev. B 40 (3): 1748-1755 (1989).

S. L. Pyshkin, S. I. Radautsan, and S. V. Slobodchikov. "Electrical Properties of Gallium Phosphide Activated with Elements of the Lanthanide Group," Sov Phys. Semicond. 1 (7): 847-849 (January 1968).

D. J. Robins and P. J. Dean. "The Effect of Core Structure on Radiative and Non-radiative Metal Ions Substituents in Semiconductors and Phosphors," Advances in Physics, 27 (4): 499-532 (1978).

C. Rocaix, A. Rolland, P. N. Favennev, B. Lambert, A. Le Corre, H. L'Harridon and M. Salvi. "Erbium Implanted in III-v Materials." Japanese Journal of Applied Physics, 27 (12): L2348-L2350 (December 1988).

A. Rolland, A. Le Corre, P. N. Favennec, M. Gaunea, B. Lambert, D. Lecrosnier, H. L'Harridon, D. Moutonnet, and C. Rochaix. "Erbium-Doped GaAs Light-Emmiting Diode at 1.54 μm," Electronics Letters 24 (11): 718-719 (August 1989).

Riichiro Saito and Tadamasa Kimura. "Cluster Calculations of Rare-Earth Ions in Semiconductors," Phys. Rev. B, 46 (3): 1423-1428 (July 1992).

M. Salvi, H. L'Harridon, P. N. Favennec, D. Moutonnet, M. Gauneau, and M. Kechouane. "A Composite Layer of Al-Er-O Particles in a Silicon Matrix," J. Electrochem. Soc. 138 (6): 1761-1764 (June 1991).

D. Seghier, T. Benyattou, G. Bremond, F. Ducroquet, J. Gregoire, G. Guillot, C. Lhomer, B. Lambert, Y. Toudic, and A. Le Corre. "Electrical Behavior of Yb Ion in p- and n-type InP" Appl. Phys. Lett., 60 (3): 983-985 (February 1992).

J. Shaffer and F. Williams. "Energy Transfer from Donor-

Acceptor Pairs to Deep-Lying Impurity States in Semiconductors," Phys. Sta. Sol. 38 : 657-663 (1970).

K. F. Shtel'makh, L. F. Zakharenkov, V. V. Romanov, I. A. Terletskiĭ, and S. V. Shtel'makh. "Investigation of the Composition, Structure, and Magnetic Properties of Europium Doped Indium Phosphide," Sov. Phys. Semicond. 24 (8): 928-929 (August 1990).

R. S. Smith, H. D. Muller, H. Ennen, P. Wennekers, and M. Maier. "Erbium Doping of Molecular Beam Epitaxial GaAs," Appl. Phys. Lett. 50 (91): 49-51 (January 1987).

K. Swiatek, A. Suchocki, and M. Gaodlewski. "Three-center Auger Ecitation Mechanism of Ytterbium Intrashell Emission in ZnS," Appl. Phys. Lett. 57 (1): 40-42 (July 1990).

K. Świątek, A. Suchocki, and M. Godlewski. "On the Correlation Between Energy Structure and the Mechanism of Recombination for Rare Earth Ions in Solids," Journal of Luminescence 48 & 49: 527-530 (1991).

A. Tagushi, H. Nakagome, and K. Takahei. "Thermal Quenching Mechanism of Yb Intra-4f-shell Luminescence in InP," J. Appl. Phys., 70 (10): 5604-5607 (November 1991).

Akihito Tagushi, Moriyuki Taniguchi, and Kenichiro Takahei. "Direct Verification of Energy Backtransfer from Yb 4f-shell to InP Host," Appl. Phys. Lett., 60 (8): 965-967 (February 1992).

Kenichiro Takahei, Kunihiko Uwai, and Hiroshi Nakagome. "Photoluminescence Characterization of Rare-Earth (Er,Yb)-Doped InP Grown by Metalorganic Chemical Vapor Deposition," Journal of Luminescence 40&41: 901-902 (1988).

K. Takahei, A. Tagushi, H. Nakagome, K. Uwai, and P. S. Withney. "Intra-4f-Shell Luminescence excitation and Quenching Mechanism of Yb in InP," J. Appl. Phys. 66 (10): 4941-4945 (November 1989).

Kenichiro Takahei, Peter S Withney, Hiroshi Nakagome, and Kunihio Uwai. "Temperature Dependence of Intr-4f-shell Photo- and Electroluminescence Spectra for Erbium-doped GaAs," J. Appl. Phys., 65 (3): 1257-1260 (February 1989).

Moriyuki Taniguchi, Hiroshi Nakagome, and Kenichiro Takahei. "Luminescence Lifetime Study of Nd-doped GaP and GaAs," Journal of Luminescence, 52 : 251-257 (1992).

K. Thonke, K. Pressel, G. Bohner, A. Stapor, J. Weber, M. Moser, A. Molassioti, A. Hangleiter, and F. Scholz. "On

Excitation and Decay Mechanisms of the Yb_{3+} Luminescence in InP," Semicond. Sci. Technol. 5: 1124-1131 (1990).

V. V. Ushakov, A. A. Gippius, V. A. Dravin, and A. V. Spitsyn. "Luminescence of a Rare-Earth (Erbium) Impurity in Gallium Arsenide and Phosphide," Sov. Phys. Semicond. 16 (6): 723 (June 1982).

Kunihiko Uwai, Hiroshi Nakagome, and Kenichiro Takahei. "Rare-Earth Ion-Doped InP grown by Metalorganic Chemical Vapor Deposition" In Gallium Arsenide and Related Compounds 1986, number 83 in Inst. Phys. Conf. Ser.: 87-92 (1986).

K. Uwai, H. Nakagome, and K. Takahei. "Yb-doped InP Grown by Metalorganic Chemical Vapor Deposition," Appl. Phys. Lett. 50 (15): 977-979 (April 1987).

J. P. van der Ziel, M. G. Oberg, and R. A. Logan. "Single longitudinal mode operation of Er-doped 1.5-μm InGaAsP lasers," Appl. Phys. Lett. 50 (19): 1313-1315 (May 1987).

J. Wagner, J. Windscheif, and H. Ennen. "Photoluminescence Excitation Spectroscopy on InP:Yb," Phys. Rev. B 30 (10): 6230-6231 (November 1984).

J. Wagner, H. Ennen, and H. D. Muller. "Neodymium Complexes in GaP Separated by Photoluminescence Excitation Spectroscopy," J. Appl. Phys., 59 (9): 1202-1204 (February 1986).

J. Weber, A. Molassioti, M. Moser, A. Stapor, F. Scholz, G. Horcher, A. Forchel, A. Hammel, G. Laube, and J. Weidlein. "InP:Yb Layers Grown InP:Yb by Metalorganic Vapor Phase Epitaxy Using $Yb(MeCp)_3$ as a New Doping Source," Appl. Phys. Lett. 53 (25): 2525-2527 (December 1988).

J. Weber, M. Moser, A. Stapor, F. Scholz, G. Horcher, A. Forchel, G. Bohnert, A. Hangleiter, A. Hammel, and J. Weidlein. "MOVPE Grown InP:Yb Layers Using $Yb(IpCp)_3$ as a New Doping Source," Journal of Crystal Growth 100: 467-470 (1990).

D. M. Williams and B. W. Wessels. "Yb-doped InP grown by metalorganic vapor phase epitaxy using a beta-diketonate precursor," Appl. Phys. Lett. 56 (6): 566-568 (February 1990).

P S. Withney, K Uwai, H Nakagome, and K Takahei. "Erbium-Doped GaAs Light-Emmiting Diodes Emmiting Erbium f-Shell Luminescence at 1.54 μm," Electronic Lett. 29 (12): 710-711 (June 1988).

Peter S. Withney, Kunihiko Uwai, Hiroshi Nakagome, and Kenichiro Takahei. "Electrical Properties of Ytterbium-doped

InP Grown by Metalorganic Chemical Vapor Deposition," Appl. Phys. Lett. 53 (21): 2074-2076 (November 1988).

L. F. Zakharenkov, V. A. Kasatkin, F. P. Kesamanly, B. E. Samorukov, and M. A. Sokolova. "Photoluminescence of Epitaxial InP:Yb films," Sov. Phys. Semicond. 16 (8): 946 (August 1981).

Xinwei Zhao, Kazuhiko Hirakawa, and Toshiaki Ikoma. "Intracenter Transitions in Triply Ionized Erbium Ions Diffused into III-V Compound Semiconductors," Appl. Phys. Lett., 54 (98): 712-714 (February 1989).

Xinwei Zhao, Kazuhiko Hirakawa, and Toshiaki Ikoma. "Diffusion and Photoluminescence of Erbium in GaAs and InP," In Gallium Arsenide and Related Compounds 1988, number 96 in Inst. Phys. Conf. Ser.: 277-282 (1988).

REPORT DOCUMENTATION PAGE

Form Approved
OMB No 0704-0188

1. AGENCY USE ONLY (Leave blank)	2. REPORT DATE	3. REPORT TYPE AND DATES COVERED
	March 1993	Doctoral Dissertation

4. TITLE AND SUBTITLE
Luminescence Study of Ion-Implanted and MBE-Grown Er-Doped GaAs and $Al_xGa_{1-x}As$

5. FUNDING NUMBERS

6. AUTHOR(S)
José E. Colón

7. PERFORMING ORGANIZATION NAME(S) AND ADDRESS(ES)
Air Force Institute of Technology, WPAFB OH 45433-7765

8. PERFORMING ORGANIZATION REPORT NUMBER
AFIT/DS/ENP-93-01

9. SPONSORING/MONITORING AGENCY NAME(S) AND ADDRESS(ES)
Lt Col Gernot S. Pomrenke
AFOSR/NE (Bldg 410)
Bolling AFB DC 20332-6448

10. SPONSORING/MONITORING AGENCY REPORT NUMBER

11. SUPPLEMENTARY NOTES

12a. DISTRIBUTION/AVAILABILITY STATEMENT
Approved for public release; distribution unlimited

12b. DISTRIBUTION CODE

13. ABSTRACT *(Maximum 200 words)*

The excitation and de-excitation mechanisms of the Er^{3+} emissions near 1.54 μm from ion implanted and MBE-grown GaAs:Er and $Al_xGa_{1-x}As$:Er were studied through photoluminescence, lifetime measurements, and selective excitation luminescence as a function of Er concentration, Al mole fraction, n- and p-type doping level, and annealing temperature. It was found that there are multiple Er-related luminescence centers in ion implanted and MBE-grown GaAs:Er and $Al_xGa_{1-x}As$:Er. Lifetime measurements showed that the decay of the 1.54 μm emission is mainly a single exponential decay with a characteristic lifetime of approximately 1 msec. The $Al_xGa_{1-x}As$:Er samples showed in addition to the near 1.54 μm emissions, various sharp emissions near 988 nm, and they were assigned to the intra-4f-shell transition between the $^4I_{11/2}$ excited state and the $^4I_{15/2}$ ground state of Er^{3+}. In addition, O and Er co-doping studies were done, and it was found that for $Al_xGa_{1-x}As$, the Er^{3+} emissions from the co-doped samples were consistently much stronger than those from the Er-doped samples, but the Er^{3+} emissions from GaAs:Er were not enhanced by the O co-doping. The enhancement of the Er^{3+} emissions from $Al_xGa_{1-x}As$:(Er+O) was attributed to the formation of the Er-Al-O complex.

14. SUBJECT TERMS
rare earth, erbium (Er), GaAs, AlGaAs, ion implantation, MBE, photoluminescence, selective excitation luminescence.

15. NUMBER OF PAGES
252

16. PRICE CODE

17. SECURITY CLASSIFICATION OF REPORT	18. SECURITY CLASSIFICATION OF THIS PAGE	19. SECURITY CLASSIFICATION OF ABSTRACT	20. LIMITATION OF ABSTRACT
Unclassified	Unclassified	Unclassified	